FLOW AND SEDIMENT TRANSPORT AT HYDRAULIC JUMPS

BY ROBERT GORDON MACDONALD

A thesis submitted to the School of Environmental Sciences at the University of East Anglia
for the degree of Doctor of Philosophy

Acknowledgements

SAND THIS WAY

Abstract

Where river discharge is highly variable or channels poorly confined, hydraulic jumps are common. Hydraulic jump deposits should be far more common in the rock record than has been documented, or than is implied by classical fluvial facies models. The only sedimentary structures classically recognised as originating from hydraulic jumps are backset bedding and chute-and-pool structures, whereas flume experiments reported in this thesis demonstrate that a far greater range of structures occur.

Hydraulic jumps were formed downstream of a bed-attached hemisphere, acting as a boulder on a stream bed. Flow velocities and water surface shapes were recorded. Vorticity patterns were inferred from observations and theory. Sediment transport patterns were observed in runs with selected pumping rates, each with water surface patterns involving discrete forms of hydraulic jump. Small amounts of sediment were used, and the starved bedload features that formed are compared to published bedload features with a hemisphere but no hydraulic jump.

Flow and sediment transport patterns were also measured in a hydraulic jump that spanned the channel width. Sediment fell from suspension and formed downstream-thickening wedges, which I term *basal wedges*. Bedload features formed, with an anatomy not seen in other bedload features, and are defined as *hydraulic-jump unit bars*. Growth of sediment deposit volume downstream of hydraulic jumps caused the hydraulic jump to move upstream and series of *hydraulic-jump unit bars* formed at intervals, above and upstream of the previous unit bars. The resulting *hydraulic-jump bar complex*es aggraded up to 0.5 m thick. Their formation preserved sets of shallow upstream dipping laminae that passed downstream into cosets of climbing and upward-thinning avalanche foresets with topset preservation. These cosets overlay the *basal wedges*. The architecture of hydraulic jump deposits, where preserved, provides diagnostic criteria to condition the 3D geological modelling of some important reservoirs for groundwater and hydrocarbons.

Contents

Symbols

A	Cross-sectional area of *channelised* flow
b	Channel width
C	Concentration of suspended sediment
d	The change in water surface height above a smooth channel floor-attached obstacle compared to water surface height not influenced by the obstacle
D_{50}	The fiftieth percentile of the grain size distribution
$\overline{D_{50}}\big|_x$	Cross-channel mean D_{50} of samples at the same streamwise location within the same sediment bed
$\overline{D_{50}}$	Mean D_{50} of samples in the same bed
E_{kw}	Kinetic energy of water
Fr	Froude number
Fr_{umax}	Maximum Froude number upstream of the hemisphere for a given series of runs
g	Acceleration due to gravity
h	Flow thickness
$\bar{h}$	Flow thickness half way along the streamwise length of the stoss face of a sediment bed feature
H	Height of the water surface above the flume floor
H	Vertical thickness of flow above the 'detached jet'
L	Development length for a parabolic velocity profile
L_j	Streamwise length of a hydraulic jump
P	Pressure
Q	Volume discharge of water and sediment
Q_{sd}	Volume of sand added to a deposit
r	Radius of hemisphere
Re	Reynolds number
S	Channel floor slope
s_t	Distance along-transect
t	Time from the start of an experimental run
Tke	Turbulent kinetic energy
u	Streamwise velocity component
$\bar{u}$	Time-averaged streamwise velocity
$\bar{u}_{max}$	Maximum value of time-averaged streamwise velocity within an upward profile
u_j	Streamwise velocity of the motion of a hydraulic jump
u'	Instantaneous deviation from mean streamwise velocity
U	Depth-averaged streamwise velocity
v	Cross-stream velocity component
w	Velocity component normal to the flume floor
w'	Instantaneous deviation from mean vertical velocity
x	Streamwise coordinate
y	Stream transverse coordinate
z	Coordinate perpendicular to the flume floor
Z_{Umax}	Value of z at which streamwise velocity maximum occurs

Δx_{hj}	Streamwise displacement of the hydraulic jump location
Γ	Height of an obstacle above the channel floor
θ	Relative slope of a deposit and a water surface
λ	Water wave length
μ	Dynamic viscosity
ρ	Fluid density
τ	Shear
τ_{zx}	Reynolds shear
§	Section

Appendages to the symbols

$\square$	A symbol listed above (with no appendage)
$\square_A$	upstream of a lateral constriction of the flow
$\square_B$	within a lateral constriction of the flow
$\square_b$	above the brink of a sediment feature
$\square_d$	downstream of a hemisphere
$\square_s$	of supercritical flow
$\square_u$	upstream of a hemisphere
$\square_1$	immediately upstream of the hydraulic jump
$\square_2$	immediately downstream of the hydraulic jump
$\square = O(\ )$	is equal to the order of the quantity in the bracket
$\square\big|_{x=nm}$	evaluated at $x = n$ m

List of Figures

List of Tables

for Caroline
because I love you

1. Introduction to the thesis

1.1 RATIONALE FOR STUDYING HYDRAULIC JUMPS

A hydraulic jump is a wave with a stationary mean position and an increase in flow depth from upstream to downstream (Fig. 1.1). As flow passes through a hydraulic jump a lot of kinetic energy is transformed to gravitational potential energy, heat and sound (Paterson, 1983 p. 377 - 380). You will be able to hear most hydraulic jumps in rivers when walking past them along the riverbank. Hydraulic jumps are also eye catching in rivers because they entrain air into the flow via a complex system of breaking at their surface, causing the flow to appear white. They add to the excitement of white water rafting (Fig. 1.2) and canoeing but can be dangerous to recreational users of rivers. People have been dragged under hydraulic jumps and drowned (Taggart *et al.*, 1984).
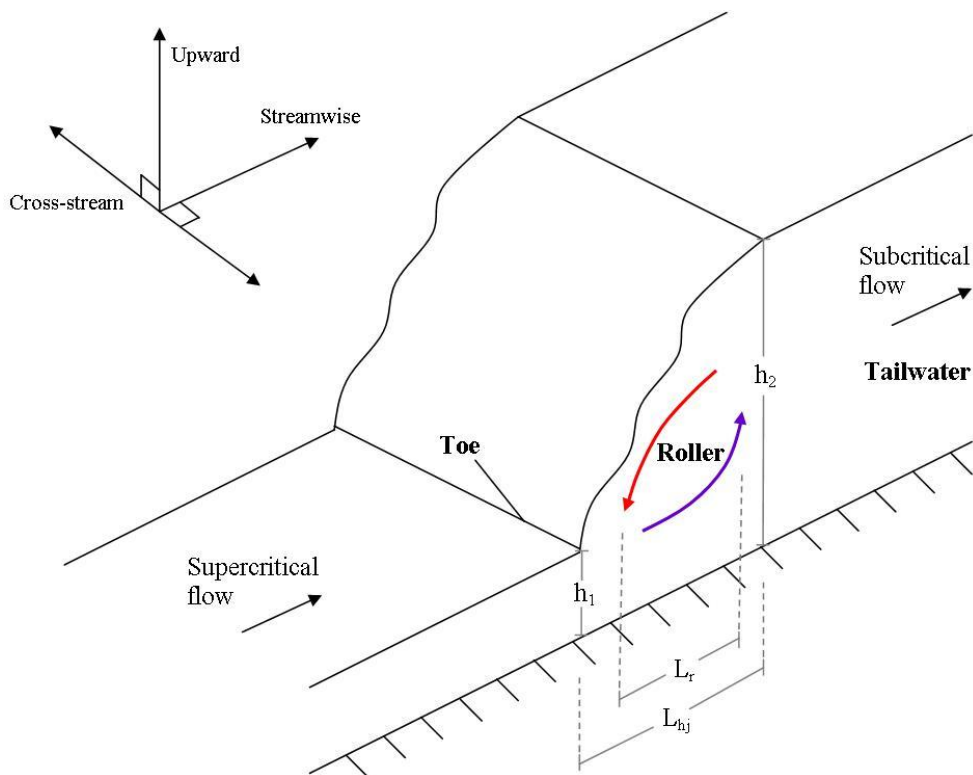
Figure 1.1 Perspective line drawing of a cylindrical supercritical flow, hydraulic jump and tailwater above an impermeable floor. The toe is the upstream limit of the hydraulic jump. The length of the hydraulic jump, L_{hj} is the streamwise distance between the toe and the highest point of the hydraulic jump. The roller is a recirculation of flow within the hydraulic jump; sense of rotation is indicated by the curved arrows. The length of the roller, *Lr* is shorter than the length of the hydraulic jump. The arrows in the top left corner indicate the upward, streamwise and cross-stream directions. The cross-stream and upward directions and the cross-stream and streamwise directions are perpendicular to each other. The upward and streamwise directions are only perpendicular where the channel floor is horizontal.

Because most hydraulic jumps entrain air they are a source of oxygen, influencing aquatic habitats. The amount of oxygen brought into the flow generally increases with the size of a hydraulic jump. In consequence, ecologists and river managers have used properties of hydraulic jumps to assess habitat for macrophytes, invertebrates and fish (Gregorian & Thorp, 1992; Kemp *et al.*, 2000) that thrive in water with high oxygen concentration downstream of hydraulic jumps. Fish and invertebrates spend some time in the hydraulic jump itself (Gregorian & Thorp, 1992) and use them as an aid to ascend waterfalls (Kim, 2001). Hydraulic jumps should be a concern to ecologists and river managers when planning engineering works that fish would have to ascend or descend.

Figure 1.2 White water rafters making impact with a hydraulic jump immediately downstream of emergent boulders which acted as a lateral constriction to flow on the river Treweryn, Wales. Photograph downloaded from Wikipedia on 30 January 2010. Photograph has been released into the public domain by an unknown photographer and has no copyright associated with it.

The deposition of sediment and the erosion of sediment and bedrock associated with hydraulic jumps are concerns to river managers and engineers. Large pressure fluctuations associated with hydraulic jumps can generate uplift forces that weaken joint seals in engineered structures leading to severe damage of the structures (Toso & Bowers, 1988). In

bedrock rivers the same uplift forces can remove bedrock blocks from the channel floor (a process called hydraulic plucking; Whipple *et al.*, 2000). A variety of channel floor materials can be eroded by hydraulic jumps (Annandale, 1995), affecting channel capacity and flood risk. Although sediment is transported by hydraulic jumps and can deposit downstream of them (Jopling & Richardson, 1966; Martini, 1977; Seidl *et al.*, 1994; Carling, 1995), patterns of sediment transport and deposition associated with hydraulic jumps have received little attention. Sediment transport at hydraulic jumps can affect the transport of pollutants in floodwaters (including sediment transported into buildings). Accumulating sediment will be preserved in the rock record if not subsequently eroded. The signature that a hydraulic jump leaves in rock could be economically important because hydraulic jumps form in environments in which large volumes of sediment are deposited and ancient deposits of these types may contain valuable groundwater or oil resources. Hydraulic jumps can also occur in environments in which placer deposits form e.g. beaches (hydraulic jumps can occur in backwash) and mineral bearing rivers and the processes of sediment movement associated with them may concentrate minerals.

This thesis is concerned with flow patterns in hydraulic jumps and patterns of sediment transport and deposition associated with hydraulic jumps. The few investigations into sediment transport at hydraulic jumps have used a variety of approaches. Using an experimental approach, Jopling and Richardson (1966) showed how a deposit feature called *backset bedding* can form downstream of a hydraulic jump at the upstream limit of a bed feature (to form *backset beds* an upstream-dipping upstream sediment front moves upstream with time). Using computational models of sediment transport at a hydraulic jump, Savery and Zech (2007) and Goutiere *et al.* (2008) showed how sediment bodies downstream of hydraulic jumps can have downstream-dipping downstream fronts that move downstream with time. Using a numerical modelling approach, Needham and Hey (1991) replicated both upstream and downstream progradation, separately.

There is still a long way to go to understand sediment transport and deposition at hydraulic jumps. Ultimately this thesis is concerned with finding sediment patterns of hydraulic jumps that can be recognised in rocks. In general, signatures of depositional events involve patterns of laminae, grain fabric or grain size within a deposit architecture. To form a deposit from which signatures can be deduced, one of the approaches that have already

produced bed features (experimental, computational and numerical approach) can be modified. I chose the experimental approach because I think a lot can be achieved by direct observation. I also think a lot more basic work needs doing on hydraulic jumps before numerical and computational models can suitably replicate the physical processes involved in sediment transport. It is advantageous to use flume channels with transparent sidewalls to simulate hydraulic jumps within river flows, because direct observation of flow patterns and sediment transport patterns may be made below the water surface. Whilst experiments have problems of scaling and space limitation, they are a good first way to study sediment depositional patterns at hydraulic jumps. In order to devise experiments on hydraulic jumps that could have occurred in ancient rivers I first studied the character of hydraulic jumps in modern rivers.

1.1.1 Rationale for selecting rivers as the context for the study

Although *hydraulic* means *of liquids in motion*, waves equivalent to hydraulic jumps can form in air flows (colloquially termed hydraulic jumps, Kuettner, 1959; Hertenstein & Kuettner, 2005) and loose granular flows (termed shock waves, Savage, 1979; Gray *et al.*, 2003). Hydraulic jumps are involved in a diverse range of liquid flows in nature; too many to consider in one Ph.D. They occur in unchannelised deep-water turbidity currents (Menard, 1964), volcanic surges (Schmincke *et al.*, 1973), freshwater flash-floods (Karcz, 1972), marine flows over obstacles such as fjord sills (Long, 1954; Gargett, 1976) and freshwater flows over obstacles such as transverse boulder ribs (Valle & Pasternack, 2006). Hydraulic jumps formed in turbidity currents can rapidly decrease the density of the current (Waltham, 2004). In this investigation fresh water flows through subaerial open channels were studied directly both in natural and laboratory settings. Hydraulic jumps in open channel flows are common in natural settings and are easy to produce and control in flumes. The air that open channel flows entrain does not generally affect flow behaviour to the same degree as air entrained into volcanic surges or water entrained into submarine flows. Open channel flows provide a good first way to investigate natural sediment transport and depositional process in hydraulic jumps.

1.2 AIMS

The aims of my Ph.D research were to:

1. Increase knowledge of the character of flow through hydraulic jumps.
2. Increase knowledge and understanding of sediment transport processes that occur in association with hydraulic jumps.
3. Investigate depositional patterns formed in association with hydraulic jumps and consider their preservability in natural open channel environments.
4. Develop personal knowledge and skills in sedimentology.

1.3 OBJECTIVES

The objectives of my Ph.D research were to:

1. Observe hydraulic jumps in rivers and document (A) the range of forms they have, (B) how long individual hydraulic jumps exist and (C) situations in which hydraulic jumps are stationary and when they are not. Focus on British rivers in a range of environments including steep upland rivers with coarse sediment load and lowland rivers with gentler gradient and finer sediment load.
2. Record velocity, vorticity and sediment transport patterns within selected hydraulic jumps in rivers.
3. Create hydraulic jumps in a flume channel with the same forms as the hydraulic jumps that were selected for study during the river work. Adjust the flume pumping rate, water volume and channel slope until the hydraulic jumps are formed repeatably.
4. Record the patterns of the water surface and flow velocity in the hydraulic jumps in the flume.
5. Devise and conduct experiments to examine how sediment is transported to a hydraulic jump and how sediment deposits build up under hydraulic jumps. Monitor sediment transport patterns, bed topography and deposit character using established methods (e.g. Bridge & Best, 1997; Leclair *et al.*, 1997; Alexander *et al.*, 2001).
6. Document the character of the resulting deposits (patterns of lamination, grain size, grain sorting etc.) and relate them to the flow and sediment movement patterns that

formed them. Assess the sedimentary structure of the deposits to detect the signature that a hydraulic jump leaves in the deposit.

7. Define reliable criteria, if they exist, to recognise hydraulic jump deposits in the rock record. Compare the deposit architecture formed by hydraulic jumps in flume experiments with features in the rock record that may have been made by hydraulic jumps, to test the value of the diagnostic criteria.

8. Assess the preservation potential of deposits containing the signature of a hydraulic jump.

1.4 THEORETICAL DESCRIPTION OF HYDRAULIC JUMPS

Flow thickness, velocity and kinetic energy of hydraulic jumps in open channels are governed by a set of equations. Patterns of water surface shape, velocity, vorticity, turbulent characteristics and energy transformations of hydraulic jumps in open channels can be described by physical reasoning. Using the equations and physical reasoning presented below, I manipulated hydraulic jumps in a flume to optimise the experimental designs used to achieve some of my objectives. Specific experimental designs are presented in Chapters 2 – 5. Flows in closed channels may be pressurised and consequently governed by different sets of equations to open channel flows. Closed channels are not considered any further in this thesis.

1.4.1 The Froude number

The Froude number, Fr is the ratio of flow velocity and surface wave velocity:

$$Fr = \frac{\bar{u}}{(gh)^2} \tag{1.1}$$

where $\bar{u}$ is the depth-averaged and time-averaged streamwise velocity, g is gravitational acceleration and h is the flow thickness. The ratio, the right hand side of Equation 1.1, was originally published by Belanger (1828) in his revised numerical treatment of the hydraulic jump. The ratio was named in honour of William Froude after he introduced the same ratio for scale experiments of flow past ship hulls (Froude, 1872). Regardless of the presence or absence of a ship or other obstacle, flow is Froude-supercritical where the flow velocity is greater than the velocity of surface waves, Froude-critical where the two velocities are equal

and Froude-subcritical where the velocity of surface waves is greater. In this thesis, "Froude-" is dropped from these phrases, which are simply stated as supercritical, critical and subcritical.

The denominator of Belanger's ratio is the speed of a wave. Any disturbance to a supercritical flow that is manifest as a wave on the water surface passes downstream immediately on inception. Some disturbances stop passing downstream at the location that flow becomes critical and some pass downstream into the subcritical flow (location of critical flow considered in Section 1.5.2). Hydraulic jumps are the waves that are formed by the disturbances located around the position of critical flow. Waves moving upstream in the subcritical flow cannot move beyond the hydraulic jump.

Froude number on smooth sloping channels

A floor is described as being smooth where friction, drag and other retarding forces are negligible compared to accelerating forces. Flow over a smooth floor that slopes downward from upstream to downstream accelerates down the slope under gravity. From upstream to downstream along the slope flow increases in streamwise velocity and becomes thinner (it must do to conserve volume flux). Because velocity increases and flow thickness decreases down slope, the Froude number increases down slope. In this way flow can gradually transform from subcritical to supercritical down a smooth slope. The change in *Fr* with distance down slope is constant on a constant smooth slope (cf. Fig. 1.3A). It increases with
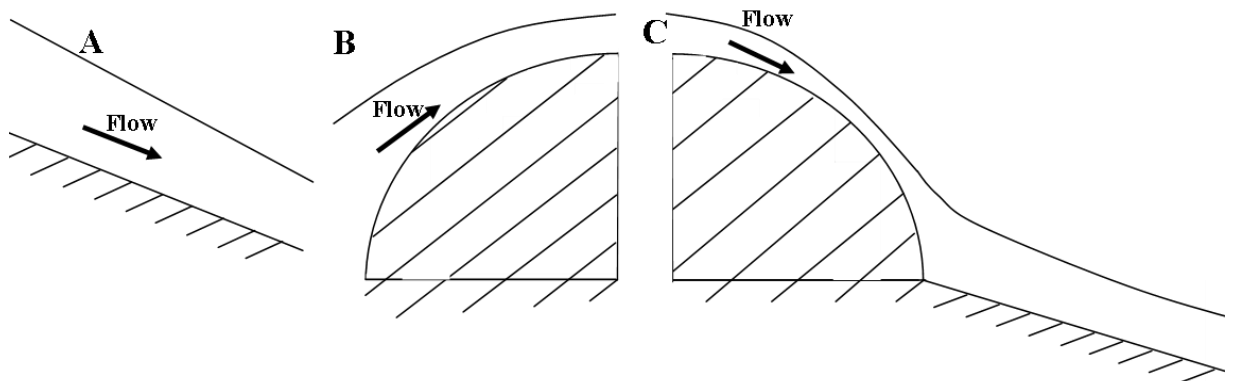
Figure 1.3 Line drawings depicting water surface shapes over sloping channel floors; (A) channel floor with constant slope. The Froude number of the flow increases constantly with distance down slope as flow thickness decreases and streamwise velocity increases. (B) Gradient of slope decreases from upstream to downstream along the slope. The Froude number of the flow increases with distance up slope as flow thickness decreases and streamwise velocity increases. (C) Gradient of slope increases from upstream to downstream along the curved part of the slope. The Froude number of the flow increases with distance down the curved part of the slope as flow thickness decreases and streamwise velocity increases. The Froude number of the flow increases constantly with distance down slope along the constant part of the slope.

7

distance downstream where slope gradient decreases with distance downstream (cf. Fig. 1.3B) and decreases with distance downstream where slope gradient increases with distance downstream (cf. flow over the curved slope in Fig. 1.3C). Supercritical flows can occur on horizontal floors (floors with zero slope) if flow travels supercritically onto the floor, but because *Fr* does not increase over a horizontal slope a transition from subcritical to supercritical cannot occur without external forcing. One common example of a hydraulic jump on a horizontal floor is the ring of curling overturning flow that forms when water from a tap runs onto the floor of a sink (Fig. 1.4).
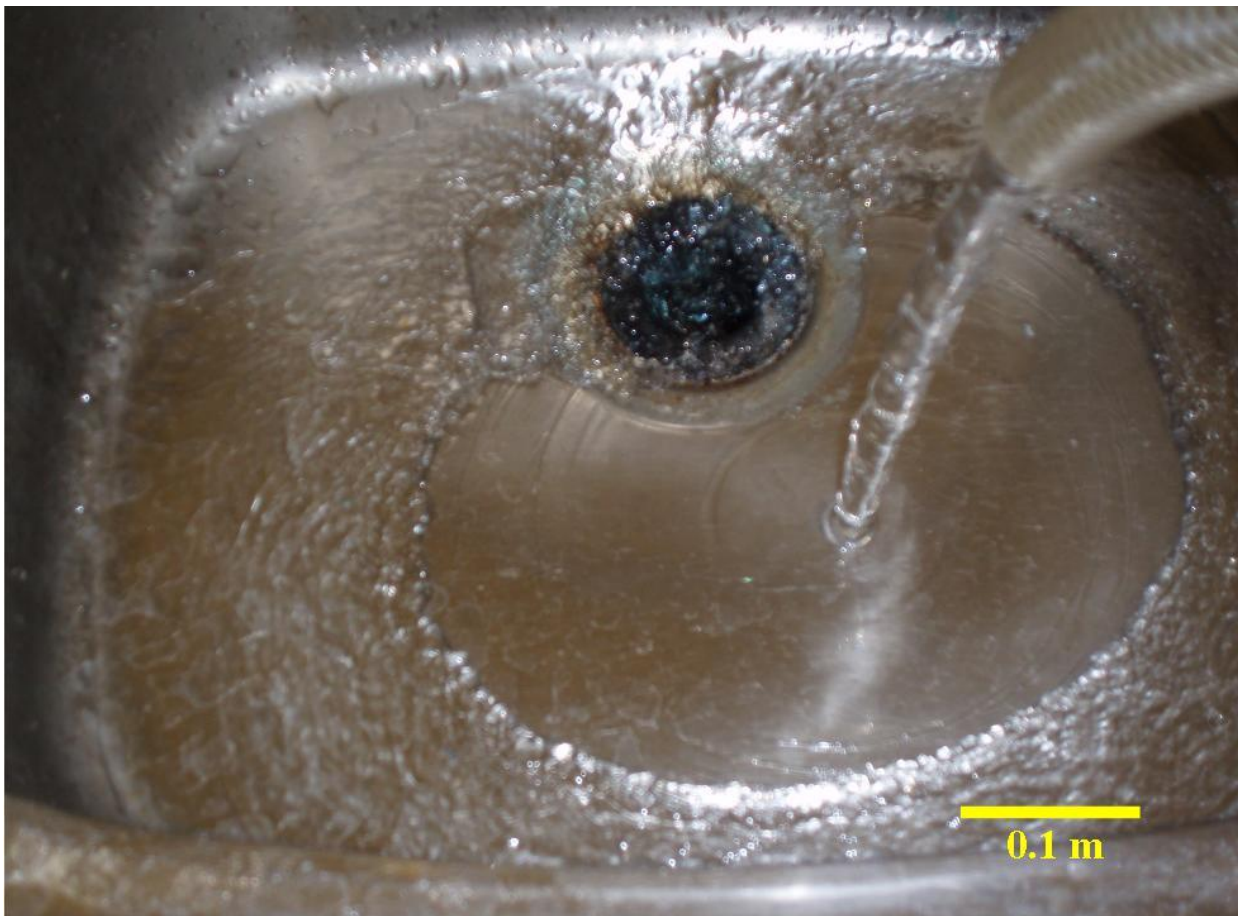
Figure 1.4 Supercritical flow and a hydraulic jump in a sink with an approximately horizontal, impermeable floor. The supercritical flow radiates from the impingement point of the water falling vertically from the hose (top right corner of the photograph).

Using the Froude number to calculate subcritical flow properties from supercritical flow properties

Every supercritical flow and subcritical flow has particular values of flow thickness and velocity that can be measured and a particular value of the Froude number that can be calculated (Eqn. 1.1). When designing experiments I used Equations 1.1 – 1.3 to calculate properties of hydraulic jumps because I wanted to form hydraulic jumps that matched hydraulic jumps in rivers, the properties of which have limited ranges (§1.6).

For a hydraulic jump in a flume or river, if any two variables in Equation 1.1 (flow thickness, flow velocity and Froude number) are known or designed, the other property can be calculated. With the thickness and Froude number of the supercritical flow known, Belanger's (1828) equation allows the depth of flow at the downstream limit of a hydraulic jump, h_2 to be calculated:

$$\frac{h_2}{h_1} = 0.5\left(-1 + \sqrt{1 + 8Fr_1^2}\right) \tag{1.2}$$

where subscripts 1 and 2 denote immediately upstream and downstream of the hydraulic jump. Next, derived from Bernoulli's equations of motion, popular hydraulics texts show that:

$$Fr_2^2 = \frac{(h_1 + h_2)h_1}{2h_2^2} \tag{1.3}$$

See e.g. Paterson (1983, p. 379) for derivations. Using Equation 1.3 Fr_2 can be calculated because h_1 and h_2 are already known (via Equations 1.1 and 1.2). Finally u_2 can be calculated using Equation 1.1.

Commensurate with Paterson's (1983) derivations for Equation 1.3, the equation

$$Fr_1^2 = \frac{(h_1 + h_2)h_2}{2h_1^2} \tag{1.4}$$

can also be derived. Replacing Equation 1.3 with Equation 1.4 and with some rearranging, the set of calculations presented above can be used to determine the properties of supercritical flow provided that two of the variables of Equation 1.1 are known for the subcritical flow.

1.4.2 The anatomy of hydraulic jumps

The upstream limit of a hydraulic jump is called the toe (Fig. 1.1; Hager & Bremen, 1989). Water thickens from the toe to the downstream limit of the hydraulic jump. The streamwise position of h_2 is the upstream limit of the tailwater downstream of the hydraulic jump. The length of the tailwater depends on the reach flow conditions. Between the toe and the tailwater the water surface generally increases in height and in association hydrostatic pressure increases. Because the thickening of water from the toe to the downstream limit of a hydraulic jump can be predicted from Equation 1.2, the increase in height of the water surface over the same region can be predicted. For a known fixed h_1, h_2 increases linearly with Fr_1. If Fr_1 increases from 1 to 4, h_2 increases from $1h_1$ to $5.2h_1$.

The water near the upper surface of most hydraulic jumps travels down slope towards the toe (from downstream to upstream, red arrow, Fig. 1.1) under the hydrostatic pressure gradient. Water at the toe travels downstream because of the drag associated with the supercritical flow as it enters the hydraulic jump (purple arrow, Fig. 1.1). In this way a recirculation occurs in the hydraulic jump, termed the roller (Darcy & Bazin, 1865; Bakhmeteff & Matzke, 1936). A shear layer between the roller and the downstream travelling flow below it, extends almost horizontally from the toe (Hornung *et al.*, 1995; Fig. 1.1). The velocity structure in a hydraulic jump with a roller can be seen clearly in Figure 2 of Hager and Bremen (1989). Where Fr_1 is not far above 1 the slope of the upper surface of the hydraulic jump has a shallow gradient. All water within the hydraulic jump flows downstream because the drag of the supercritical flow is greater than the force of gravity in the direction of the hydrostatic pressure gradient everywhere in the hydraulic jump. The velocity structure in a hydraulic jump without a roller can be seen clearly in Figure 7 of Lennon and Hill (2006). Binney and Orkney (1955) and Chanson (1995) determined that rollers occur in hydraulic jumps with $Fr_1 > 1.76$ and $Fr_1 > 1.5$ respectively. By trial and error and using Equations 1.1 – 1.4, I designed flume experiments with hydraulic jumps with and without rollers (Chapters 2 – 5).

1.4.3 Designing the position of a hydraulic jump in a channel

Where neither Fr nor the shape of the channel floor varies with time, the disturbance pattern of the flow does not vary either and the hydraulic jump has a stationary mean position. The

position of the hydraulic jump oscillates upstream and downstream constantly around the stationary mean position because at any time three forces are unlikely to be in balance: (1) Gravity acting in the same direction as the hydrostatic pressure gradient. (2) Frictional drag of the supercritical flow as it passes underneath the hydraulic jump, opposing the hydrostatic pressure gradient. (3) Forces associated with the disturbance pattern of waves moving upstream towards the hydraulic jump. In most open channel flows the oscillation has a constantly varying amplitude and period because flows are unsteady and so the disturbance pattern is unsteady.

The mean position of a hydraulic jump in a channel can be manipulated by making changes to the flow or the channel conditions. If Fr_1 is caused to increase (by decreasing h_1 or increasing u_1, Eqn. 1.1) the hydraulic jump will move downstream. If Fr_1 is caused to decrease (by increasing h_1 or decreasing u_1, Eqn. 1.1) the hydraulic jump will move upstream. To design the position of the hydraulic jumps in my flume experiments I varied h_1 and u_1 by varying slope and discharge (Chapters 2, 4 and 5). Whilst h_1 and u_1 have also been successfully controlled using undershot sluice gates (e.g. Rajaratnam, 1965; Hager *et al.*, 1990; Imai & Nakagawa, 1995) I chose not to use one because they may impart patterns in the flow that did not occur in ancient rivers.

The oscillating character of a hydraulic jump can be manipulated by making the flow more or less steady. I monitored the steadiness of the pumping rate by observing a time series of discharge. I monitored the steadiness of the flow by recording time series of velocity data over longer periods than the turbulent fluctuation.

If an obstacle is placed a short distance downstream of a hydraulic jump, the hydraulic jump will move upstream. The presence of an obstacle a short distance downstream of a hydraulic jump instantaneously increases h_2 above the value specified by Equation 1.2. A consequence of the increase in h_2 is that the hydraulic jump moves upstream, because of gravity, and a new time-averaged balance of forces (1) $-$ (3) is established. Both the disturbance pattern within the hydraulic jump and the value of Fr_1 may change. If that same obstacle is removed the original condition will re-establish. The streamwise displacement of the hydraulic jump location, Δx_{hj} is given by

$$\Delta x_{hj} = \frac{\Delta(h_2 - h_1)}{S} \tag{1.5}$$

(Bradley & Peterka, 1957) where S is the dimensionless channel floor slope and $\Delta(h_2 - h_1)$ is the change in magnitude of the difference in height from upstream to downstream of the hydraulic jump, in this case between the times before and immediately after the arrival or removal of an obstacle in the tailwater. I used overshot weirs as obstacles downstream of a hydraulic jump to optimise the hydraulic jump position in a flume. I chose not to manipulate the position of the hydraulic jump by changing the roughness of the flume floor and chose not to use a break in slope. In this way the deposits would be controlled by the flow and not the channel topography.

Water surface shape above obstacles under subcritical and supercritical flow

In situations where subcritical or supercritical flow passes over a bed-attached obstacle that makes a smooth contact with the channel floor, the water surface height changes above the obstacle compared to flow upstream and downstream of the obstacle, by a factor

$$d(x) = \frac{\Gamma(x)}{\dfrac{1}{Fr_u^2} - 1} \qquad (1.6)$$

where Fr_u is the spatially averaged Froude number upstream of the obstacle and Γ is the height of the obstacle above the channel floor (Fig. 1.5). The sign of $d(x)$ is positive when flow is supercritical and negative when flow is subcritical: The water surface height is higher above the obstacle than elsewhere where flow is supercritical, and is lower above the obstacle than elsewhere when flow is subcritical. This is relevant to the design and understanding of experiments involving subcritical or supercritical flow over isolated bed-attached obstacles (Chapter 3). It is also relevant for a thought experiment in discussion in Chapter 6.

1.4.4 Turbulence properties of hydraulic jumps in rivers

Parameters used to describe general turbulent properties of a flow

The Reynolds number, Re is the ratio of inertial to viscous forces, first published by Stokes (1851) and popularised by Reynolds (1883). Considering depth-averaged properties of a flow,

$$Re = \frac{\rho u h}{\mu} \qquad (1.7)$$

where ρ is water density and μ the dynamic viscosity. In laminar flow the velocity pattern of the flow does not vary unless the flow is accelerated. In turbulent flow in the Reynolds description of turbulence, time variations of the velocity pattern occur everywhere in the flow without the flow being accelerated, and *Re* is generally higher than in laminar flow. As *Re* increases, bursts, sweeps, vortices and other small scale components of a flow become more prevalent. Although the values of *Re* are a bit arbitrary when defining a threshold for turbulent flow they suffice as an order of magnitude guide of the general turbulent state and I use them for no more than a general description of turbulence in this thesis.
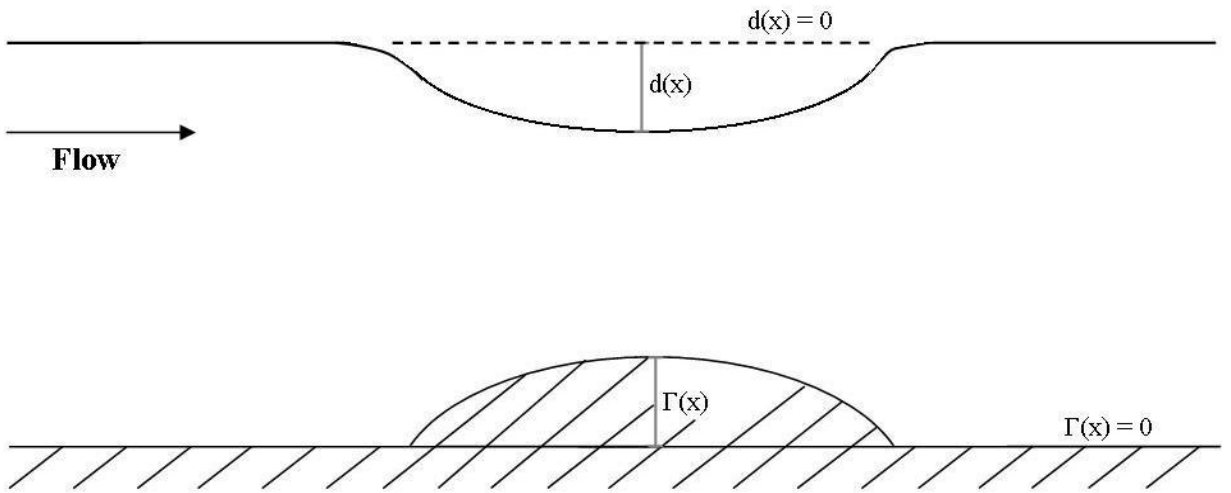
Figure 1.5 Flow over a smooth obstacle that makes a smooth contact with the channel floor. The upper surface of the obstacle has a height $\Gamma(x)$ above the channel floor and the water surface above the obstacle is dipped by factor $d(x)$ compared to the flow further upstream and further downstream.

In the *x-z* plane, turbulent kinetic energy per unit mass, *Tke* is the kinetic energy of flowing fluid that is associated with the small scale components of the flow:

$$Tke = \frac{1}{2}\left(\overline{u'^2 + w'^2}\right)$$
(1.8)

where *u'* and *w'* are deviations from the time-averaged velocity components. It is used as a general description of the energy associated with flow that is already known to be turbulent. As a flow becomes more turbulent, both *Tke* and the size and prevalence of coherent rotating structures increase.

Reynolds shear per unit mass is expressed as

$$\tau_{zx} = -\overline{u'w'}$$
(1.9)

for incompressible Newtonian fluids. Localised viscous stresses within the flow are expressed by the velocity deviations, mathematically described in the turbulent acceleration term of the Navier-Stokes equations: the gradient of τ_{zx} accelerates the local fluid. As a flow becomes more turbulent both Reynolds shear and the number and magnitude of instantaneous deviations from mean velocity increase.

Designing the general turbulent character of experimental hydraulic jumps

In most modern rivers the inertial forces of depth-averaged water flow are greater than viscous forces by at least four orders of magnitude ($Re > 10^4$, Equation 1.7) and small scale components of the flow are prevalent. River flows may be described as fully turbulent in the Reynolds description of turbulence. I designed my experimental flows to have $Re > 10^4$.

Scale of turbulence in hydraulic jumps

Flow thickness determines the largest spatial scale of patterns in the time variation of the velocity pattern of the flow (Fiorotto & Rinaldo, 1992). Because subcritical flow downstream of a hydraulic jump is generally thicker than the supercritical flow upstream of the same hydraulic jump, the largest spatial scale of turbulence in that subcritical flow is larger than the largest spatial scale of turbulence in the supercritical flow. Consequently discrete turbulent structures such as vortices are likely to be smaller in supercritical flow than subcritical flow.

1.4.5 Energy transformations within hydraulic jumps

As water flows from upstream to downstream of any hydraulic jump, some of its kinetic energy (including turbulent kinetic energy) is transformed to gravitational potential energy, sound and heat. Where air or sediment is present within the flow, some of the kinetic energy of the water may be transformed to kinetic or gravitational potential energy of the air or sediment. Some of the kinetic energy of the sediment load may be transformed to kinetic energy of the water. Considering hydraulic jumps containing water only, it can be shown that the rate of loss of kinetic energy is

$$\frac{\Delta E_{kw}}{\Delta t} = \frac{1}{4} \rho \overline{u_1} g \frac{(h_1 - h_2)^3}{h_2} \qquad (1.10)$$

joules per unit time, moving with the water (cf. Patterson, 1983, p. 379), where t is time and E_{kw} is the kinetic energy of the water.

1.5 CHARACTERISTICS OF SUPERCRITICAL FLOWS IN OPEN CHANNELS

Because water, sediment and air transported to a hydraulic jump will have passed through the supercritical flow, the character of the supercritical flow is likely to affect the character of sediment transport and deposition at a hydraulic jump. I observed supercritical flows in more than thirty British rivers and read reports of observations of supercritical flows and data recorded from supercritical flows by other investigators of open channel flows. I assessed the range of shapes, positions, turbulent properties, prevalence and lifetime of supercritical flows. I used the range of observed supercritical flows in open channels to select characteristics to reproduce in experiments.

1.5.1 Most characteristics of supercritical flows are predicted by theory

In most respects supercritical flows in open channels are alike the supercritical flows over smooth floors in theory (§1.4.1). Regardless of the characteristics of the floor of a channel, all supercritical flows I observed in British rivers and read about in other settings had a hydraulic jump associated with them. Most supercritical flows were thinner than the water downstream of the hydraulic jump that was associated with it. The value of h in most supercritical flows generally decreased from up slope to down slope. All supercritical flows that I observed were less than 0.3 m thick and most were less than 0.2 m thick. In all supercritical flows I observed, coherent flow structures (expressions of the largest scales of turbulence) were too small to see. Bursts and sweeps must have occurred (§1.4.4) but at too small a scale to see. Where supercritical flow passed over a smooth undulation on a bedrock floor the water surface height rose over it.

Some characteristics of supercritical flow are not predicted by theory (§1.5.2 – 1.5.5). I observed the hydraulic jumps in the modern British rivers and read all the literature to (1) assess the spatial prevalence of supercritical flows and hydraulic jumps in modern natural open channel flows. (2) Assess how long individual stretches of supercritical flow persist for in modern open channel flows. These two assessments allowed me to optimise open channel

environments or paleo environments in which to look for hydraulic jump deposits (presented in Chapter 6). (3) Assess the range of shapes of supercritical flows in modern natural open channels. This allowed me to design experimental supercritical flows with shape characteristics that supercritical flows in ancient rivers might have had.

1.5.2 Mechanism of formation of supercritical open channel flows

Parts of river flows can become supercritical because the flow accelerates under gravity, when passing over smooth sloping planar floors (e.g. Kieffer, 1985; Fig. 1.6) and when passing over the downstream face of large roughness elements (e.g. Grant *et al.*, 1990; Fig. 1.7). Flows can become supercritical because they are made narrower by passing through a constriction. Flow can be constricted from many sides when passing into a slot (cf. Fig. 1.8). Flow can be constricted from above where undershot sluice gates are present in channels (cf. Rajaratnam, 1965; Fig. 1.9), from below by levees (e.g. Fildani *et al.*, 2006; Fig. 1.10) and from the sides by emergent obstacles or downstream-narrowing valley walls (e.g. Kieffer, 1985; Grant *et al.*, 1990; Figs 1.2 and 1.11). In the flume I used for the experiments I chose a high pumping rate
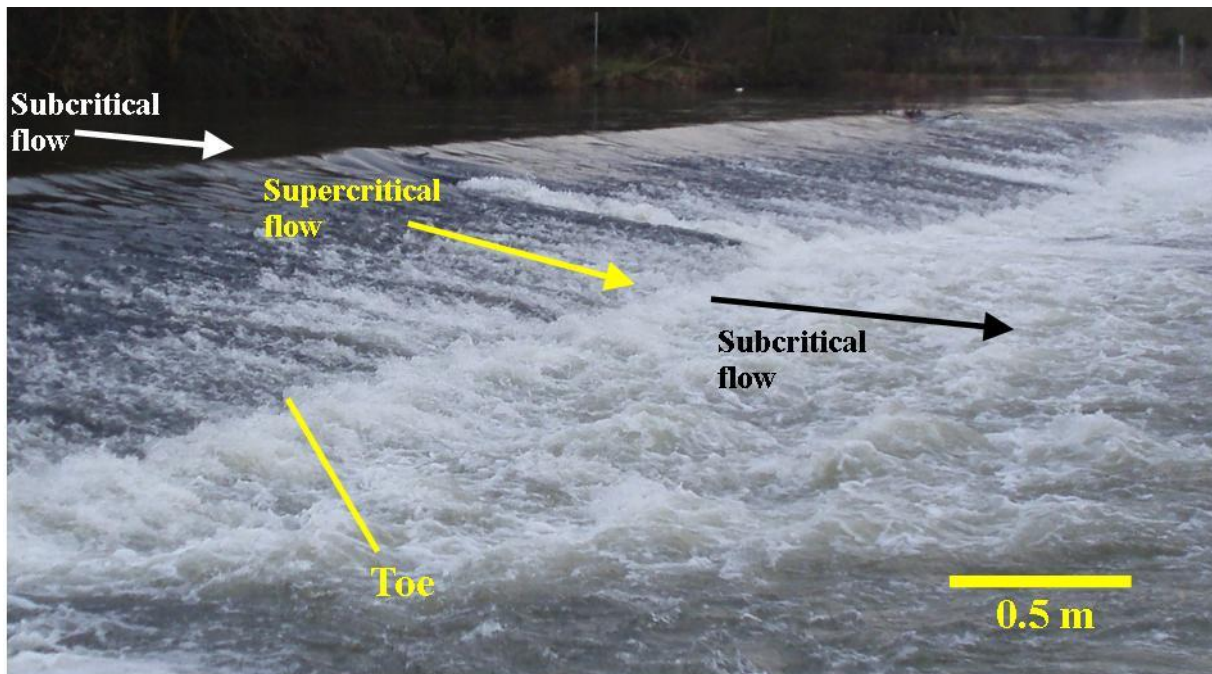
Figure 1.6 Flow becoming supercritical over a downstream dipping planar slope and passing through a hydraulic jump at a break in slope, Yearl weir, River Derwent, Cumbria, England photographed on 12 January 2008 at 16:19. The Froude-supercritical flow over the weir is breaking and is entraining air. Bed roughness elements on the surface of the weir were large compared to the flow depth.
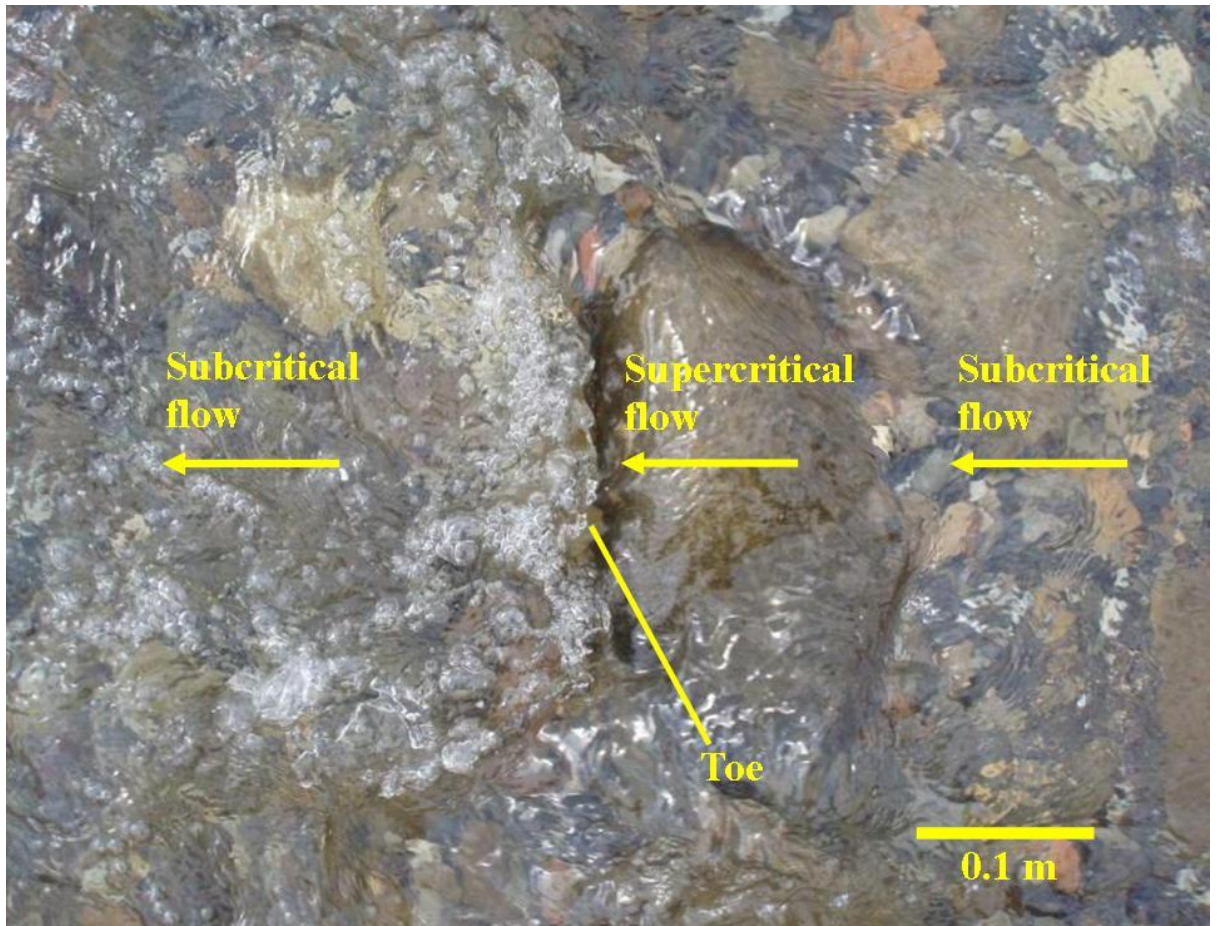
Figure 1.7 Flow becoming supercritical over a bed attached cobble and passing through a hydraulic jump immediately downstream of the cobble, Lowca Beck, Cumbria, England photographed on 18 April 2008 at 17:34.

to discharge water supercritically through a restricted pipe so that flow entered the open test channel supercritically.
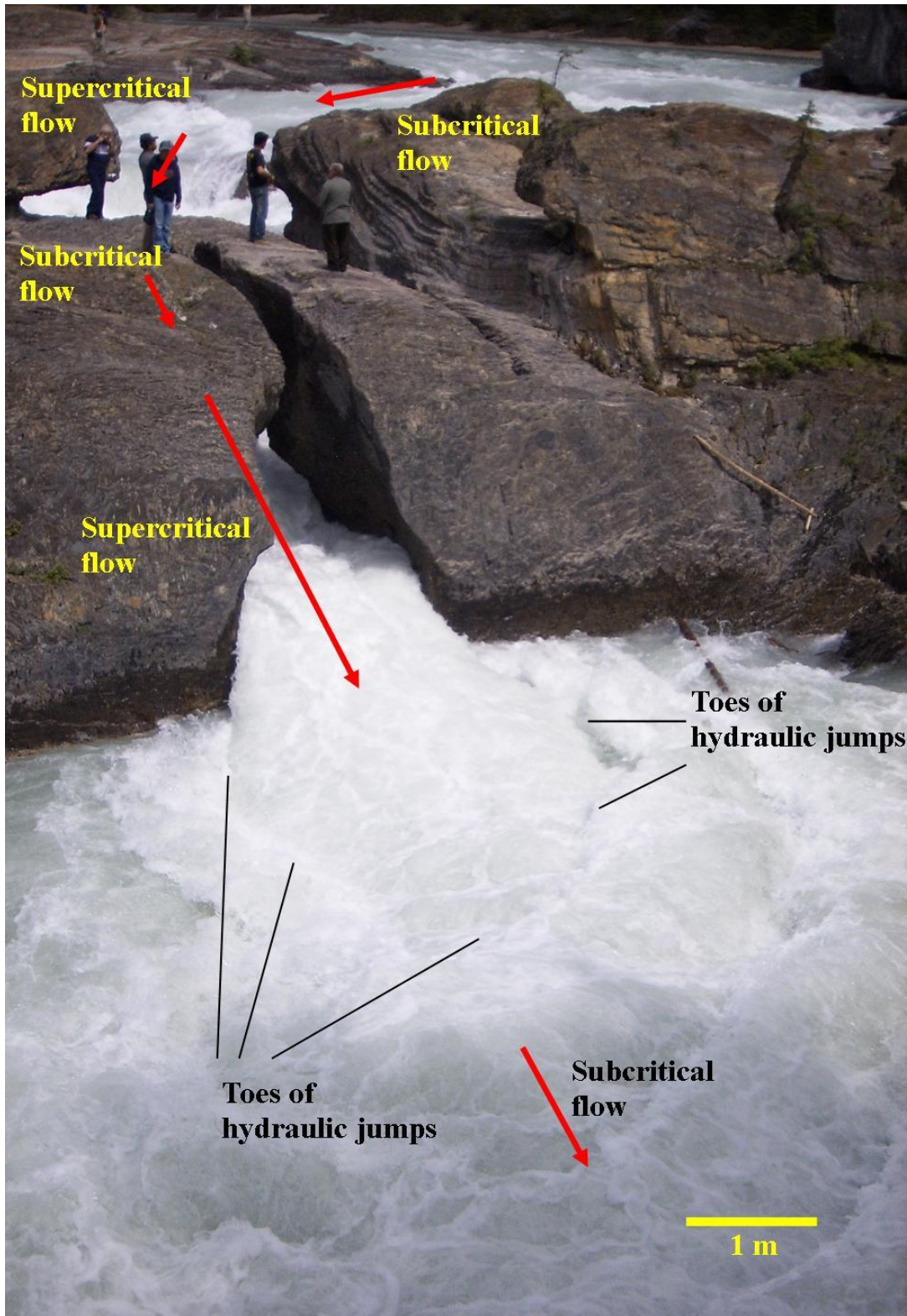
Figure 1.8 Flow becoming supercritical through a very narrow constriction. At the downstream limit of the supercritical flow I saw five hydraulic jumps (position of the toes of the hydraulic jumps indicated). Photograph taken on 12 June 2007 by Maurits van Dijk.

Figure 1.9 Flow becoming supercritical as it passes under an undershot sluice gate in an Armfield sediment demonstration flume. Reproduced with permission of Armfield.

Figure 1.10 Flow becoming supercritical as it passes over a levee of the Mississippi river. Photograph sourced from http://lassiegethelp.blogspot.com /2008/06/lawless-stream.html and has been released into the public domain.

Figure 1.11 Flow becoming supercritical through a lateral constriction. At the downstream limit of the supercritical flow I saw one hydraulic jump (position of the toe of the hydraulic jump indicated). Photograph courtesy of Lucy Clarke.

1.5.3 Spatial prevalence of supercritical flows in rivers

Supercritical flow can be absent from large stretches of most rivers because friction, drag and other retarding forces are equal to or greater than gravitational acceleration of the flow. However supercritical flow can be common in space (e.g. where shallow flow passes over many boulders, Fig. 1.12). Individual stretches of supercritical flow can be at least tens of metres long and wide (e.g. immediately downstream of abrupt lateral expansions, Fig. 1.8; glacial outburst reported by Cassidy *et al.*, 2003). Grant *et al*. (1990) assessed that supercritical flows and hydraulic jumps constitute up to 10% of flow over riffles and 15 - 50% of flow in rapids (as typical ranges of values).

Where flow travels over chutes and pools and cyclic steps, supercritical flows, hydraulic jumps and subcritical flows occur in a repeating streamwise sequence. Cyclic steps on steep hill slopes frequently repeat on the order of tens of centimetres to tens of metres (Fig. 1.13). In my flume experiments I chose to form a single stretch of supercritical flow over a floor-attached boulder in my experiment in Chapter 3. I chose to use a supercritical flow several metres long that spanned the channel width in my experiment in Chapters 4 and 5.

1.5.4 Time persistence of supercritical flows in rivers

Supercritical flows in rivers have a maximum possible lifetime equal to the length of time that a channel maintains its course, but most supercritical flows have shorter lifetimes because the Froude-state of flow is sensitive to discharge and local channel conditions. Supercritical flows in rivers with very variable discharge (e.g. the Burdekin river, Wohl, 1992; Alexander *et al.*, 1999) have a maximum possible lifetime equal to the duration of the flow. Flow being supercritical down a slope is sensitive to discharge decreasing because retarding forces have a greater combined effect, decreasing u and Fr. Flow being supercritical over an obstacle is sensitive to discharge increasing and decreasing. A decreasing flow stage associated with decreasing discharge can cause flow to cease travelling over an obstacle (where thin flow over the obstacle was supercritical) but continue to travel around the obstacle. If discharge increases, flow directly over the obstacle generally increases in thickness; decreasing Fr. Discharge varies constantly in all natural rivers. It is more likely that more hydraulic jumps will have shorter lifetimes the more variable discharge is.
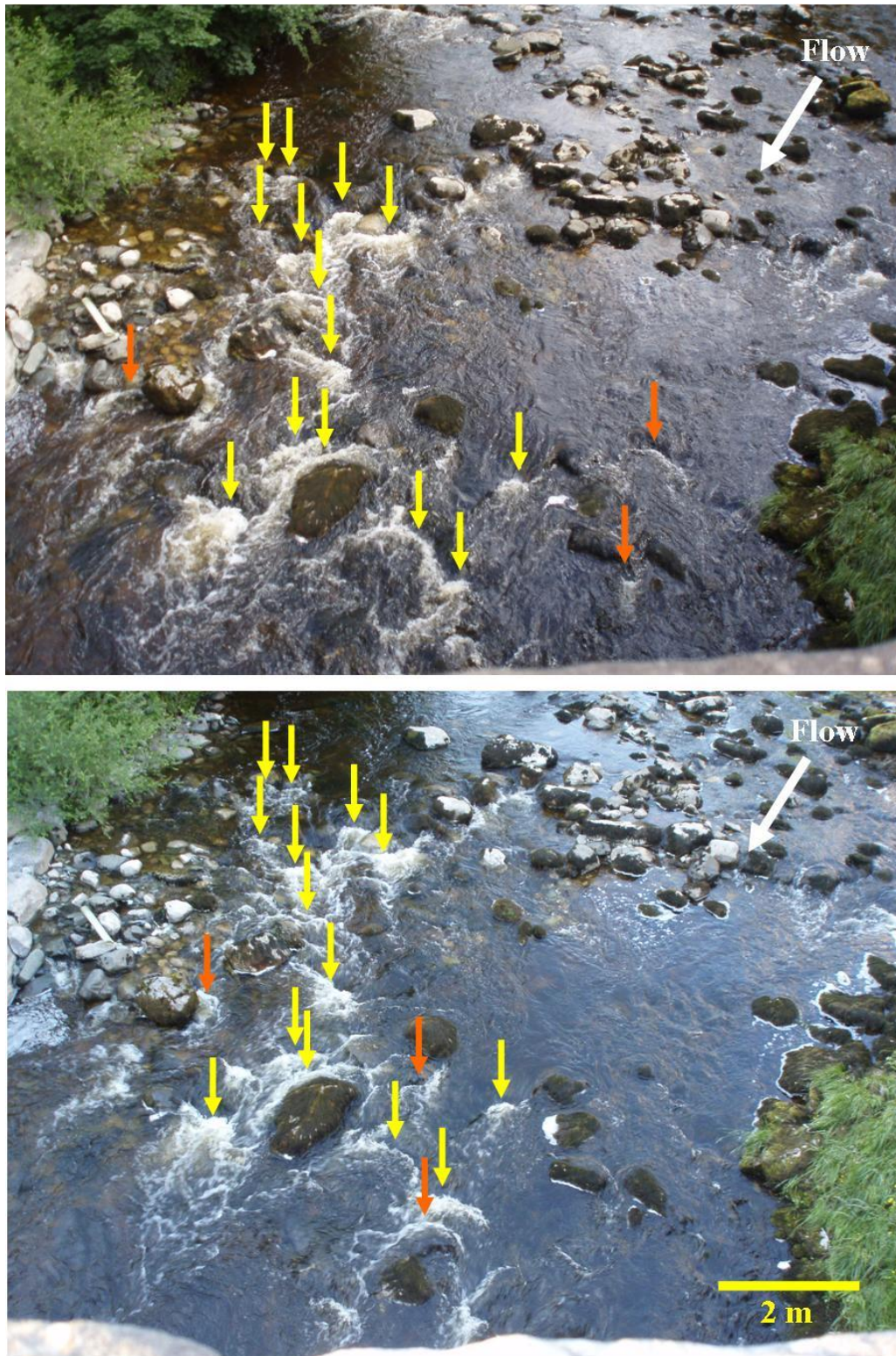
Figure 1.12 Photographs of the river Twiss, Lancashire, England taken on 20 June 2008 at (A) 12:43 hr, (B) 22:15 hr. Arrows indicate hydraulic jumps. Yellow arrows: Hydraulic jumps that appear in the same place within the river at both times. Orange arrows: Hydraulic jumps that appeared in the field of view at one time but not the other. Stage was approximately 0.1 m higher at 12:43 than at 22:15. At both times 17 hydraulic jumps were observed. The channel floor is predominantly cobbles and boulders.

Because changing discharge, sediment supply and vegetation can change channel boundary conditions over time, they have a long term effect on the potential for flow to become supercritical. Large flows can change the pattern of channel floor obstacles by eroding and redepositing sediment bed topography. Because the sediment transport pattern over chute and pools and cyclic steps varies with time (Alexander *et al.*, 2001) it can influence the character of supercritical flow and even cause it to switch on or shut down.

In my flume experiments I chose to set initial conditions (at time, $t \leq 0$) involving constant discharge and constant channel floor characteristics (involving no sediment transport) so that the hydraulic jump would persist in character before sediment was supplied to it. Having a steady system at the start of a run involving sediment made the effect of the supercritical flow and hydraulic jump on the sediment transport patterns easy to isolate.

Figure 1.13 Cyclic steps in a small degradational channel on a steep slope, Banff, Canada.

1.5.5 The shape of supercritical flows in rivers

Having designed the mechanisms by which supercritical flows would form in the experiments and designed that the supercritical flows would persist for a long time before sediment was allowed to influence the flow, I wanted to design the supercritical flows to have shapes similar to those that occur in modern rivers. I present a range of shape characteristics of supercritical flows that I have seen, or were presented by other authors, in **bold italic** type. My choices for further study are discussed in plain type.

Supercritical flows in rivers do not generally span the full width of the channel. In general the characteristics of river channel floors are not uniform across stream and some parts of channel floors are more prone to flow travelling supercritically over them than others are, for given ranges of discharge. I designed one experiment such that supercritical flows did not span the width of a flume in most runs (Chapter 3); a different setup to all experimental supercritical flows in flumes (or pipes) that I have come across in literature. The full width of natural narrow channels or subchannels can be supercritical (e.g. in slots or tunnels and at knickpoints in resistant bedrock) and I selected for supercritical flows to span the width of a flume in one experiment (Chapters 4 and 5).

Supercritical flows above smooth channel floor obstacles are themselves smooth. Equation 1.6, which predicts that flow over a smooth obstacle rises over the obstacle, was qualitatively satisfied by most supercritical flows that I observed over obstacles in river channels (e.g. Fig. 1.12). Equation 1.6 was only partially satisfied where supercritical flow travelled into a hole (an obstacle with negative topography, $\Gamma(x) < 0$). The water surface heights of the supercritical flows generally became lower from the top to the bottom of the upstream face of the hole, satisfying Equation 1.6 in that region, and then passed through a hydraulic jump (Fig. 1.14) causing Equation 1.6 to break down.
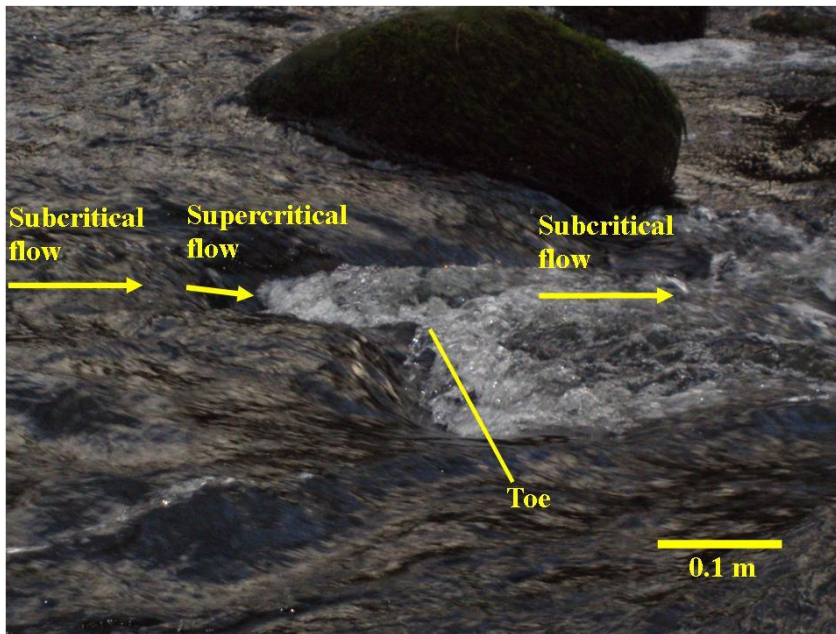
Figure 1.14 Supercritical flow passing through a hole in the floor of a channel and passing through a hydraulic jump at the bottom of the upstream face of the hole.

Supercritical flow generally changes in thickness along smooth slopes. As predicted by the physical reasoning in Section 1.4.1, supercritical flow generally becomes thinner down smooth slopes. This was designed into the experiments (Chapters 3 – 5). Where two smooth slopes make an abrupt contact with each other, supercritical flow can be thicker at the contact and thinner immediately upstream of the contact (e.g. Fig. 1.3C). Because an abrupt contact occurred between the smooth slopes of the obstacle and the flume floor in the experiment in Chapter 3, this characteristic was permitted in that experiment. It was not permitted in the initial condition of the experiment in Chapter 4 and 5 because there was only one slope (slope of the flume floor).

In general the more irregular the boundary conditions, the more complicated the water surface shape of a supercritical flow. Supercritical flows over smooth channel floors tend to have smooth upper surfaces and supercritical flows over flat smooth floors tend to be cylindrical (cf. Fig. 1.1). Surface breaking of supercritical flow can occur during passage over bed roughness elements that are large compared to the depth of flow (e.g. Fig. 1.6). Flow over densely packed large roughness elements invariably causes the water surface to have an intricate shape (Pagliara & Chiavaccini, 2006). Water surface breaking causes dissipation of the energy of supercritical flows (Pagliara and Chiavaccini, *loc. cit.*) and causes Equation 1.8 to break down. I decided to integrate a non-breaking surface into the supercritical flow in the experiments so that energy transformations might occur predictably.

Supercritical flow passing through a constriction can be thicker than subcritical flow downstream of the constriction. Where a channel has a lateral constriction, flow accelerates through the constriction (it must do to conserve the volume flux of water). If flow is subcritical upstream of the constriction, it can be transformed to supercritical through the constriction. Supercritical flow may be thinner, the same thickness or thicker than the subcritical flow upstream of it depending on the values of the Froude number upstream of the constriction, $Fr_A{}^2$ and the ratio of channel width upstream of and through the constriction, $\dfrac{b_A}{b_B}$

(conditions in which flow is thicker, the same thickness or thinner within the constriction than upstream of it, are derived in Appendix 1).

1.6 DOCUMENTATION OF HYDRAULIC JUMPS

I documented hydraulic jumps in more than thirty British rivers and read reports of observations of hydraulic jumps and data recorded from hydraulic jumps, by other investigators of open channel flows. I assessed the ranges of characteristics of flow through hydraulic jumps and the general prevalence of each characteristic. With the range of documented hydraulic jumps in open channels to hand I selected characteristics to reproduce in experiments.

Some characteristics of hydraulic jumps are alike in open channels and in theory. Most hydraulic jumps have one supercritical flow associated with them. Most do not occur periodically. Most hydraulic jumps generally thickened between their upstream limit and their downstream limit. I observed flows at the downstream limit of hydraulic jumps that were several centimetres thick, up to more than a metre thick. In general, hydraulic jumps associated with cylindrical supercritical flows were themselves cylindrical (cf. Fig. 1.1). The use of the word *cylindrical* is discussed in Section 1.9.2. The hydraulic jumps and the flow immediately downstream of them contained coherent turbulent structures, some of which were large compared to the flow depth and larger than the depth of the associated supercritical flow. Long *et al*. (1991) recorded video footage of hydraulic jumps in a flume with $Fr_1 = 4 - 9$ and $h_2 = 0.3$ m. Vortices formed approximately 0.2 m in diameter and had a cross stream axis of rotation. The height of the water surface of both hydraulic jump and tailwater was locally increased by the presence of vortices close to the water surface.

As was the case for supercritical flows, the spatial prevalence, time persistence and range of shapes of hydraulic jumps are not predicted by theory. I observed the hydraulic jumps in the modern British rivers and read literature on hydraulic jumps to assess these three attributes of hydraulic jumps in modern natural open channel flows. These assessments allowed me to design experimental hydraulic jumps with shape characteristics that hydraulic jumps in ancient open channel flows might have had (experiments presented in Chapters 3 – 5). The assessments also helped me to optimise open channel environments or paleo environments in which to look for hydraulic jump deposits (presented in Chapter 6).
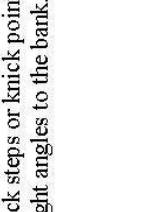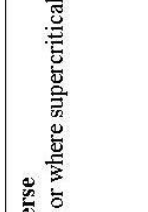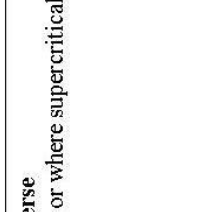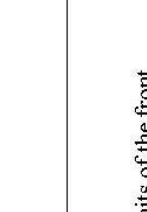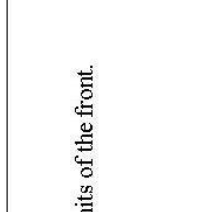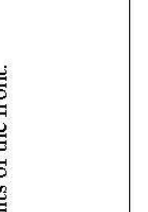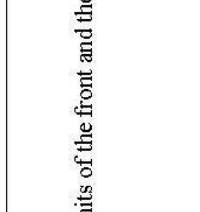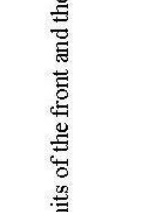
1.6.1 Position of formation of hydraulic jumps

All hydraulic jumps formed at positions that were associated with one or more topographic controls and the position varied with the Froude number of the supercritical flow (hence varied with discharge). All hydraulic jumps were seen in regions of significant flow deceleration (e.g. at a downstream transition from smooth to rough channel floor, at a break in slope gradient, at a position where flow abruptly widened from upstream to downstream or where an end wall of a flume, or an overshot weir slowed the flow). The mean position of a lot of hydraulic jumps that I watched did not change by more than the excursion of the oscillation of the toe because discharge did not vary significantly. In general though hydraulic jumps do move downstream with significant increases in discharge. For instance Kieffer (1985), Valle and Pasternack (2002) and Wyrick and Pasternack (2008) reported hydraulic jumps moving downstream by as much as several metres when flow increased above the mean annual flows of the Colorado river and the American river, California, USA.

1.6.2 Spatial prevalence of hydraulic jumps in rivers

Hydraulic jumps can be absent from large stretches of most rivers because flow does not become supercritical. Hydraulic jumps are common in space where supercritical flows are common in space (§1.5.2). Hydraulic jumps can also be common in space at the downstream limit of a single stretch of supercritical flow that passes downstream into an abrupt channel expansion (Fig. 1.8). The downstream limit of the supercritical flow, in the wider part of the channel, often has an arc shape in plan view with the apex of the arc pointing downstream and many hydraulic jumps, each with toes that are slightly curved in plan view, form around the arc. The hydraulic jumps are distinct from each other because their fronts are slightly offset upstream or downstream from each other.

In general hydraulic jumps that I observed had a smaller plan area than the supercritical flows I observed (e.g. Figs in Table 1.1). Downstream of the abrupt channel expansions where one supercritical flow produced many hydraulic jumps, the hydraulic jumps had a smaller combined plan area than the supercritical flow. I saw hydraulic jumps that were several centimetres long, up to several metres long (cm $\leq L_{hj} \leq$ m, Fig. 1.1; I had seen supercritical flows that were tens of centimetres to metres long). In my experiments the hydraulic jumps spanned a smaller plan area than the supercritical flow.

Plan shape	Example	Description
I		**Straight fronted; front oriented to stream-transverse** Generally form on weirs, bypass channels and at sites where rock steps or knick points occur. The hydraulic jump generally spans the full channel width at right angles to the bank.
II		**Straight fronted; front oriented obliquely to stream-transverse** Generally form at sites with a near-constant cross-stream slope or where supercritical flow enters a reach obliquely. The hydraulic jump generally spans the full channel width.
III		**U-fronted with apex pointing downstream** Generally form downstream of lateral constrictions to flow. The nodes of the constriction are generally the cross-stream limits of the front.
IV		**V-fronted with apex pointing downstream** Generally form downstream of lateral constrictions to flow. The nodes of the constriction are generally the cross-stream limits of the front and the V shape is generally associated with shock waves.
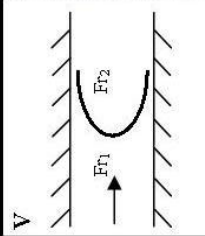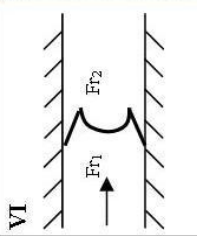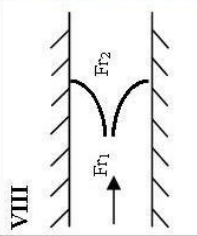
Plan shape	Example	Description
V		**U-fronted with apex pointing upstream** Generally form downstream of isolated roughness elements. The front of the hydraulic jump is generally slightly wider than the roughness element and does not span the channel.
VI		**W-fronted with two apexes pointing downstream and one pointing upstream** Generally form in narrow channels. The front of the hydraulic jump is generally as wide as the channel. The outermost parts of the hydraulic jump forms where shockwaves emanate from the channel sides.
VII Sculpted. Shape is similar to the shape of the underlying topography.		**Fronts sculpted by the shape of underlying topography** Associated with immobile floors with sculpted topographies, typical of bedrock channels. In general shape is similar to shape of underlying topography.
VIII		**"overturning arcs"** Generally form downstream of isolated roughness elements. The front of the hydraulic jump is wider than the roughness element and generally does not span the channel.

Table 1.1 Eight plan shapes of hydraulic jumps that I have seen in natural settings, along with photographic examples and descriptions of the shape and locations where it occurs. The photographic example of shape VIII is from a flume experiment because I have only seen this once in a natural setting and do not posess a good quality image of it.

28

1.6.3 The shape of hydraulic jumps in rivers

Hydraulic jumps have at least eight plan shapes in natural settings. I present the eight shapes to show the range that the hydraulic jumps that I saw had and it is possible that more will be recognised in the future. I do not call this range of eight shapes a classification because a continuum of shapes might exist and I do not feel it useful to devise arbitrary boundaries at this stage. One type of hydraulic jump had a straight front oriented transverse to the stream (I, Table 1.1). One had a straight front oriented obliquely to the main flow direction (II, Table 1.1). One had a U-shaped front (III, Table 1.1) and one a V-shaped front (IV, Table 1.1) with the apex of the 'U' or 'V' pointing downstream. Both these U and V shaped hydraulic jumps commonly occur downstream of lateral constrictions to flow. The V-shaped fronts may be associated with shock waves projecting downstream from the constriction. Hydraulic jumps downstream of isolated bed-attached obstacles may have U-shaped fronts with the apex of the 'U' pointing upstream (V, Table 1.1). A hybrid shape can form, with a U-shaped front pointing upstream plus two limbs associated with shockwaves that extend between the channel side and the cross stream limits of the U-shaped front (VI, Table 1.1). The hybrid shape made by the U-shaped front and the two limbs looks like the letter W to me and I term it a W-shaped hydraulic jump. The shapes of hydraulic jumps might be sculpted by the shape of underlying topography (VII, Table 1.1). Pasternack *et al.* (2007) studied a sculpted hydraulic jump in the context of a horseshoe waterfall. An eighth shape of hydraulic jump occured in wave backwash on a beach and I hypothesise that it could form in shallow open channel flows in suitable discharge conditions. The cross stream limit of the shape was two arcs of curling overturning water (VIII, Table 1.1). The arcs were very close together at their upstream limit and the cross stream separation of the arcs increased downstream. Whilst cylindrical hydraulic jumps with straight toes oriented across stream have been the focus of most studies on hydraulic jumps by experimentalists and applied theoreticians, hydraulic jumps of all eight plan shapes could have influenced sediment transport and deposition in ancient river flows and could have a recognisable signature in the rock record. I chose to study hydraulic jumps with shape I because it is the simplest shape of hydraulic jumps (can be fluid-dynamically modeled in two dimensions) so provides a good first way in to studying sediment transport patterns. It is the most common shape of engineered hydraulic jump, with much already known about its dynamics, and that literature is drawn on when I discuss sediment transport patterns in

Chapters 4 and 5. I chose to study hydraulic jumps with shape V because it was the shape I most commonly saw when observing hydraulic jumps in British rivers, and also hydraulic jumps with shape VIII to test my hypothesis that they canform in open channel flow.

Patterns of the water surface of hydraulic jumps

Since the first reported experiments of Bidone (1819) hydraulic jumps have been described as having surfaces that break. Whilst some small hydraulic jumps that I observed did not have rained air into the hydraulic jump (e.g. Figs in Table 1.1). Valle and Pasternack (2002) documented air contents of 19, 23 and 42 % in three hydraulic jumps in the south fork of the American river. In general air within hydraulic jumps causes h_2 to be higher that the value predicted by Equation 1.2. Some of the hydraulic jumps that I devised experimentally had breaking surfaces and air entrainment so it was not important for me to calculate the specific value of h_2, but instead record whole water surface shape profiles. In my experience it is difficult to discern the plan position that h_2 occurs at in hydraulic jumps in rivers.

Figure 1.15 Hydraulic jump with a non-breaking surface in the demonstration flume, School of Environmental Sciences, University of East Anglia. Each square drawn onto the flume sidewall is 0.005 m across.

1.6.4 Time persistence of shapes of hydraulic jumps

A hydraulic jump exists for as long as supercritical flow exists (§1.5.4). The size and position of hydraulic jumps can change with changing discharge (§1.4). The shape of some hydraulic jumps can also change with changing discharge. All hydraulic jumps I observed in rivers maintained their general shape as discharge varied but when watching backwashes of waves travel over a pebble on medium sand on Whitby beach (North Yorkshire coast, England) I saw one hydraulic jump form and change shape twice (Video file 2, Appendix 2; video shows 2.8 seconds of swash followed by 9.84 seconds of backwash). As the backwash traveled down slope towards the sea it became faster, flow over the pebble became thinner and *Fr* generally increased. After 0.32 seconds of the start of a backwash, a hydraulic jump formed, seawards of

the pebble (video file time, $t_{vf} = 3.12$ seconds). The hydraulic jump had a U-shaped front with the apex of the U pointing upstream (Shape V, Table 1.1). Over a further 3.92 seconds the hydraulic jump changed shape to the arcs of overturning water (Shape VIII, Table 1.1) and then back to the U-shaped front with apex pointing upstream. I hypothesise that this variation in shape could occur in channelised flows.

1.7 SEDIMENT TRANSPORT PATTERNS AT HYDRAULIC JUMPS

Some characteristics of sediment transport patterns at hydraulic jumps can be assessed by simple physical reasoning. Other characteristics have already been deduced from field and experimental observations and from computational and numerical modelling. Experimental and modelling results are more commonly recorded than field results because of the danger of accessing some sites of hydraulic jumps and because high sediment loads preclude an observer seeing below the water surface (Fig. 1.16). To best plan my experiments I derived some expectations of sediment transport patterns at hydraulic jumps (expectations in emboldened italicised text below) and undertook trial experiments (Chapter 2).

Figure 1.16 Sediment laden flow passing through a hydraulic jump. Flow through culvert MEL-C-3 of Norman Creek underneath Ridge Street, Brisbane, Australia in flood on 31 December 2001 around 6:10 am at the end of a rainstorm. Photograph courtesy of Hubert Chanson.

Flow downstream of a hydraulic jump is more likely to be depositional than flow upstream of a hydraulic jump. Bedload is more likely to stall downstream of a hydraulic jump because flow is less competent there than upstream of a hydraulic jump. Sediment is more likely to fall from suspension downstream of a hydraulic jump than upstream of it for the same reason and according to the mathematical treatment of Parker *et al*. (1986), flow downstream of hydraulic jumps must be nett depositional. Applying Parker *et al*'s (*loc. cit.*) treatment to the Hikurangi submarine channel, offshore New Zealand, Lewis and Pantin (2002) found that energy within subcritical flows necessarily decreased downstream: If it does in real flows then it is a physical requirement that sediment fall from suspension or saltation to be deposited on the channel floor downstream of a hydraulic jump. Seidl *et al*. (1994) and Carling (1995) described how conditions of low kinetic energy downstream of hydraulic jumps caused a lot of transported sediment to stall and cover the channel floor in a veneer of sediment. However, sediment can be brought into suspension on the arrival of a bore (a stationary hydraulic jump in the frame of reference moving with the bore) and sediment could be maintained in suspension downstream of a hydraulic jump by the large scale turbulence that can occur there. Chanson (2008) described bed sediment becoming suspended on the arrival of the bore front on the Dordogne river and then advecting downstream relative to the bore front (note particularly his Fig. 6-1, which documents sediment in the process of entering suspension).

Bedload features can form downstream of hydraulic jumps. Carling (1995) described a V-shaped hydraulic jump in a bedrock channel in northern England, downstream of an abrupt lateral expansion (location details given in original paper) and a berm forming in association with it. Carling (*loc. cit.*) described slowly recirculating eddies in a region adjacent to the channel sides immediately downstream of the hydraulic jump. Small boulders, cobbles and pebbles were transported to the hydraulic jump, were swept into the eddies and accumulated to form the berm. Carling (*loc. cit.*) did not describe the manner of the accumulation. Martini (1977) described how a gravel bedload can come to an abrupt halt on the steep upstream face of obstructions downstream of hydraulic jumps.

Sediment features with flat upper surfaces and steep downstream terminations have formed in open channel flumes, in association with straight fronted hydraulic jumps with toes oriented across stream (Jopling & Richardson, 1966; Needham & Hey, 1991; Bellal *et al.*,

2003). The features described by all of these experimenters grew downstream over time by the progradation of an avalanche face at their downstream limit. Although none of these authors used the phrase, the bedforms had the characteristics of unit bars: The features grew over time as sediment was supplied to them; they did not migrate and did not form periodically (although this could be because the flumes were too short to see periodic formation). The feature described by Jopling and Richardson (1966) formed immediately downstream of a hydraulic jump of $Fr \sim 4$, in an 0.20 m wide flume, from gravelly sand with median sediment size, $D_{50} = 0.077$ m. As well as prograding downstream it prograded upstream because sediment accumulated at its upstream face. A photograph of Needham and Hey's (1991) experiment (their Fig. 13) showed that two unit bars formed, one above the other, immediately downstream of their hydraulic jump of centimeters thickness and unknown Fr. The first unit bar formed within tens of seconds of sediment transport and the second formed between 15 – 17 minutes later. The higher of the two unit bars was similar in length to the lower of the two but it had an avalanche front less than half as thick. Flow was supercritical above the feature formed in Bellal et al's (2003) experiment. The downstream avalanche face of the feature was at the upstream limit of a hydraulic jump. Gradually as the avalanche face prograded downstream, flow directly above it became supercritical and the hydraulic jump moved downstream in tandem with it.

Cyclic steps and chute and pools are sediment bed features that form periodically in space in association with hydraulic jumps. In both features flow is supercritical in a downstream-dipping section that terminates in an abrupt change in slope; a prime site for a hydraulic jump to occur if flow into it is supercritical. Over time the bed features of chutes and pools and cyclic steps move upstream in tandem because the supercritical flow is erosional and sediment accumulates at the abrupt change in slope. Taki and Parker (2005) suggested that chute and pools are one sub class of cyclic steps. Alexander et al. (2001) described aggradational chutes and pools being separated by areas of relatively plane bed in a flume with slope = 0.015%. According to Alexander et al. (loc. cit.) the length of each depositional unit is controlled by both flow depth and particle transport properties (themselves indirect functions of each other). Cyclic steps have been inferred most often where a channel bed is in nett degradation (Wintwerp et al., 1992; Parker & Izumi, 2000; Sun & Parker, 2005; Taki & Parker, 2005) but have also been inferred on aggrading beds (Straub & Mohrig, 2009).

According to Taki and Parker (2005) the length of each step cycle is controlled by flow depth and is limited to the range of 100 − 500 times the flow depth. Whilst hydraulic jumps have also been associated with erosional features (Karcz, 1972; Gorrell & Shaw, 1991), these are somewhat in the realms of speculation and I will seek aggradational sedimentary signatures of hydraulic jumps through my experiments.

Cross sets form because the bedload features downstream of hydraulic jumps prograde. Sets of downstream dipping laminae at the downstream end of the unit bars described above (Jopling & Richardson, 1966; Needham & Hey, 1991; Bellal *et al.*, 2003) formed concurrently with the downstream avalanche face prograding downstream. No topset or bottomset formed in association with any of these sets of downstream dipping laminae. Jopling and Richardson's (*loc. cit.*) set of downstream dipping laminae was about 0.04 m thick and the flow above it was about 0.02 m thick (deduced from photographs from the original paper). Needham and Hey's (*loc. cit.*) sets of downstream dipping laminae were 0.07 − 0.09 m thick and flow above them was 0.06 − 0.08 m thick. Bellal *et al*. (*loc. cit.*) did not describe characteristics of the cross set that formed in their experiment. They described the hydraulic jump diminishing in amplitude as it moved downstream.

The set of upstream dipping laminae at the upstream end of Jopling and Richardson's (1966) feature was approximately one third as long as the set of downstream dipping laminae at the downstream end of their feature (their Fig. 3c). It was approximately 0.04 m thick and the laminae dipped at angles of 30 − 35˚. Jopling and Richardson (*loc*. *cit*.) called the set of upstream dipping laminae *backset bedding*. No upstream dipping laminae formed in Needham and Hey's (1991) or Bellal *et al's* (2003) experiments. Backset bedding commonly forms in association with hydraulic jumps in the pools of chute and pool bedforms and cyclic steps (Alexander *et al.*, 2001). The orientation of the backsets is controlled by the geometry of the pool and the speed at which the cycle moves upstream; however the origin of the laminae, the laminaset geometry and bedform development are known only rudimentarily. Martini (1977) described that backsets can form from gravel abruptly stalling (Martini used the word "plastering") at the upstream face of sediment bed features immediately downstream of hydraulic jumps. The gravel was well imbricated and if a sedimentary structure formed, it too would be well imbricated.

1.8 SEDIMENTARY STRUCTURES INFERRED TO HAVE BEEN FORMED IN ASSOCIATION WITH A HYDRAULIC JUMP

The presence of a hydraulic jump in the deposit-forming flow has been used to explain different distinctive features in ancient sedimentary deposits. Most commonly, "backset beds" have been attributed to hydraulic jumps, in alluvial fans, fan deltas and jökulhlaup and pyroclastic deposits (e.g. Postma & Roep, 1985; Massari & Parea, 1990; Nemec, 1990; Macías *et al.*, 1998; Fralick, 1999; Russell & Knudsen, 2002; Cassidy *et al.*, 2003; Russell & Arnott, 2003; Breda *et al.*, 2007; Duller *et al.*, 2008). Steep-sided scours filled with massive or diffusely graded deposits have been attributed to hydraulic jumps (e.g. Gorrell & Shaw, 1991; Russell *et al.*, 2003), as have normally graded and cross stratified gravels with scoured bases (e.g. Hornung *et al.*, 2007) notably in sites downstream of glacial debouchment. Reviewing sedimentary structures formed by upper phase beds and hydraulic jumps, Fielding (2006) recognised that little is certain about what hydraulic jump deposits look like, but sedimentary structures associated with hydraulic jumps are reported in Chapters 4 and 5.

1.9 BREAKING BARRIERS IN COMMUNICATION

Terms used within this thesis are defined below, to avoid misinterpretation or because the term is used to mean different things by Earth Scientists, Engineers and Mathematicians.

1.9.1 Standing waves: A common misconception in terminology

Colloquially termed "standing waves", waves which stay stationary in space as water passes through them are termed *stationary waves*. In accordance this type of wave is called a *stationary wave* in this thesis. In contrast *standing waves* (whether water waves or not) only oscillate vertically, repeatedly "standing up" and "sitting down again" without travelling or oscillating in plan position. Trains of standing waves have nodal points (plan positions of zero oscillation). *Standing waves* are the direct opposite of *progressive waves* which only travel horizontally: *progressive* refers only to the direction of travel.

1.9.2 Cylindrical: Another common misconception in terminology

Cylindrical refers to something three dimensional, for which the shape is independent of the axis perpendicular to the cylinder ends. Critically for understanding, the ends of cylinders can be any shape bounded by a closed curve. For instance the cylindrical supercritical flow depicted in Figure 1.1 has a rectangular end following the curve ABCD and the cylindrical hydraulic jump depiucted in Figure 1.1 has a hydraulic-jump shaped end following curve CDEF. Being an adjective of shape, *cylindrical* is not used to infer rotation, oscillation or any other time-varying phenomenon in this thesis.

1.9.3 Use of the word "bed"

Bed has been used to mean the lower boundary of a channel, the surface of a deposit of sediment and a discrete unit of sediment within a deposit. All three of these "beds" are present in this thesis, often all at the same time within the experimental runs. To avoid having a bed overlying a bed overlying a bed, only a discrete unit of sediment within a deposit is referred to as a *bed*. The lower boundary of a flume channel is referred to as a *flume floor*. The upper surface of a deposit is called a *sediment surface*.

1.9.4 Use of the word "jet"

Jets are often thought of as streaming fluid or particulate material with a distinct material surface. In this study the word *jet* is taken to mean a portion of flow that has distinctly higher velocity than the surrounding flow, the strict meaning of the word. A jet need not have a material surface. *Jet edges* are defined in the situation that the transition in velocity from a jet to the flow surrounding it is sufficiently abrupt for an inflexion point to exist. I define that the *jet core* exists between *jet edges* where they exist. A *wall jet* has one edge adjacent to a solid boundary. A *submerged jet* is overlain by further water region(s) where immediately upstream it was overlain by air or a solid surface. A *detached jet* is overlain and underlain by at least one water region, where immediately upstream one edge is adjacent to a solid boundary.

1.9.5 Terms used to describe the shape of curved surfaces

Surfaces that undulate in the streamwise direction only (are cylindrical in the cross-stream direction) are referred to as *undular* rather than cylindrical-undular, for brevity. Surfaces that

undulate in the streamwise and cross-stream directions are referred to as *undulant*, to distinguish them from undular surfaces and avoid the cumbersome term "non-cylindrical undular".

1.10 GENERAL CONTENT OF THE FOLLOWING SIX CHAPTERS

Having observed and read reports of hydraulic jumps in open channel flows, I know of eight shapes of hydraulic jumps and selected three for further study. To find sediment transport patterns associated with hydraulic jumps I chose to undertake two flume experiments. Using flumes allows me to control discharge and sediment flux so that deposits formed in well defined conditions. In Chapter 2 I describe equipment I use in the experiments and briefly report trial experiments undertaken in a small flume. In Chapters $3 - 5$ I report the specific experimental procedure for the experiments reported there, and the water surface shapes involving hydraulic jumps, patterns of velocity, vorticity, sediment transport, bed topography and deposit character associated with hydraulic jumps. I discuss experimental runs individually and come to conclusions for the individual runs. In Chapter 6 I discuss the potential characters of deposits formed in channels larger than the flume channel used. I propose diagnostic criteria for the presence of a hydraulic jump as a deposit was lain down and I test the criteria against two field deposits in which hydraulic jumps are likely to have formed. I assess the preservation potential of hydraulic jump deposits in open channel settings where hydraulic jumps are known to form. In Chapter 7 I present all my conclusions and assess how well each of my objectives was achieved.

2. Equipment, deployment, accuracy and coordinates

2.1 INTRODUCTION

Results from flume experiments on flow and sediment transport patterns in a range of hydraulic jumps are presented in Chapters 3 – 5. The flumes and all of the experimental equipment deployed in them during the experiments are housed in the Sedimentary Fluid Dynamics Laboratory at the University of East Anglia (UEA). In the experiments acoustic Doppler instruments were used to measure velocity. Point gauges were used to measure the water surface shapes. Video cameras and still cameras were used to record the flows and developing deposits. A laser diffraction particle sizer was used to measure the sizes of grains in sediment samples from the experimental deposits. Details of the methods specific to the experimental runs presented in Chapters 3 – 5 are given at the start of each chapter. Chapter 2 describes the general physical and operational principles of the equipment, my rationale for selecting the equipment I used, the way in which it was deployed in the experiments and the errors that the equipment introduced in collecting experimental data. A co-ordinate system is defined, specific to the flumes used.

2.2 THE FLUMES USED IN THE EXPERIMENTS

2.2.1 The small flume used for trial experiments

A small flume that was used for trial experiments is called the sediment transport demonstration flume by the manufacturers and is referred to in this thesis as *the demonstration flume* (Fig. 2.1; trial experiments described in Section 2.9). It recirculates water but not sediment. The test channel is straight, is 0.077 m wide and 1.5 m long. It has a flat stainless steel floor and colourless vertical Perspex sidewalls that are 0.11 m high. At the downstream end of the test channel, water passes over a fixed sharp-crested overshot weir (Fig. 2.1). The weir is 0.060 m wide and 0.050 m high. Passing over the weir, water falls into a holding tank. Water in the holding tank is drawn by a pump, through a recirculation pipe, back into the test channel. A filter on the entry to the recirculation pipe prevents the recirculation of sediment. Discharge in the recirculation pipe is adjusted by a tap valve. Pumping rate is user-selected

from three discrete factory default pumping rates. The volume of water in the flume can also be varied. The slope of the test channel is adjustable between $0 - 5.7°$ using a jacking screw. Sediment can be put directly into the test channel and removed from the test channel or holding tank by scooping. Squares of 0.005 m are drawn on the outside of the right hand sidewall between $x = 0.525 - 1.025$ m, between the bottom and the top of the sidewall. The set of squares provides a scale for video recordings and photographs. It was beneficial to use the demonstration flume to trial experiments because it can be cleaned of sediment and re-set up in hours whereas it took approximately three days to clean out sediment put into the flume used for the main experiments and set it up for a new experimental run.
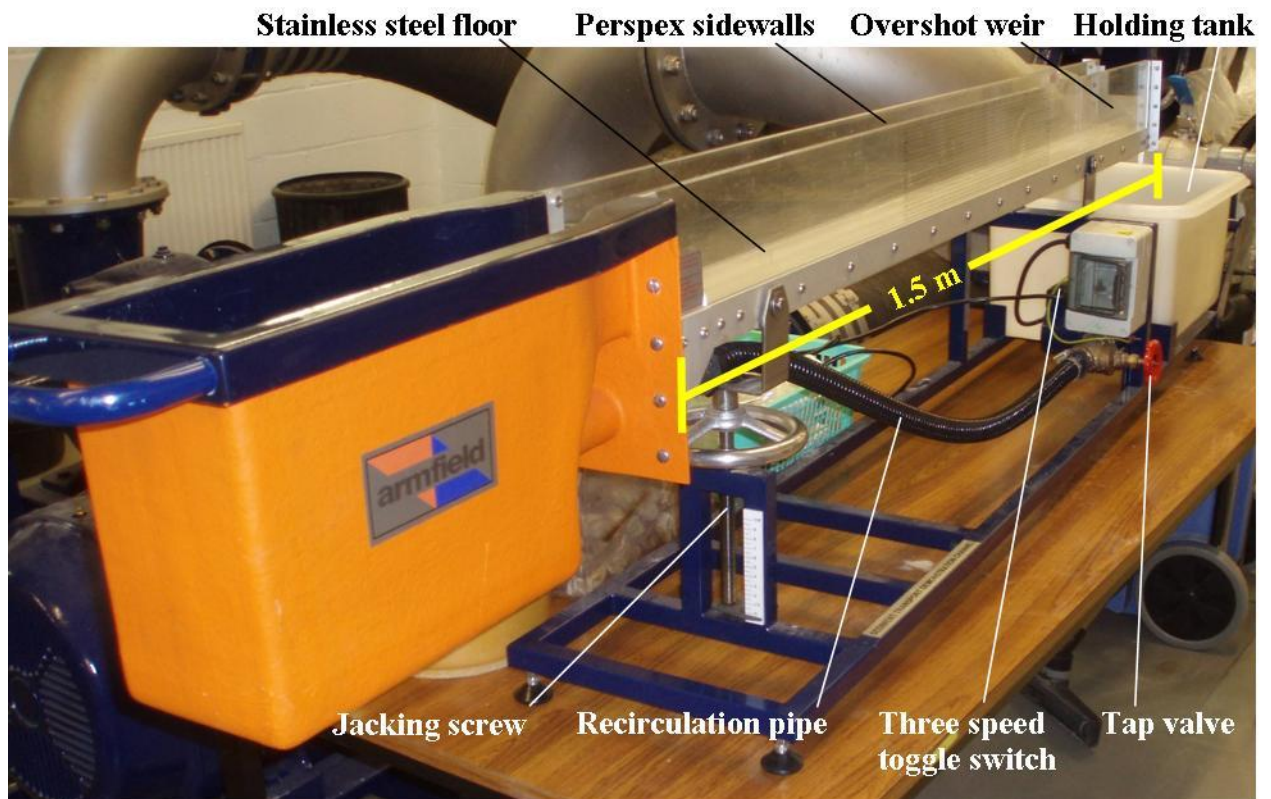
Figure 2.1 Photograph of the 1.5 m long demonstration flume. The test channel tilt can be adjusted using the jacking screw. Flow discharge can be varied using three pump settings, using a tap valve, and by varying the volume of water.

2.2.2 The flume used for the main experiments

The experiments reported in Chapters $3 - 5$ of this thesis used the largest flume in the Sedimentary Fluid Dynamics Laboratory, which is referred to throughout the thesis as *the*

flume. It recirculates water and sediment in a closed pumped loop (Fig. 2.2A). The test channel has 11 pairs of blue vertical supports (Fig. 2.2B). It is straight, 10 m long and has a square (1 x 1 m) cross section. The sidewalls of the test channel are vertical and made of eight colourless glass plates that are 1 m high and 2.5 m long. The contacts between adjacent glass plates of the sidewalls are generally flush, with one exception: the contact between the second and third plates on one side is under-filled with silicone sealant and is rougher than the glass. In flows where the water surface is otherwise smooth a shockwave is generally seen on the water surface, emanating downstream from this contact. Upstream and downstream of the test channel, the sidewalls are made of stainless steel (Fig. 2.2B). Both sidewalls of the test channel have a stainless steel rail to fix equipment mounts to. There are five 1 m wide stainless steel plates on the flume floor. One is 2 m long and is immediately upstream of the test channel. Four are 2.5 m long and are in the test channel. The steel plates are aligned to within 0.001 m in height such that the plates do not lie perfectly flush. The contact between the plates is sealed with mastic sealant, which is less smooth than the steel plates.

The recirculation system of the flume involves the test channel, the discharge tank, two 15 m long recirculation pipes, two pumps and two return pipes that join into a single curved cylindrical pipe leading back into the test channel (Fig. 2.2B). The discharge tank has a recess in the flume floor 0.165 m downstream of the test channel, designed to trap bedload and is called *the bedload trap* in the thesis (Fig. 2.2A). The bedload trap is as wide as the channel, 0.365 m long and 0.170 m deep. Downstream of the bedload trap, the discharge tank has a break in slope of the channel floor, that dips downstream, and a second break in slope causes water to turn and flow downwards into the recirculation pipes. A honeycomb structure between 1.025 – 0.625 m upstream of the test channel, and the design of the pipes leading to the test channel, minimise cross stream flow in water entering the flume (reducing corkscrew flow or meandering that occurs in some experimental flumes).

Sediment was put into the discharge tank via a conveyor (§2.3) so that sediment entering the test channel had already passed through at least 15 m of pipes and pumps and would be well mixed. Removal of sediment from the flume was done in two stages. The first stage involved several iterations of shovelling sediment from the test channel, refilling the flume with water, recirculating the water to bring the sediment out of the pipe work, stopping and draining the flume and shovelling sediment from the test channel. This removed the
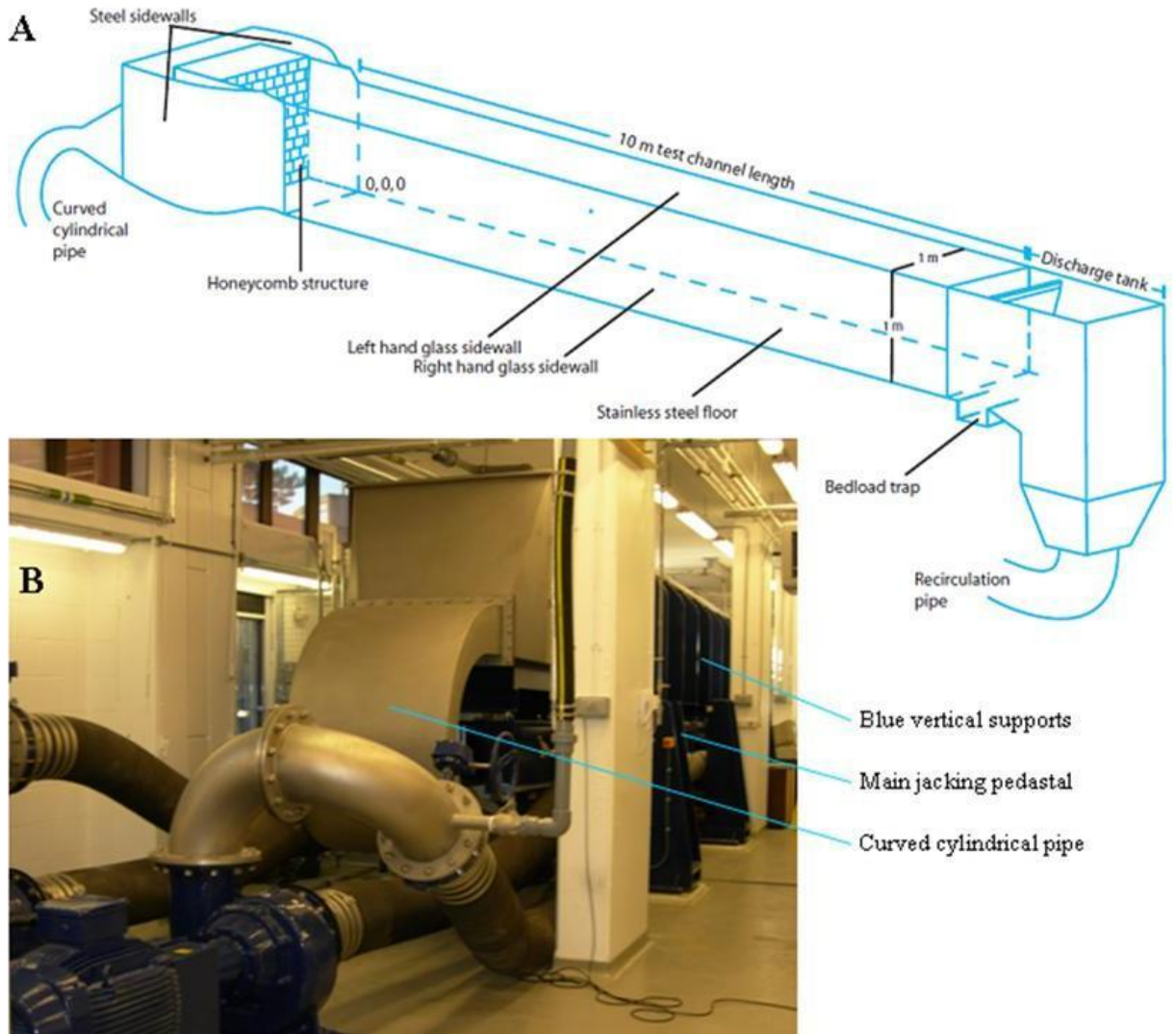
Figure 2.2 The flume used for the main experiments (not to scale).

majority of the sediment from the flume. The second stage involved several iterations of water and remnant sediment being pumped into the flume sump below the discharge tank, the flume being stopped and sediment being washed or scooped out of recesses.

Slope and discharge measurements

The test channel can be tilted about a pivot at the inlet end of the flume by controlling machine screw jacks. The range of tilt is -0.03 – 4.29°, determined via a linear transducer on the main jacking pedestal (Fig. 2.2B). The transducer measures the vertical movement of the test channel (Armfield Limited, 2005 p. 19). A converted reading of slope (in percent) is displayed on the main control box.

Discharge through the flume is measured with two electromagnetic flow meters, one in each of the two recirculation pipes. Discharge was accurate to 0.2% of the discharge displayed on the main control box (Euromag, 2009). There is no setting for a zero pumping rate of the water and sediment: Pumping is at or above a minimum pumping rate which in my experience is a function of the volume of water in the system. Pumping rate can be varied gradually above the minimum value and the flume is designed to discharge up to 0.45 m^3 s^{-1} (Armfield Limited, 2005). Both pumps were used at the same pumping rates in the experiments reported in Chapters 3 – 5 of this thesis, which helped to reduce corkscrew flow or meandering in the test channel.

The fixed steps in the flume induce waves in the water flows

Because the floor of the honeycomb structure sits on top of the flume floor it creates a step-up in the channel floor at its upstream limit and a step-down in the channel floor at its downstream limit. The bedload trap creates a step-down at its upstream limit and a step-up at its downstream limit. Steps in water channels induce waves in water flows (e.g. Lighthill, 1978 p. 262). Above a threshold of depth averaged velocity equal to 0.23 m s^{-1}, the waves are sinusoidal in the streamwise direction and are cylindrical in shape (e.g. . 2.3A). Below 0.23 m s^{-1} the water surface pattern is not cylindrical but is undulant (e.g. Fig. 2.3B; undulant defined in §1.9.4). The water surface shape associated with the wave pattern depends on *Fr* and in analysis of the experimental runs I use *Fr* to characterise the flows.
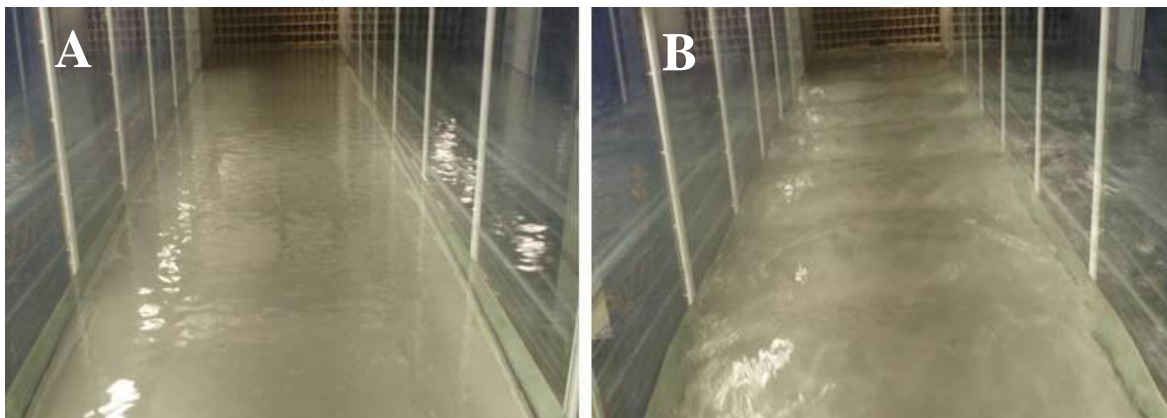
Figure 2.3 Water surface patterns in the flume. (A) In flows below 0.23 m s^{-1} the water surface pattern is undulant (defined in §1.9.3) and (B) above 0.23 m s^{-1} cylindrical sinusoidal waves form.

2.2.3 Coordinate systems and dimensions in the flumes

When I describe the left or right-hand side of a channel it is when looking down-channel. The coordinate system used in both flumes is Cartesian with x, y and z denoting the streamwise, cross-stream and floor-perpendicular dimensions. The origin of the coordinate system ($x = y = z = 0$) is the position of the upstream limit of the test channel, at the left hand sidewall, on the flume floor (Fig. 2.2A). The direction x is positive downstream, y is positive towards the right hand sidewall and z is positive upwards perpendicular to the flume floor. The line $y = 0.5$ is the channel centreline in plan view. In 3d view $y = 0.5$ is the centre plane but in both views I term it *the centreline* in the thesis. The streamwise, cross-stream and vertical components of velocity are u, v and w, where u is positive to downstream, v is positive towards the right and w is positive upwards perpendicular to the flume floor. Flow thickness is measured perpendicular to the flume floor and given the nomenclature h. The water surface height, $H = h$ except over an obstacle or a deposit where $H > h$. Time, t has the value 0 at the start of an experimental run. Downstream-dipping slopes are positive whilst upstream-dipping slopes are negative.

2.2.4 Reynolds number is constant in the test channels

Treating a test channel as being of unit width (unit of 1 m in the flume), Equation 1.7 becomes

$$\mathrm{Re} = \frac{\rho Q}{\mu} \qquad\qquad (2.1)$$

within the test channel. Discharge, Q is as constant as the pumping rate in a recirculating system. Taking density and viscosity to be constants, the value of *Re* is equal when comparing any cross-section of the flume test channel. Since *Re* is a measure of the turbulent character of a flow (§1.4.4) this fact made the turbulent character of the experimental flows easy to control. If the rest of the loop does not have unit width, Equation 2.1 will not be valid there and the value of *Re* will vary around the loop.

2.3 THE CONVEYOR USED TO PUT SAND INTO THE FLUME

A motor-driven looped conveyor belt (Fig. 2.4) is used to transport sand into the flume. It is 4.89 m long and has a fixed tilt. During use it was located with the high end overhanging the

discharge tank and sediment was manually shovelled onto it. A metal structure funnels shovelled sediment onto the belt, minimising spillage.

Sediment input rate to the flume is as constant as the shovelling rate onto the conveyor. Seventeen paddles on the belt prevent the sediment from rolling down slope past them (Fig. 2.4). Generally neither wet nor dry sand sticks to the belt; most of the sand falls into the discharge tank on reaching the top of the conveyor. In the setup used, the belt revolved at a constant rate (240 times per hour).
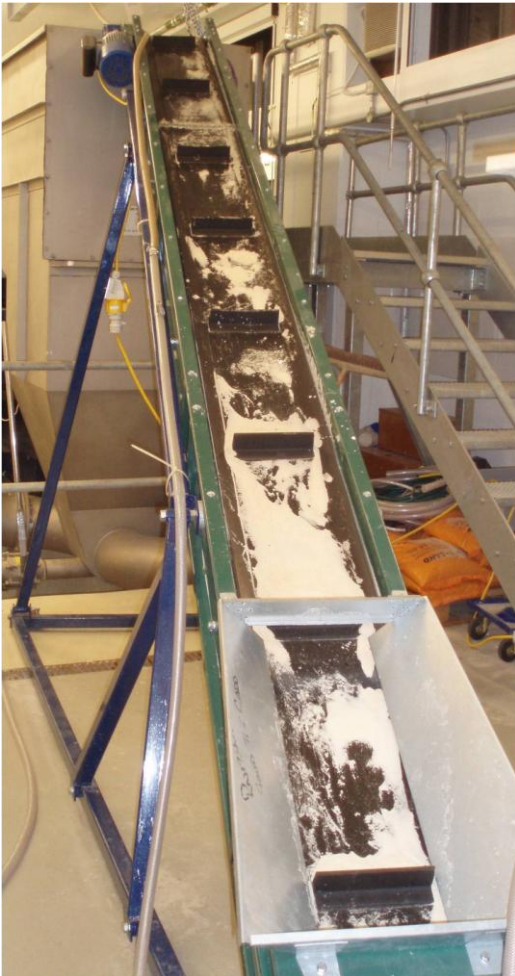
Figure 2.4 The conveyor belt used to transfer sediment into the flume. A metal structure to funnel sediment onto the conveyor is fixed at the low end of the conveyor.

2.4 ACOUSTIC EQUIPMENT USED TO MONITOR VELOCITY

I chose to use acoustic Doppler velocity meters (Fig. 2.5) and ultrasonic Doppler velocity meters (Fig. 2.6A) to measure velocity in the experimental flows. Acoustic Doppler devices do not intrude on the flow they record (when set up suitably). They record velocity precisely and

rapidly. They have been used successfully to study three component (u, v and w) velocities of hydraulic jumps with Fr = 2.0, 2.5 and 3.3 (Liu *et al.*, 2004) and streamwise velocity and shear velocity in bores (Koch & Chanson, 2005; 2007). Each of the three studies just cited contained air bubbles but no sediment. Reynolds shear and other turbulent characteristics have been successfully calculated from acoustic Doppler velocity data. These properties could potentially affect sediment transport patterns in hydraulic jumps. Particle image velocimeters and laser Doppler velocimeters have also been used successfully to determine these properties in hydraulic jumps (Hornung *et al.*, 1995; Svendsen *et al.*, 2000), but it is unnecessary to apply every technique available.

Figure 2.5 A Nortek Vectrino$^+$ acoustic Doppler velocimeter. The black casing houses the circuit boards. The 0.008 m diameter stem joins the circuit boards to the probe head, which has five blue parts that emit and sense acoustic signals.
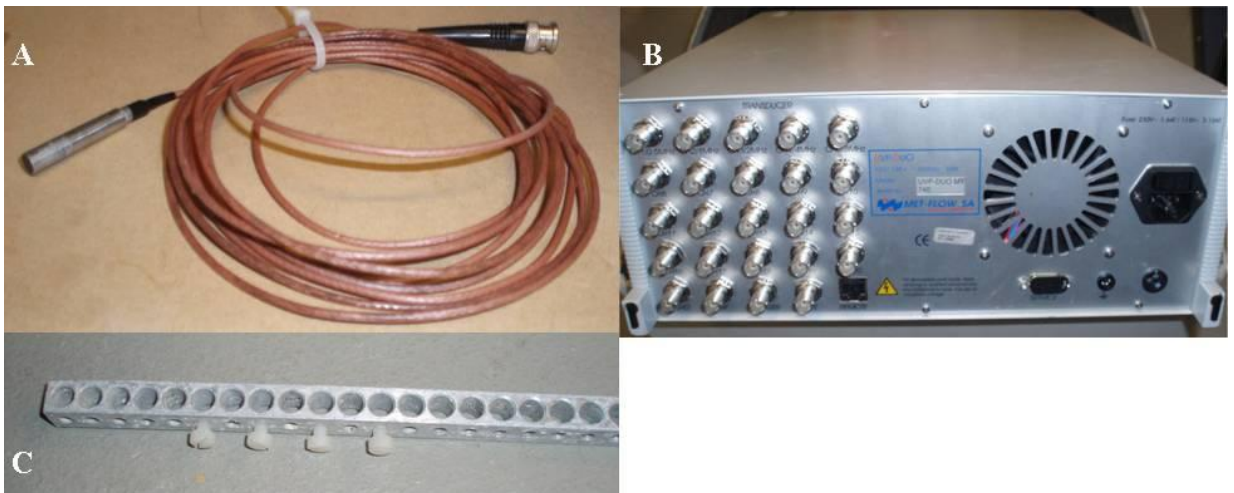
Figure 2.6 Photographs of (A) a MetFlow UVP-DUO ultrasonic Doppler velocity profiler (UDVP), (B) The UVP-DUO control box and (C) the mount used to secure profilers within experimental flows in the flume. The mount has 100 slots to hold individual profilers.

Acoustic Doppler devices repeatedly send acoustic signals to at least one measuring volume, in a user-specified regime. Particulate material within the measuring volume reflects the acoustic signal, causing a Doppler shift of the incident acoustic wavelength. The Doppler shift is proportional to the particle velocity (Lane *et al.*, 1998) and velocity is calculated from the Doppler shift within software programs. In consequence it is the fluid-sediment velocity of the flows that the devices record. This two-phase velocity is taken as a proxy for the fluid velocity. Rapid repeated measurements at a single point are used to construct velocity time series. However the value of time averaged fluid-sediment velocity is generally between the values of time averaged fluid velocity (without particulates) and the time averaged velocity of particulate material (treating the particulate flow as if the water were not present, Kiger & Pan, 2002).

Although successfully deployed in flows containing bubbles, bubbles increase noise in acoustic Doppler velocity data compared to flows without bubbles (Anderson & Lohrmann, 1995; Nikora & Goring, 1998). Robinson *et al*. (2000) found that the ADVs under-represent velocity values in flows with high air contents and Liu *et al*. (2004) detected spikes in velocity data when air bubbles passed through sampling volumes. To avoid misrepresenting velocity and subsequently miscalculating turbulent characteristics I used a despiking method when post-processing velocity time series (§2.8.1). Other problems in acoustic Doppler velocity data stem from uncertainty in Doppler phase shift measurements due to acoustic beam divergence (McLelland & Nicholas, 2000). This is thought to be associated with the finite residence time of suspended material within a bin (Ljermitte & Serafin, 1984). Doppler noise is associated with velocity shear in the sampling volume (McLelland & Nicholas, 2000). Data aliasing can also be a problem with acoustic devices.

2.4.1 Acoustic Doppler velocimeters

Up to three Nortek Vectrino[+] acoustic Doppler velocimeters (ADVs, Fig. 2.5) were deployed in the experiments described in Chapters 4 and 5. Each ADV has black plastic casing around its circuit boards, a cylindrical stem 0.008 m in diameter and a probe head with three mutually orthogonal branches emanating from the end of the stem. Each of the branches has a sensor on, and a fourth sensor is attached to the end of the stem. In every deployment the black casing was above the flow. The stem was oriented perpendicular to the flume floor and was partially

submerged. The probe head was fully submerged. In this orientation none of the mountings used to fix the ADV to the flume were in the flow. Each ADV emits acoustic pulses at 2 MHz, from the three mutually orthogonal sensors, to one measuring volume 0.05 m from the end of the stem. The measuring volume is cylindrical, 0.003 – 0.015 m long (user selectable) and 0.006 m in diameter. Particles in the measuring volume reflect the pulses and the three mutually orthogonal sensors receive the reflected pulses. The Norwich tap water used in the experiments contained sufficient fine particles to reflect acoustic signals without needing to seed the flow. Via software, three mutually orthogonal components of velocity are returned for the measuring volume. Outputs were monitored in real time to ensure aliasing was prevented. Velocity recordings were made at 600 Hz in my experiments for periods of at least 540 s, to allow accurate assessments of time-averaged velocities allowing for turbulent fluctuation (assessments described in §2.8.2).

Each velocity reading made by the ADVs used was accurate to ± 0.5% of the measured value ± an additional 0.001 m s^{-1} (NORTEK AS, 2006). In practice the error in an individual velocity measurement was ± 0.0178 – 0.0213 m s^{-1}. Sturdy mounting of the ADV is required because the probe head can be 0.9 m below the flume traverse and flow past the ADV stem and probe head can cause the ADV to vibrate.

In addition to recording velocity, each ADV recorded the distance to the nearest solid boundary in a straight line from the sensor on the end of the stem, at the time each deployment began. This distance is accurate to half of the length of the measuring volume when reflected from a smooth fixed surface and was less accurate when the surface was rough or not fixed.

2.4.2 Ultrasonic Doppler velocity profilers

Up to ten MetFlow *UVP-DUO* ultrasonic Doppler velocity profilers (UDVPs; Fig. 2.6A) were deployed in arrays (one array per run) in experiments described in Chapters 3 – 5, using standard operating procedures (Best *et al.*, 2001). (Note that the manufacturers MetFlow drop the initial for Doppler from the acronym.) Streamwise velocity, *u* was measured using profilers aligned parallel to the flume floor and *w* was measured using a probe aligned normal to the floor and sampling downward. In any one deployment all of the UDVPs were run through one control unit (Fig. 2.6B). Each profiler works by emitting ultrasonic pulses at a frequency of 4 MHz to one row of cylindrical bins with cylinder axes in the direction of

orientation of the profiler (Ozaki *et al.*, 2002). The bins near each UDVP had diameter of 0.005 m and the diameter of the bins increased with distance from the profiler due to beam divergence.

To deploy them in the flume, the UDVPs are held in drilled slots in an aluminium frame by screws (Fig. 2.6C). I deployed the frame perpendicular to the flume floor with one end on the floor and the other end fixed in a mount above the flow. The frame was 0.01 m long in streamwise and cross-stream dimensions. With ten profilers and ten screws attached, wakes downstream of the frame were observed to be 0.08 m – 0.15 m long in the streamwise direction at the water surface, in the experimental conditions used. In every deployment profilers were oriented to face upstream in order to measure velocity unaffected by the frame. Like the ADV (§2.4.1), the frame needs to be fixed firmly so that it does not vibrate in the flow.

UVP for Optek firmware

Within the firmware *UVP for Optek* the user defines 16 parameters relating to the expected velocity range of the flow to be studied, the signal emitted from the probes and the distance from the probes in which velocity is to be measured (white boxes, Fig. 2.7; Met-flow, 2002). Within the firmware, the range of measurable velocity, the distance over which velocity is measured and the time to take and record a velocity measurement (Fig. 2.7) are interlinked. Before each deployment, settings were chosen to minimise the time taken and maximise the other two parameters. Three other parameters are not user definable (grey boxes, Fig. 2.7) and these vary with the user-selectable parameters.

When using an array of profilers, each one is nominated as Profiler 1 – Profiler n in *UVP for Optek*, where n is the total number of profilers used. The sequential deployment made by the firmware is: Profiler 1 signal sent, Profiler 1 return signal received, Profiler 1 return signal processed. Profiler 1 is then inactive whilst the sequence is repeated for Profiler 2 to Profiler n. One measurement from each of Profilers 1 - n is one cycle and the cycle sampling time was less than 1.04 s in all deployments. A user-definable time delay follows each cycle and a user defined number of cycles are undertaken.

The resolution of velocity in an individual bin is $\pm$ 0.4% of the user-defined velocity range detectable by the profilers (Met-flow, 2002). In practice the magnitude error in an

individual velocity measurement was ± 0.00623 – 0.01624 m s^{-1}. For illustration an error of ± 0.01624 m s^{-1} would have occurred if a UDVP was misaligned by 5.1°. The rigid, tight-fitting profiler mount (Fig. 2.6C) ensured that any misalignment was the same for all profilers used in one deployment. Because the mount is long the overall alignment was easier to judge than if it were short. Velocity and validity readings were monitored in real time to ensure aliasing was prevented. Velocity recordings were made at 600 Hz in my experiments for periods of at least 540 s, to allow accurate assessments of time-averaged velocities allowing for turbulent fluctuation (§2.8.2).
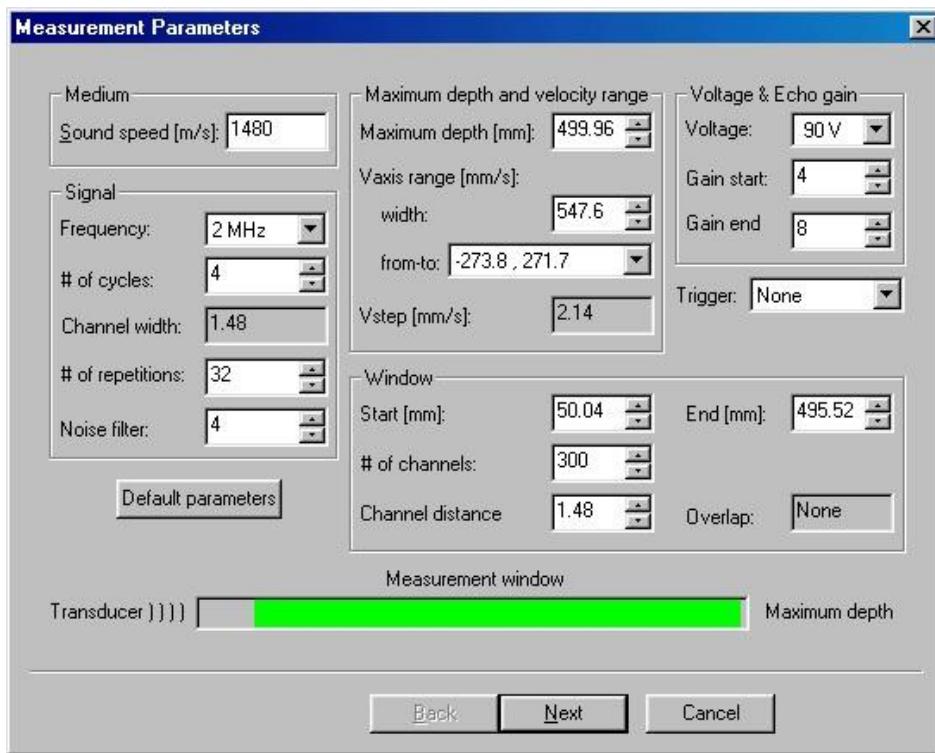
Figure 2.7 Screenshot from the firmware UVP for Optek, used to run the UDVPs

2.5 NON-ACOUSTIC EQUIPMENT DEPLOYED IN THE EXPERIMENTS

2.5.1 The point gauge

Water surface elevations recorded through the sidewall may overestimate true surface elevation by up to several millimetres because of a meniscus adjacent to the glass. A point

gauge was used to determine the height of the water surface above the flume floor, H from upstream to downstream of the hydraulic jumps, away from the sidewalls (cf. Sarma & Newnham, 1973). Sufficient data were recorded to represent the water surface shape, because h_2 was not distinguishable by eye (something true of most hydraulic jumps in open channel flows, §1.6.3). The point gauge has a 1 mm graduated scale that was oriented perpendicular to the flume floor. When fixed in the mount used, the point could reach within 0.066 m of the sidewalls and within 0.010 m of the ends of the test channel. In the situation of a water surface that fluctuated in position with time, H was determined to be where the point was wetted for half of the time spent at the plan location of the measurement, and the accuracy of the measurement of H was generally ± 3 mm.

2.5.2 The video recorders

A Canon XL1S video camera was used to record some of the experiments. The video camera records images at 25 frames per second. Video was viewed directly at this frequency and using Windows Movie Maker, both at 25 frames per second and frame by frame. In some runs in the experiment presented in Chapter 3 an Olympus µ 700, 7.1 megapixel digital camera was used to capture video in a different view to the Canon XL1S. The Olympus camera was also used to take still images of the equipment, the experimental runs and the rivers and outcrops observed during fieldwork. The camera mode was varied between pictures to improve image quality. Pictures taken by others working in the laboratory were also examined.

2.6 THE LASER DIFFRACTION PARTICLE SIZER

Associated with the different ways in which they measure, the various pieces of equipment available to measure grain size are known to return different apparent textural qualities of sediment samples (Agrawal *et al.*, 1991; Shillabeer *et al.*, 1992; Blott & Pye, 2008). I used a Malvern Mastersizer 2000 laser diffraction particle sizer to determine the grain size distributions of samples of the sediment used in experimental runs and sampled from outcrop, because small samples can be analysed for 3d grain size properties quickly. The name of the particle sizer is abbreviated to Mastersizer in the rest of the thesis. Standard operating procedures were used (American Society for Testing and Materials, 2000; Blott *et al.*, 2004;

Blott & Pye, 2006). Specifically water and sediment were pumped around a closed loop within the Mastersizer and particle sizes were measured by the obscuration of laser light within a section of the loop. Sediment samples with masses between 3.2 – 4.5 g were run through the Hydro G dispersal unit and where only a very small sample was available the Hydro S dispersal unit was used (full descriptions of the Hydro G and Hydro S are written by Malvern, 2009). The Mastersizer detects 3d particle sizes between 0.02 – 2000 μm and grain size distributions of reference materials within this range are accurate to 1% (Quality Audit Standard, Malvern 2009). Blott and Pye (2006) found grain size distributions to be accurate to 0.03% for reference materials, 1% for well sorted sand and 1.4% for bimodal sand.

Mastersizer pumping rates were tested in the range 1200 – 3000 Hz using small amounts of the sediment used in the experiments (Chapters 3 – 5). Following testing, a pumping frequency of 2200 Hz was used. Below 2200Hz the coarsest sand fractions were underrepresented because they were not in continuous motion around the loop. Between 2200 – 2500 Hz the coarsest fraction did not change. At pumping frequencies above 2500 Hz air bubbles were entrained; they obscured laser light and were recorded within the grain size distribution.

2.7 DESIGNING THE INITIAL POSITION OF HYDRAULIC JUMPS IN THE FLUME TEST CHANEL

Flows through the test channels of the flumes were designed to involve hydraulic jumps that can form in modern river channels. Most supercritical flows in modern rivers have under-developed velocity profiles; that is to say their streamwise length is too short for flow to have a parabolic velocity profile (for whatever length of time the supercritical flow is steady for). Kirkgöz and Ardiçlioğlu (1997) determined that the streamwise distance over which a velocity profile develops, L is given by

$$\frac{L_s}{h_s} = 76 - 0.0001 \frac{\mathrm{Re}_s}{Fr_s} \tag{2.2}$$

where L_s, h_s Fr_s and Re_s are the development length, depth, Froude and Reynolds numbers of the supercritical inflow. Equation 2.2 is modified from Kirkgöz and Ardiçlioğlu's Equation (5), which does not involve the supercritical notation. In my experiments I designed

supercritical flows to have streamwise lengths less than L_s to recreate this property of hydraulic jumps in natural rivers.

The first procedure for physically forming hydraulic jumps was to fill the flume with Norwich tap water. The level that the test channel was filled to was varied between experimental runs. For each flume run pumping conditions were preset using the flume control box. Pumping conditions took up to 30 s to equilibrate and during that 30 s a hydraulic jump had formed in the test channel. In the trial experiments and in the experiment described in Chapters 4 and 5, water was pumped in such a way that it entered the test channel supercritically. The hydraulic jump initially formed above the discharge tank because water was reflected from the downstream end wall of the flume. After it formed, the hydraulic jump moved upstream rapidly and within 30 s it stalled within the test channel (a hydraulic jump in translation became an arrested surge with a stationary mean position, Chanson, 2007). Overshot weirs (Fig. 2.2A) were used to adjust the stationary mean position of the hydraulic jump before any measurements were taken or sediment was added.

In the experiment of Chapter 3 the supercritical flow and hydraulic jumps were associated with a bed attached obstacle that simulated an immobile boulder on the floor of a channel. The supercritical flows and hydraulic jumps formed within 30 s of pumping. They had a stationary mean position controlled by the flow and the boulder only. In all experiments, once optimum conditions for hydraulic jumps were achieved, I ensured that the position, shape and oscillating character of the hydraulic jumps were reproducible. Then I undertook the experimental runs.

2.8 POST-PROCESSING VELOCITY DATA

2.8.1 Defining and removing erroneous data

Calculating accurate time-averaged velocity components and presenting accurate time series of velocity from individual spatial points (from one ADV or UDVP measuring volume) requires post-processing of the velocity time series because of minor inherent problems with the acoustic method of data capture (§2.4). Nikora and Goring (1998) and Goring and Nikora (2002) devised a method to screen out data that are erroneous because of acoustic beam

divergence and Doppler noise. I used their method to remove erroneous velocity data. A parameter called validity, returned by the UVP for Optek firmware for every datum, also incorporates Doppler noise and data with less than 100% validity were removed. The above methods of data screening led to the removal of up to 20 data points (out of at least 520) per bin.

2.8.2 Time-averaging velocity data

Mean streamwise velocity for a cross section within the test channel was determined by considering the conservation of volume flux of water through the flume. This was chosen over the method of fitting curves to velocity profiles because the velocity pattern within a hydraulic jump may not be cylindrical. Mean streamwise or vertical velocity was determined at individual spatial points, from the mean of at least 500 data, after erroneous points had been removed. Averaging over random selections of 400 data for any particular time series produced mean velocity values less than 3% different to averaging over 500 data. The mean of 300 data were up to 8% different to averaging over 500 data and the mean of 200 data up to 11.1% different.

2.8.3 Calculating turbulent kinetic energy and Reynolds shear

When an instantaneous profile was measured by a vertically oriented UDVP, the position of some of the bins intersected one bin of each of the upstream-oriented UDVPs. From these coincident time series of velocity data, *Tke* (Eqn. 1.8) and Reynolds shear (Eqn. 1.9) were calculated. The magnitude of *u* and *w* data independently were not affected by each profiler not sampling at the same instant but calculations of *Tke* and τ_{zx} might have been. Gray (2004) calculated *Tke* and τ_{zx} using *u* and *w* UDVP data from his original time series and also from adjusted time series. Gray's (*loc. cit.*) adjustment effectively made time series of all UDVPs instantaneous by fitting a cubic spline to the series, but τ_{zx} and *Tke* were hardly different. I chose only to remove erroneous data before calculating τ_{zx} and *Tke*, without making the time series instantaneous.

2.9 TRIAL EXPERIMENTS FOR SEDIMENT PATTERNS

2.9.1 Objectives of making trial experiments

1. Form a hydraulic jump in the test channel of the demonstration flume. Put sediment into the flow in regimes where the sediment is transported to the hydraulic jump as suspended load and bedload.

2. Obtain a general idea of sediment transport patterns within hydraulic jumps. Devise procedures for recording patterns of sediment transport through hydraulic jumps in flume test channels.

3. Obtain a general idea of how the flow and sediment transport patterns change and feed back with each other over time.

4. Change the input regime through iterations so that a deposit forms underneath or downstream of the hydraulic jump and grows in volume for as long as the flume pumping conditions and sediment input regime are maintained.

5. Determine if any patterns within sediment deposits (patterns of grain size, grain fabric, lamination etc.) are detectable by eye. Obtain a general idea of what information can be derived from the depositional patterns.

2.9.2 The setup used for the sediment trial experiments

A hydraulic jump was formed in the test channel, with the supercritical flow about as long as the tailwater and shorter than L_s (Equation 2.2). The supercritical flow was 0.015 m thick. The hydraulic jump was cylindrical with its toe oriented across-stream (shape 1, Table 1.1). Its streamwise shape was alike the shapes of hydraulic jumps reported by Sarma and Newnham (1973). The channel sloped from upstream to downstream and the subcritical flow thickened downstream. Sediment was put directly into the supercritical flow using a scoop in three regimes. In two of the trial runs pumping rate and channel slope was kept constant whilst deposits formed. In a third trial run the slope of the test channel was increased after ten minutes to increase the Froude number of the hydraulic jump. A written record of the trial runs was kept and Trial Run 3 was videoed.

2.9.3 Observations of sediment transport through a hydraulic jump

To best transfer the observations from the trial experiments to the main experiments presented in Chapters 3 – 5, I present my observations in the order of the objectives.

1. Hydraulic jumps form readily on slopes greater than 3° in the demonstration flume. Very little sand or fine gravel travelled in suspension all the way through the supercritical flow because it was very thin.

2. Bedload moved through the supercritical flow as a cylindrical mound (cylinder axis across-stream). On entering the hydraulic jump the mound became longer and thinner but remained cylindrical. Bedload initially stalled downstream of the hydraulic jump by about half the length of the roller. Lee and stoss faces formed within minutes from the start of sediment input. The lee face was steep compared to the stoss face, with respect to the channel floor. Subsequent cylindrical mounds climbed the stoss face of the deposit that formed and became thinner as they did. Some sediment was deposited on the stoss side, forming and preserving upstream-dipping laminae. Most avalanched down the lee face. The bedload feature became long over time. Its height was limited because flow was thin. No bedload stalled on top of the feature.

3. Growth of the feature caused the hydraulic jump to move upstream (the hydraulic jump was a progressive wave, §1.9.2). The flow and deposit thickness were always contained within the test channel of the demonstration flume and the trial experiments were ended when sediment covered most of the channel floor and the hydraulic jump was at the upstream limit of the channel.

4. Grain size segregation was distinct when poorly sorted sediment was supplied to the hydraulic jump. Patterns of lamination were also obvious. Over several days a drying pattern formed in the deposits, which highlighted lamination. The drying process did not obviously disturb the pattern of grain size in the deposits.

2.10 THE STYLE OF THE EXPERIMENTS REPORTED IN THE FOLLOWING THREE CHAPTERS

In Chapter 2 I reported the equipment and methods of deploying it, and in Chapters 3 – 5 I report the experimental methods and results. In Chapter 3 I report a method of generating

hydraulic jumps in a laboratory flume using a bed attached obstacle. The shape, velocity and vorticity patterns of flows that resulted from interaction with the obstacle are reported. Observations of non-equilibrium transport of bedload through selected flows are also reported. In Chapters 4 and 5, I change emphasis from studying the plan pattern of sediment transport to forming aggradational sediment deposits in association with a hydraulic jump, and analysing deposits in streamwise and cross-stream section for characteristics that could be seen in the rock record.

3. The flow field around a hemisphere where a hydraulic jump is created and implications for sediment deposition

3.1 INTRODUCTION

This flume study was designed to improve understanding of water and sediment movement around channel floor obstacles. In a physical process common to steep or shallow rivers, flow becomes supercritical as it passes over the top of bed-attached large roughness elements and a hydraulic jump appears downstream of the crest of the roughness element (e.g. Fig. 1.7, Fig. 1.12 and shapes V and VI of Table 1.1). Difficulties in anticipating flow stage in natural settings make systematic field studies problematic. Following the paper of Schlichting (1936), the many flume studies of water flow, and the few studies of water and sediment flow, around hemispheres have involved only subcritical flow (studies involving sediment listed in Table 3.1). To simulate a cobble or boulder in a shallow stream a hemisphere was positioned on the

Investigators	Macdonald (Chapter 3)	Werner *et al*. (1980)	Best and Brayshaw (1985)
Runs without sand	67	0	0
Runs with sand	5	9	8
Froude number of flow upstream of the hemisphere	0.15-0.83	<< 1	UNKNOWN
Hemisphere diameter (m)	0.24	0.10-0.122	0.09
Ratio of channel width to hemisphere diameter	0.42		
Thickness of sand bed in test channel at $t = 0$ (m)	0	UNKNOWN	0.015
Sediment introduced during the experiment?	Yes (rate varied)	No	Yes (UNKNOWN rate)
Sediment used	250 μm sand in four runs. 1800 μm sand in one run.	Different in every run. Median grain size ranged between 6 μm silt to 225 μm quartz sand	810 μm quartz sand with 9% 450 μm magnetite

Table 3.1 Details of the experimental setups used during three investigations which are discussed in Chapter 3. Information of the runs of Werner *et al*. (1980) and Best and Brayshaw (1985) is derived from the respective papers. Further information from the runs of Macdonald are given in Chapter 3.

floor of a flume. Flow stage and pumping rate were varied in a range where hydraulic jumps formed downstream of the hemisphere. Water flow patterns around the hemisphere were observed and measured and then sand was introduced to selected pumping conditions.

3.1.1 Flow patterns around immobile boulders in subcritical flows

The experimental flows in Chapter 3 were designed with *Re* $\mathbf{O}(10^5)$ so that they can be directly compared with river flows that become supercritical over obstacles (§1.5.2; *Re* defined in §1.4.4). Flow with $\mathbf{O}(10^5)$ separates from the upper boundary of floor-attached hemispheres and does not reattach within 20 obstacle diameters: the length of test channel downstream of the hemisphere (e.g. van Dyke, 1982, his Fig. 48). Associated with the flow separation a turbulent wake must form downflow of the hemisphere.

Vortex patterns around hemispheres form as soon as flow approaches the hemisphere, and form in a similar way over erodible and non-erodible floors (Darghai, 1990). The boundary layer of flow approaching the hemisphere is likely to roll up immediately upstream of the hemisphere as described by Fraenkel (1961) and visualised by Tamai *et al.* (1987). This is an expression of the vorticity pattern, and is associated with higher shear stress than flow further upstream than the hemisphere (Sutton & McKenna-Neuman, 2008b). The vorticity travels with the flow. In subcritical flows vorticity travels around most of the hemisphere edge in a horseshoe-shaped track and is associated with increasing fluid stress from upstream to downstream (Sutton & McKenna-Neuman, 2008b). Further downstream than the hemisphere some authors have illustrated the vorticity travelling in spiral tracks downstream from the obstacle-attached horseshoe (e.g. Paola *et al.*, 1986; Sutton & McKenna-Neuman, 2008b). Flow visualisations reported in van Dyke (1982; his Fig. 48) indicate that discrete vortices form within 0.5 diameters downstream from an obstacle and take irregular paths within the wake of the obstacle. The location and movement of vorticity will affect sediment transport. Because supercritical flow over the hemisphere flow is generally thin, vorticity at the smallest scales travels over the hemisphere. Other accepted patterns of flow around a bed attached hemisphere under subcritical water flow were altered by the supercritical flow and hydraulic jump present in the flows described here, with consequent effects on bedload transport patterns.

3.1.2 Sediment features around immobile boulders in subcritical flows

On river floors that are predominantly gravel, sand can be transported and redeposited in the lee of boulders: Carling and Reader (1982) and Laronne *et al*. (2001) describe this occurring during waning flows and Wohl and Cenderelli (2000) during high stage flows. In predominantly sand bed streams too, Karcz (1968) described accumulations of sand in the lees of boulders. The cross-stream width and height of Karcz's (*loc. cit*.) accumulations decreased with distance downstream and their longest axis extended into the lee of the boulder; a counterpart to Bagnold's (1941) aeolian *sand shadows*. In more recent publications Bagnold's *sand shadows* have been termed *current shadows* (Allen, 1982) and *shadow dunes* (e.g. Gunatilaka & Mwango, 1989). Laronne and Carson (1976) described boulder shadows, which were accumulations immediately to the stoss and lee sides of boulders in Seale's Brook, Quebec. The lee accumulations were well imbricated coarse pebbles, whereas the stoss accumulations were small pebbles thought to have accumulated during a flood recession. Johansson (1963) defined *wake bars* with similar properties to sand shadows but not necessarily having an upstream limit on the downstream face of the boulder. Johansson (*loc. cit*.) reported that *wake bars* are flanked by two erosional features (of undefined nature). Werner and Newton (1975) defined *comet marks* in current-affected submarine settings, which were obstacle-induced erosional features with the obstacle at the upstream end of the feature, forming the comet head, and with the longest axis of the feature extending into the lee of the obstacle. *Comet marks* may be the erosional counterpart to Bagnold's (1941) *sand shadows*. In all of these examples the flow that formed the features was not observed, but the depth-averaged flow was inferred to be subcritical everywhere.

The high shear stress at the plan locations of horseshoe vortices (§3.1.1) should often cause these locations to be associated with scour features (Richardson, 1968; Allen, 1982). Horseshoe scours have been recognised by Shaw (1994). Scours with similar general appearance form immediately upstream of cylindrical obstacles, such as bridge piers (see Darghai, 1982) and tree trunks (Fielding & Alexander, 2001). Because obstacle shape is important in affecting the flow and scour patterns I will not compare the scour pattern equations around cylinders with scour patterns around hemispheres.

3.2 EXPERIMENTAL PROCEDURE

3.2.1 Runs to characterise flows around the hemisphere

A hemisphere of radius, $r = 0.12$ m was fixed flat-side down at the centre of the flume floor, which was set at 0° tilt (Fig. 3.1; Flume descriptions in §2.2.2). The ratio of channel width to obstacle diameter, $\dfrac{b}{2r}$ was 4.2.

Sixty seven experimental runs were undertaken in sediment-free conditions in four series (Table 3.2, presented at the end of Chapter 3). The first run of each series used the lowest working discharge and in each subsequent run discharge was greater. Each series had a different water volume in the closed loop, giving different water depths in the test channel. Series H1 involved 18 runs and was the deepest series with the pre-series (stationary) water level at a height twice that of the hemisphere crest. For each subsequent series the pre-series water level was decreased by 25% of the Series H1 depth, down to half of the crest height in Series H4. Series H2 included 18 runs, Series H3 17 runs and Series H4 14 runs. Flow in the experimental channel deepened slightly from the start to the end of each of these four series, concurrently with discharge increasing: There was a fixed volume of water in each series, it recirculated in a closed loop and the only open channel sections of the loop were the test channel, 2 m of channel upstream of it and the discharge tank (§2.2.2). Because water was increasingly drawn down into the discharge tank with increasing pumping rate in each series the volume of water in the test channel increased (it must have done for volume flux to have been conserved around the closed loop). In the first five runs of Series H4 only, water did not flow over the hemisphere.

In all runs the flume pumping conditions were maintained for at least several tens of minutes and each run was undertaken at least four times to make repeat observations. In runs with water flow over the hemisphere, four distinctive patterns of the water surface were observed. In one example of each of these, a vertical array of eight UDVP probes (Fig. 3.2A) was deployed at 40 plan locations in the flow (Fig. 3.2B) at separate times, to record a representation of the velocity patterns (§2.4.2 for UDVP deployment characteristics). The examples were from Series 2, using the first run in which each new form of the hydraulic jump first appeared (Table 3.2). Ten of the forty locations were along the streamwise centerline of
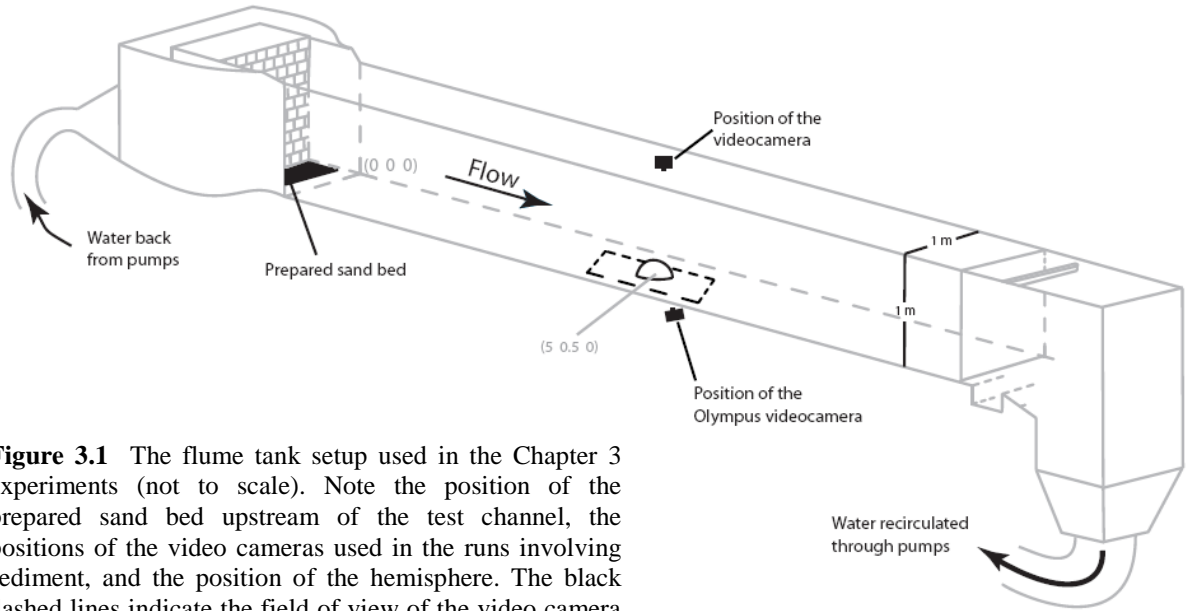
Figure 3.1 The flume tank setup used in the Chapter 3 experiments (not to scale). Note the position of the prepared sand bed upstream of the test channel, the positions of the video cameras used in the runs involving sediment, and the position of the hemisphere. The black dashed lines indicate the field of view of the video camera when pointing downwards.

the test channel ($y = 0.5$ m) and thirty locations were within the left hand side of the flow (along lines $y = 0.4$, 0.25 and 0.1 m); it was assumed that flow was symmetrical about $y = 0.5$ m. All eight probes were oriented to face upstream. At some locations in some of the flows, some of the probes or sampling locations were above the water surface and in these cases the probes were not deployed. At least 1800 data points were recorded by each probe over 612 seconds to allow an accurate assessment of the time-averaged velocity, allowing for turbulent fluctuation (see §2.8.2 for discussion of "accurate" average velocity).
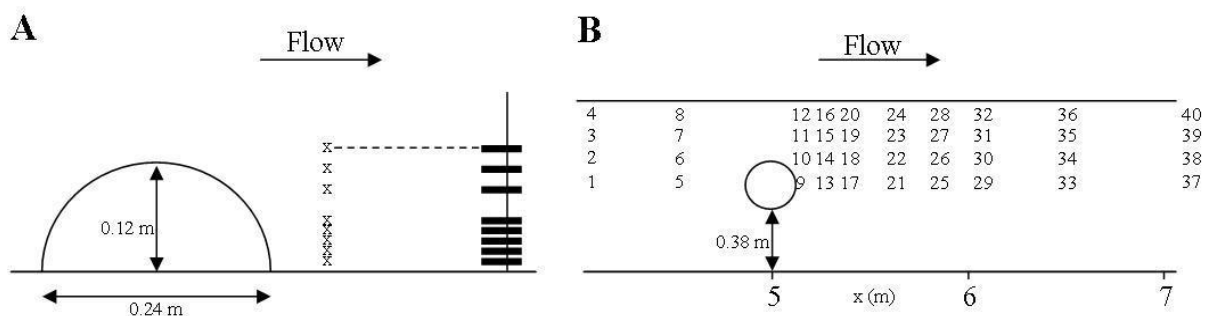
Figure 3.2 The UDVP setup (not to scale) showing (A) the distribution of probes and the orientation of the probe array, (B) plan view of the deployment positions for the array. The numbers mark the plan positions of the velocity measurements recorded by the UDVP array for deployment positions 1 – 40. Vertical profiles of velocity calculated from the UDVP data and presented in Figs 3.13, 3.15 and 3.17, are given the same numerical code as their associated deployment position.

The water surface pattern and the velocity field were investigated in three ways to detect any influence of the presence of the hemisphere on the patterns: (1) Observation of the shape of the water surface with the naked eye. Orientation, shape and oscillating character were compared between waves upstream of the hemisphere. (2) The water surface shape generally did not vary for as long as each pumping condition was maintained and because of this it was possible to use a point gauge to detect the amplitudes and wavelengths of cylindrical waves. This enabled streamwise changes in shape to be detected, which were not otherwise visible. (3) Measurement of the $\bar{u}$ profiles.

3.2.2 Runs to characterise bedload transport patterns around the hemisphere

A fifth series of four runs involved a medium sand (D_{50} 250 µm, Table 3.3; Fig. 3.3) and the hemisphere. The run codes for this series use "MH2". A single run named CH2.02 involved coarse sand and fine gravel (D_{50} 1800 µm, Table 3.3; Fig. 3.3) and the hemisphere. Flow conditions were equivalent to runs of Series H2 with equivalent Pumping Condition Number (Table 3.2).

Before each run that involved sediment, 30 kg of the sediment was spread evenly across the full width of the flume floor between 6.0 and 5.5 m upstream of the hemisphere under still water (-1 ≤ x ≤ -0.5 m, Fig. 3.1). At time, $t = 0$ the flume pumps were started, the predetermined pumping rate was reached within 90 seconds and the sand movement was observed. Over the duration of each run in Series MH2 and Run CH2.02 (Table 3.3) all of the sand was moved by the flow from the prepared bed. The runs were stopped when all sand had passed downstream into the test channel. At this time some had reached the downstream end of the test channel but some had not reached the hemisphere. The sand bed was always visible through the water column; any distinct regions of stationary sand on the flume floor, and of sediment movement, could be seen easily. Most of the bedload that reached the downstream end of the flume was stopped from recirculating by the sediment trap so that transport patterns of non-recirculated bedload could be determined (trap described in §2.2.2). The pattern of sediment on the flume floor at the end of each run was photographed to give a snapshot of the bedload transport pattern.

Run code	Pumping condition	D_{50} of the prepared bed (μm)	Run duration (seconds)	Nature of the hydraulic jump	Plan shape of hydraulic jump from Table 1.1
MH2.2	H2.2	250	3600	Undular	I
MH2.2a	H2.2	250	3600	Undular	I
MH2.4	H2.4	250	900	Arcuate-fronted	V
MH2.6	H2.6	250	720	Overturning arcs	VIII
CH2.2	H2.2	1800	4500	Undular	I

Table 3.3 Details of the experimental setup for runs of Series MH and for Run CH2.2
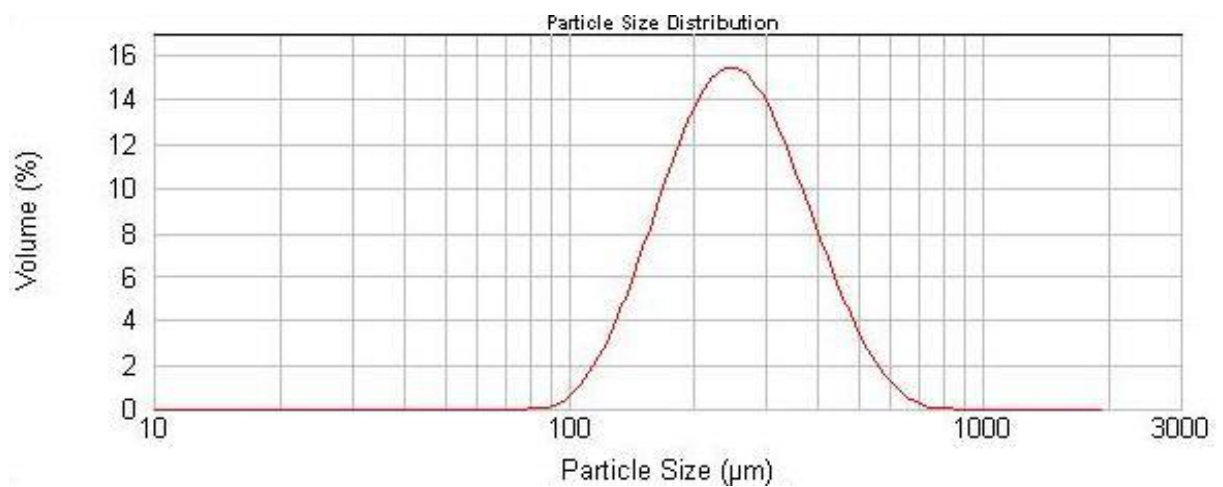
Figure 3.3 Grain size distributions of the sediment used in the experiments reported in Chapter 3.

3.3 GENERAL CHANGES TO FLOW CHARACTERISTICS WITH INCREASING PUMPING RATE

At the lowest three pumping rates in Series 1 and the lowest one in Series 2, the water surface pattern was similar over the whole area of the test channel. The water surface was undulant; bumps and dips in the water surface were up to 0.1 m long both in the streamwise and cross-stream directions (Fig. 3.4A; undulant defined in §1.9.4). The bumps and dips constantly moved and varied in amplitude between 0 – 0.004 m, detected using the point gauge. Both at higher pumping rates and the initial pumping rates of Series 3 and 4, stationary water surface waves occurred upstream of the hemisphere and these were sinusoidal in shape in the streamwise direction (Fig. 3.4B). These sinusoidal waves were cylindrical, varying little across stream. The amplitude and length of the waves increased with increasing pumping rate

in each series (Table 3.2). The surface of the cylindrical sinusoidal waves appeared smoother with increasing pumping rate.
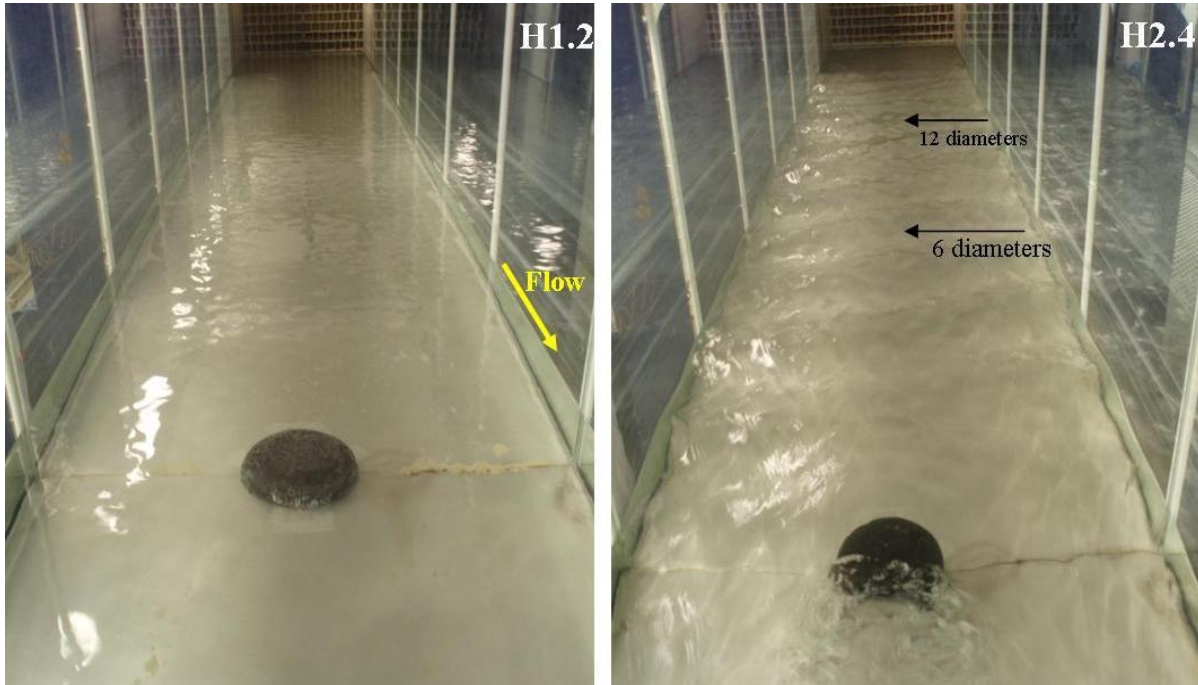
Figure 3.4 Photographs of two forms of the water surface upstream of the hemisphere. (A) An undulant surface, defined as a complicated 3d pattern composed entirely of bumps and dips in the water surface, of similar size and cross-stream and streamwise extents much smaller than the width of the channel. (B) Cylindrical sinusoidal waves. The shape of the waves is independent of the cross-stream dimension. The character of the water surface is the same at 6 diameters upstream of the hemisphere as at 12 diameters upstream of the hemisphere, but closer to the hemisphere surface waves were non-cylindrical.

Except for the lowest pumping rates tested, the water surface shape over and downstream of the hemisphere was different in appearance to that upstream of it and was 3d. Where water flowed over the hemisphere a single hydraulic jump formed within a dish-shaped depression of the water surface (concave up) in the lee of the hemisphere in association with flow accelerating over the downstream half of the hemisphere (Fig. 3.5). Where h over the downstream half of the hemisphere was less than 0.01 m, Fr was in excess of 20. The water surface above the downstream half of the hemisphere became steeper with increasing pumping rate below $Fr_u = 0.49$ where Fr_u is the mean Froude number upstream of the hemisphere (mean over time and plan area; Fig. 3.6). In the flows where $Fr_u > 0.49$ the water surface over the downstream half of the hemisphere became less steep with increasing pumping rate. Each hydraulic jump maintained both its position and shape (with oscillations on the order of

millimetres to a few centimetres) for as long as the associated pumping condition was maintained. The toe of the hydraulic jump generally moved downstream with increasing pumping rate (Fig. 3.7) but occasionally did not (notably between the first three runs of Series H2, §3.4.2). In runs with equivalent Fr_u the toe of the hydraulic jump was further downstream in deeper runs. Note that Fr_u is used to compare runs because it controls water surface shape (§1.4.3, §2.2.2).
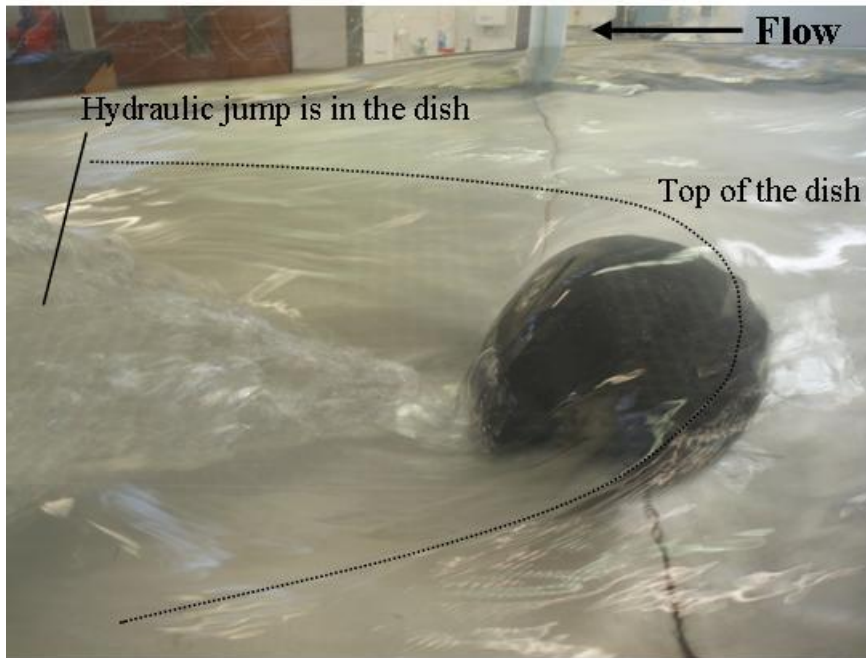
Figure 3.5 Photograph of the dish shaped depression in the water surface downstream of the hemisphere and a hydraulic jump within it. Example is Run H3.2.
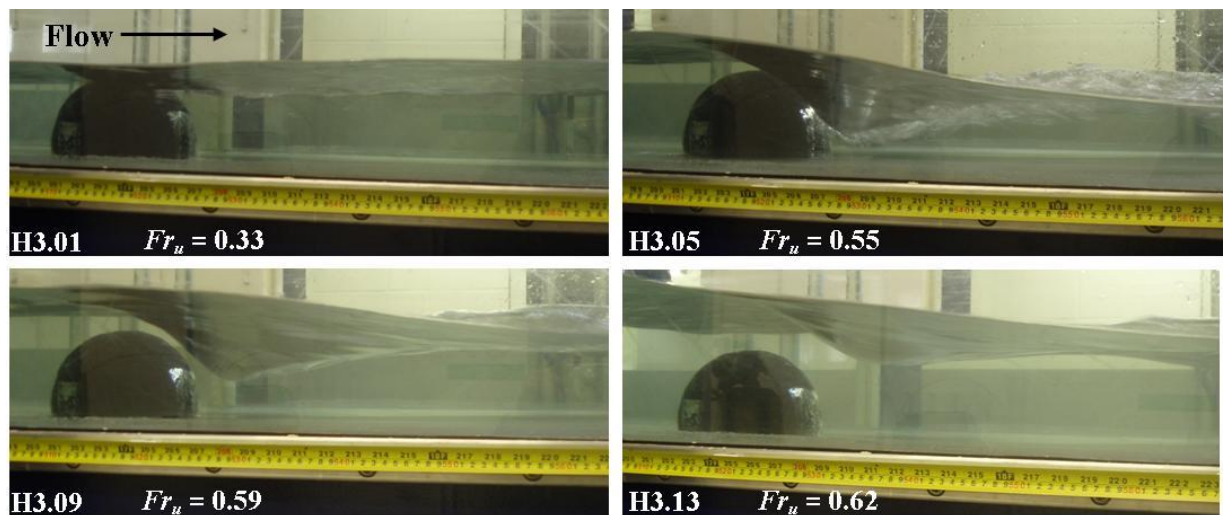
Figure 3.6 Photographs of flows over and downstream of the hemisphere from Series 3. Flow became steeper over the hemisphere into the water surface depression, between H3.01 – H3.05, and shallower from H3.05 to later runs of Series 3. The experimental conditions are listed in Table 3.2.
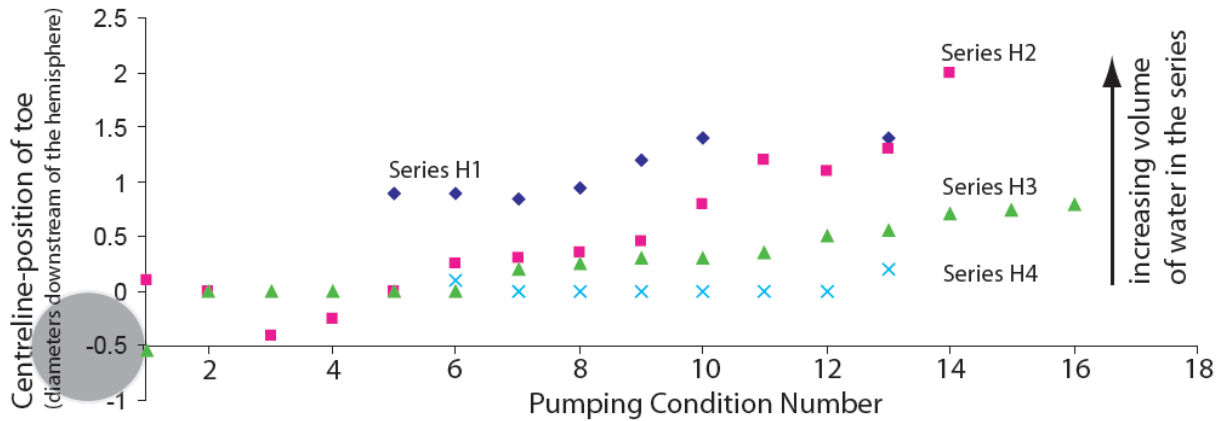
Figure 3.7 The time-averaged streamwise position that the toe of the single hydraulic jump had at the channel centreline ($y = 0.5$ m), observed in runs where water flowed over the hemisphere. Different symbols are used for the different Series H1 – H4. The horizontal axis is labelled with the Pumping Condition Numbers. The vertical axis is a streamwise length scale based on the downstream limit of the hydraulic jump having the value 0, positions downstream of the hemisphere having positive values and upstream of the hemisphere having negative values. The hemisphere is depicted in plan view in grey with the same length scale as the horizontal axis. In Runs H1.11 and H1.12 the toe was not easily distinguished.

All runs had subcritical flow upstream of the hemisphere ($Fr_u < 1$, Table 3.2). With increasing pumping rate through each series, Fr_u and Fr_d (Froude number downstream of the hydraulic jump) generally increased (Table 3.2; Fig. 3.8). In all series apart from the shallowest one, Fr_u and Fr_d approached a maximum parabolically. When both were less than 0.4, $Fr_d = Fr_u$ (Fig. 3.8). In runs in which both were above 0.4, Fr_d was greater than Fr_u. In the shallowest series both Fr_u and Fr_d reached a maximum (at pumping condition 09) whilst Fr decreased with increasing pumping rate. When pumping rate was increased further both Fr_u and Fr_d decreased.

The Reynolds number increased with increasing pumping rate. In the initial runs of Series H1 – H3, $Re = 40000$ and in Series H4 the initial run had $Re = 17400$ (Table 3.2). In the final run of Series H1 $Re = 216000$, Series H2 $Re = 197000$, Series H3 $Re = 151000$, Series H4 $Re = 93000$. Further details of flow characteristics specific to individual runs are presented in Sections 3.4 – 3.7.
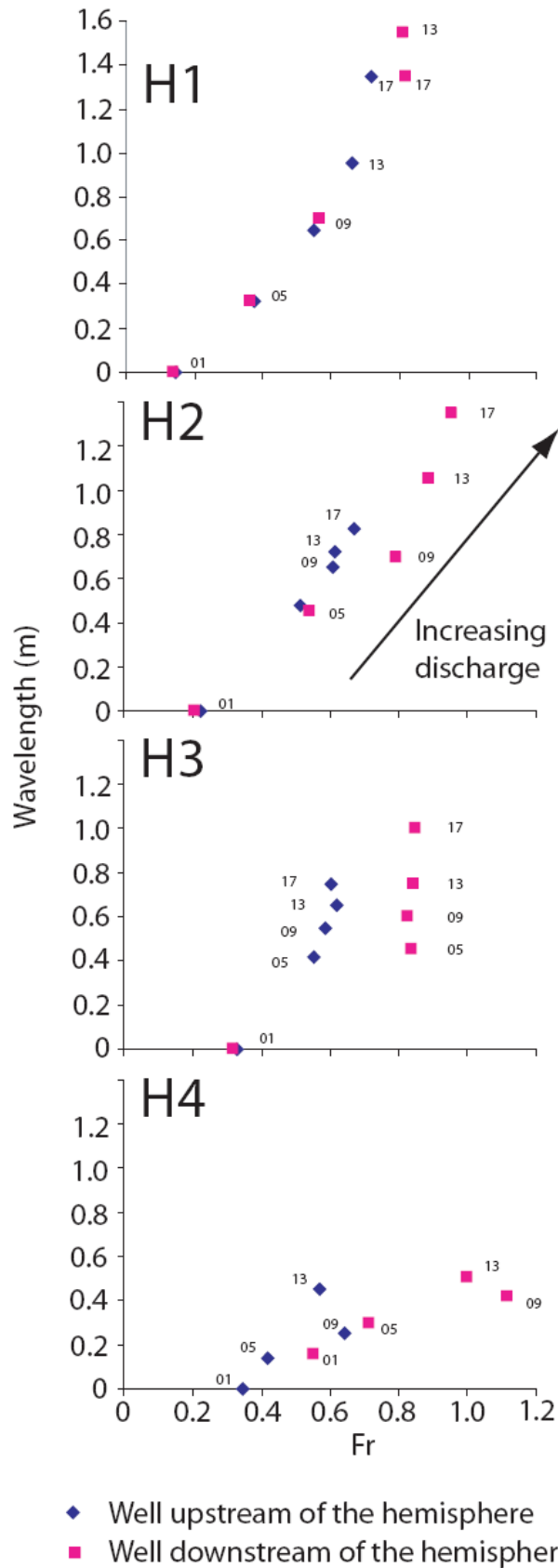
Figure 3.8 Graphs of the variation in Froude number and wavelength of flow upstream of the hemisphere in Series H1 – H4. Numbers indicate the Pumping Condition Number of the adjacent symbol and correspond to the Pumping Condition Numbers listed in Table 3.2. Each subsequent data point towards the top-right corner of each graph is, in general, a later Run Number in order 01, 05, 09, 13, 17. Series H4 was undertaken up to Run H4.14 and so the fourth graph contains eight data points.

3.4 OBSERVATIONS OF THE WATER SURFACE PATTERN AS PUMPING RATE INCREASED

3.4.1 The water surface patterns in Series H1

The water surface was undulant in flows with $0.15 < Fr_u < 0.27$ (H1.1 – H1.3, Table 3.2) and at each pumping condition in this range h varied on the order of millimetres. Sinusoidal surface waves were seen where $Fr_u > 0.27$. Above $Fr_u = 0.46$ sinusoidal waves were present and oscillated in the streamwise direction by $0.005 – 0.050$ m. The oscillation increased with increasing Fr_u. Above $Fr_u = 0.67$ the sinusoidal waves broke continuously close to the sidewalls.

Flow was not supercritical anywhere in the first three runs, where $\overline{h_u} = 0.21$ m and $Fr_u < 0.2$. In all other runs, the dish-shaped depression of the water surface (§3.3) had an upstream limit at the crest of the hemisphere. Its length increased from 0.5 hemisphere diameters, where $Fr_u = 0.2$, to more than four diameters where $Fr_u = 0.71$. The hydraulic jump was in the downstream half of the depression. Its shape changed with discharge and Fr_u through the same series. (1) An arcuate-fronted undular crest formed with an apex that pointed upstream (Fig. 3.9A; the toe had shape V, Table 1.1). (2) With slightly higher Fr_u a convex-upstream, arcuate-fronted hydraulic jump developed (Fig. 3.9B). The arc had greater plan convexity than the undular crest and the apex of the arc pointed upstream. (3) At yet greater Fr_u a hydraulic jump formed with stream-transverse limits that were two arcs of overturning water, a shape not previously reported as a hydraulic jump. The arcs were several centimetres apart at their upstream limit and their cross-tank separation increased with distance downstream (shape VIII, Table 1.1). The arcs overturned upstream perpendicular to their plan curvature (to upstream) without appearing to entrain air into the flow. The upper surface of the hydraulic jump between the arcs was concave up (Fig. 3.9C). (4) In the highest range of Fr_u in each series, the surface pattern was similar to (3) but the central part of the hydraulic jump was convex up (Fig. 3.9D). Like (3), this pattern of hydraulic jumps has not been reported in the literature. The transition from (1) – (2) occurred at $Fr_u = 0.32$, the transition to (3) at $Fr_u = 0.55$ and to (4) at $Fr_u = 0.63$.
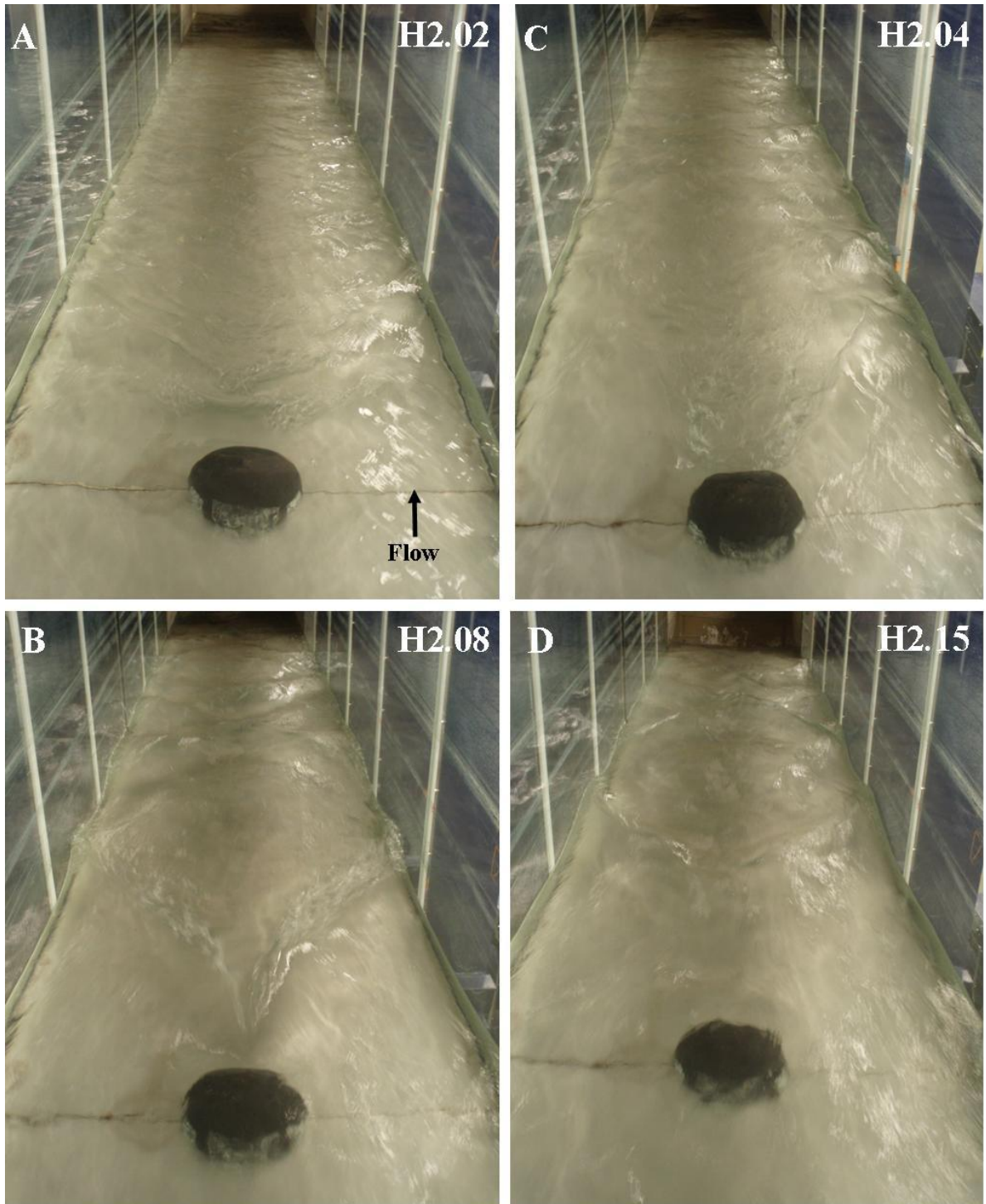
Figure 3.9 Oblique views of flow fields from upstream of the hemisphere to the downstream end of the flume, from Series H2. From photograph A − D the flume pumping rate increases. Flow became supercritical as it travelled over the hemisphere and each photograph shows an example of one of the four forms of hydraulic jump that formed downstream of the hemisphere. The toes of the hydraulic jumps are depicted on the overlays along with the Froude-scaled flow conditins upstream of the hemisphere. . In Run H2.02 an undular jump occurred and it had an arcuate shaped front. In Run H2.04 an arcuate-fronted jump occurred (Shape V, Table 1.1). In Runs H2.08 and H2.15 the arcs of overturning water occurred (Shape VIII, Table 1.1). In Run H2.08 the water surface between the arcs was concave-upwards and in Run H2.15 it was convex-upwards.

3.4.2 The water surface patterns in Series H2

Flows upstream of the hemisphere were similar in appearance to those observed in Series H1 except that (A) the transition from the undulant water surface upstream of the hemisphere to sinusoidal waves occurred at $Fr_u = 0.30$, (B) the sinusoidal waves did not break at any pumping condition and (C) wavelength increased less with increasing Fr_u (compare Fig. 3.8A and B).

The dish shaped depression of the water surface occurred in all runs. It was a factor of $2 - 3$ deeper than the dish-shaped depressions observed in Series H1. Whilst the general trend was for the toe of the hydraulic jump to move downstream with increasing pumping rate (§3.3), between H2.01 and H2.03 the toe moved upstream by 0.12 m (0.5 hemisphere diameters, Fig. 3.7). Flow thickened with increasing discharge (§3.2.1) and I think that from Run H2.01 to H2.03 the value of Fr for the flow over the hemisphere decreased causing the upstream motion: although u increased, h increased by a greater proportion (Eqn. 1.1). The toe moved downstream by 0.60 m between H2.04 and H2.18, more than twice its displacement in equivalent runs in the other series.

In Series H2, as Fr_u increased the hydraulic jump changed in shape in the same order $(1) - (2) - (3) - (4)$ as seen in Series H1. These transition in shape occurred at similar values of Fr_u to the equivalent transitions in Series H1. Specifically the transition to (2) occurred at $Fr_u = 0.30$, to (3) at $Fr_u = 0.54$ and (4) $Fr_u = 0.64$.

3.4.3 The water surface patterns in Series H3

Flows upstream of the hemisphere were similar in appearance to those observed in Series H2 except that (A) the transition from the undulant water surface upstream of the hemisphere to sinusoidal waves occurred at $Fr_u = 0.39$ and (B) wavelength increased less with increasing Fr_u (compare Fig. 3.8B and C).

The dish shaped depression of the water surface occurred in all runs. It was a factor of $2 - 4$ deeper than the dish-shaped depressions observed in Series H1. The dish was deepest in Run H3.05 where it was as deep as the radius of the hemisphere (Fig. 3.6). Between Runs H3.01 and H3.17 the toe of the hydraulic jump moved downstream gradually by 0.35 m.

The undular jump was not seen in Series H3. In Run H3.01 a hydraulic jump with an arcuate front, shape (2) above, was seen. With increasing pumping rate the shape transformed

to (3) in Run H3.06 and (4) in Run H3.17. The transition to (3) occurred at $Fr_u = 0.56$ and to (4) at $Fr_u = 0.61$.

3.4.4 The water surface patterns in Series H4

Upstream of the hemisphere the pattern of the water surface was undulant at the lowest pumping rate (H4.01). As pumping rate increased, firstly the pattern became an association of non-cylindrical sinusoidal waves. Water surface height increased towards the centre of the wave crests, which were 0.2 – 0.6 m long and oriented at -20 – 20° to the y axis (H4.02 – H4.06). Tens of the non-cylindrical sinusoidal waves were present at any one time and they moved upstream and downstream with an excursion of up to 0.3 m. Their amplitude changed continuously, within a range of several centimetres, when observed by eye over several tens of minutes. Individual sinusoidal waves were observed to move into and merge with adjacent sinusoidal waves. The water surface pattern associated with the non-cylindrical sinusoidal waves was transient and at any one time the wave pattern was elaborate in plan view. A pattern of cylindrical sinusoidal waves was observed at higher pumping rates (H4.07 – H4.14). The wavelength of the cylindrical sinusoidal waves increased less in Series H4 than in the other series, in association with the smaller studied range of Fr_u (Table 3.2). No cylindrical sinusoidal waves were seen to break in any of the H4 runs.

In Runs H4.01 – H4.09 Fr_u and Fr_d increased with increasing discharge (Fig. 3.8D). Run H4.09 had the highest values of Fr in the series, being $Fr_u = 0.64$ and $Fr_d = 1.12$. In Run H4.09 only, the flow was supercritical on average downstream of the hemisphere, but was subcritical upstream of the hemisphere. In Runs H4.10 – H4.14 Fr_u and Fr_d decreased with increasing discharge (Fig. 3.8D); I think because of flow thickening (cf. H2.01 – H2.03). The non-cylindrical sinusoidal waves formed at $Fr_u \sim 0.44$ and the transition to cylindrical sinusoidal waves occurred at $Fr_u \sim 0.57$.

In the first seven runs (H4.01 – H4.07) water did not flow over the hemisphere but passed around it. Between $4.65 \leq x \leq 6.08$ m (4 diameters downstream of the hemisphere) flow became thinner downstream and became thinner towards the channel centreline ($y = 0.5$ m). The depressed part of the water surface was not obviously dish shaped; its shape was constrained laterally by the sidewalls.

In the runs in which the hemisphere was not overtopped (Runs H4.01 – H4.07, Table 3.2) four hydraulic jumps formed at the same time, within the depression. Two hydraulic jumps formed with their toes approximately parallel to the channel centreline, approximately one hemisphere diameter apart (Fig. 3.10A). At the lowest pumping rates (lowest value of Fr_u) both of their toes were 2.3 diameters long. Between the two jumps flow was subcritical and had a complex swirling pattern, dominantly with a vertical axis of rotation. Swirling coherent flow structures were seen to pass downstream. As Fr_u increased the toes of the hydraulic jumps became shorter, and closer together at their upstream limit (Fig. 3.10B). Two further hydraulic jumps had toes that were much more flow-transverse in orientation. Their upstream limit was the downstream limit of the other two hydraulic jumps. The time-averaged shape of their toes was straight-fronted and at any time a complicated breaking pattern was seen. The toes extended symmetrically away from the centreline to the sidewalls at an angle of 40°. This pattern is reported because it occurred, but no further analysis is undertaken on it because the focus of the research is single hydraulic jumps formed by flow acceleration over the hemisphere (§3.1).

Downstream of the four hydraulic jumps there were two straight-fronted converging waves; these made a diamond pattern with the more downstream hydraulic jumps (Fig. 3.10B). Swirling flow from between the two upstream jumps passed downstream into the diamond but was not observed downstream of the diamond. Swirls of flow within the diamond rotated more slowly than swirls of flow between the more upstream hydraulic jumps. Downstream of the diamond cylindrical water surface waves spanned the channel width, with 0.16 m wavelength and 0.002 m amplitude.

At and above $Fr_u = 0.43$ (Run H4.08 – H4.14) some water flowed over the hemisphere and the pattern of the water surface over and downstream of the hemisphere was different to that below $Fr_u = 0.43$. A single hydraulic jump formed downstream of the hemisphere, within a depression in the water surface (Fig. 3.10C and D). The single hydraulic jump was arcuate fronted in Runs H4.08 – H4.12, and had the form of arcs of overturning water in Runs H4.13 and H4.14: In Run H4.13 the water surface was concave up between the arcs and in Run H4.14 the water surface was convex up between the arcs.
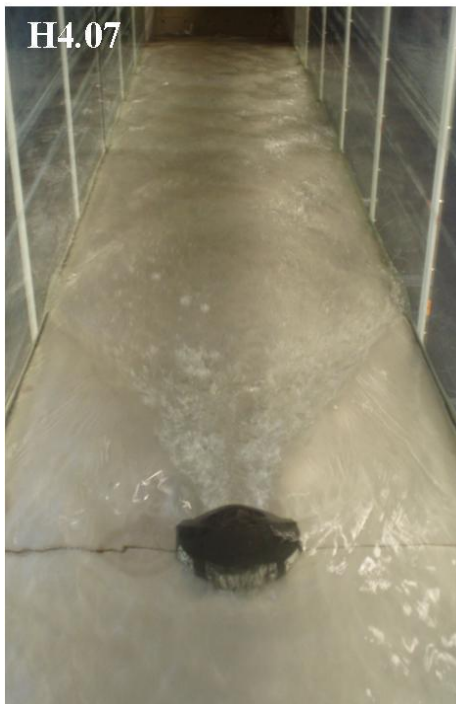
Figure 3.10 Oblique views of flow fields from a few tens of centimetres upstream of the hemisphere to the downstream end of the flume, from Series H4. From photograph A – D the flume pumping rate increases. Flow became supercritical as it travelled around or over the hemisphere and the pattern of hydraulic jumps varied with the Froude condition of flow upstream of the hemisphere (marked on the overlay). In (A) and (B) the flow did not overtop the hemisphere. Hydraulic jumps were straight-fronted and oblique to the main flow direction (Shape II, Table 1.1) Note how the fronts of the flow-parallel hydraulic jumps closed from (A) to (B) and then widened from (B) to (C) as the hemisphere was overtopped by flow. In (C) the hydraulic jump has an arcuate front (Shape V, Table 1.1). Between (C) to (D) the hydraulic jump has transformed into the arcs of overturning water (Shape VIII, Table 1.1).

73

3.5 FLOW PATTERNS HIGHLIGHTED BY BUBBLES

Air did not enter the flow during any of the runs of Series H1, but did in the runs involving arcuate-fronted jumps within series H2 – H4, in the form of bubbles (the range of conditions in which the hydraulic jump was arcuate-fronted is indicated in Table 3.2). Tracking the bubbles highlighted patterns in the water flow. The bubbles were observed through the right-hand sidewall of the test channel. Bubbles formed and followed well defined tracks in continuous streams whilst the fronts of the hydraulic jumps were breaking.

For most flows in which an arcuate-fronted hydraulic jump was present, flow (and bubbles) passed downstream along a curved track descending from the surface towards the flume floor and rising in the more downstream part of the track (Fig. 3.11). As pumping rate increased and the arcuate-fronted jump increased in size, and the depth to which the bubbles descended increased, to a maximum of 0.3 hemisphere diameters below the water surface at $Fr_u = 0.44$. The streamwise distance over which bubbles remained in the flow increased with pumping rate, from 2 – 5 hemisphere diameters. Flow at the surface of the hydraulic jump constantly travelled in the upstream direction. At the downstream limit of the track, where bubbles reached the water surface, they travelled downstream for several tens of centimetres before bursting.
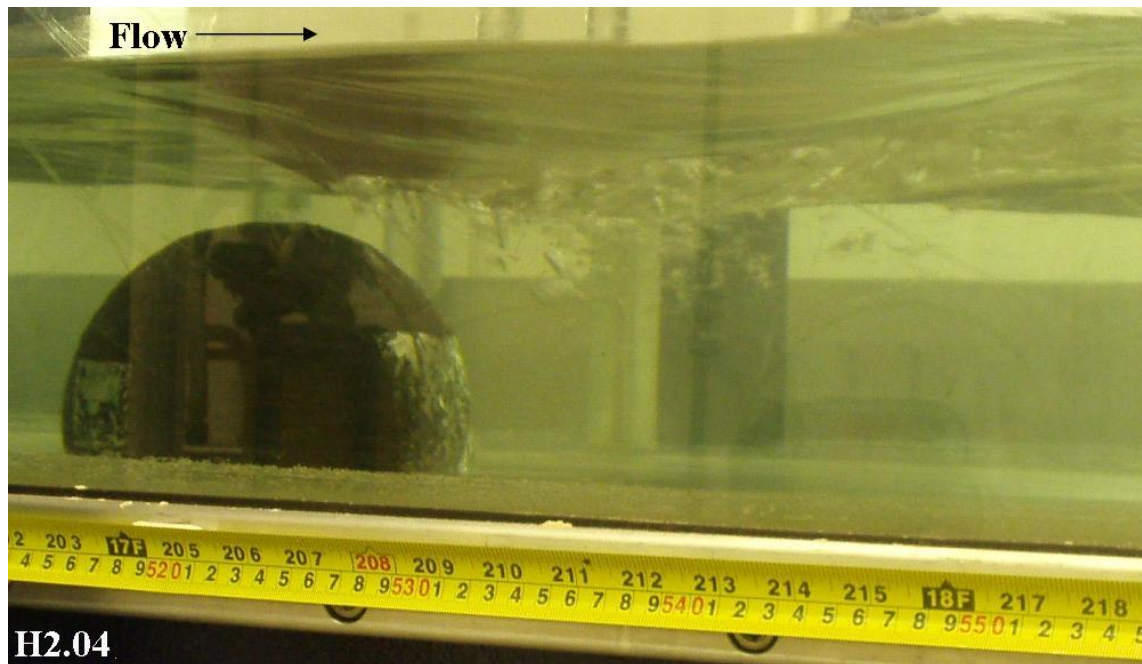
Figure 3.11 Photograph of bubbles that passed in a downstream direction, downstream of the hemisphere. The track of the bubbles got deeper in its more upstream half. In the more downstream half of the track the bubbles rose to the water surface.

At Fr_u = 0.49 in Series 3 (H3.04), most bubbles passed downstream with the track of the flow described above but some passed upstream close to the water surface. Instead of terminating at the water surface and bursting, the bubbles were trapped within the flow and coalesced into a bubble between the hemisphere and the water surface (Video file 3, Appendix 2). A single bubble repeatedly formed at this position, grew to 0.04 m in streamwise length, and after several seconds to tens of seconds passed downstream along the underside of the water surface. As this large bubble entered the downstream track described above, it broke into many tens of smaller bubbles.

3.6 DETAILS OF THE FLOW IN THE HYDRAULIC JUMPS

The undular jump, arcuate fronted hydraulic jump and arcs of overturning water were documented from Series H2 using the runs they first appeared. All four forms occurred in Series H1 and H2; Series H2 was used as an example. The water surface shapes were mapped between 0.75 m upstream and 3.25 m downstream of the hemisphere using a point gauge, in an 0.04 by 0.04 m plan grid with additional measurements where the water surface slope was steep (point gauge and mapping procedure described in §2.5.1). Except where stated in the text, the water surface was stationary for tens of hours whilst the point gauge maps were recorded. The time-averaged streamwise velocity ($\bar{u}$) structure within the flow was determined for the same plan area using the procedure outlined in §3.2.1.

3.6.1 Run H2.2: The undular jump (Fr_u = 0.30)

Water surface shape

Upstream and either side of the hemisphere crest, $\bar{h}$ = 0.165 m (Fig. 3.12). The undulant water surface had amplitude of several millimetres. Further downstream, the undulant surface was disturbed in association with the presence of the hemisphere.

The water surface shape above the upstream half of the hemisphere was similar to the shape of the upstream half of the hemisphere, with lower curvature; H increased towards the hemisphere crest (Fig. 3.12) where it was the highest within the test channel. The value of h

decreased from the upstream limit of the hemisphere to the hemisphere crest and flow became supercritical.

Downstream of the hemisphere crest, the water surface was depressed (Fig. 3.12). The depression was dish-shaped except over the downstream half of the hemisphere where the depression was similar in shape to the hemisphere below, with slightly greater curvature. At the downstream limit of the depression, 0.6 diameters downstream of the hemisphere crest, the supercritical flow passed through the most upstream wave of the undular jump. This most upstream wave was 0.026 m in amplitude and had an arcuate-shaped front. The undular jump diminished in amplitude to 0 over three wavelengths (total of 0.40 m). The three undular waves each extended to the flume sidewalls and were not reflected from the sidewalls in an obvious way.

For a distance of 7 diameters downstream of the undular jump in a central *water surface shadow* 1.7 diameters across-stream, the water surface was generally flat and oscillated in H by less than 0.001 m (the smoothest area on Fig. 3.12). Isolated dimples formed on the upper surface of the shadow with water rotating around them. Between two and ten dimples could be seen at any time and these were constantly in downstream motion. They were the water surface expression of vortices with a vertical axis of rotation (Brocchini & Peregrine, 2001) that emerged from the undular jump and passed downstream through the shadow close to the water surface. The water surface downstream of the shadow, and either side of it, undulated with amplitude on the order of several millimetres.

Flow passed the hemisphere from upstream to downstream through a mean cross-sectional area two thirds the size of the cross-sectional area upstream of the hemisphere. In association $\bar{u}$ around the hemisphere was on the order 1.5 times that of $\bar{u}$ upstream of the hemisphere. Considering Bernoulli's famous equation (Eqn. 3.1) there is necessarily a pressure drop between flow upstream of the dish shaped depression and flow through the dish shaped depression, associated with increased u.

$$P + \frac{1}{2}\rho u^2 + \rho gh = constant \qquad (3.1)$$

where P is pressure. On the water surface it can be assumed that P is constant and $u = \bar{u}$. The pressure drop affected sediment transport patterns presented and discussed later in this chapter.

Velocity patterns

At a distance of more than five diameters upstream of the hemisphere the velocity profile was parabolic (Profile 0, Fig. 3.13). As flow passed downstream the $\bar{u}$ profile changed. In a region extending 3 diameters upstream from the hemisphere, the parabolic $\bar{u}$ profile was decreased by half, below $z = 2/3\ r$ (compare Profiles 0, 1 and 5, Fig. 3.13). In the same region $\bar{u}$ close to the water surface was increased threefold compared to Profile 0 (to 1 m s^{-1}): flow appeared to have two layers. The velocity height gradient, $\dfrac{\partial \bar{u}}{\partial z}$ between the layers was the highest recorded from the $\bar{u}$ pattern. Towards the sidewalls the boundary between the two layers rose to $z = r$ and $\dfrac{\partial \bar{u}}{\partial z}$ between the layers decreased in magnitude (Profiles 4 and 8).

As flow passed either side of the hemisphere, between $4.88 < x < 5.12$ m, $\bar{u}$ increased in the lower layer (below $z = r$) and the two layers became indistinct. The $\bar{u}$ profile shape was approximately parabolic. Immediately downstream of the hemisphere, the $\bar{u}$ profile shape was the most complicated within the test channel (Profile 9, Fig. 3.13). In the region $0.15r < z < 0.45r$ and also above $z = r$, $\bar{u}$ was above 0.5 m s^{-1}. At most other positions within the profile $\bar{u}$ was less than 0.4 m s^{-1}; an upper jet edge was apparent at $z = 0.45r$ and a core of highest velocity within the jet was adjacent to the upper surface of the jet. Passing downstream from $x = 5.15$ m (the position of Profile 9) to 5.85 m (2.5 diameters further downstream), passing through the undular jump, flow slowed in the regions $0.15r < z < 0.45r$ and $z > r$. Over the same distance, at the other heights within the $\bar{u}$ profile, $\bar{u}$ increased. At the downstream limit of the undular jump, $\bar{u}$ was nearly constant through the full flow thickness with rapid decrease near the flume floor. Jet flow was no longer distinct.

Beyond 3.5 diameters downstream of the hemisphere, flow was faster underneath the shadow region (mean 0.55 m s^{-1}) and slower near the sidewalls (mean 0.45 m s^{-1}). Beyond 6 diameters downstream of the hemisphere the $\bar{u}$ profile shape was parabolic everywhere across the channel and $\bar{u}_{max}$ was below the water surface.
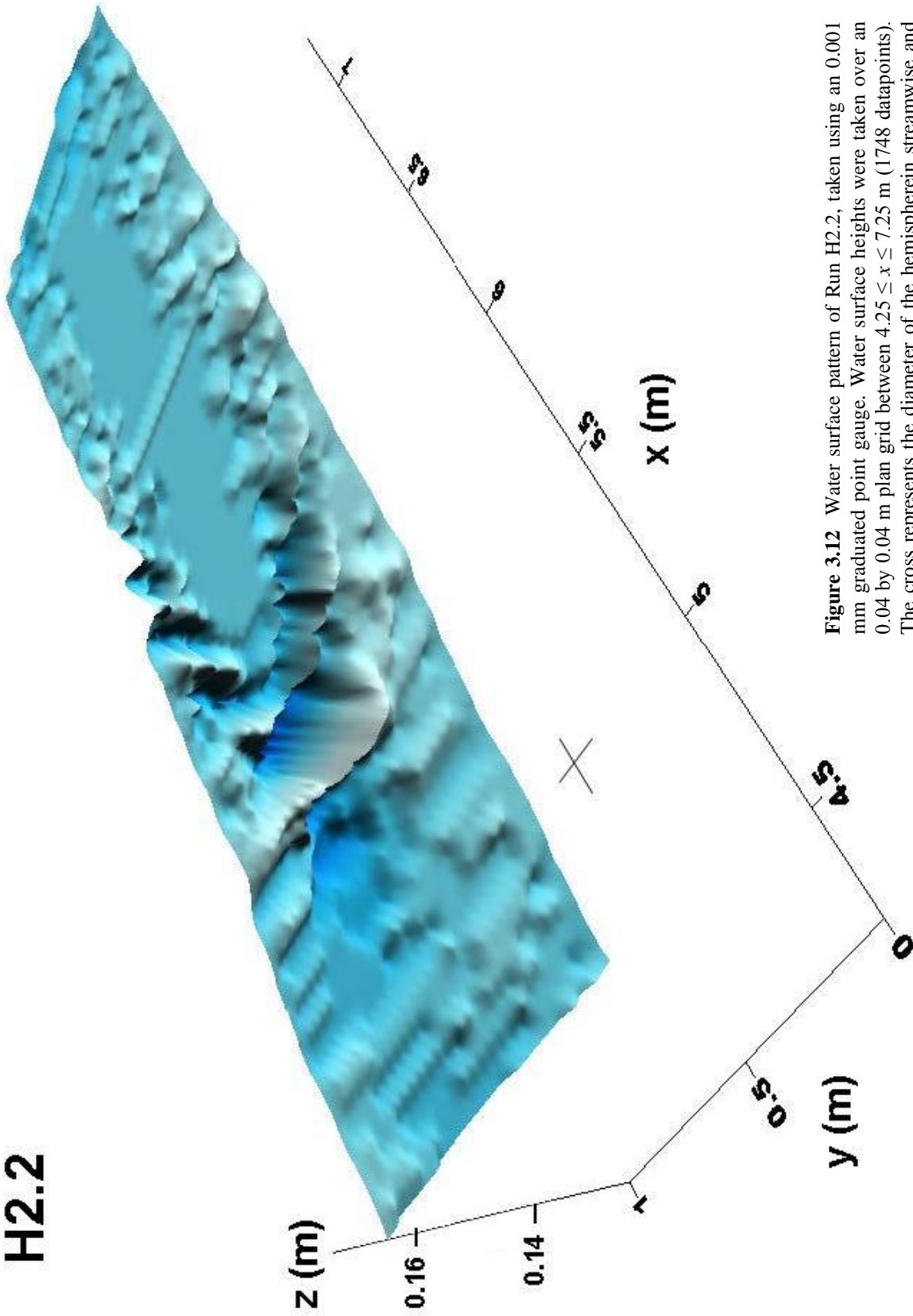
Figure 3.12 Water surface pattern of Run H2.2, taken using an 0.001 mm graduated point gauge. Water surface heights were taken over an 0.04 by 0.04 m plan grid between $4.25 \le x \le 7.25$ m (1748 datapoints). The cross represents the diameter of the hemispherein streamwise and stream-transverse orientations (drawn in perspective).
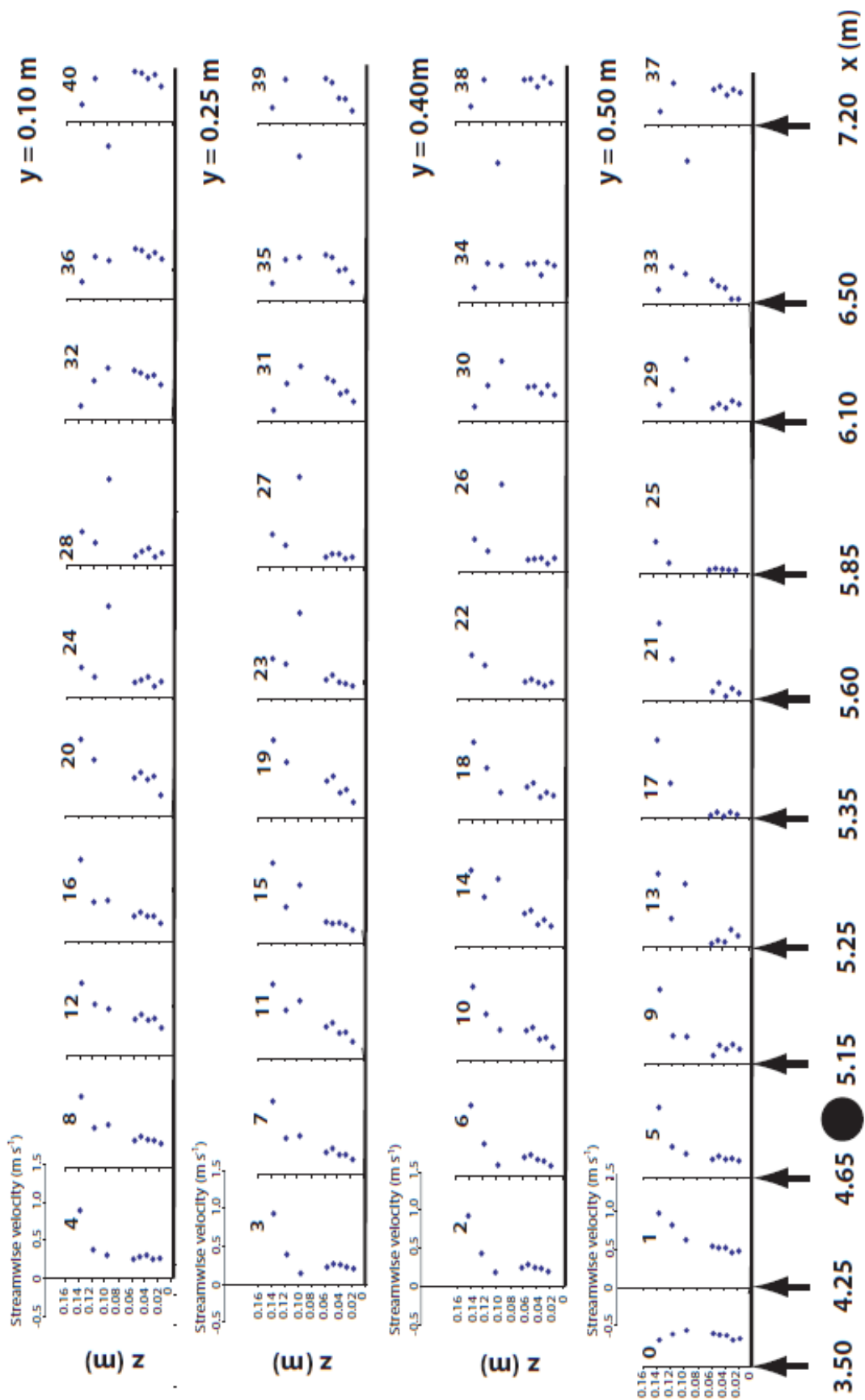
Figure 3.13 Velocity profiles 1 – 40 in the arrangement illustrated in Figure 3.2 for Run H2.2. An additional profile (Profile 0) was recorded at the position $x = 3.50$ m, $y = 0.50$ m. The black circle is used to indicate the streamwise position of the centre of the hemisphere ($x = 5.00$ m).

79

3.6.2 Run H2.4: The arcuate-fronted jump (Fr_u = 0.44)

Water surface shape

The cylindrical sinusoidal waves upstream of the hemisphere (§3.3) were 0.20 m in amplitude and 0.27 m in wavelength (Fig. 3.14). One cylindrical sinusoidal wave occurred at the streamwise position of the hemisphere and it was the most downstream of the sinusoidal waves. It was longer than the waves upstream of it and the amplitude was lower, both over the upstream half of the hemisphere where H was higher and either side of the hemisphere where H was lower. As H rose over the hemisphere, h decreased by 5/6 and became supercritical. The curvature of the dish shaped depression of the water surface did not appear to be affected by the curvature of the surface of the hemisphere. The depression spanned the width of the test channel, and was deepest at x = 5.10 m, at which position h = 0.12 m. At a distance of 0.4 diameters downstream of the hemisphere crest, flow passed through a hydraulic jump (Fig. 3.14). The hydraulic jump had a surface flow in the upstream direction, on the downstream face of the dish-shaped depression (the water surface expression of a roller, §1.4.2). In passing downstream through the hydraulic jump, flow thickened to just over 9/10 its thickness upstream of the hemisphere. Downstream of this thickening there was a shadow 1.3 diameters wide and 5.5 diameters long, in which water surface waves had an amplitude 5 – 10 times less than waves outside of the shadow (Fig. 3.14). Waves were cylindrical across the width of the shadow, had amplitudes on the order of millimetres and groups of adjacent waves occurred in patches approximately 0.25 m long.

Waves that flanked the shadow abutted the sidewall and had amplitudes up to 0.015 m (Fig. 3.14). The most upstream of these waves flanked the hydraulic jump; it had the highest water surface height (H) within the test channel. The waves that flanked the shadow decreased in amplitude over 4 wavelengths (2 m) as they increased in cross-stream span (Fig. 3.14). Their streamwise position oscillated on the order of 4 mm. The waves did not noticeably oscillate in the stream-transverse direction. In consequence, the accuracy of the point gauge values over these waves was ± 0.003 m.

Velocity patterns

At all measurement positions upstream of the hemisphere, the $\bar{u}$ profile had a parabolic shape with $\bar{u}_{max} = 0.9$ m s^{-1} at $z = r$ (e.g. Profile 1, Fig. 3.15).

For a distance of six diameters directly downstream of the hemisphere, the pattern of $\bar{u}$ was influenced by the presence of the hemisphere. Within the hydraulic jump, $\bar{u}$ was less than 0.01 m s^{-1} below $z = 0.2$ r and increased to 0.33 m s^{-1} at 0.5 r (Profile 9, Fig. 3.15) : the supercritical wall jet plunged down the downstream half of the hemisphere face underneath the hydraulic jump. Above this, $\bar{u}$ was negative at $z = 0.8$ r, according with the flow that was constantly seen to travel upstream. From this position to 1.5 diameters downstream, the negative peak in the $\bar{u}$ profile decreased to zero (compare Profiles 9 – 13 – 17 – 21, Fig. 3.15). Flow below 0.2 r also increased in $\bar{u}$, and $\bar{u}$ between 0.2 r and the negative part of the profile, decreased. Consequently $\bar{u}$ approached being uniform with height as the flow travelled downstream (compare Profiles 21 – 25 – 29 – 33, Fig. 3.15). The jet was indistinct downstream of $x = 6.50$ m. Either side of the hydraulic jump, as flow passed downstream, the $\bar{u}$ profiles generally maintained their parabolic shape, and additionally had a minimum in $\bar{u}$ at $z = 0.8$ r (Fig. 3.15). Further than six diameters downstream of the hemisphere the $\bar{u}$ profiles were generally parabolic in shape.

3.6.3 Run H2.6: The overturning arcs ($Fr_u = 0.53$)

Water surface shape

In Run H2.6, without varying the flume discharge the hydraulic jump repeatedly changed in form, spending up to tens of seconds in the arcuate-fronted state and up to several minutes in the arcs of overturning water shape (both shapes first described in §3.4.1). All waves upstream of the hemisphere were cylindrical, sinusoidal in the streamwise direction, 0.19 m in amplitude and 0.5 m in wavelength. One of the wave peaks was a short distance upstream of the hemisphere (Fig. 3.16). The height of the water surface above the flume floor remained as high as the wave crest over the upstream half of the hemisphere but decreased either side of the hemisphere. Flow thickness decreased by 9/10 where the water flowed over the hemisphere and in association the flow became supercritical. The dish shaped depression of the water surface had an upstream limit at $x = 4.93$ m, was 1.3 long and was truncated laterally

H2.4
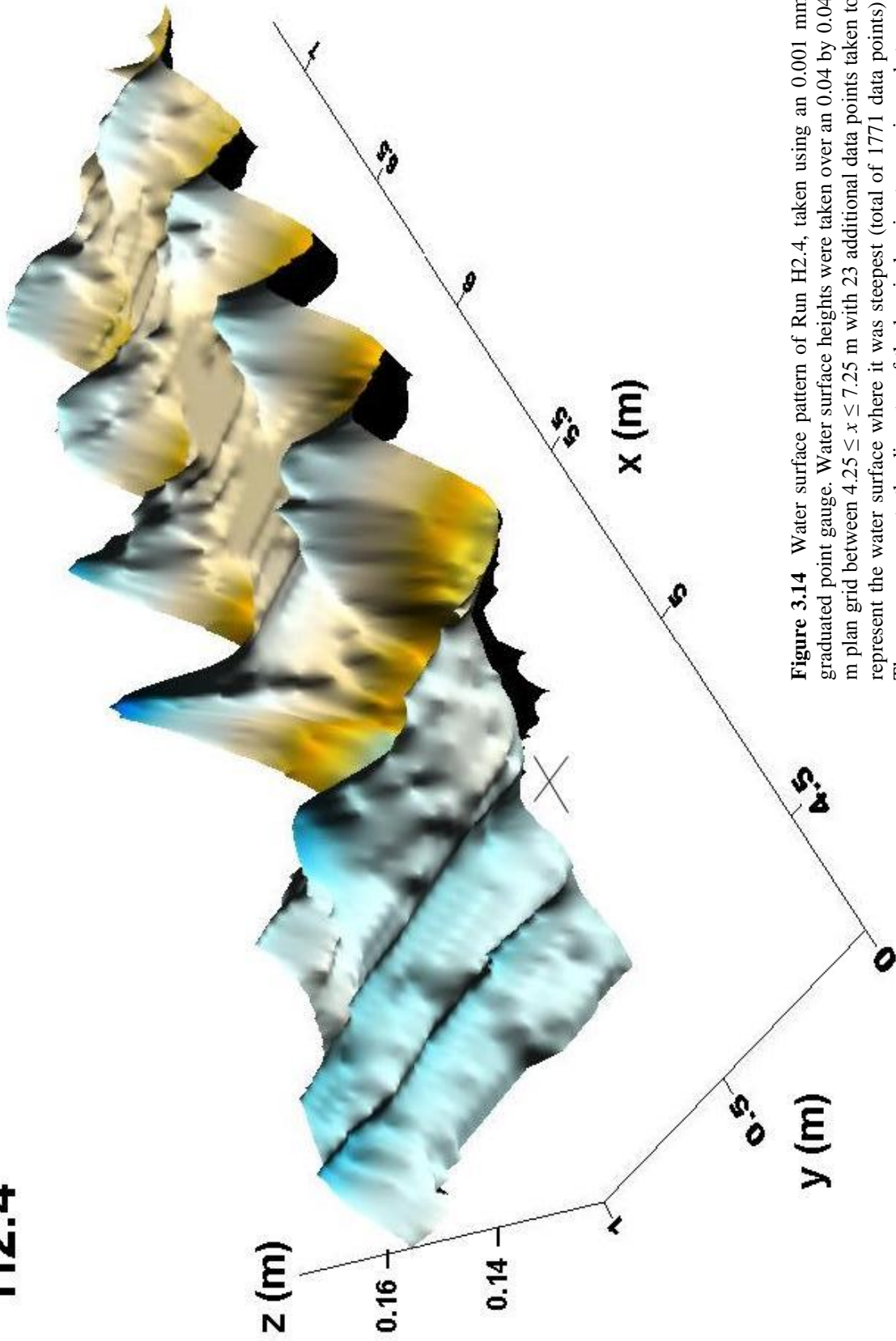
Figure 3.14 Water surface pattern of Run H2.4, taken using an 0.001 mm graduated point gauge. Water surface heights were taken over an 0.04 by 0.04 m plan grid between $4.25 \leq x \leq 7.25$ m with 23 additional data points taken to represent the water surface where it was steepest (total of 1771 data points). The cross represents the diameter of the hemispherein streamwise and stream-transverse orientations (drawn in perspective).
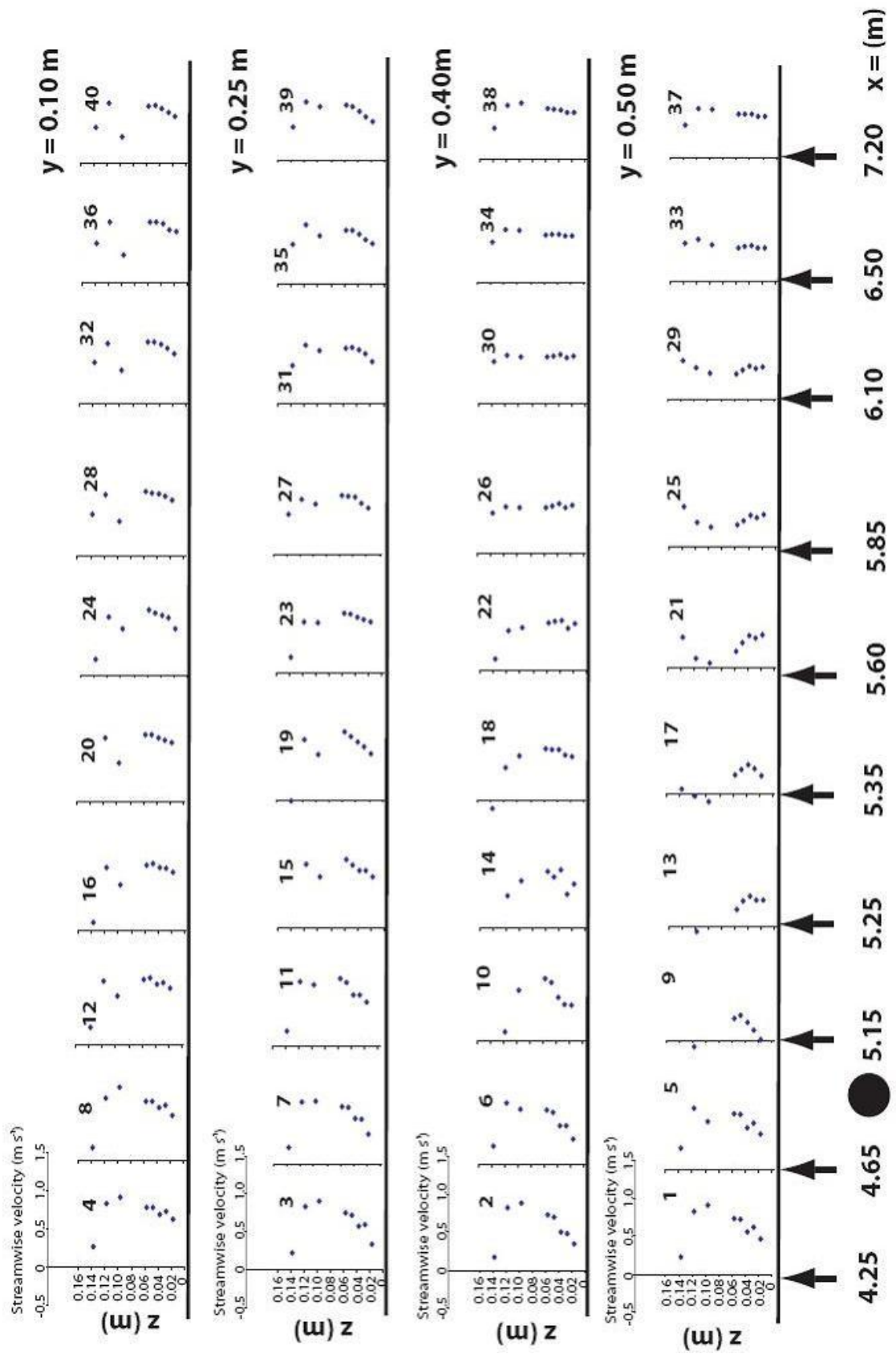
Figure 3.15 Velocity profiles 1 – 40 in the arrangement illustrated in Figure 3.2 for Run H2.4. The black circle is used to indicate the streamwise position of the centre of hemisphere ($x = 5.00$ m).

by the sidewalls. The upstream limit of the hydraulic jump was 0.8 diameters downstream of the hemisphere crest, on the upstream half of the face of the depression. There was no water surface shadow along the centre of the channel downstream of the hemisphere, instead a series of cross-flow waves occurred downstream of the hydraulic jump, making a diagonal pattern across the width of the test channel. The water surface was concave-up within the diamonds.

Velocity patterns

In Run 2.6 velocity was only recorded downstream of the hemisphere. Flow was 0.07 m thick at the bottom of the concave up depression and the trends in the shape of the $\bar{u}$ profiles (Fig. 3.17) were different to those within the depressions of Runs H2.2 and H2.4 (Figs 3.13 and 3.15). Considering flow along the channel centerline: One diameter downstream of the hemisphere $\bar{u}_{max}$ was within 0.02 m of the flume floor and $\bar{u}$ decreased with height (Profile 13, Fig. 3.17). By 1.5 diameters downstream of the hemisphere the flow had gone through the hydraulic jump. $\bar{u}_{max}$ had more than doubled and its position had risen to 0.8 h whilst the lower half of the flow had very low $\bar{u}$ (Profile 17, Fig. 3.17). The core of highest velocity was in an upper part of the flow and a lower jet edge could be detected around $z = 0.09$ m (jet edges defined §1.9.3). Further downstream the lower part of the flow quickened and the upper half slowed; $\dfrac{\partial \bar{u}}{\partial z}$ between the upper and lower parts decreased (compare Profiles $17 - 21 - 25$, Fig. 3.17). At $x = 5.60$ m, and further downstream, the jet became indistinct and the $\bar{u}$ profile had a parabolic shape (compare Profiles $25 - 29$, Fig. 3.17). Away from the centerline, flow had a parabolic shape upstream of the depression (Profile 16, Fig. 3.17). Within the depression $\bar{u}$ generally increased with height and $\bar{u}_{max}$ was the highest within the test channel (e.g. Profile 19, Fig. 3.17). As flow thickened through the downstream half of the depression, $\bar{u}$ approached being uniform with height (e.g. Profile 27, Fig. 3.17) and further downstream the shape of the $\bar{u}$ profile approached being parabolic (separately compare Profiles $27 - 31$ and Profiles $26 - 30$, Fig. 3.17).
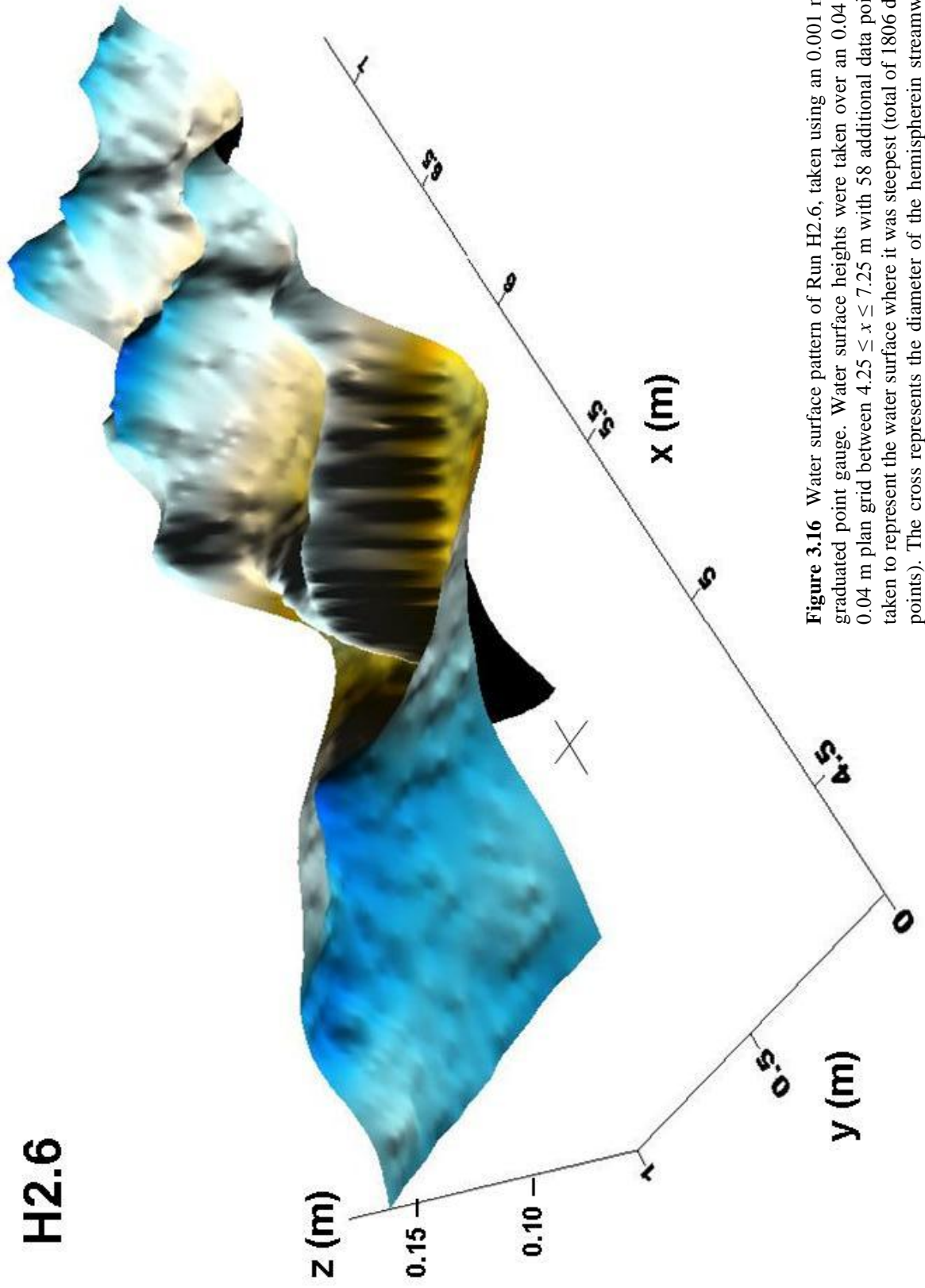
Figure 3.16 Water surface pattern of Run H2.6, taken using an 0.001 mm graduated point gauge. Water surface heights were taken over an 0.04 by 0.04 m plan grid between $4.25 \leq x \leq 7.25$ m with 58 additional data points taken to represent the water surface where it was steepest (total of 1806 data points). The cross represents the diameter of the hemispherein streamwise and stream-transverse orientations (drawn in perspective).

85
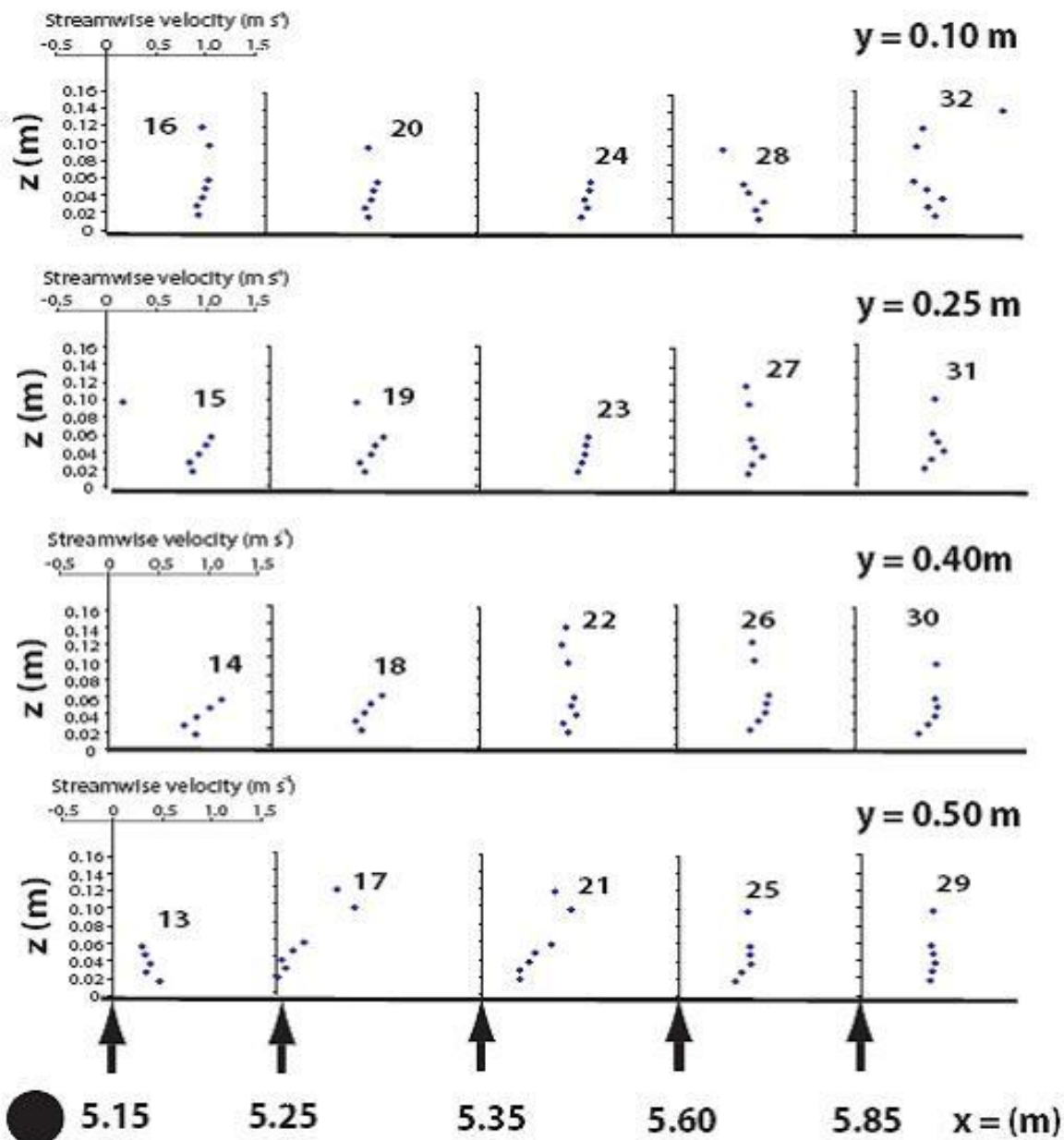
Figure 3.17 Velocity profiles 13 – 32 in the arrangement illustrated in Figure 3.2 for Run H2.6. Measurements were not taken at locations 1 – 12 or 33 – 40. The black circle is used to indicate the streamwise position of the centre of hemisphere ($x = 5.00$ m).

3.7 THE PATTERNS OF SEDIMENT TRANSPORT

As soon as pumping was started in each run involving sediment, small amounts of sediment travelled in suspension and within 240 s a pattern of bedload transport had formed over the

whole flume floor. The suspended sediment hardly impaired the view of the floor. The developing bedload transport patterns described here were directly observed. Bedload features formed. Regions of the bedload features are defined as plan areas in which at least one pair of adjacent bedload features were the same type and the same order of magnitude in height and length. The regions of the bedload features were documented, first with the hemisphere present (§3.8) and then with the hemisphere not present (§3.9). Following the description of all the runs involving sediment, and comparing results with published reports of subcritical runs, the influence of the hydraulic jumps on the bedload transport patterns is picked out (§3.10 and §3.11).

For the duration of each run involving sediment, the movement of sediment did not obviously change the patterns of the water surface, velocity or vorticity. Sediment left the prepared bed as a sheet or as isolated grains and moved downstream. Generally more sediment left the prepared bed than fell into the sediment trap downstream of the test channel (Fig. 2.2A) so the total bedload transport within the test channel increased with time. The bedload features and the regions of bedload features both generally grew with time but for occasional durations of up to tens of seconds some bed features did not grow or reduced in size. Almost all bedload features were transitory and because run durations were short it is unlikely that the transport pattern reached equilibrium condition.

All bedload transport patterns involved two regions with upstream limits at the honeycomb structure at the upstream end of the flume, between the sidewall and 0.15 m closer to the channel centreline, in which only a few small bedforms appeared (honeycomb structure introduced in §2.2.2). The bedforms in this region had the appearance of ripples and were less than a few centimetres in length and width. Both regions narrowed downstream. All bedload transport patterns also involved at least one region of incipient dunes upstream of the hemisphere (Fig. 3.18 B – D). Each incipient dune was almost ubiquitously separated from the next upstream or downstream one by bare flume floor (i.e. was "starved"), because of the small volume of sand used in the runs and the associated low bedload transport rate. All ripples and incipient dunes that were observed had a shallow stoss face and a steep lee face. The bedload transport patterns also involved one region either side of the hemisphere in which bedload travelled faster than within any other region: these regions are termed the regions of rapid bedload transport. Directly upstream of the hemisphere, no bedload was observed to

Subcritical

A

Werner et al. (1980)

Flow direction in all examples

B Undular

C Arcuate fronted

Bedform-free shadow

Region of rapid bedload transport

D Overturning arcs

Incipient dunes

Horseshoe gaps

88

Figure 3.18 (above) Photograph montage of the sediment transport patterns at the end of Runs H2.2, H2.4 and H2.6 taken from above. The sediment transport pattern of Werner *et al*. (1980), formed under subcritical flow, is displayed for comparison. All photographs are reproduced at same scale. The curved black lines represent the positions of the toes of the hydraulic jumps. Each bedload transport pattern has at least one region of incipient dunes, one horseshoe gap, two regions of rapid bedload transport either side of the hemisphere and one bedform-free shadow downstream of the hemisphere.

enter a region approximately 0.4 diameters in length with upstream limit the same shape as the upstream edge of the hemisphere. This region extended around both sides of the hemisphere underneath the horseshoe shaped vortex (§3.1.1) and termed *the horseshoe gap* (Fig. 3.18A – D). One final region containing no bedload features formed underneath and downstream of the water surface shadow and is termed the *bedform-free shadow* (Fig. 3.18A – D). A small amount of sand entered the bedform-free shadow from the bedload features both sides of it, and was transported downstream through the shadow area.

Most bedload features migrated downstream through the regions. As bedload features migrated close to the hemisphere from upstream, they either changed shape or accumulated onto a larger feature close to the hemisphere. As bedload features closer to the sidewalls migrated downstream they were washed out in the regions of rapid bedload transport either side of the hemisphere (Fig. 3.18B – D). No bedload was observed to travel over the top of the hemisphere in any of the runs. Sediment grains that travelled between bedforms along the flume floor did so an order of magnitude faster than the bedforms travelled.

3.7.1 Runs MH2.2 and MH2.2a: Transport of medium sand involving an undular jump
The regions adjacent to the sidewalls with upstream limit at the honeycomb structure, pinched out to the flume sidewalls well upstream of the hemisphere (Fig. 3.18B). Although little sediment was directly observed to pass through them, obvious mounds of sediment developed at their downstream limits.

One type of bedload feature, with shallow stoss face and steep lee face, formed upstream of hemisphere. These bedload features are termed incipient dunes because the flow and sediment characteristics plot in the dune phase of the bedform phase diagrams of Carling (1999) and Van den Berg and Van Gelder (1993). They occurred at all streamwise locations between the upstream limit of the test channel and the upstream limit of the horseshoe gap (Fig. 3.18B). They grew laterally until they spanned the width of the test channel and were approximately cylindrical. They generally remained cylindrical as they migrated downstream;

occasionally one would split into two lateral parts, or two would combine by joining laterally or by streamwise cannibalisation. They took longest to develop their cylindrical shape in a triangular area immediately upstream of the hemisphere (cf. Fig. 3.19; the base of the triangle is indicated). Initially, the base of the triangle was the same width as the hemisphere and the area extended 2.6 m upstream along the centreline. The triangle diminished in size as the crest length of the bedforms increased, and could no longer be detected by $t = 25$ minutes.
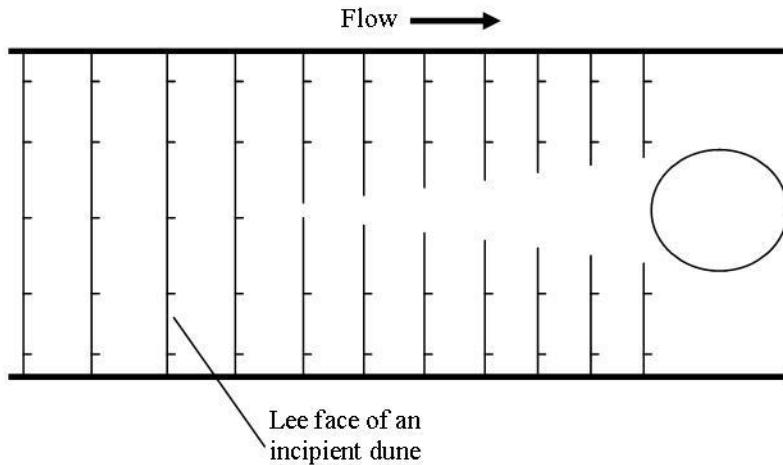
Figure 3.19 The pattern of incipient dunes upstream of the hemisphere. Dunes took longest to develop in a triangular region immediately upstream of the hemisphere; not to scale.

As the incipient dunes migrated downstream into a region $1 - \sim 0.4$ diameters upstream of the hemisphere they changed shape, taking on the same curvature as the leading edge of the hemisphere (Fig. 3.18B). At all times during both runs, either two or three bedforms were curved. The curved parts of the bedforms were as wide as the hemisphere. The curved bedforms never amalgamated. Each bedform approached the hemisphere but stalled at the horseshoe gap. Sand grains travelled outward, along the lee face of the stationary bedform, or along the flume floor a few millimetres downstream of it. Sand grains left the stationary bedform at its stream-transverse limits and entered the regions of rapid bedload transport that flanked the hemisphere. Each most downstream curved feature reduced in size over time until it disappeared. It was replaced by the next-most-upstream curved feature. The part of the incipient dunes closer to the sidewalls remained cylindrical as they approached the sides of the hemisphere. They were washed out alongside the upstream limit of the hemisphere (Fig. 3.18B), the upstream limit of the region of rapid bedload transport. Bedload sheets formed in the region of rapid bedload transport with a lunate downstream edge (Fig. 3.18B; what class of bedform they were, is discussed in §3.11.3). Up to six sheets up to 10 grain diameters thick

were present in each region of rapid bedload transport at any time; they were up to 0.18 m long and 0.15 m across and travelled downstream faster than the incipient dunes.

Downstream of the region of rapid bedload transport, cylindrical starved incipient dunes developed (Fig. 3.18B) and migrated downstream on the order of one millimetre per second. At their upstream limit these incipient dunes had the same cross-stream span as the regions of rapid bedload transport, and their crest lengths increased downstream. Either side of the bedform-free shadow the crests were generally mirror images. Their plan orientation changed gradually downstream from (1) the end of the dune crest adjacent to the bedform-free shadow being further upstream than the end adjacent to the sidewall, to (2) the end of the dune crest adjacent to the bedform-free shadow being further downstream than the end adjacent to the sidewall (Fig. 3.18B). The most upstream 6 − 7 incipient dunes were in orientation (1) and the other incipient dunes were in orientation (2).

The bedform-free shadow was a distance of 15 diameters long (Fig. 3.18B). It was 0.40 m wide at its upstream limit and became narrower downstream as the crest lengths of the cylindrical bedforms either side increased. Its width varied by less than a few centimetres over the duration of each run. At the downstream limit of the bedform-free shadow, bedforms developed with lunate plan form (Fig. 3.18B). These bedforms grew laterally slowly compared to all other features in the bedload pattern, associated with the low sediment flux through the bedform-free shadow. When each bedform reached the downstream end of the test channel, it fell into the sediment trap (Fig. 2.2A).

3.7.2 Run MH2.4: Transport of medium sand involving an arcuate-fronted jump

Bedload transport patterns more than one diameter upstream of the hemisphere were very different to those observed in Runs MH2.2 and MH2.2a. After $t = 240$ seconds fewer bedforms were observed upstream of the hemisphere and they were spaced further apart (compare Fig. 3.18B and C). I saw a body of sand, the largest in the bedload transport pattern, with two downstream-pointing tails that were 0.2 m wide at their upstream limit and decreased to 0 m wide over their length (Fig. 3.18C). Mounds of sand formed underneath the peaks of the cylindrical waves (mounds Fig. 3.18C; waves Fig. 3.14). The mounds were approximately four times as long in the streamwise direction as the incipient dunes of Runs MH2.2 and MH2.2a. Short streamwise-oriented streaks were seen in a region around $y = 0.5$ m (Fig.

3.18C). The two regions of bare flume floor adjacent to the sidewall with upstream limit at the honeycomb structure extended the whole length of the test channel.

Bedload transport patterns around and downstream of the hemisphere had distinct similarities to those observed in Runs MH2.2 and MH2.2a. Another body of sand, the second largest in the bedload transport pattern, formed upstream of the hemisphere in the area that curved ripples formed in Runs MH2.2 and MH2.2a (compare Fig. 3.18B and C). It grew in height, length and width throughout Run MH2.4. From t = 240 seconds onwards it had a concave-downstream avalanche face that was stationary, at the upstream limit of the horseshoe gap and was wider than the hemisphere. Bedload was transported away from the body of sand, from the stream-transverse limits of its avalanche face, fed directly from bedload transport over the stoss face of the body as well as from grains travelling outward along the avalanche face.

The regions of rapid bedload transport that flanked the hemisphere were longer in the streamwise direction compared to Runs MH2.2 and MH2.2a (compare Fig. 3.18B and C). No bedload sheets formed as sand was transported through them. Downstream of these regions, mounds of sand formed underneath the wave peaks (mounds, Fig. 3.18B; wave peaks, Fig. 3.14). These are incipient starved antidunes according to the bedform phase diagrams of Carling (1999) and Van den Berg and Van Gelder (1993). The mounds had the same cross-stream width as regions of rapid bedload transport. Bedload moved between the mounds on the order tens of centimeters per second, and at times the mounds were indistinguishable in plan view because of the sediment being transported between them. The mounds could be distinguished from the bedload, through the sidewall because they were at least four grains thick and because they contained stationary sediment at their base. No other bedload features were seen downstream of the hemisphere.

The bedform-free shadow extended to the downstream end of the test channel: where it had been 15 diameters long in Runs MH2.2 and MH2.2a it was more than 20 diameters long in Run MH2.4. Its width was 0.44 – 0.60 m throughout. The small amount of bedload transported through this shadow area fell directly into the sediment trap without stalling.

3.7.3 Run MH2.6: Transport of medium sand involving arcs of overturning water

The pattern of bedload transport was similar to that observed in Run MH2.4 (compare Fig. 3.18C and D; flow conditions in Table 3.2). The largest body of sand in the bedload transport pattern was similar in appearance to the largest body of sand observed in Run MH2.4 (§3.8.2) but was longer in the streamwise direction (compare Fig. 3.18C and D). Between the two tails of the largest body of sand, incipient dunes were seen in two streamwise rows (Fig. 3.18D). The stream-transverse limits of these bedforms abutted the tails; they did not lie on top of the tails. The region of rapid bedload transport around the hemisphere was 1.3 times as long as in Run MH2.4 and had a smaller cross-stream extent at its downstream limit (compare Fig. 3.18C and D). The incipient starved antidunes that formed under wave peaks downstream of the regions of rapid bedload transport were wider in the cross-stream direction than the region of rapid bedload transport.

3.7.4 Run CH2.2: Transport of coarse sand and fine gravel involving an undular jump

Flow over the prepared bed of coarse sand and fine gravel reworked the bed into a feature with a complicated shape well upstream of the hemisphere. This bed feature was still developing at the end of the run. The feature migrated downstream as it developed. At least several tens of grains left the feature per second, and passed downstream. On several occasions each up to several minutes long, grains did not leave the downstream limit of the feature but left a more upstream part of the feature and reattached to the feature further downstream without passing the hemisphere or hydraulic jump. At these times there was no nett transport of sediment away from the feature.

When grain supply away from the feature was from the centre of the downstream limit of the shape, another bedload feature developed upstream of the hemisphere with a similar character to that which developed in Runs MH2.4 and MH2.6. It had a stationary lunate downstream edge, at the upstream limit of the horseshoe gap. Grains were transported off its stream-transverse limits. At times when grains were not supplied to the feature along the centre of the test channel the feature diminished in size. No other bedload features formed within the test channel. All grains that passed the hemisphere continued in motion until they fell into the sediment trap.

3.8 WATER SURFACE PATTERNS WITHOUT THE HEMISPHERE OR HYDRAULIC JUMP

Three runs were undertaken with equivalent water conditions and pumping rate to Runs H2.2, H2.4 and H2.6 but without the hemisphere, to determine the effect of the hemisphere on the flow and sediment transport patterns. They were termed Runs N2.2, N2.4 and N2.6 with N denoting no hemisphere. The water surface pattern throughout the test channel was equivalent to the water surface pattern at a distance of more than six hemisphere diameters upstream of the hemisphere in Runs H2.2, H2.4 and H2.6. Specifically, in Run N2.2 the water surface was undulant with amplitude of several millimetres and a mean water surface height of 0.165 m. In Run N2.4 there were cylindrical sinusoidal waves on the water surface that were 0.20 m in amplitude and 0.27 m in length. In Run N2.6 there were cylindrical sinusoidal waves on the water surface that were 0.19 m in amplitude and 0.5 m in length.

3.9 SEDIMENT TRANSPORT PATTERNS WITHOUT THE HEMISPHERE OR HYDRAULIC JUMP

Four runs were undertaken with the same experimental conditions as Runs MH2.2, MH2.4, MH2.6 and CH2.2, except that the hemisphere was not present in the test channel (Table 3.3). These runs were assigned the codes MN2.2, MN2.4, MN2.6 and CN2.2, with N indicating *no hemisphere*. In each one the bedload transport patterns between $0 \leq x \leq 4.64$ m were similar to the equivalent runs with the hemisphere. The bedload transport patterns further downstream than $x = 4.64$ m (equivalent to one diameter upstream of the hemisphere) are described:

In Run MN2.2, incipient dunes were seen at all streamwise and stream-transverse locations (Fig. 3.20A). None were curved; none had an apex pointing upstream or downstream. The pattern made by the incipient dunes was complicated. In general the dunes became less cylindrical with increasing distance downstream. Bedload transport rate was increasingly variable with distance downstream. Bedload transport rate was lowest in the region $6 \leq x \leq 10$ m, $0.35 \leq y \leq 0.65$ m (Fig. 3.20A). In this region bedforms took tens of minutes to grow and coalesce into bedforms that spanned the width of the test channel.

In Run MN2.4, bedload travelled downstream at all streamwise locations (Fig. 3.20B). Mounds formed underneath the peaks of the cylindrical sinusoidal waves between $0.1 \leq y \leq 0.9$ m and had lower height than the incipient starved antidunes formed in Run MH2.4. These mounds were difficult to detect in Fig. 3.20B because they were substantially reworked by the waning flow as pumping was stopped.

In Run MN2.6 the only bedforms observed were mounds of sediment under the peaks of the cylindrical sinusoidal waves. At the end of Run MN2.6, waning flow reworked the pattern out of all recognition, within several seconds. Consequently no photographs of the bedload transport patterns are presented.

In Run CN2.2 a bedload feature with a complicated shape formed upstream of $x = 4.64$ m. All grains that left the complicated feature were transported downstream by the flow, without stalling, and fell into the sediment trap.

3.10 DISCUSSION OF THE PATTERNS OF THE FLOW

Because a toe was common to all forms of the hydraulic jump and was a more distinct feature than the position of h_2 it is used as a point of reference in the following discussion.

3.10.1 Influence of the hemisphere and hydraulic jump on vorticity patterns

No quantitative analysis of vorticity was made but several aspects of the water surface, velocity patterns and boundary conditions (§3.4 – §3.6) allow aspects of the pattern of vorticity within the flow to be stated. Turbulent sweeps and bursts, inherent in flows of high *Re* (Allen, 1982) are associated with the production of vorticity near a boundary; some vorticity would have been present at all plan positions of the flow.

The rolling up of the boundary layer upstream of the hemisphere (§3.1) was a source of vorticity in the flow, but this vorticity is unlikely to have travelled along a horseshoe-shaped track as occurs around hemispheres in subcritical flows (cf. Fig. 3.21B). Instead vorticity would travel more laterally, below the dish shaped depression above the hemisphere (§3.3). Associated with the shape of the depression a hydrostatic pressure gradient acted radially towards the centre of the dish. Vorticity, transported with the fluid, would have travelled from higher to lower pressure. A more lateral release of vorticity is depicted in Figure 3.21C.

The continual breaking and spilling of the fronts of the hydraulic jumps were another source of vorticity. The physical mechanism for the creation of vorticity on a breaking front has some qualitative similarities to that invoked for plunging breakers by Hornung *et al*. (1995) and Brocchini and Peregrine (2001). The vorticity introduced into the flow in this way added to the vorticity in the roller (itself an expression of vorticity in the upper part of the hydraulic jump). The vortices seen emanating downstream from the arcuate fronted jumps (cf. §3.6.2) were expressions of vorticity passing downstream from the hydraulic jump.
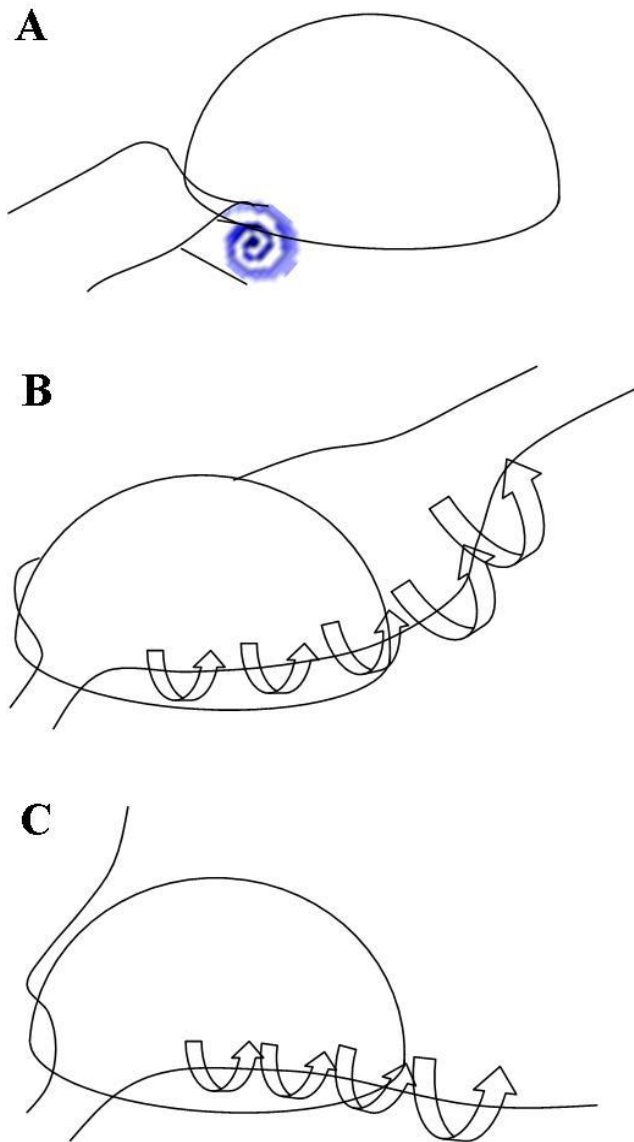
Figure 3.21 (A) Rolling-up of the boundary layer and (B) the horseshoe vortex system around a hemisphere under subcritical flow (after Best & Brayshaw, 1985). (C) The track of vorticity transport in association with supercritical flow: the tubular vortex is released more laterally, over and around the hemisphere.

3.10.2 Water surface patterns with and without the hemisphere

Three of the features of the water surfaces that were present only when the hemisphere was present (the dish shaped depression, supercritical flow and hydraulic jump; §3.3, §3.4) were influenced directly by the hemisphere. Two of the features (the water surface shadow and the waves that flanked it) were influenced indirectly by the hemisphere but directly by the hydraulic jump. The size, position and curvature of the dish shaped depressions was controlled by the shape of the hemisphere and the Froude number of the supercritical flow via Equation 1.6 (§1.4.3).

3.10.3 Shape and plan position of the hydraulic jumps

The undular form of the jump was expected first, with increasing pumping rate, because it is associated with flows slightly above supercritical (Chanson, 1999). Arcuate fronts of single undular and hydraulic jumps have been seen in other situations of converging supercritical flow such as downstream of a horseshoe waterfall (e.g. Pasternack *et al.*, 2007). In the case of the horseshoe waterfall the plan shape of the toe can be partly sculpted by the shape of the waterfall, but downstream of isolated obstacles arcuate fronted jumps are not surrounded by solid topography. The arcuate fronts I saw in my experiments were sculpted by the dish shaped depressions of the water surface, themselves deformable boundaries. The Froude number of the supercritical flow and the shape of the boulder, that controlled the size, position and curvature of the depression (§3.10.2) indirectly controlled the shape of the arcuate fronted jump. The position of the downstream face of the obstacle may act together with the flow conditions (chiefly the Froude number of flow overtopping the hemisphere) to fix the upstream limit of the toe, but it would not sculpt the toe.

Pairs of overturning arcs have been described in open channel flows before, firstly by Kennedy (1961) who called them *rooster tails*. They are sometimes seen on stationary waves above sand bedforms (cf. Fig. 3.22). The sand bedforms in Fig. 3.22 were not bluff bodies: a bluff body is not required for the arcs of overturning water to form. Pairs of overturning arcs have not previously been described as hydraulic jumps but in this chapter it has been shown that they certainly are; flow being supercritical upstream of the overturning arcs and subcritical between them (§3.6.3). Kennedy (1961) postulated that the arcs were caused by shock waves emanating from his flume sides and Montes (1986) described a diamond pattern

of water surface waves that he inferred was the pattern of shock waves, with the upstream limit being adjacent to his flume sidewalls. However, because the upstream limit of the diamond pattern of water surface waves was a diamond apex at the channel centreline ($y = 0.5$ m), unlike the diamond pattern of Montes (1986), the pattern observed in my experiments cannot be attributed to shock waves emanating downstream from the flume sidewall.
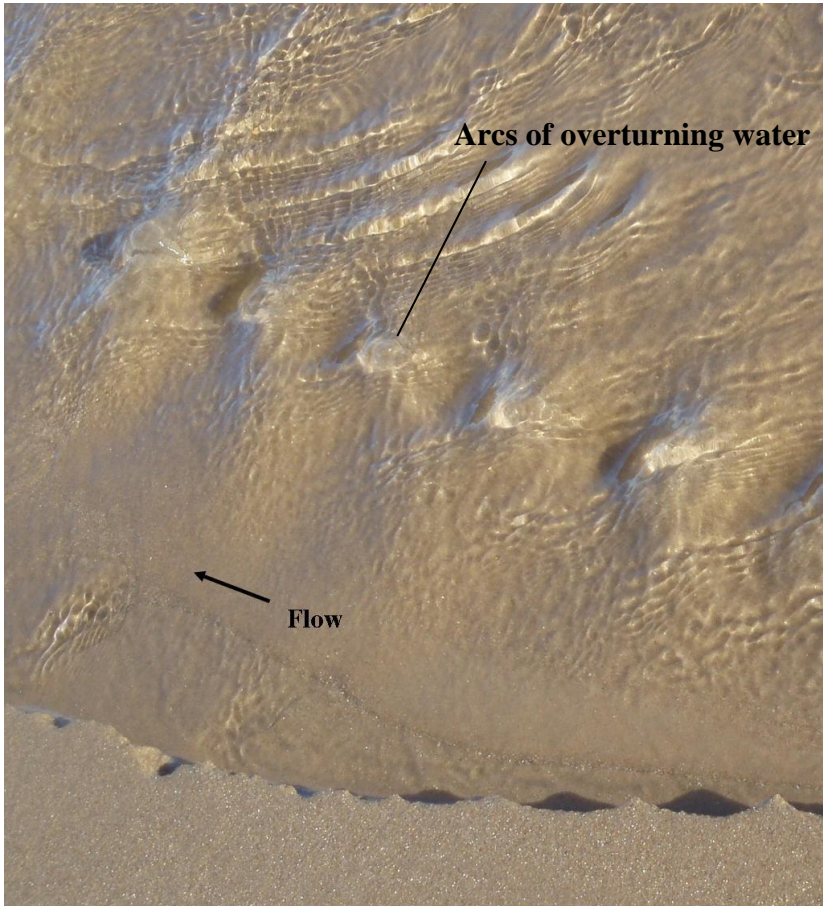
Figure 3.22 Photograph of the arcs of overturning water (Fig. 3.9C and D) documented within a train of supercritical antidunes. Kennedy (1961) described these features as looking like "rooster tails". In the photograph, flow was a few centimetres thick and the channel bed was medium sand.

3.10.4 The change in form between undular jumps, arcuate fronted jumps and arcs of overturning water

Whilst transitions between forms of cylindrical hydraulic jumps are classified as being gradual (cf. Massey, 1983), transitions between each of the forms (1) – (4) of the hydraulic jumps in my experiments were abrupt. Each form (1) – (4) was a discrete flow component and existed in a discrete range of values of Fr_u. The transition from form (1) to form (2) may have been a transition from undular to weak hydraulic jump in the classification of Massey (1983).

Because the steady pumping rate in Run H2.6 resulted in flow conditions on the cusp of (form 2) the arcuate fronted hydraulic jumps and (form 3) the arcs of overturning water, the transition between these two forms of hydraulic jump must have been sensitive to some controlling parameter(s). Flow stage (or Froude number of flow overtopping the hemisphere by association with flow stage) can influence the transition from (2) to (3), which can also be seen in wave backwash on beaches, a process involving decreasing flow stage (Video file 2, Appendix 2). Hydraulic jumps would not form in wave swashes because there is not a continuous flow downstream of the swash (it has a downstream limit) but the reverse transition, (3) to (2) is potentially controlled by an increasing flow stage. In the steady pumping rate of Run H2.6, changes in flow stage over the hemisphere could have been associated with streamwise oscillation of the cylindrical sinusoidal wave with crest just upstream of the hemisphere (Fig. 3.16). Other candidate parameters for the repeated change of form between overturning arcs and arcuate-fronted hydraulic jumps are the length and position of the track taken by the jet of water passing over the hemisphere into the hydraulic jump. Flow into hydraulic jumps have been modelled using wall jets (defined in §1.9.3) since Rajaratnam (1965). Silberman (1959) determined that when a wall jet passes into a hydraulic jump the jet can detach from the channel floor. In Chapter 4 and Macdonald *et al*. (2009) it is shown that for $Re > 10^5$, the position of the jet core (§1.9.3) can vary between directly under a roller (defined in §1.4.2) and closer to the channel floor, with minimal changes in stage or pumping rate. In the overturning arcs, the jet had "fully detached", defined as being the case where the upper jet edge is the free water surface and a region of separated flow exists below a lower jet edge. Because jet detachment is sensitive to Re (Silberman, 1959) the position of the jet increased in height with Re (undular jump to arcuate fronted jump to overturning arcs, Table 3.2). The jet also diverged symmetrically away from the centreline (along the crest of the arcs). The divergence was possibly stimulated by upwelling of flow passing around the dish shaped depression and underneath the arcs, but the occurrence of the diverging flow is a topic for future research.

3.11 DISCUSSION OF THE PATTERNS OF SEDIMENT TRANSPORT

3.11.1 Comparisons of bedload transport patterns with and without a bed-attached hemisphere

The patterns of sediment transport in Series MH are compared to Series MN (without the hemisphere) to determine the effect of the hemisphere on the sediment transport pattern, and to published bedload transport patterns around obstacles under subcritical flow to determine the effect of the hydraulic jump on the sediment transport pattern. Werner *et al*. (1980) and Best and Brayshaw (1985) monitored sediment transport around hemispheres (Table 3.1) and their studies are comparable with most of my runs because of the following important similarities:

- The hemisphere was fixed flat side down on the centreline of the flume.
- The hemisphere was fully submerged by the flow.
- The ratio y/d was less than 10 (§3.2.1) and the hemispheres caused a blocking effect on the flow (Chanson *pers*. *comm*.).
- Bedload transport occurred over the flume floor at all streamwise locations.

Sutton and McKenna-Neuman (2008a) produced sediment transport patterns around cylinders in air flows, with important similarities. I also make comparisons between sediment transport immediately downstream of the hemisphere and sediment transport downstream of Thompson's (2008) bed attached cuboids. Thompson (*loc*. *cit*.) prepared sediment mounds immediately downstream of the cuboids and monitored the development of the mounds in sediment starved conditions whilst rising stage, steady and falling stage flows passed over them.

3.11.2 Influence of the hemisphere on the patterns of sediment transport

In most respects the bedload transport patterns with and without the hemisphere were similar except for five features that were present only when the hemisphere was present. The hemisphere caused these five features to occur.

Extending a long way upstream of the hemisphere, the triangular region in which bedload features took longest to develop (§3.8.1) was associated with the hemisphere rather

than with the hydraulic jump and was due to low rates of bedload transport into and within the region.

Immediately upstream of the hemisphere the horseshoe gap was affected by rolling up of the boundary layer at the upstream limit of the hemisphere (Fraenkel, 1961), and not by the hydraulic jump, which is downstream of it (§3.10.1). The rolling up of the boundary layer must have occurred constantly in order for no sediment to have entered the horseshoe gaps of Runs MH2.2, MH2.4 and MH2.6 and also Werner *et al*'s (1980) similar gap in which sediment was eroded. The horseshoe gap was similar in general appearance to scours that form upstream of cylinders (§3.1) and would have been a scour feature if formed on a non-erodible floor.

The regions of rapid bedload transport that flanked the hemisphere did not occur in Werner *et al*'s (1980) runs or Sutton and McKenna-Neuman's (2008a) runs. The regions of rapid bedload transport were probably controlled directly by the hydraulic jump and supercritical flow, themselves directly controlled by the hemisphere (§3.6). Incipient dunes were washed out as they entered the regions because flow was thinner and 1.5 times faster in these regions than over the dune further upstream. The initial washing out of the dunes is likely to have been caused by the vorticity that originated immediately upstream of the hemisphere (from the rolling up of the boundary layer, §3.10.1) because it was associated with high shear stress. In the runs with lowest pumping rates the incipient dunes were washed out alongside the hemisphere approximately 0.2 diameters upstream of it, commensurate with a lateral release of vorticity. With increasing pumping rate, the dish became deeper (§3.3) and the track of the vorticity generated by the rolling up of the boundary layer would have been generally further upstream. Commensurately the streamwise position at which the washing out occurred moved upstream. The position that they were washed out the flow was in the dune forming phase and not the upper stage plane bed phase according to Carling (1999) and Van den Berg and Van Gelder (1993), although a different sediment was used to these investigators. The increased sediment reworking that is associated with dune migration (Huettel *et al.*, 1996) could have affected the dunes being washed out.

As in Werner *et al's* (1980) run, a region with no sediment present was seen downstream of the hemisphere. In Werner *et al's* (1980) run sediment was eroded to form this region and in the runs described here little bedload entered the region. The bedform-free

shadow was produced by the hemisphere wake and not directly a product of supercritical flow. Overall the shadow downstream of the hydraulic jump must have been less turbulent than the flow either side of it, because either side of it was the surface expressions of waves (Brocchini & Peregrine, 2001), however very little bedload moved from the more turbulent region to the less turbulent region. Werner *et al*. (1980) noted a "sweeping effect" of flow around the hemisphere that pushed grains towards the edge of what is here termed the *bedform-free shadow*. In Series MH the small amount of bedload supply to the *bedform-free shadow* travelled downstream; none travelled towards the sidewalls and joined a bedform further downstream within the regions that flanked the *bedform-free shadow*. Apparently no sweeping effect was present, and this is associated with the supercritical flow and hydrostatic pressure gradient changing the track of the horseshoe vortex.

3.11.3 The bedload sheets that formed in Runs MH2.2 and MH2.2a

The sediment features that developed in the regions of rapid bedload transport in Runs MH2.2 and MH2.2a were given the name bedload sheets because of their shape (Bennett & Bridge, 1995) and because they generally scaled with sediment supply (Nelson *et al.*, 2009). In particular (1) they were only a few grain diameters thick, (2) they had height to length ratios of around 1:10 and (3) they were on the order of tens of centimetres long (sand sheets can be on a scale from cm – m long, Whiting *et al.*, 1988). With greater sediment flux and a longer time of development, they may have become recognisable as other forms.

Perhaps more likely they were *washed out ripples*: bed features with symmetrical to slightly asymmetrical, convex up profile and low angle foresets (e.g. Baas & de Koning, 1995). The shape of the bedload sheets fits this description (§3.8.1 for plan shape; Video file 4, Appendix 2 for the 3d shape). The shape of the bedload sheets was quite well developed and the time for an equilibrium shape of washed out ripple to form is inversely proportional to velocity: even at lower range of velocity at which they form the equilibrium shape is seen by t = 30 minutes (Baas, 1994). Washed out ripples are known to form under flow conditions between those forming ripples and upper stage plane beds (Southard & Harms, 1972) and u increased to upper stage plane bed flow conditions within the regions of rapid bedload transport according to the bedform phase diagrams of Carling (1999) and Van den Berg and Van Gelder (1993). Washed out ripples are known to have decreasing height and more

constant spacing with increasing velocity (Bridge & Best, 1988) but the velocity was constant with time and the plan area over which *u* changed was small (only $6 - 10$ *bedload sheets* occurred in each region of rapid bedload transport, §3.8.1). A test for if these *bedload sheets* were *washed out ripples* could be to form longer regions of rapid bedload transport in a new experiment. No recognisable washed out ripples occurred between the mounds of sediment downstream of the hemisphere adjacent to the sidewalls, because there was sufficient material travelling in modified saltation to suppress bedform development (Baas, 1994)

3.12 CONCLUSIONS

1. A hemisphere was fixed to the floor of a flume, acting as a cobble or boulder on a river channel floor. Flow conditions were generated in the flume, with properties commonly attained in natural streams, such that flow accelerated over the hemisphere, became supercritical and a hydraulic jump formed.

2. Patterns of the water surface and of streamwise velocity downstream of the hemisphere were similar to the upstream flow field where a hydraulic jump did not form but were radically different from the upstream flow field where a hydraulic jump formed.

3. Where flow overtopped the hemisphere supercritically, a dish shaped depression of the water surface occurred over and downstream of the hemisphere. Associated with the depression was a radial hydrostatic pressure gradient.

4. With increasing pumping rate a series of four hydraulic jumps formed within the dish shaped depression: (1) An arcuate-fronted, undular jump with the apex of the arc pointing upstream. (2) An arcuate-fronted hydraulic jump with the apex of the arc pointing upstream. This form of hydraulic jump was sculpted by the dish-shaped depression, itself a deformable boundary. (3) A hydraulic jump with a shape not previously reported as a hydraulic jump, whose stream-transverse limits were two arcs of overturning water whose cross-tank separation increased with distance downstream. The upper surface of the hydraulic jump between the arcs was concave up. (4) In the highest pumping rates in each series the surface pattern was similar to (3) but the central part of the hydraulic jump was convex up. Both the dish and hydraulic jump maintained their shape and position for at least tens of minutes.

5. The pattern of vorticity known to form around a hemisphere under subcritical flow conditions was disrupted by the supercritical flow and the hydrostatic pressure gradient: The vorticity was not simply transported around the edge of the hemisphere but had a significant cross-stream component.

6. By the end of each run involving sediment, distinct regions of bedload features had developed. Most aspects of the sediment transport patterns around the hemisphere in supercritical conditions were controlled by the hemisphere and not the supercritical flow and hydraulic jump. Similarities to bedload transport patterns with subcritical flow included: (1) a region upstream of the hemisphere equivalent in streamwise length to 0.4 hemisphere diameters, in which sediment never entered; (2) immediately upstream of the gap, bedload features had a curved downstream face where elsewhere bedload features were not curved; and (3) a region directly downstream of the hemisphere where bedload transport rates were low, in which no bedload features formed.

7. The supercritical flow, hydraulic jump and flume sidewalls controlled one part of the transport pattern of bedload around a hemisphere, causing regions either side of the hemisphere in which bedload features were washed out.

3.13 THIS SECTION BRIDGES CHAPTERS 3, 4 AND 5

Chapter 3 described a method of generating 3d hydraulic jumps in a laboratory flume using a bed attached obstacle and described 3d patterns of flows that resulted from the flows interacting with the obstacle. It also included observations on non-equilibrium transport of bedload through some of the flows, selected for their distinct differences in the shape of the hydraulic jump. In the future this would be an interesting research path to follow but in the context of this thesis, following it risks marginalising hydraulic jumps because little sediment passed through the hydraulic jumps. From Chapter 3 to Chapters 4 and 5, I change emphasis from studying the plan pattern of sediment transport to analysing deposits in streamwise and cross-stream section. The hydraulic jump, supercritical flow and tailwater were the only water features in the channel; because of this fact, patterns in the sediment could easily be detected as relating to the hydraulic jump. As well as changing the nature of the flow I also changed the sediment input, from 30 kg to 5000 kg and from a prepared bed upstream of the test channel to

input by conveyor feed. This increase in sediment used per experiment gave the advantage that the sediment features that formed could be sampled and sections could be cut within them.

Run Code	Pre-run water level (hemisphere diameters)	Discharge $(m^3 s^{-1})$	Fr_u	λ_u (m)	Re (10^3)	Hemisphere overtopped?	Form of the hydraulic jump
H1.01	1	0.05	0.15	undulant	40	Yes	No jump
H1.02	1	0.07		undulant		Yes	No jump
H1.03	1	0.09		undulant		Yes	No jump
H1.04	1	0.10				Yes	Undular
H1.05	1	0.12	0.38	0.32	108	Yes	Undular
H1.06	1	0.13				Yes	Arcuate
H1.07	1	0.15				Yes	Arcuate
H1.08	1	0.16				Yes	Arcuate
H1.09	1	0.18	0.55	0.65	144	Yes	Overturning arcs
H1.10	1	0.19				Yes	Overturning arcs
H1.11	1	0.21				Yes	Overturning arcs
H1.12	1	0.22				Yes	Overturning arcs
H1.13	1	0.24	0.66	0.95	189	Yes	Overturning arcs
H1.14	1	0.25				Yes	Overturning arcs
H1.15	1	0.26				Yes	Overturning arcs
H1.16	1	0.28				Yes	Overturning arcs
H1.17	1	0.29	0.71	1.35	216	Yes	Overturning arcs
H1.18	1	0.30				Yes	Overturning arcs
H2.01	0.75	0.05	0.22	undulant	39	Yes	Undular
H2.02	0.75	0.07				Yes	Undular, arcuate
H2.03	0.75	0.09				Yes	Arcuate
H2.04	0.75	0.10				Yes	Arcuate
H2.05	0.75	0.11	0.51	0.48	94	Yes	Arcuate
H2.06	0.75	0.12				Yes	Arcuate, overturning arcs
H2.07	0.75	0.13				Yes	Overturning arcs
H2.08	0.75	0.14				Yes	Overturning arcs
H2.09	0.75	0.15	0.61	0.65	126	Yes	Overturning arcs
H2.10	0.75	0.16				Yes	Overturning arcs
H2.11	0.75	0.17				Yes	Overturning arcs
H2.12	0.75	0.18				Yes	Overturning arcs
H2.13	0.75	0.19	0.61	0.72	159	Yes	Overturning arcs
H2.14	0.75	0.20				Yes	Overturning arcs
H2.15	0.75	0.21				Yes	Overturning arcs
H2.16	0.75	0.22				Yes	Overturning arcs
H2.17	0.75	0.24	0.67	0.83	197	Yes	Overturning arcs
H2.18	0.75	0.25				Yes	Overturning arcs

H3.01	0.5	0.05	0.33	undulant	40	Yes	Arcuate
H3.02	0.5	0.07				Yes	Arcuate
H3.03	0.5	0.08				Yes	Arcuate
H3.04	0.5	0.09				Yes	Arcuate
H3.05	0.5	0.10	0.55	0.42	81	Yes	Arcuate
H3.06	0.5	0.11				Yes	Overturning arcs
H3.07	0.5	0.12				Yes	Overturning arcs
H3.08	0.5	0.13				Yes	Overturning arcs
H3.09	0.5	0.13	0.59	0.55	110	Yes	Overturning arcs
H3.10	0.5	0.14				Yes	Overturning arcs
H3.11	0.5	0.14				Yes	Overturning arcs
H3.12	0.5	0.15				Yes	Overturning arcs
H3.13	0.5	0.16	0.62	0.65	133	Yes	Overturning arcs
H3.14	0.5	0.17				Yes	Overturning arcs
H3.15	0.5	0.18				Yes	Overturning arcs
H3.16	0.5	0.18				Yes	Overturning arcs
H3.17	0.5	0.18	0.60	0.75	151	Yes	Overturning arcs
H4.01	0.25	0.04	0.34	undulant	17	No	Pattern of 4 jumps
H4.02	0.25	0.05				No	Pattern of 4 jumps
H4.03	0.25	0.06				No	Pattern of 4 jumps
H4.04	0.25	0.06				No	Pattern of 4 jumps
H4.05	0.25	0.07	0.42	0.14	40	No	Pattern of 4 jumps
H4.06	0.25	0.08				No	Pattern of 4 jumps
H4.07	0.25	0.09				No	Pattern of 4 jumps
H4.08	0.25	0.10				Yes	Overturning arcs
H4.09	0.25	0.10	0.64	0.25	82	Yes	Overturning arcs
H4.10	0.25	0.10				Yes	Overturning arcs
H4.11	0.25					Yes	Overturning arcs
H4.12	0.25					Yes	Overturning arcs
H4.13	0.25		0.57	0.45	93	Yes	Overturning arcs
H4.14	0.25			0.50		Yes	Overturning arcs

Table 3.2 General conditions of the flow in Series H1, H2, H3 and H4. Discharge was measured by the electromagnetic flow meters (§2.2.2). Wavelength upstream of the hemisphere, λ_u was measured using a point gauge. The forms of the hydraulic jump are described in §3.4 and §3.6.

4. Flow patterns, sedimentation and deposit architecture under a hydraulic jump on a non-eroding bed; defining *hydraulic-jump unit bars*

4.1 INTRODUCTION

Over the last two to three decades various sedimentary depositional architectures, seen in the geological record of various environments, have been associated with hydraulic jumps (§1.8). Some of these are erosional features and some are depositional features. Despite the fairly common occurrence of hydraulic jumps in natural flows, the deposits associated with them have been poorly documented and poorly quantified. Identification of ancient "hydraulic jump deposits" is difficult or impossible without diagnostic criteria for the presence of a hydraulic jump, and without the diagnostic criteria the association of hydraulic jumps with more recent deposits is generally speculative.

This chapter reports on two experimental runs undertaken in the flume (§2.2.2). In Run 1 I quantified patterns of flow velocity, Reynolds shear stress, turbulent kinetic energy and vorticity in a supercritical flow, hydraulic jump and tailwater, that would be an initial condition for Run 2. New acoustic technology (§2.4) was deployed to document the velocity patterns in more detail than had previously been reported. Run 2 involved a continuous sediment addition. The sediment entering the hydraulic jump caused bed features and a deposit containing sedimentary structures, to form. The sediment transport behaviour and the changes in the patterns of the flow as the sediment bed evolved below it are documented. Sediment bed features and lamination patterns were quantified as the sediment transport pattern evolved. Feedback between flow and sediment transport patterns are discussed and the chapter concludes with the presentation of a model describing how a sediment depositional architecture forms in association with a hydraulic jump and one pattern of sediment transport through it. Runs 1 and 2 are also reported in Macdonald *et al*. (2009) which was written during this research. In Chapter 5 I report two further runs involving sediment addition and I reproduce the depositional architectures that formed. In light of the lack of basic data on deposits associated with hydraulic jumps, I investigated an initially planar, inclined, non-erodible flume floor so that deposition would be controlled by the flow not the channel

topography. Two further experimental runs, with different depositional outcomes, are presented in Chapter 5. Discussion of the deposit architectures is postponed to Chapter 6 where I propose diagnostic criteria for hydraulic jump deposits based on the flume experiments and then test the criteria on field data from deposits inferred to have formed in association with hydraulic jumps.

Highlights of Chapter 4 include flow separation from a smooth planar wall, descriptions of two newly defined architectural elements: the *hydraulic-jump unit bar* and the *hydraulic-jump bar complex* and an unusual mechanism of grain segregation by size, by which those architectural elements formed.

4.1.1 Experimental procedure

Runs 1 and 2 used the co-ordinate system and the equipment described in Chapter 2, in the procedure outlined below.

Run 1: sediment-free hydraulic jump

A hydraulic jump was formed in the flume in the way described in §2.7, using a channel tilt of 4.25° and a constant water discharge of 0.26 $m^3 s^{-1}$. The mean position of the toe was set at $x = 4.68$ m (Fig. 4.1) using an 0.1 m high overshot weir (toe defined in §1.4.2). At this position the hydraulic jump could be viewed past structural building pillars and the blue vertical supports (Fig. 2.3A). It was sufficiently far down the flume for the supercritical jet free surface to be uniform across-stream. The hydraulic jump was sufficiently far up the flume for sediment accumulation downstream of the jump to be largely unaffected by the conditions downstream of the test channel (i.e. the pattern of flow above the sediment trap, draw down into the recirculation system).

The hydraulic jump toe oscillated in the streamwise direction between $x = 4.38$ m and 4.88 m (total excursion of 0.50 m). Flow depth upstream of the toe, $h|_{x=4.68} = 0.09$ m, and immediately downstream of the hydraulic jump, $h|_{x=6.40} = 0.25$ m. Further downstream of the hydraulic jump h increased slightly because the water surface slope was shallower than the slope of the flume floor. As the wall jet entered the jump, $Fr_s = 2.73$, $Re = 282000$ and $L_s = 5.91$ (flow conditions possible in natural streams §1.4; wall jet defined in §1.9.3). Such a high Reynolds number confirms that the flow was fully turbulent throughout
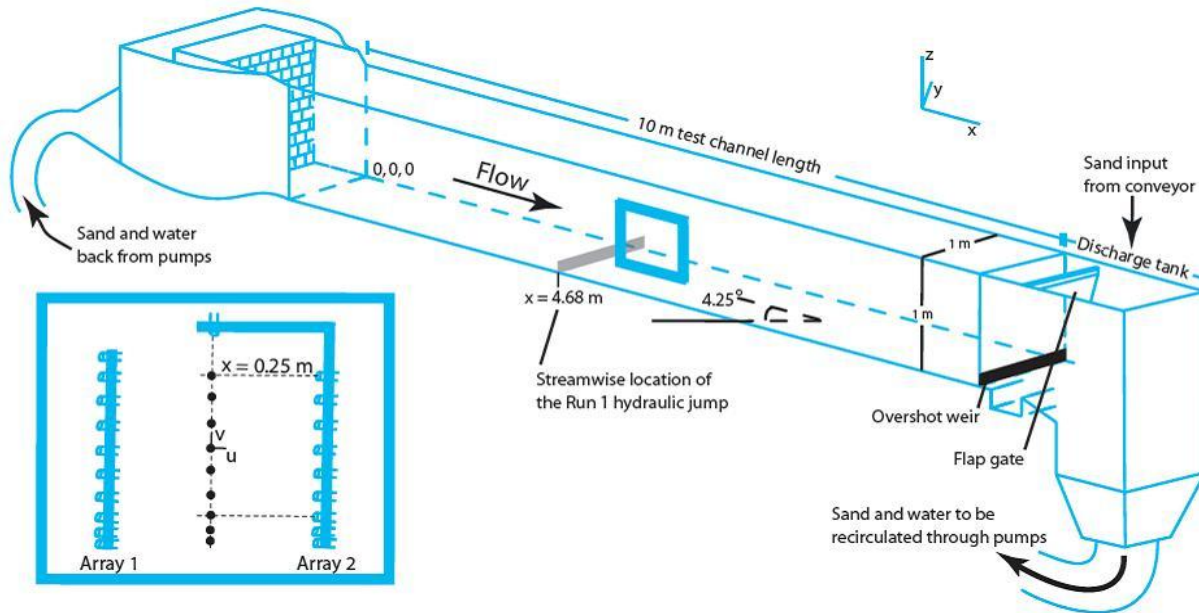
Figure 4.1 The flume used for these experiments (not to scale). The inset box shows the pattern of UDVP probes, used in the two different arrays along the flume centreline. The mean streamwise position of the hydraulic jump in Run 1 is marked with a grey rectangle, which is also its mean position at the start of Run 2.

Run 1 (§1.4.4). Immediately downstream of the jump, $Fr|_{x=6.40} = 0.24$. At the end of the test channel $Fr|_{x=10.00} = 0.20$. The decrease in Fr between $6.40 \leq x \leq 10.00$ m was associated with the simultaneous increase in h.

Ultrasonic Doppler velocity profiler (UDVP) probes deployed in arrays, measured high frequency time series of beam-parallel velocity components, in transects away from the probes. A UDVP array of ten probes, parallel to the flume floor and pointing upstream (array 1; Fig. 4.1), was deployed at 13 positions along the channel centreline to measure u just upstream, within and downstream of the hydraulic jump. Two-dimensional (u and w) turbulent characteristics were assessed with data from a second UDVP array (array 2; Fig. 4.1) at 4 positions. Velocities in the supercritical flow were measured with a single probe and mean velocities are the average of 12000 readings at each point. Vectrino[+] acoustic Doppler velocimeters recorded time series of all component velocities at isolated points.

Run 2: hydraulic jump with sand addition

The hydraulic conditions that formed the Run 1 hydraulic jump were run in the flume. Well sorted sand was added to the flume at approximately 4000 kg per hour over the duration of the

75 minute run (sand, Fig. 4.2; input regime, Table 4.1). There was a short hiatus in sand loading when each full crate was manoeuvred into place (Table 4.2). The input sand was well mixed and unimodal (modal class was 250 – 300 μm), with mean grain size 368 μm and standard deviation 222 μm. The shape of the sand deposit adjacent to the sidewalls was recorded at 23 instants and the position of the water surface was recorded at 13 instants (Table 4.3) by tracing onto the sidewalls. This frequency of recording was sufficient to represent any changes that occurred. A point gauge was used to measure the water surface shape away from the sidewalls to determine the error introduced by the meniscus adjacent to the sidewall (§2.5.1) and the error associated with the meniscus could be corrected.

| | Run duration (Minutes) | The input sediment | | | | | Input rate | Hiatuses in sand loading |
		D_{50} (μm)	Modal class (μm)	Sorting	Standard deviation (μm)	Density (kg m^{-3})	(kg hr^{-1})	
Run 2	75	368	250 - 300	Poor	222	2650	4000	Yes
Run 3	45	368	250 - 300	Poor	222	2650	6700	No
Run 4	75	250		Good		2630	4000	No

Table 4.1 Details of Runs 2 – 4, which involved sediment input to the Run 1 hydraulic jump. Sorting is quoted relatively; the full grain size distributions are depicted in Figures 4.2 and 5.1. The hiatuses in sand loading to the flume were whilst interchanging some of the six crates which contained the sand, and lasted up to two minutes.

**Timeline of the formation of beds and changeover
of crates of sand in Run 2**

t (mins)	Action
0	Crate 1 started.
0	Suspension fallout unit (1) and youngest bar (2) start.
7 – 12	Crate 2 moved into place
12	Crate 2 started
12 – 15	New bar (3) incepted
23 – 30	New bar (4) incepted
30 – 32	Crate 3 moved into place
32	Crate 3 started
42 – 52	New bar (5) incepted
45 – 50	Crate 4 moved into place
50	Crate 4 started
63 – 66	New bar (6) incepted
65 – 66	Crate 5 moved into place
66	Crate 5 started

Table 4.2 Timeline of Run 2 indicating the timings of loading of sand into the flume from five crates (black text) and the timings of development of bed features (blue text). Hiatuses in sand loading were five minutes long before crate two and crate four but only two minutes before crate three and crate five.
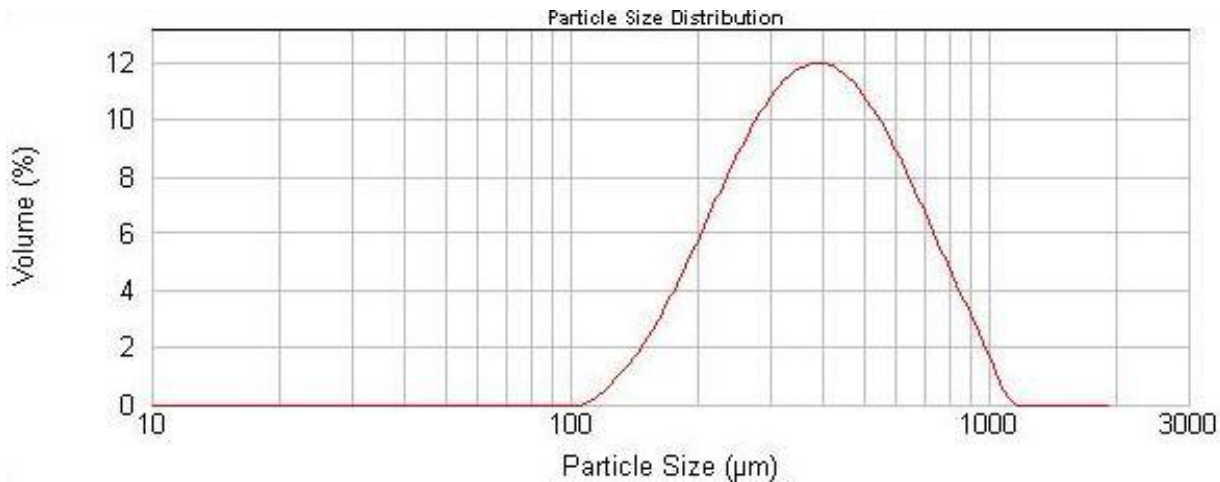
Figure 4.2 Grain size distribution of the sand used in Run 2. Grain size distribution was analysed using a laser diffraction particle sizer (§2.6).

Sand was manually loaded onto the conveyor at as steady a rate as could be maintained by shovelling and fell into the discharge tank in near shovel-full lumps from 1 m above the water, with minimal splashing. Sand added to the discharge tank mixed with sand recirculating past the downstream limit of the test channel (discharge tank indicated in Fig. 4.1). The sand travelled through more than 15 m of recirculation pipes and pumps before entering the test channel. This acted to damp any fluctuation in sand flux. After initiation of sand input, the sand flux to the hydraulic jump did not cease until the run was stopped and no abrupt change in sediment flux was observed within the test channel. Suspended sand accounted for a mean of 1 volume percent of the supercritical flow and about 0.3 volume percent of the flow through the tailwater immediately downstream of the hydraulic jump.

Times sand surface was recorded at:			Times water surface was recorded at:		
0	17	57	0	30	
1	19	58	2	39	
5	20	60	5	44	
7	23	63	8	53	
8	30	66	12	63	
12	37	72	15	66	
15	42		20		
16	52		24		$t = n$ minutes

Table 4.3 Lists of the times that the surface of the sand deposit and the water surface were recorded at in Run 2. Run 2 was started at 09:45 ($t = 0$ minutes) and completed at 11:00 ($t = 75$ minutes).

The UDVP array 2 was fixed in position at $x = 6.10$ m throughout the run with each probe measuring three bins between $5.78 \leq x \leq 5.92$ m. Because the jump moved slowly upstream, the UDVP probes recorded the streamwise velocity component, u at increasing distances downstream of the hydraulic jump. Vectrino[+] acoustic Doppler velocimeters recorded time series of all component velocities at isolated points.

The end of the run was defined to be the point in time when all 5000 kg of sand had been input. On reaching the end of the run the pumps were stopped. This avoided further transport of sediment, or erosion of the deposit, under conditions of decreased sediment flux.

After the run was ended, the flume was drained. One stream parallel section was cut 0.3 m from the right hand sidewall, measured and photographed and then nine stream transverse sections were cut, measured and photographed. Because of the very low clay concentrations in the sediments used, post-run dewatering of any sediment deposits formed is unlikely to have altered the grain size distribution at any position within the deposit.

4.2 RUN 1: HYDRAULIC JUMP IN A SEDIMENT-FREE FLOW

Observations of the flow through the glass sidewall (e.g. Figs 4.3 and 4.4A) indicated a more complicated time dependent flow structure than is usually illustrated in theoretical models of a hydraulic jump (Hornung *et al.*, 1995; Chanson, 1999). Despite the steady flow conditions in the supercritical flow and at some distance downstream of the hydraulic jump, within the hydraulic jump a lot of the internal structures were transitory; repeatedly forming, changing and dissipating at consistent locations within the flow.

The components of the flow defined in §1.4.2 and §1.9.3 are illustrated in Fig. 4.3. The supercritical flow into the hydraulic jump maintained the form of a steady submerged wall jet (§1.9.3) for 0.67 m downstream of the toe (the most upstream point of abrupt flow thickness change). The submerged wall jet thinned downstream (from 0.09 to 0.06 m). At 0.67 m downstream of the toe, the submerged wall jet expanded vertically (maintaining contact with the flume floor) and the core of the jet rose to follow the highest position of the expanding jet, as a detached jet (Fig. 4.3; core of a jet defined in §1.9.3). The detached jet approached the water surface and thickened downstream to span the entire flow depth (green arrow, Fig. 4.4A) and from this position downstream the flow was called the tailwater (defined in §1.4.2).
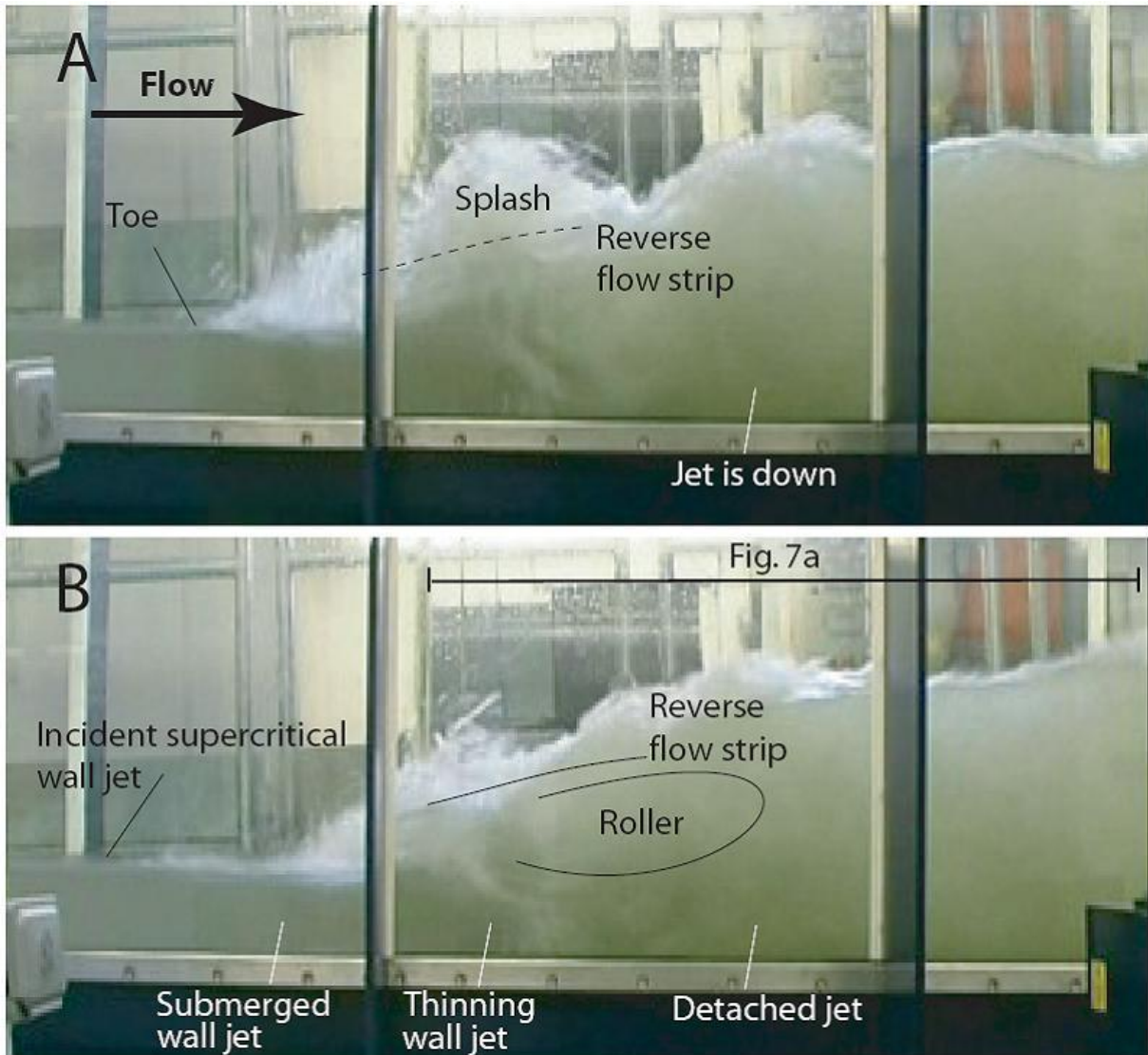
Figure 4.3 Still video images of the hydraulic jump in Run 1 at two instants, taken from a consistent distance, through the flume sidewall. Definition diagram of the hydraulic jump. The vertical sidewall supports are 0.80 m apart. A: Image of surface splash. B: Image taken 0.32 s after A without splash.

In the volume of fluid below the lower boundary of the detached jet, there was no obvious flow movement except when bubbles (described below) highlighted discrete eddies. Because the jet was detached from the flume floor it had a lower edge as well as an upper edge, and one shear layer was associated with each edge.

Above the submerged wall jet and detached jet was a recirculating roller (Figs 4.3 and 4.4A). The upper surface of the roller was also the surface of the hydraulic jump. It oscillated with an 0.05 m vertical amplitude (Fig. 4.4A) and had a complex system of localised breaking (Fig. 4.5). The upper surface of the hydraulic jump at all times had many folds in all

orientations. Localised peaks of the water surface height, typically spanning less than half the flow width, rose above this oscillation and spilled upstream in seconds (Figs 4.3A and B). In this thesis these are termed *splashes* and were observed at 5 – 45 s intervals throughout Run 1. Splash height and position varied, with maximum heights recorded on Fig. 4.4A. There was a thin, highly aerated, upstream flow along the uppermost 0.05 m of the roller (immediately below the water surface) and this is termed the "reverse flow strip" (Fig. 4.3). It persisted throughout Run 1. The toe oscillation was a local feature and had a frequency not simply related to the vertical, surface oscillation of the roller. Splashes were particularly high when the toe was in its most upstream position (Video file 5, Appendix 2).

The continuous breaking of the water surface of the hydraulic jump entrained air into the flow, in the form of bubbles. Incident supercritical flow was not aerated; but bubbles constituted a considerable fraction of the roller and the flow downstream of it. The highest concentration of bubbles was at the turbulent shear layer between the upper surface of the submerged wall jet and the roller. The submerged wall jet and the core of the detached jet contained few bubbles compared to the water above and below.

Figure 4.4 (below) Flow characteristics of Run 1. (A) Flow structure. The blue free-surface line indicates the maximum recorded splash heights, above the maximum and minimum instantaneous surface positions when a splash was not present (two brown lines). The larger arrows represent components of the flow structures whose streamwise direction did not alter. The arrows are red in the 'roller', green in the 'detached jet' and blue within the 'tailwater'. The small blue arrows indicate the path of bubbles in the tailwater. (B) Profiles of time-averaged streamwise velocity component, $\bar{u}$, averaged over 540 seconds of measurement with UDVP probes at $y = 0.500$ m. Profile position is indicated by the down-pointing grey arrows in A. The dashed lines adjacent to Profiles I and J are the time-averaged velocity profiles with velocity data outlying steady upper or lower bounds removed. The insert graph shows velocity profiles measured in the supercritical flow (dark blue) and the toe of the hydraulic jump (pale blue) with expanded vertical scale. (C) Vertical profiles of *Tke* and τ_{yx} calculated from UDVP array 2 data at four locations along the flume centreline for Run 1. The *Tke* profiles are drawn in pink and the τ_{yx} in black. The lowest position of the surface is also drawn (compare with A).
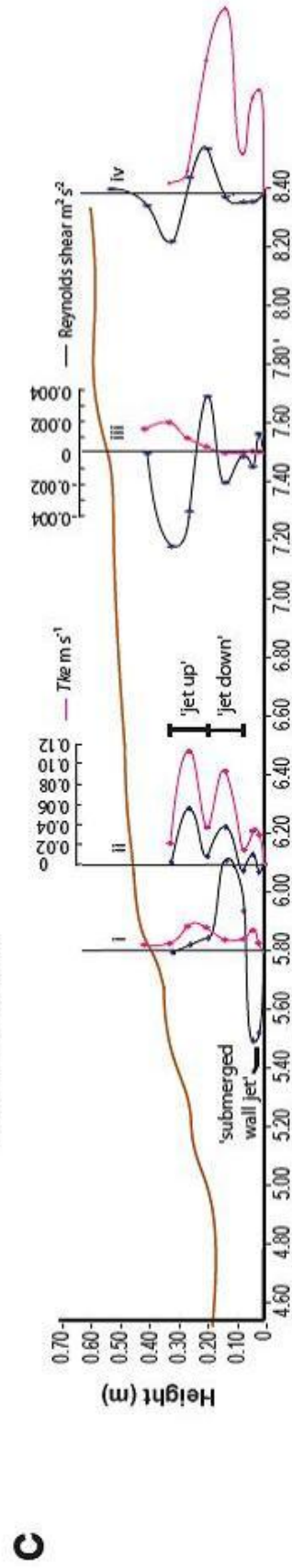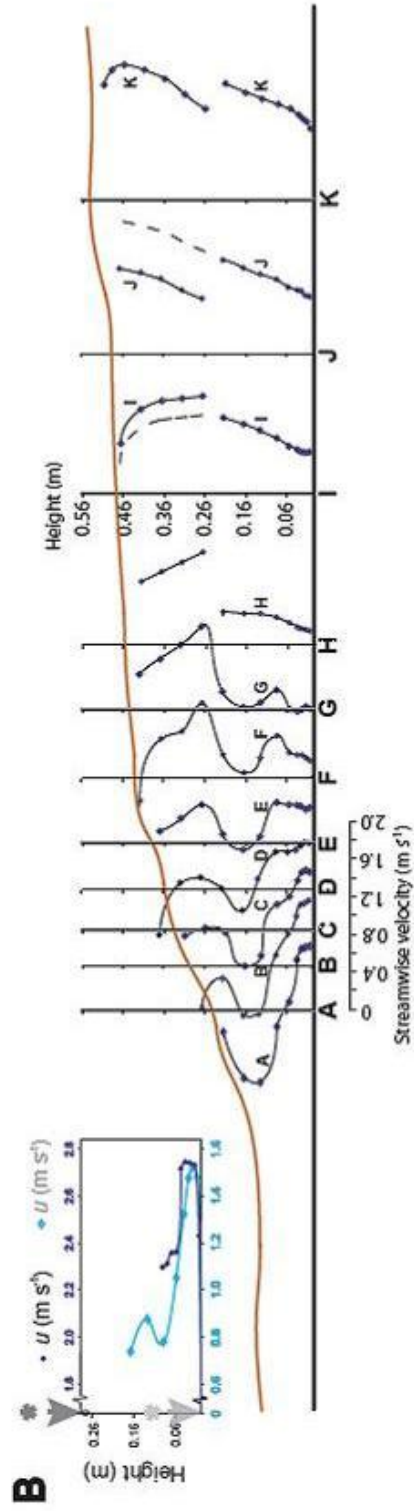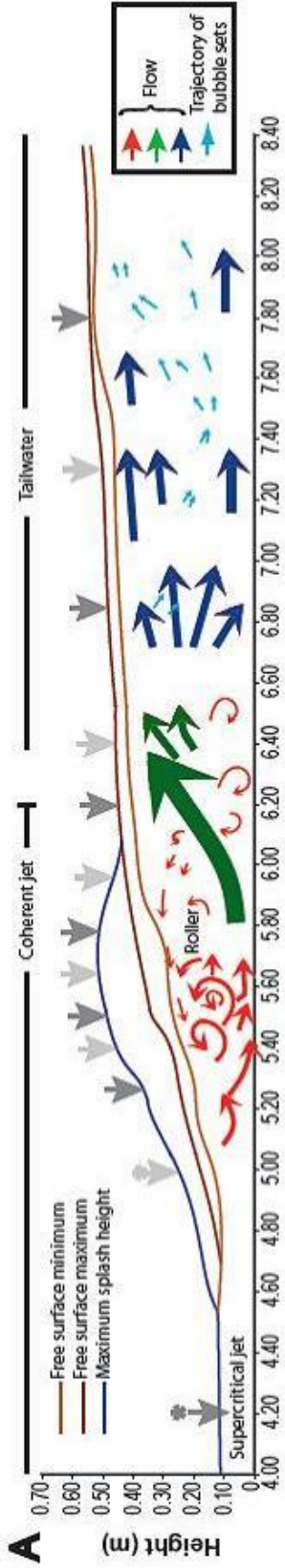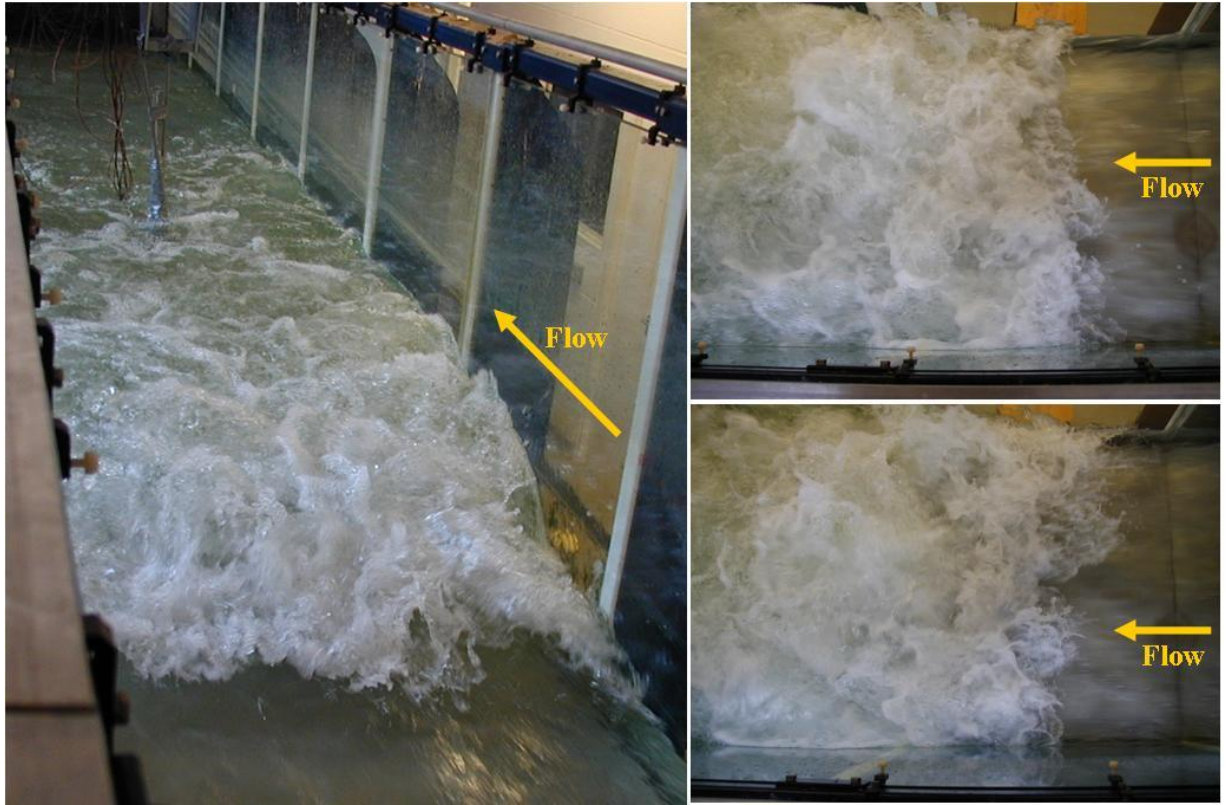
Figure 4.5 Photographs of the Run 1 hydraulic jump.

Immediately downstream of the toe there was a zone of vortex generation. Vortices formed within the shear layer between the submerged wall jet and roller (§1.4.2). When they began forming, the diameter of the rotating part of the flow was more than 0.2 m. Over several seconds they tightened to 0.05-0.09 m in diameter and were seen to be coherent structures. Some vortices followed the upper edge of the detached jet. Others were deflected downwards, and became smeared out in the streamwise direction because their lower boundaries passed downstream along the flume floor, upstream of jet detachment. Throughout Run 1, further vortices were shed from the lower boundary of the detached jet and these rotated slowly without tightening as they moved into the quiescent region below the detached jet. These vortices were generally larger than, contained more diffuse bubbles than and rotated in the opposite sense to those generated in the shear layer. All vortices had axes of rotation across-stream.

Bubbles exited the upper portion of the downstream edge of the roller in sets, defined as bubbles in close proximity surrounded by fluid without bubbles, in pulses approximately

every 5 s. They followed a curved trajectory within the expanding jet and tailwater and burst at the surface within the flume length (Fig. 4.4A). The bubble sets were restricted to the top quarter of the flow just downstream of the roller, extended down to three quarters of the flow depth about 1.1 m downstream (at $x = 7.50$ m) and had all escaped by 1.9 m downstream.

4.2.1 Velocity data

At 0.4 m upstream of the hydraulic jump ($x = 4.28$ m) u reached a maximum (2.74 m s^{-1}) at $z = Z_{Umax}$ (0.033 m above the flume floor, Fig. 4.4B inset). Supercritical flow was generally steady between upper and lower bounds and additionally had instances of slower flow (mean 1.18 m s^{-1}, half the lower bound) of up to 0.1 s duration with no apparent periodicity (Fig. 4.6D).

As the supercritical wall jet became submerged, $\bar{u}_{max}$ slowed by 85% in 0.9 m (to 0.41 m s^{-1} in Profile F, Fig. 4.4B). Z_{Umax} moved down over a horizontal distance of 0.67 m, to within 0.001 m of the flume floor and moved up to 0.03 m by Profile D (Fig. 4.4B). In Profiles A – D, u decreased smoothly upwards, across the shear layer and became negative within the recirculating roller. The time-averaged jet expanded downflow of Profile D and Z_{Umax} moved upwards following the upper limit of the expanded jet. In both Profiles F and G, two peaks in $\bar{u}$ were recorded because the jet core position changed repeatedly between a *jet up* and *jet down* state. The u time series at Z_{Umax} ($z = 0.27$ m, Fig. 4.6A) shows that most data were spread uniformly around a steady mean and additionally u minima, each lasting for less than 2 s, were recorded at times when the whole detached jet was in the *jet down* state. The detached jet was transient in vertical space, through time.

Underneath the length of the roller, the upper jet edge was abrupt (jet edges defined in §1.9.3). The lower edge of the detached jet was less abrupt. The upper edge of the detached jet rose to 0.75 of the flow depth within a streamwise distance of 0.6 m, and downstream of this the jet became indistinct.

Above the time-averaged jet, there was a minimum in $\bar{u}$ at $z = 0.20$ m. This was negative at the upstream end of the roller (-0.76 m s^{-1}) and increased to 0.03 m s^{-1} downstream through the roller (Profiles A – F; Fig. 4.4B). The integrated mean $\bar{u}$ for velocity Profile A is negative, indicating nett upstream volume flux. This resulted from the greatly aerated state of the recirculating flow within the roller; the negative (up-flume) volume flux of water (rather than water and air bubbles) was less than the down-flume volume flux of the submerged wall

jet (that contains no bubbles). The highest magnitude of negative u in each of profiles A – D coincided with the stream of vortices above the detached jet.
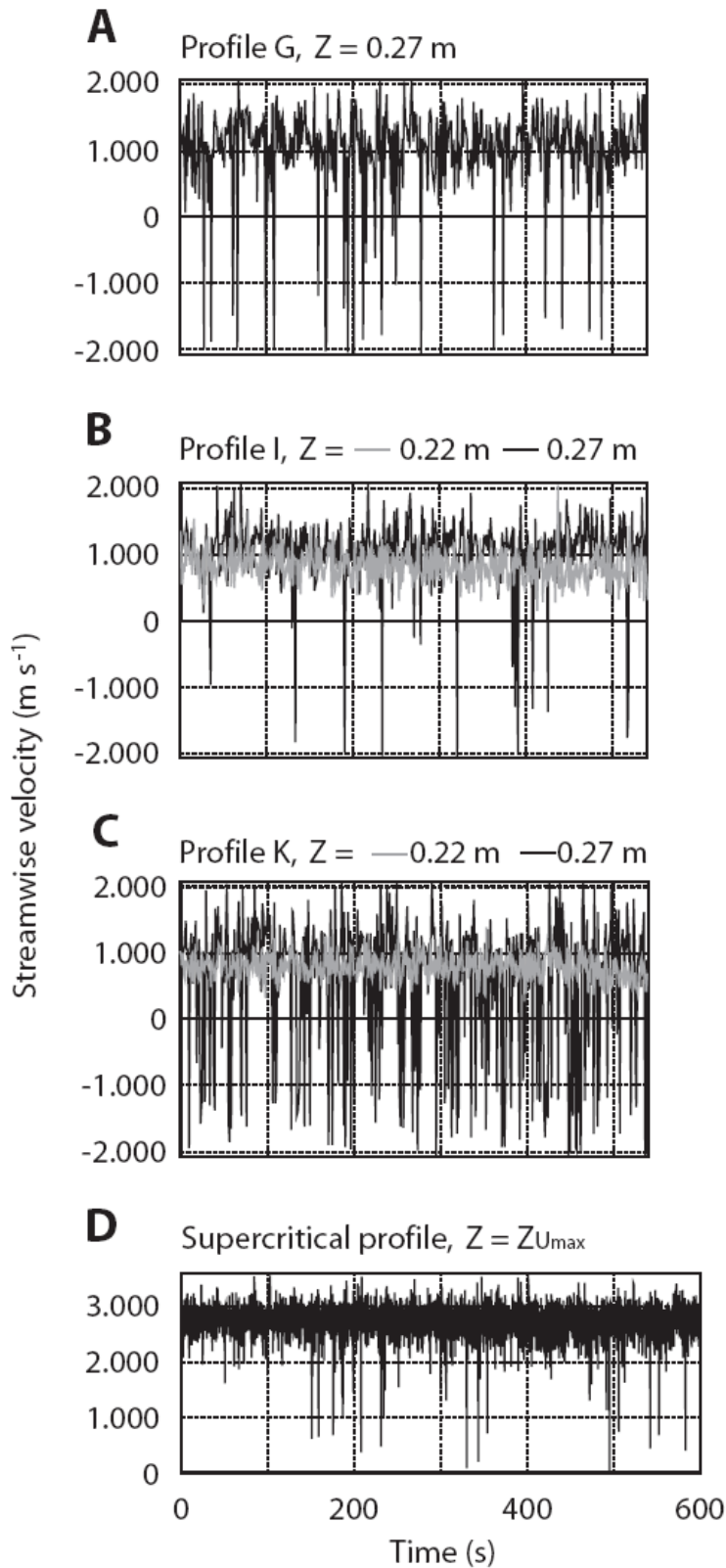
Figure 4.6 Time series of u at positions downstream through the jet and tailwater. (A) – (C) shows 500 data points from array 1 at the position: (B) within the detached jet. (C) two positions within the tailwater near the upstream limit of the bubble pulses. (D) within the tailwater, further downstream than the bubble pulses. Note that in (D) the bubble pulses reach down to $z = 0.27$ m more regularly than in (C). (D) 12000 data points from a single probe, at $z = Z_{Umax}$ in the supercritical flow. Compare inset, Figure 4.4B.

The flow below the time-averaged detached jet was directed downstream. Profile G was in the region below the jet, between the detachment point and the point where the tailwater was fully developed. In this region the water near the flume floor was nearly static (less than 0.04 m s^{-1} below $z = 6$ mm). The near floor velocities were greater both upstream and downstream of G.

The time-averaged tailwater velocity is drawn above and below an offset, as two unjoined lines (Profiles H – K; Fig. 4.4B). The height of offset followed the trajectory of the bubble sets (which highlighted pulses from an upper region of the roller). The velocity profiles below the offset remained unchanged throughout, with a symmetrical spread of data about a steady mean (black lines on Fig. 4.6B and C). At each position above the offset, the u time series were similar to that below the offset for most of the recording period, but with slightly wider bounds (grey lines on Fig. 4.6B and C). This recorded the non-offset pattern displayed by the dashed lines of Fig. 4.4B. In addition there were repeated short periods (up to 5 s long) when velocity varied by 2 – 3 times the excursion of the steady flow. At any point in space above the offset, the large excursions were only above or below the upper boundary of the steady part of the u time series, but not both. By Profile J, the time-averaged u profile was approximately parabolic. All bubbles had disappeared. The tailwater continued to slow downstream.

4.2.2 Turbulent kinetic energy and Reynolds shear

Turbulent kinetic energy, *Tke* and Reynolds shear, τ_{zx} (§1.4.4) were calculated from coincident u and w data generated by the UDVP array 2 (Fig. 4.7). At the jet detachment site, *Tke* was highest at the upper and lower edges of the jet (the lower edge was the flume floor) due to high shear fluctuations (Profile i, Figs 4.4C and 4.7). The *Tke* minimum in the middle of the detached jet was approximately 20% of that at the upper jet edge. *Tke* was low in the downstream half of the roller and the reverse flow strip. At Profile (ii) the detached jet had *Tke* maxima at the upper and lower edges and a mid-jet minimum, all higher in magnitude than at jet detachment. A *Tke* minimum at $z \sim 0.05$ m, underneath the detached jet was associated with the centre of diffuse vortices (§4.2). Where the pulses were nearest to the flume floor, two distinct regions were recorded, above and below the height at which bubbles were seen (Profile iii). Below the pulses (below $z = 0.14$ m in Profile iii) *Tke* was virtually zero. Above z

= 0.14 m *Tke* rapidly increased, peaking at the height of the favoured path of bubble sets within the pulses (z = 0.30 m). The tailwater downstream of the pulses exhibits a smooth *Tke* curve, peaking at the height of maximum shear which was below the break in the velocity profile (Profile iv).

A mid-jet minimum in Reynolds shear, τ_{zx} coincided with the *Tke* minimum in the submerged wall jet (compare τ_{zx} and *Tke* on Profile i, Fig. 4.4C). Rapidly accelerating sheared flow at the upper jet edge was associated with a strong positive vertical gradient in τ_{zx}. An abrupt decrease in stress occurred between the upper jet edge and the roller, and this is attributed to the presence of the upward-travelling stream of vortices. The flow above $z \sim$ 0.180 m did not deviate abruptly in speed or direction and exhibited low values of Reynolds shear. The detached jet profile at x = 6.10 m (Profile ii) highlights the jet retardation in the negative $\partial\tau_{zx}/\partial z$ around z = 0.150 m. The shorter negative gradient below (around z = 0.05 m) marked the *jet down* position. At this streamwise location the *jet up* state produced a more diffuse pattern in u because the jet spanned more of the flow depth than the *jet down* state. Strong positive values of $\partial\tau_{zx}/\partial z$ existed at the upper and lower jet edges in the *jet up* state, despite diminished direct acceleration by the retarding jet to the flow surrounding it. The region of diffuse vorticity below the detached jet had comparatively low values of τ_{zx}. The τ_{zx} peak lower in the flow was at the same height as the vortex centres as they streamed past this streamwise location. Above this peak $\partial\tau_{zx}/\partial z$ was negative and below this peak $\partial\tau_{zx}/\partial z$ was positive: the upper part of the vortex circumference is detected to have rotated downstream, whilst the lower part rotated upstream. The reverse flow strip had a low value of τ_{zx}, consistent with the zero shear stress boundary condition which exists on the surface flow within this ever-present part of the flow structure, and consistent with the low *Tke* values.

Figure 4.7 (below) Plots of the instantaneous deviation from mean streamwise velocity, *u'*, against the corresponding instantaneous deviation from mean vertical velocity component, *w'*, for Run 1 at Profiles (i) – (iv) (Fig. 4.4C). *u'* > 0 denotes downstream and *w'* > 0 denotes away from the flume floor. These plots give a visual impression of the variation in turbulence structure in space.

Height above the flume floor (m)

0.386

0.306

0.246

0.186   Roller   Jet centre

0.126

0.066

Jet centre

0.036

0.016

2.000 v'
1.000 (ms⁻¹)

u'

-2.000 -1.000 0 1.000 2.000

-2.000

5.800   6.100   7.500   8.400

Distance along test channel (m)
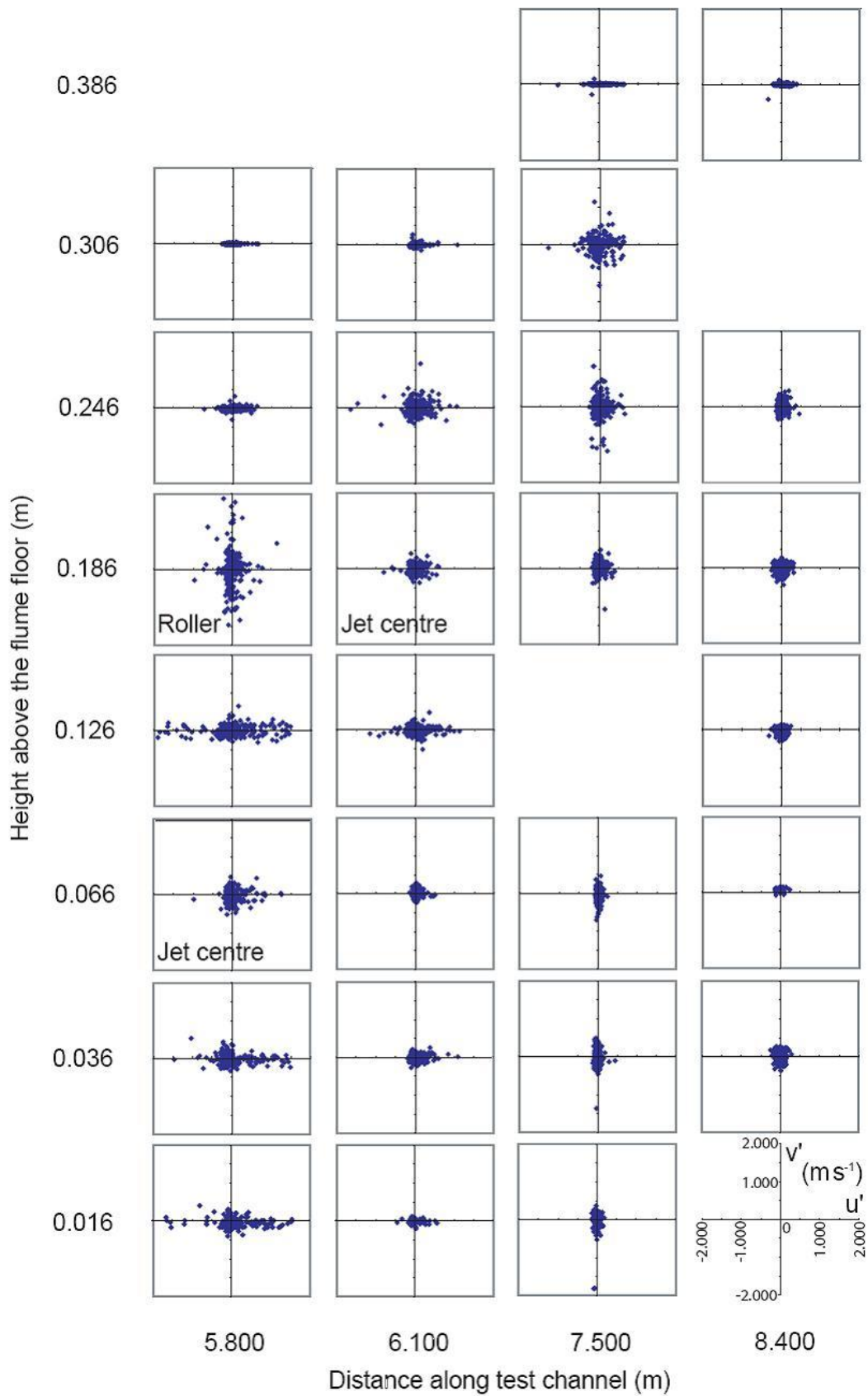
Further downstream than the jet, two modes of the flow were detected (cf. Profile iii, x = 7.50 m, Fig. 4.4C); a low-τ_{zx} tailwater, below a higher-τ_{zx} tailwater in which τ_{zx} was three times higher. The transition between these regions was at the base of the observed favoured path of bubble sets, between z = 0.120 m and 0.180 m (Fig. 4.4A). The distribution of $\partial\tau_{zx}/\partial z$ within the transition was positive: a nett acceleration of the immediately surrounding water by the lowest reaching pulses which were still travelling downstream. Above z = 0.180 m in Profile (iii), a strong negative gradient in τ_{zx} was observed because the fluid had comparable values of u and w. Because of their buoyancy, the w of bubbles may be greater than that of the water. The tailwater further downstream (Profile iv) exhibited low negative shear of slowing steady flow except for the marked peak around z = 0.18 m, consistent with the data for *Tke* and $\bar{u}$.

4.2.3 Turbulent velocity fluctuations

By definition, instantaneous deviations from mean streamwise and vertical velocity, u' and w' (§1.4.4) have a mean of zero and the data scatter indicates the predominance of horizontal or vertical fluctuations, shedding light on the time-transient flow character (Fig. 4.7). Downstream through the flow, u' and w' both generally decreased in magnitude.

Jet flow generated high instantaneous velocity fluctuations. The jet thickness was 0.12 − 0.23 m as it rose from the flume floor (Profiles i and ii, Fig. 4.7; h_s was 0.09 m). The detached-jet centre was less spread in u' and w' than the edges of the jet in the *jet up* position (Fig. 4.7). In addition there was less spread in u' and w' at the lower edge of the jet while it was in the *jet down* state and still less spread between the two states.

Profile (i) at x = 5.80 m was the location of the widest spread in u' and w' and was along the path on which vortices passed downstream. In the recirculating roller (at z = 0.186 m) w' was twice as widely spread as u'. Close to the bed at x = 5.80 m, where the wall jet was thinnest a few outlying values negative in u' and positive in w' indicated slowing, rising bursts. These data points are interpreted to be the record of times at which the jet began to detach from the flume floor at x = 5.80 m (rather than further downstream of this position).

Downstream of jet detachment, turbulence was reduced at the flume floor, but increased within the water column. Transport of suspended sediment and bedload would have been promoted by turbulence due to the jet edges at *jet up* and *jet down* conditions. The slowly

rotating vortices which spanned the flow column below the detached jet at $x = 6.10$ m accorded with a small spread in u' and w' compared to the surrounding fluid. Throughout Profile (iv) at $x = 8.40$ m, and the lower region of Profile (iii) at $x = 7.50$ m, u' and w' were clustered particularly close to the origin, corresponding to steady flow. Above $z = 0.186$ m u' and w' were more spread than u' and w' below $z = 0.186$ m, according with the minimum height that pulses reached down to. At $z = 0.246$ m data were more spread in u' than w' because the pulses which travelled deeper, also travelled further downstream before rising towards the surface. The additional turbulence which the pulses caused within the downstream water column could have caused suspended sediment to travel further downstream before settling, than if the vorticity had not passed to downstream of the roller (discussed below).

4.3 DISCUSSION OF SEDIMENT-FREE HYDRAULIC JUMP

4.3.1 Flow patterns

Despite the higher Froude number in most published experimental studies compared with that of Run 1, there are similarities in the flow pattern. The shape of the hydraulic jump is consistent with Murzyn *et al.*'s (2005) photograph for $Fr_s = 3.0$ as well as the sketch of Chanson and Brattberg (2000) who reported hydraulic jumps of $Fr_s = 6.33$ and 8.48. The shape was only marginally steeper than the surface profiles measured by Sarma and Newnham (1973) for $Fr_s = 1.10 - 3.79$ with fully developed inflow downstream of an undershot sluice gate.

The value of maximum velocity in a vertical profile of streamwise velocity, $\bar{u}_{max}$ decreased exponentially with distance downstream from the toe of the hydraulic jump, unlike the value of $\bar{u}_{max}$ in Chanson and Brattberg's (2000) hydraulic jumps, which decreased linearly downstream. I think that this would have been due to decreasing influence of friction on the lower jet edge from upstream to downstream along the path of the jet as the jet detached from the flume floor underneath the hydraulic jump. The detached jet thickened downstream as it slowed. The nature of how it thickened was unclear visually but from the detachment point downstream thickening would have been exponential, in proportional to its exponential slowing if the volume flux of water through the jet was constant in time. Because water may

have continuously been transferred between the roller and the jet, at variable rates, there may have been a non-constant volume flux of water through the jet and the thickening may not have been exponential. Because the stream of upward and downward travelling vortices widened downstream the submerged wall jet thinned downstream and slowed downstream.

Influence of vortices on the velocity pattern in the roller

Ignoring the rest of the flow, the $\bar{u}$ profile of a constant stream of vortices would be the same at any location along the stream. In the sense of rotation of the vortices seen in the roller, the lower part of the vortex stream would increase the magnitude of u of the flow and the upper part of the vortex stream would decrease the magnitude of u of the flow (Appendix 3). The upper part of the vortex stream could have been involved with the negative values of $\bar{u}$ in the roller (Profiles A – E, Fig. 4.4B; the reverse flow strip, §4.3.1 certainly was involved). The increase in velocity over the lower half of the vortex courses was magnified, and the decrease over the lower half decreased, where the jet had slowed (by up to 85%). Because of the stream of vortices, flow immediately above the submerged wall jet may have had more downstream momentum than that within the jet.

4.3.2 Detachment of the jet

Although jet separation from a lower boundary has been described in sites with positive lee-side ramps (McCorquodale & Khalifa, 1980; Mossa & Tolve, 1998; Balachandar *et al.*, 2000; Liu *et al.*, 2004; Yüksel *et al.*, 2004) and at sharp negative steps such as at a headcut (Bennett & Casali, 2001; Alonso *et al.*, 2002), wall jets entering hydraulic jumps above flat surfaces have until recently been assumed to expand into the tailwater without any separation from the floor. Run 1 confirms that wall jets in oscillating hydraulic jumps (classification of Massey, 1983) do separate from a solid floor rather than simply diffuse into a parabolic tailwater (cf. Alhamid, 2004; Lennon & Hill, 2006; Dey & Sarkar, 2007). There has been little published discussion of the cause of separation of a jet entering a hydraulic jump or other adverse pressure gradient, and none on the implications for sediment movement. From upstream to downstream through the hydraulic jump, the viscous boundary layer (of sub-millimetre thickness) moves from a region of relatively low pressure to one of relatively high pressure and it is probable that in Run 1 the viscous boundary layer, in high *Re* conditions, separated

from the flume floor. Local separation of the viscous boundary layer from the boundary can induce a larger scale change of the direction of the jet as observed in Run 1.

4.3.3 Position and motion of vortices

Distribution of vorticity

Vorticity can enter a flow, due to one part of the flow spilling onto another (first described by Hornung *et al.*, 1995) and within a shear layer across which flow velocity rapidly changes (cf. Winant & Browand, 1974). Vorticity which enters the flow at the toe, can make its way into the shear layer between the submerged wall jet and the roller, by convection (Hornung *et al.* (1995). In Run 1 the toe repeatedly spilled onto the submerged wall jet and the splashes repeatedly spilled onto the surface above the roller. In consequence the roller had the highest vorticity in the flow and most of the coherent rotating structures seen were within it. Because all vortices which passed downward from the shear layer into the submerged wall jet appeared to smear out and cease to circulate, within a few tens of centimetres as they passed downstream, this suggests that the submerged wall jet was supercritical. The lower vorticity below the detached jet compared to within the roller, was associated with lower $\dfrac{\partial \bar{u}}{\partial z}$ across the lower jet edge compared to the upper jet edge. Some vorticity below the detached jet was noticeable to observers in the form of vortices with a much slower rotation than the roller vortices (red arrows, Fig. 4.4A). Vorticity below the detached jet was associated with lower magnitude turbulent fluctuations than vorticity within the roller was. The lack of coherent rotating structures downstream of the roller (dark blue arrows, Fig. 4.4A), and presence of the pulses (that transported bubble sets, §4.2, light blue arrows), suggests that vorticity had diffused. The diffusion of vorticity, in general is promoted by small rather than large changes to $\bar{u}$ on small timescales; the much lower spread in u' and w' downstream of the detached jet compared to that within the detached jet and the roller, suggests that vorticity could diffuse on passing downstream of the roller (Fig. 4.7). This would promote the fallout of sediment from suspension. Coherent vortices shed from the lower edge of a detached jet have not previously been reported. Having a much smaller rate of circulation than the vortices within the roller, it

126

is unclear whether their presence would result in maintaining sediment suspension in the same way.

Axis of orientation of vortices within the hydraulic jump

The properties of vortices (1) having had a cross-stream axis of rotation and (2) having been incepted in a plane shear layer between relatively fast and slow parts of the flow, are consistent with reports of Winant and Browand (1974) in a different type of flow. In Winant and Browand's (*loc. cit.*) flow, *Re* was less than one thousandth that in Run 1. Brown and Roshko (1971) also noted (1) and (2) in an air flow at high *Re*. Despite the consistent axis of rotation of all vortices, each splash (defined in §4.2) did not rise up across the full width of the test channel and the folds of the breaking water surface were oriented in all directions, obliquely to the direction of flow (Fig. 4.5).

The manner in which vortices moved out of the roller

In my judgement, vortex escape from the roller caused the periodic pulses observed within the upper part of the tailwater. When a pulse was not present, the upper jet edge approached the water surface (the *jet up* state) isolating the roller from the tailwater; vortices rotated within the roller and became diffuse adjacent to the reverse flow strip. When a pulse occurred (§4.2) the diffuse tip of the jet was lower in the flow and the vortices moved downstream into the tailwater and became diffuse. The additional vorticity in the upper region of the tailwater caused the change in mean velocity profiles (the offsets to profile patterns in Fig. 4.4B).

There are three possible mechanisms for periodic release of vortices from the roller: (1) Tightly rolled vortices may have had strong enough circulation and streamwise velocity to escape the roller, pushing the upper jet edge downward as they travelled downstream, close to the surface. Those vortices which maintained outlying positive values in u ($u' >> 0$; Fig. 4.7) may escape the roller. (2) The detached jet tip, a short distance upstream of the tailwater could have moved back and forth along the path of its core of highest velocity, hypothetically fixed in space. If the tip moved upstream and downstream along the path, the vertical distance, H between the tip and the surface would have fluctuated and H changed around its time-averaged position (0.75 of the total water depth, §4.3). Vortices would be more or less likely to pass to downstream of the jet, depending on the magnitude of H. (3) At 'splash condition' (Fig. 4.3A)

a surface peak exists over the roller, and with it an additional short-lived downstream pressure gradient. It is possible that this pressure gradient forced the downstream parts of the detached jet from its usual *jet up* state to *jet down*, in which state its path was lower within the flow. In doing this, a vortex may have been let out of the roller because in *jet down* state *H* would be increased without the path of the jet being shortened. Subsequent upstream spill of the hydraulic jump would have collapsed the surface peak, and so allowed the jet to return to the *jet up* position.

The first mechanism is least likely to release the vortices which caused the offset to tailwater flow because the jet tip was not seen to move downward in response to a vortex being directly above it. This is despite the roller vortices having had smaller diameters and greater rates of rotation than vortices observed by Long et al. (1991), were always in motion and did not coalesce. The second mechanism could occur when the wall jet was slowest because under equivalent conditions of friction it would slow to the velocity of the tailwater over a shorter distance, so shortening the path to the jet tip and increasing *H*. For repeated periods of up to 2 s the supercritical wall jet was slower than the lower bound of the steady flow (Fig. 4.6A); periods of 2 s were long enough for the passage of up to 2 vortices. These periods could be due to the flume pumps (although there is no regular period) or due to the supercritical inflow being only partially developed. Friction working on the jet under the hydraulic jump is unlikely to change much through time because of the constancy of the stream of vortices above it and the constancy of the slow flow below it. The third mechanism is also considered likely to produce some of the periodic releases observed: If the constant air intake at the toe and unsteady roller surface exceeds the bubble flux out of the roller surface, the volume of the roller increases; the level of the roller surface may be periodically raised above the level of the tailwater surface. The rapid up-flume spill of the splash would rapidly allow the jet to return to *jet up* and bound the downstream extent of the roller. This process could repeat with a near constant period and the sub-second duration that splashes took to appear and then collapse compares with the durations that the jet was in the *jet down* state. The mean frequency of the jet moving into the *jet down* state does not account for pulses every 5 s but the slowing to the supercritical wall jet is much more frequent and the three mechanisms may all operate, resulting in a complex periodicity to the flow within the hydraulic jump.

4.4 RUN 2: HYDRAULIC JUMP WITH SAND FLUX

Run 2 involved the pumping conditions of Run 1 and the addition of sediment at a near constant rate, starting from time, $t = 0$ when sediment was first added. The reader is referred to Fig. 4.2 for the character of the sand and Tables 4.1 and 4.2 for the manner it was shovelled onto the conveyor.

4.4.1 Comparison of hydraulic jump behaviour with and without sediment

Because the presence of suspended sediment increases slightly the kinematic viscosity of flow, compared to the Run 1 condition *Re* was decreased but remained well over 270,000 and was nearly constant with time after sediment was first added. Despite the same pump settings the presence of suspended sediment caused the flow to be generally slower than in Run 1 causing *Fr* to be lower (Eqn. 1.1).

Flow pattern

In Run 2 the hydraulic jump moved upstream at an almost constant rate in response to sand accumulating downstream of it. Specifically it moved 2.72 m in response to almost 5000 kg of the sand accumulating on the flume floor. The position of the toe of the hydraulic jump in Run 2 oscillated to the same degree as the toe of the sediment-free jump. The system of breaking of the water surface seemed to be equally complex with folds of the water surfaces being in similar ranges of size and orientation as the folds of the water surface of the Run 1 hydraulic jump (compare Figs 4.5 and 4.8). The same fluid processes were observed, in the same geometry as in Run 1: The jet detached from the flume floor with similar angle, from the same streamwise position relative to the toe of the hydraulic jump and rose to a similar flow depth downstream; vortices were generated at locations consistent with Run 1, with a similar scale and frequency and passed downstream along similar paths. Bubbles were observed, but fewer than in Run 1 and none observably persisted downstream of the roller (Figs 4.9A and B), making flow components (e.g. vortices) more difficult to see.

Figure 4.8 Oblique photograph of the water surface of the supercritical flow, hydraulic jump and tailwater in Run 2.

Figure 4.9 (below) Photographs of Run 2 showing (A) The roller and the jet beneath, taken seven minutes after the sediment addition started. Flow structure was similar to Run 1 (compare Fig. 4.3). The blue vertical supports are 0.80 m apart. (B) The first *hydraulic-jump unit bar* which was prograding over the fine sand sheet, at thirteen minutes. The blue vertical supports are 0.80 m apart. (C) The slip face of the youngest *hydraulic-jump unit bar* prograding downstream over the fine sand sheet at twenty four minutes, after upstream progradation of the upstream part of the bar has ceased. Some slip faces contained distinctly finer sediment than others. The silver bolts are 0.15 m apart.
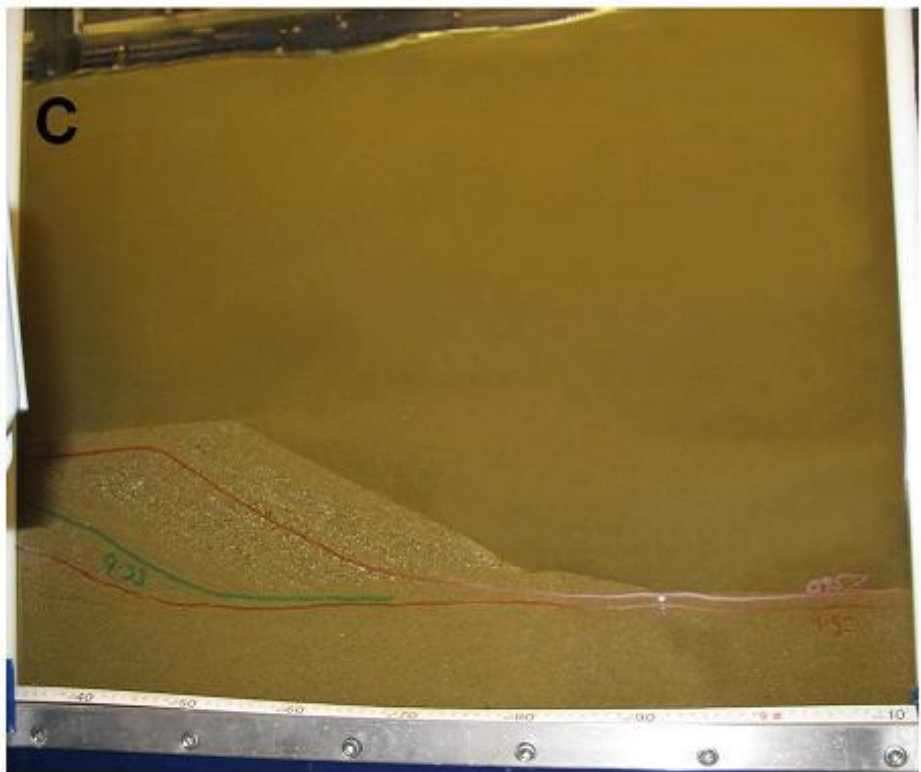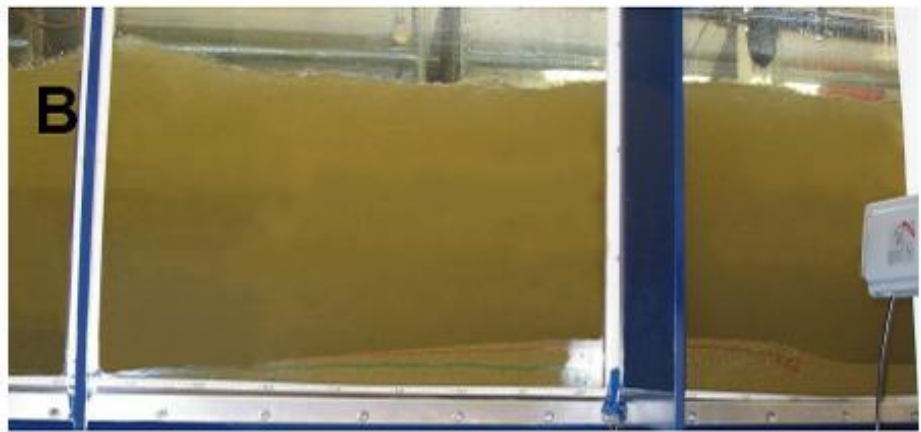
Streamwise velocity profiles were measured at $x = 6.100$ m at eight time intervals representing distances increasingly downstream of the hydraulic jump. The progressive upstream movement of the hydraulic jump made it possible to measure velocity further downstream from the hydraulic jump in Run 2 than was measurable in Run 1. The streamwise velocity field at the most upstream profile within the hydraulic jump, was similar to that at the same site in Run 1 (Profile L in Fig. 4.10 compared to Profile G in Fig. 4.4B). However, the velocity peak was 0.2 m s^{-1} compared to 0.95 m s^{-1} during Run 1. Velocity decreased more rapidly above the peak than below it in Run 2 while the opposite was true in Run 1. The near-bed velocity peak (in *jet down* conditions) was closer to the bed in Run 2 than in 1. At the downstream end of the roller the *u*-profile was offset at $z = 0.26$ m (Profile M; Fig. 4.10) above which *u* markedly increased before decreasing to the water surface, as in Run 1. Downstream from this position, the velocity field in Run 2 differed from that in Run 1. No profile offset was apparent. At the more distal sites the velocity increased towards the bed, and was 0.15 m s^{-1} at 0.01 m above the bed (the lowest measurable height; Profile Q, Fig. 4.10).
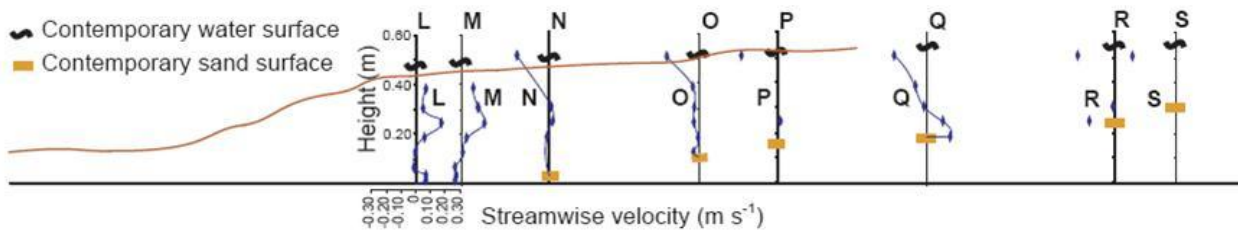
Figure 4.10 Profiles of time-averaged streamwise velocity component, $\bar{u}$ for Run 2, measured by UDVP and averaged over measuring intervals of 600 seconds. The UDVP array was fixed at $x = 6.10$ m throughout the run. The hydraulic jump moved upstream with time. The profiles are drawn in positions relative to the contemporary hydraulic jump (compare the brown line showing lowest surface position with the same line in Fig. 4.4A and B). Profiles Q to S are further downstream of the hydraulic jump than was measurable in Run 1.

Sedimentation

All patterns of sediment transport and deposition were effectively seen in 2d because the concentration of suspended sediment was at all times sufficient to occlude the view more than a few centimetres into the test channel. All sand within the supercritical flow was transported in suspension or turbulent suspension-modified saltation. As the sand entered the hydraulic jump, some of it moved from the jet into the roller and some into the water below the detached jet (Fig. 4.9A). Most of the sand remained in the jet as it detached from the bed. The sand distribution downstream of the distinct jet appeared uniform throughout the water column,

132

although suspension concentration patterns were not measured. Sand dropping from slowing and reversing-flow in the roller was instantly accelerated by the jet underneath. In the *jet up* state some sand dropped from the detached jet and through the underlying zone of separation onto the bed. When the flow pattern had switched towards the *jet down* state this sand was pushed downstream as a bedload sheet a few grains thick, to form a mound in the tailwater about 0.8 m from the jet separation point (at $x = 6.90$ m). At the same time, finer sand was dropped from suspension downstream of the mound and formed a thin sheet. While the fine sand sheet thickened, the mound grew and prograded downstream over it (Fig. 4.11B). A small relatively fine-grained set of upstream-inclined laminae formed on the upstream edge of the mound as it grew upstream, and a coarser-grained avalanche set formed on the downstream edge. As the bedform grew downstream, the topset aggraded and the avalanche face progressively overlapped the distal fine sand sheet (Figs 4.9B and 11C). The aggradation of the topset was at least ten times slower than the progradation of the foreset. The small amount of fine sand falling onto the feature surface was transported over the brink and incorporated with the coarser sand in the lee-side avalanche set and topset (Figs 4.9C and 4.11D). When this bed feature was fully developed the upstream growth slowed, at times becoming imperceptible. The fine sand sheet continued to thicken downstream of the avalanche face and a diachronous boundary formed between it and the overlying set (Fig. 4.11E).

Figure 4.11 (below) Model of *hydraulic-jump unit bar* formation and growth. (A) Initial mounding on the non-erodible bed and fine sand falling from suspension, forming a sheet downstream of it. This stage of hydraulic-jump unit bar growth is represented in Fig. 4.9B. (B) Accretion of relatively fine sand on the upstream side of the newly formed *hydraulic-jump unit bar* and formation of a coarser grained avalanche face on the downstream side. The massive fine sand sheet continues to thicken to form an elongate wedge. (C) The downstream avalanche face prograde over the massive sand wedge. (D) Reduction in the rate of upstream growth corresponds to more fine sand reaching the avalanche face. As the slip face moves further from the hydraulic jump, fine sediment settling from suspension (previously falling to the massive fine-grained wedge) is incorporated in the foresets. The topsets aggrade as the foreset prograde and the unit appears to climb. This stage of hydraulic-jump unit bar growth is represented in Fig. 4.9C. (E)The pattern formed in (D) continues with topset aggradation and downstream extension. Inset boxes (i to iii) in (B), (C) and (D) Detail of change in the shape of the front of the unit bar, explaining the blocking (and deposition) of fine grained sand and later bypass.

A

■ Finest sand deposited from suspension
□ Sand finer than the bulk load
▫ Sand coarser than the bulk load

Water surface

Initial sediment mound

Sand deposited as a sheet

B

i   Upstream edge

C

ii

D

iii

Topset   Cross set becomes finer downstream

E
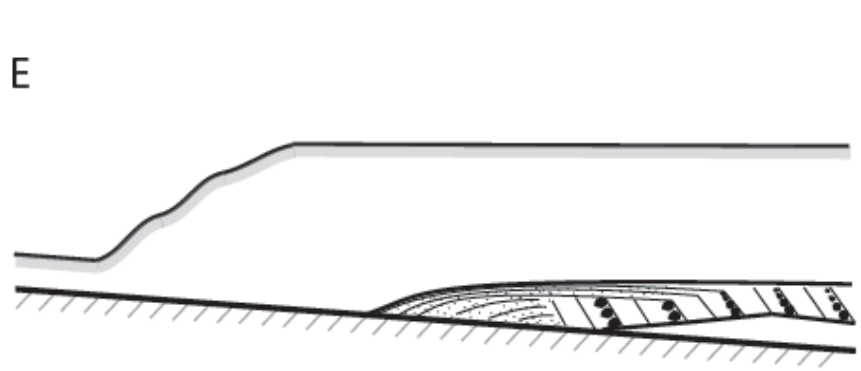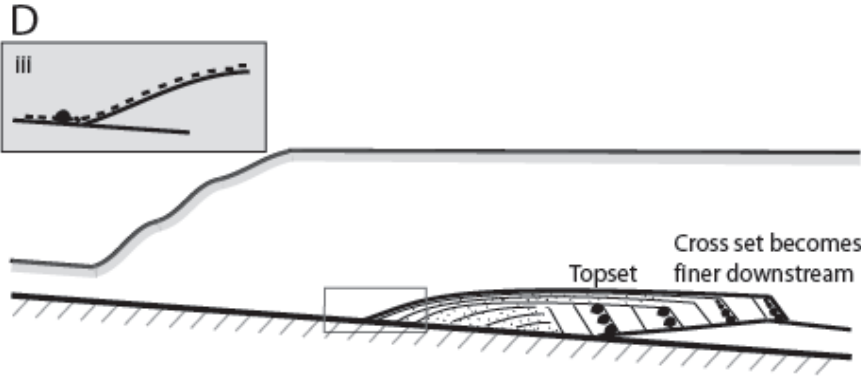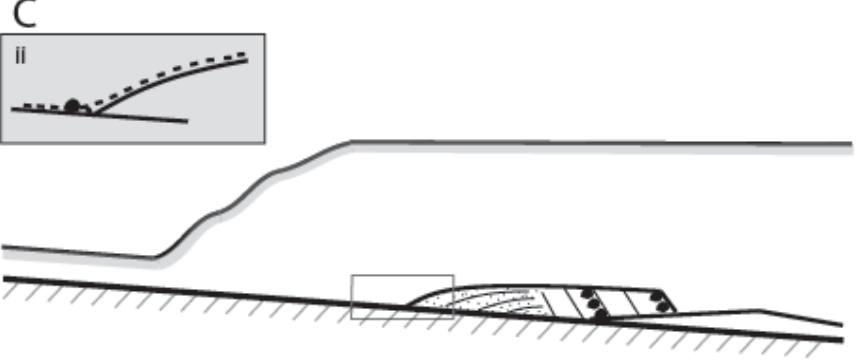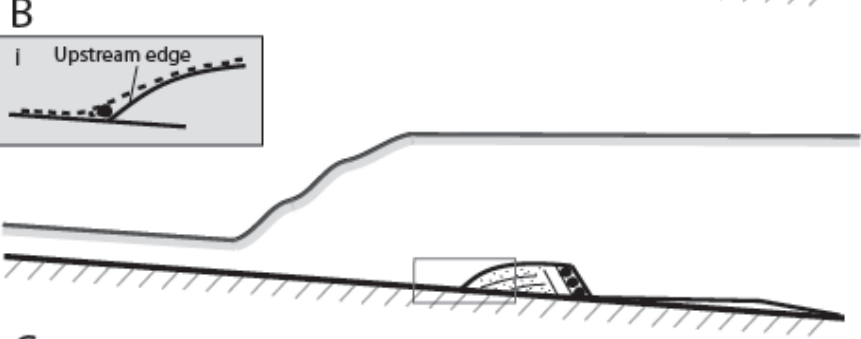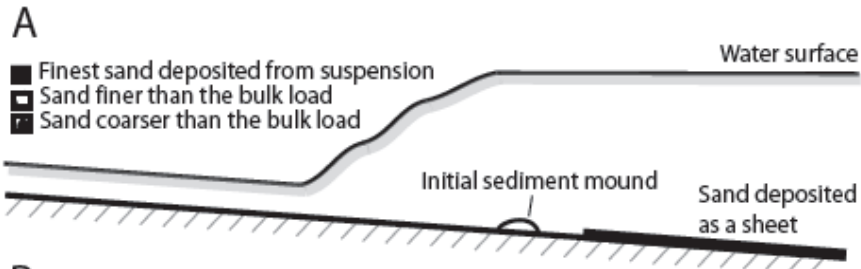
At any point in time the deposit surface had a shape that increased in height downstream asymptotically to the position $z\big|_{x=10m} = H\big|_{x=10m} - h\big|_{x=10m}$. The shape fluctuated over time from this broad shape and local changes in the surface amplitude were up to half of the deposit thickness in magnitude. Sediment accumulation caused the surface of the tailwater to rise, increasing the hydraulic jump surface gradient. This change caused the hydraulic jump to move upstream (Equation 1.6; §1.4.3). The sediment accumulation pattern moved gradually upstream in tandem with the hydraulic jump forcing positive feedback. The bed feature continued to grow, with slow upstream progradation, rapid downstream avalanching and slow topset aggradation. The tailwater above it continued to rise. Periodically a new bed feature formed above or upstream of the previous bed feature and grew in a similar way to the previous feature. As a new bed feature developed the older feature became inactive and the new downstream-dipping avalanche faces prograded and climbed over the top of it (Fig. 4.12). When the avalanche face height produced a strong enough lee separation eddy, counter-flow ripples formed and these migrated up-face up to one third of the height of the lee face before being met by an avalanche of downstream travelling bedload. If a feature prograded to further downstream than the feature below it, the avalanche faces amalgamated. At the end of Run 2 an avalanche face was still prograding downstream and a proto bed feature was forming on the upstream face of the deposit.
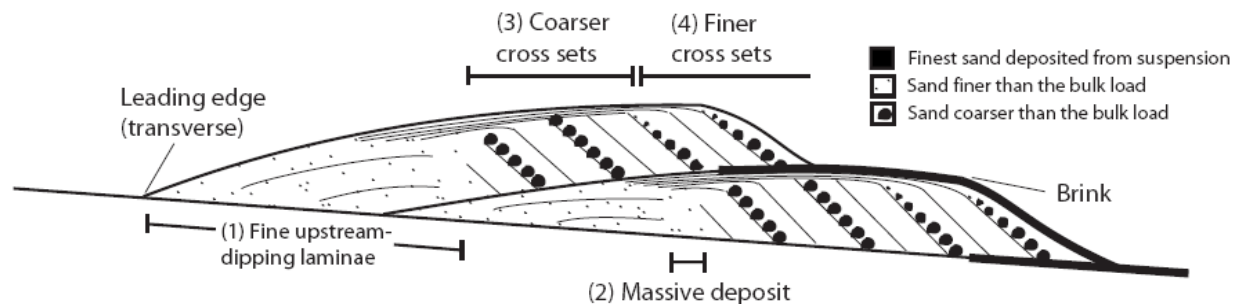
Figure 4.12 Diagrammatic representation of the architecture of the unit bars formed downstream of the hydraulic jump, with near-steady sand addition, steady pumping rate, and non-erodible flume floor. The large (small) grains depict a location where grain size distribution is negatively (positively) skewed with respect to the bulk load. The thin lines illustrate the general orientation of laminae within the unit bar and the thick line depicts the suspension fallout deposits.

4.4.2 Deposit architecture

In this experimental run six discrete beds developed (Fig. 4.13); numbered 1 – 6 upwards. The beds were too long and laboratory space too small to photograph the beds in full. Details from each bed are presented from photographs in five unnumbered subsections below. Beds 2 – 6 developed sequentially and displayed the same general internal character: The pattern of sedimentation associated with the hydraulic jump had formed distinctive bed features with a characteristic anatomy (Fig. 4.12) here termed a *hydraulic-jump unit bar*. In general the *hydraulic-jump unit bar*, when fully developed, had the form of an elongated bed with a sharp lower boundary, upstream-dipping upstream bed termination, flat upper surface and steep downstream bed termination. The cross-stream bed shape cannot be defined as the flume experiments were effectively 2d. The internal architecture of each *hydraulic-jump unit bar* was: At the upstream end, a small wedge of gently upstream-dipping (-9° to 7° relative to the lower boundary) convex up laminae with grain size smaller than the bulk composition of sediment from the crates. This graded downstream, through a small volume of massive sand, into a downstream-dipping cross set with coarser grain size. This foreset passed downstream into a finer grained foreset which approached the same grain size distribution as the bulk sediment load. The brink of the foreset was the highest point of each *hydraulic-jump unit bar*.
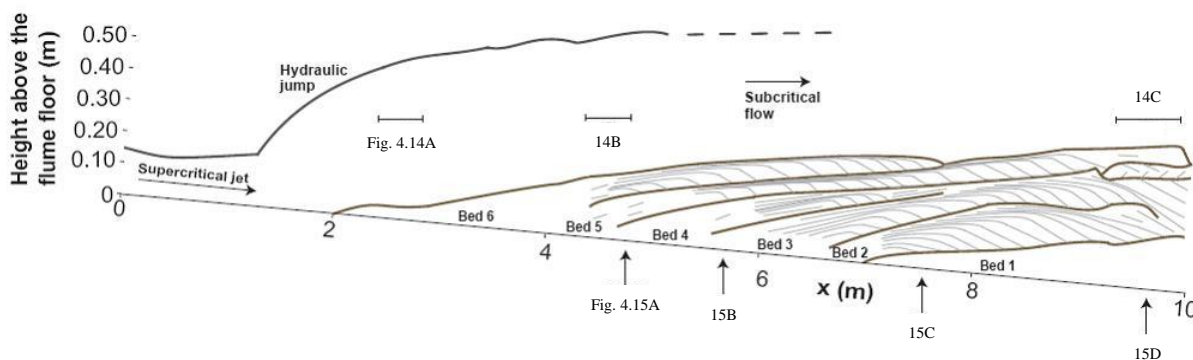
Figure 4.13 Pattern of lamination within the deposits of Run 2 represented in a stream-parallel section. The line representing the water surface corresponds to the final position of the hydraulic jump at the end of the run. The initial position of the toe of the hydraulic jump was at $x = 4.68$ m.

Above both foreset types, low-angle laminae formed a topset, which locally reached thicknesses similar to the underlying foreset. The oldest (lowest) foreset was underlain by a massive fine layer. Foresets that overrode the oldest foreset were underlain by the fine unit at

the distal end. Each *hydraulic-jump unit bar* had a bidirectional cross set pattern with greater development of the downstream sets.

The downstream part of the deposit was a coset of avalanche foresets with set boundaries dipping upstream to give a climbing and upward-thinning coset (Fig. 4.13). The set boundaries were well-defined except in the area of the upstream-dipping lamination, and graded from convex up to concave up. Each successive bed was longer than its predecessor, and pinched out to the flume floor further upstream of it. The set boundaries were less distinct in the area of the upstream-dipping lamination. The transition between the upstream and downstream dipping cross laminae occurred progressively further upstream in successive beds and contact between the two component sets became sharper. This architecture is termed a *hydraulic-jump bar complex*. The uppermost 0.1 m and downstream-most 0.8 m of Bed 5 had collapsed into the discharge tank (Figs 4.14C and 4.15D). Otherwise, the deposit was undisturbed. In the stream-parallel sections the same features were observed, and at comparable streamwise locations, as seen forming through the flume sidewalls (described above).

Details of the basal wedge

The *basal wedge* (Bed 1) gradually thickened downstream from its upstream limit at $x = 6.70$ m, to 0.18 m at the end of the test channel. Containing sediment much finer than the bulk load, it made a distinct contact with the beds which overlay it at different streamwise locations when viewed in stream-transverse section (Fig. 4.14C) but was not distinct in stream transverse section (Fig. 4.15D). No length scale can be defined for this unit as it would have continued downstream if the flume had been longer.

Details of the coset of avalanche foresets

The foresets of Beds 2 – 6 that comprised the coset of avalanche foresets are termed Foreset 2 – Foreset 6 for convenience. Foreset 2 had a downstream termination at $x = 9.74$ m. The termination dipped downstream. Foreset 4 pinched out at $y = 0.66$ m at $x = 7.55$ m. Foresets 3 and 5 terminated at the downstream limit of the test channel and would have extended further downstream if the flume were longer. Foreset 6 was still developing when the run was ended.
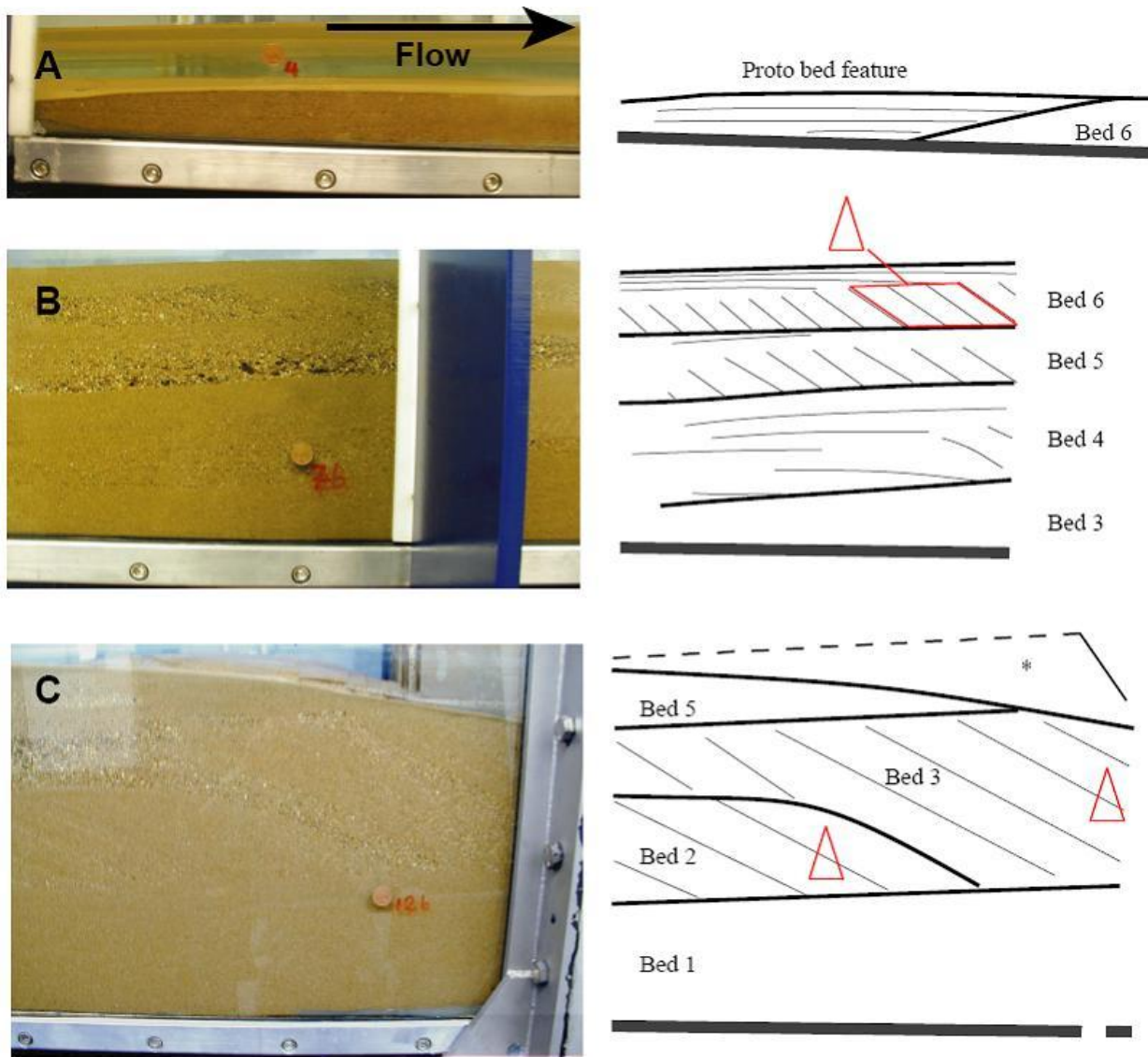
Figure 4.14 Photographs taken through the sidewall of the flume (i.e. stream-parallel sections) and corresponding line drawings of the deposits of Run 2. The location of each photograph is indicated in Fig. 4.13. The coin used for scale is a British penny and is 20 mm in diameter. The lighting conditions were varied to highlight the lamination; this gives a false impression of variation in sand colour. The line drawings are labelled with bed numbers as in Fig. 4.13. The red triangles with apexes at the top indicate that grain size is coarsening-upward within the corresponding bed. The area highlighted by the asterisk (*) was within Bed 5 before the flume was drained.

Each foreset in the coset was visually discernable from the set of fine laminae upstream because of the coarse sand fraction which it contained. At its upstream limit each coarse grained foreset was thin (approximately half the thickness of the adjacent massive deposit) and thickened rapidly downstream, with increased dip angle, as the topset above it thinned.

138
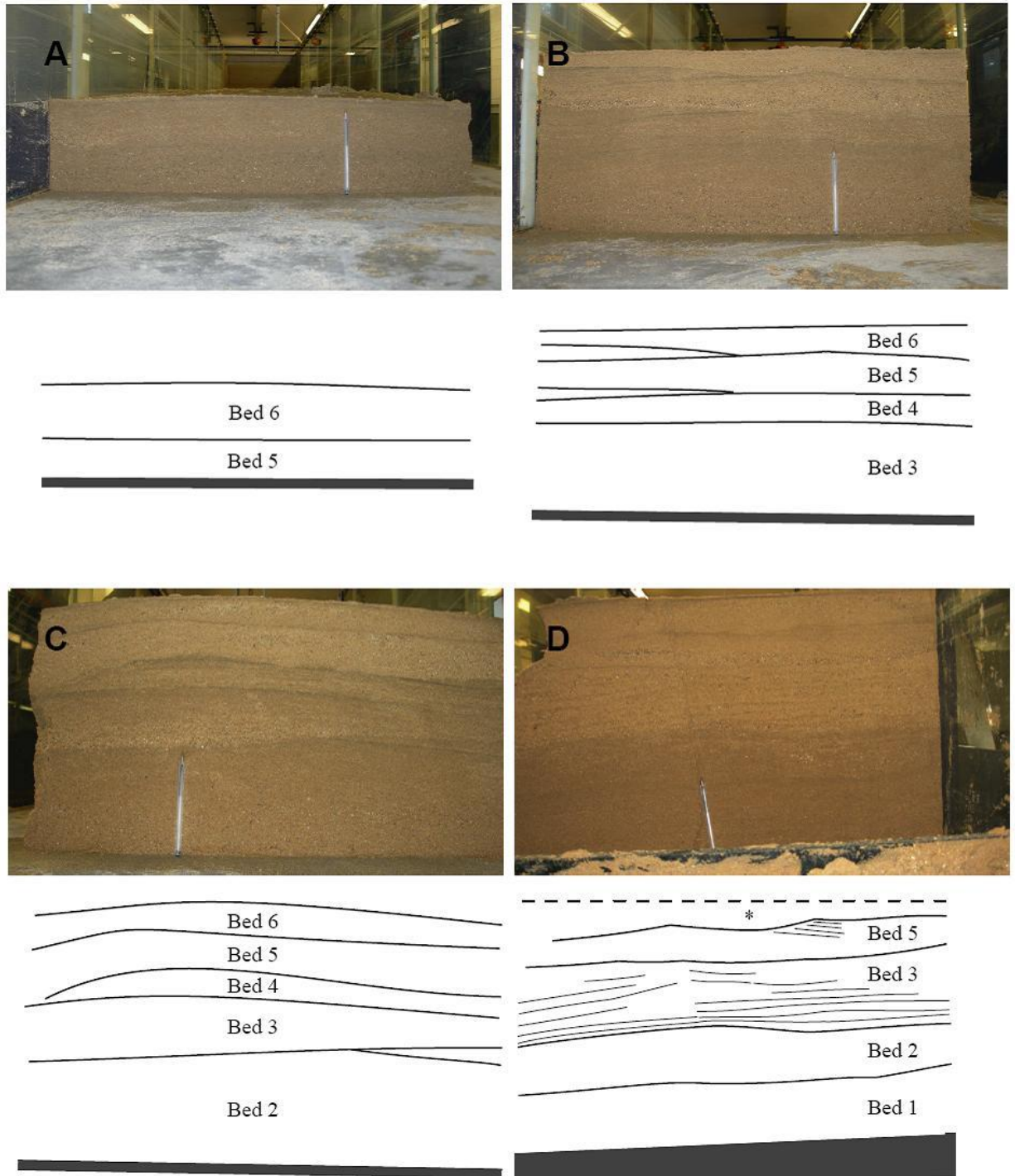
Figure 4.15 Photographs and corresponding interpretative line drawings of sections cut through the deposit perpendicular to mean flow direction (i.e. stream-transverse sections) with an 0.14 m long pen for scale. The most upstream section is A and the most downstream is D. Their positions are indicated on Fig. 4.13. A and B were photographed looking downstream, C and D are looking upstream. The thick line on each line drawing is the boundary of the deposit and the flume floor, and the laminae above are traced from the photographs in close-up view. Note that in section D, Bed 5 sits in contact with Bed 3. The area highlighted by the asterisk (*) was within Bed 5 before the flume was drained.

The maximum foreset angles occurred within the coarser foresets and the dip decreased downstream with grain fining. Each downstream transition from coarse cross set to cross set with granulometry approaching the bulk load, was streaky along the streamwise extent of transition: At the downstream termination of Bed 2, a cross set approaching bulk-load grain size was preserved (Fig. 4.14C). The *hydraulic-jump unit bar* above it (Bed 3) exhibited the patchy transition between the two cross set types at this streamwise location (Fig. 4.14C) with the coarse cross set being interspersed with foresets with bulk load granulometry. The youngest *hydraulic-jump unit bar* (Bed 6) was the only one where the downstream-most metre of the foreset contained no patches of coarser laminae, so Bed 6 displayed the complete transition to bulk-load cross set.

Towards their upstream limit, coarse grained foresets occurred in three packages a few centimetres thick at the left sidewall ($y = 0$) that pinched out within 0.35 m across the flume, at the top of Beds 2 (Fig. 4.15C), 4 and 5 (Fig. 4.15B). Towards their downstream limit they occurred across the flume width (Bed 3; Fig. 4.15C). At the base of Foreset 5 counter flow ripples had deposited upstream-dipping laminae at the downstream end of the test channel, and produced distinctly coarse sets (Fig. 4.15D).

Details of the topsets above the foresets
The topsets of Beds 2 – 6 are termed Topset 2 – Topset 6 for convenience. Topsets abruptly overlay the foresets (Bed 6; Fig. 4.15B) and generally thinned downstream. Being incepted further upstream, each topset was thinner and finer grained than the topset of the bed below at the same streamwise location (compare the Foresets 5 and 6 in Fig. 4.14B). Many of the individual topset laminae could be traced for several metres in the streamwise direction, particularly in the more upstream portion of each bed, above the coarser grained cross set. Topset 2 pinched out downstream, upstream of the downstream termination of the bed (Fig. 4.14C). The contact between each topset and the foreset directly above was sharp.

Details of the volumes of massive sand between upstream and downstream dipping lamina sets
The volumes of massive sand between the cosets (the original mounds) were observed in Beds 2 – 6 (Fig. 4.13). They spanned up to 0.3 m in the streamwise direction and were preserved with a similar shape to the *hydraulic-jump unit bars* that developed from them, with upstream-

dipping upstream bed termination and low angle arcuate upper surface (Fig. 4.14B; Right hand side of Bed 4). The downstream terminations of each of these volumes of the massive sand were arcuate and more abrupt than the upstream terminations of the beds (though not sharp, Fig. 4.14B; Left hand side of Bed 5).

Details of the area of upstream dipping lamination

Upstream-dipping lamination was distinct in the proto bed feature (Fig. 4.14A) which had been developing for three minutes only. The contact between the proto bed feature and larger bed feature below was not easy to distinguish (Figs 4.14A and 4.15A). In the section shown in Fig. 4.15A, one set of upstream-dipping laminae directly overlay another and the inter-set contact appeared indistinct except adjacent to the flume sidewall. Both sets consisted of sand finer than the bulk load, which fined towards the top of the set. Because upstream-dipping laminae in more developed *hydraulic-jump unit bars* had a similar shape in streamwise section to the bed contacts (e.g. Bed 4 in Fig. 4.14B) the bed contacts were difficult to distinguish.

4.5 DISCUSSION OF SEDIMENT TRANSPORT AND DEPOSITION

4.5.1 The Run 2 velocity profiles

In Run 2, the lower jet edge in *jet up* conditions was more distinct than in Run 1 and the velocity peak in *jet down* conditions was closer to the flume floor; both of these promoted bedload transport underneath the jet and a more distal inception of the initial sediment mound than was anticipated from observations of Run 1. The rapid decrease in u above the mid-detached jet maximum within the roller, and associated decreased vorticity production compared to Run 1, would lead to less vorticity passing downstream into the tailwater. This provided a hypothetical negative feedback between suspended sediment concentration and the preferential length scale of the massive basal unit.

4.5.2 Sediment transport through a hydraulic jump

A massive basal unit is thought typical of deposition downstream of a hydraulic jump because of (a) the ability of the turbulence within the hydraulic jump to maintain sediment in

suspension and lift it into the downstream-expanding flow depth of the hydraulic jump and (b) the decline in turbulent regime downstream of the hydraulic jump where fallout from suspension takes place. The distribution of grain size that fell onto the *basal wedge* could have been controlled both by the distribution of grain size that entered the hydraulic jump and the segregation of grains that fell to bedload within the hydraulic jump (§4.4.1). As each *hydraulic-jump unit bar* developed above the *basal wedge*, sand was deposited from suspension within the prograding system, particularly at the downstream part of the *hydraulic-jump unit bar*. In consequence it was the base of the deposit that the only body of massive sand more than a few millimetres thick that formed within the *hydraulic-jump bar complex*. The 'rare mud drapes between coarse laminae' described by Massari (1996) were thin and could have been suspension fallout deposits.

Despite the uniform streamflow in the tailwater (affected in an upper region by vortex release from the roller) at no time were downstream migrating bedforms superimposed on any *hydraulic-jump unit bar* surface. It is common for other barforms to have bedforms on their upper surface and, whilst the reason for the absence of bedforms is yet unknown to me, it is exciting and interesting to report their absence. The flow above the developing *hydraulic-jump bar complex* (§4.4.1) could in other situations be associated with the formation of dunes in the medium sand used according to the bedform phase diagrams of Carling (1999) and Van den Berg and Van Gelder (1993). The most likely explanation is that bedload flux was sufficiently high to suppress bedform development and the rate of bedload flux over a *hydraulic-jump bar complex* could be quantified through further work.

A foreset brink climbing a slope greater than 5.7° raises the deposit height more than the topset aggradation, which was an order of magnitude slower than foresets prograded in the slopewise direction. The upstream movement of the hydraulic jump was affected more by the brink whilst Bed 2 was growing, and more by the topset whilst Beds 1 and 3-6 were growing. After Bed 2 was deposited, each new bed made the *hydraulic-jump bar complex* surface shallower and topset aggradation had increasingly more effect than brink progradation on the upstream movement of the hydraulic jump. Local increases in the deposit surface height increased the tailwater levels irrespective of how close they were to the hydraulic jump, shown to be true for a constant increase in height at fixed x by Vide *et al*. (1993).

4.5.3 The Run 2 deposit architecture

A distinct sequence of beds was formed in the flume in conditions of constant water recirculation and near-constant sediment transport. There was no obvious correlation between the timing of initiation of new unit bars and sediment input rate variation. Notably there was no obvious correlation with the short hiatuses in the sediment addition resulting from changing crates; two new unit bars formed during loading of the sand from the second crate (Table 4.2). The first two unit bars to form, formed straight after sand was loaded onto the conveyor from the first two crates, but the next three unit bars were formed more than ten minutes after a new crate was put in place.

The periodic formation of new *hydraulic-jump unit bars* successively above and upstream of the previous unit bar occurred because of the upstream movement of the hydraulic jump and the migration with it of the pattern of sediment transport. The formation of a new unit bar was not controlled directly by the boundary condition below the sediment transport pattern, which changed between flume floor and sediment surface, and between downward and upward slope, during Run 2. New mounds of sediment could have formed if the jet did not enter the *jet down* state for a sufficiently long time, though there are no data to suggest this happened periodically. More likely the mounds formed at times of highest bedload transport to the upstream limit of the deposit, within a periodic fluctuation in bedload transport. All the bedload transport that was observed was from upstream to downstream, so it was sediment that fell from suspension below the detached jet that became the bedload transported to the upstream limit of the deposit. The volume of flow between the lower jet edge, the flume floor and the upstream limit of the deposit contained the sediment that formed each new mound. Generally this volume increased gradually with the upstream motion of the hydraulic jump, but periodically it decreased suddenly when each new mound formed. It is likely that this volume has a maximum volume, at which a new mound forms; the maximum volume would be a function of the shape of the hydraulic jump and the grain size distribution of sediment transported through it.

In Run 2 the deposits did not have architecture similar to classic backset beds described from the rock record (§1.8). The finer grained proximal part of the *hydraulic-jump unit bar* did have low-angle upstream-dipping cross bedding, and the set boundaries between the unit bars dipped upstream at a low angle. The absence of relatively steep upstream-dipping

surfaces as described from the rock record may relate to the absence of bed erosion in a flume. If the bed were erodible, scour upstream of the hydraulic jump would increase the amplitude of bed topography and the deposits would form above a scoured surface (e.g. Massari, 1996).

Height and length scales of the sediment features

Further to the concentration of the suspended load the length scale of the basal unit is also controlled by the segregation of bedload below the detached jet, and the grain size distribution (hence settling velocity) which remained in suspension. Because flow slowed downstream and turbulent fluctuations decreased in magnitude through the tailwater, a streamwise gradient of suspension fallout would have occurred (fallout increasing from upstream to downsteream). Because of the srtreamwise gradient of suspension fallout, the character of the *basal wedge* thickening downstream was a function of space. Because the *basal wedge* was overridden by two foresets, the character of it thickening downstream was a function of time as well.

The shape and the length scale of the fully developed *hydraulic-jump unit bars* were different from the massive basal unit (which would form in the absence of a bedload feature). *Hydraulic-jump unit bars* which terminated within the flume length had ratios of height for [upstream-dipping lamina set : mound : coarser foreset : finer foreset] of [2 : 5 : 8 : 6] and length ratios of [2 : 3 : 3 : 6]. Further discussion of these length scales is postponed to Chapter 5.

Grain size segregation in a hydraulic-jump unit bar

The bedload initially mounded on the flume floor at a position within the tailwater and this mound had sharp upstream and downstream edges (Fig. 4.11A). The mound built slowly compared to the flow velocity, which encountered the mound as if it were stationary (Needham & Hey, 1991). The presence of the mound was seen to influence flow velocity, in the lower region of the tailwater close to the mound. Well upstream of the mound, the velocity increased rapidly with distance above the flume floor, whereas immediately upstream of the mound the rate of velocity increase above the bed would have been less, up to the height of the mound. As the bedload approached the upstream edge of the mound, it slowed. In this setting sand at the finer end of the bedload grain size distribution come to a halt on the flume floor at the upstream face (Fig. 4.11B). The coarser grains, having greater momentum as they

approached the mound and protruding higher into the flow where they would have been influenced by greater velocities, moved over the mound. The velocity gradient *blocking effect* segregated the finer bedload on the upstream face of the mound from coarser bedload downstream.

As the upstream edge of the deposit prograded upstream, its dip decreased (Fig. 4.11C) and the velocity gradient immediately upstream would have steepened. As the dip decreased, increasingly finer grained sand was forced over the mound by the flow. The accumulation of relatively fine sand decreased bed roughness and coarse grains more readily traversed the smooth slope in a positive feedback. The blocking effect decreased with time until all bedload was forced across the feature and upstream growth of the unit bar stopped (Fig. 4.11D and E). This contributed to the downstream fining of the foreset (described above) as the finer bedload components were transported to and deposited on, the lee. A more significant cause of downstream foreset-fining was likely to have been that as the unit bar extended downstream, more fine sand fell onto it from suspension and was incorporated in the topset and foreset.

4.6 CONCLUSIONS

1. In the wave of a hydraulic jump of $Fr = 2.73$ a flow recirculation was seen, commonly termed a roller, in which flow travelled upstream in the upper part and downstream in the lower part. Vortices were seen within the roller, itself an expression of vorticity. The vortices travelled along part of the path of flow within the roller before becoming diffuse.

2. Water that flowed into this hydraulic jump under the roller detached from the flume floor, taking a path that rose from the flume floor as flow passed downstream. The path reached as high as 0.75 of the flow thickness and had an indistinct downstream limit. Underneath the path, time-averaged streamwise velocity was more than one order of magnitude lower than along the path.

3. The flow pattern within the hydraulic jump controlled the nature of the resulting deposits and when sediment was added to the system, a deposit developed downstream of the hydraulic jump causing the tailwater to rise and the hydraulic jump to migrate upstream.

4. Most of the finer-grained sediment was deposited from suspension in the slowing tailwater to form a sheet, thickening downstream. Concurrently, coarser sediment dropped to the bed from the flow structure within the hydraulic jump and was pushed downstream to a point at the upstream limit of the fine sheet where it mounded. The mound developed into a *hydraulic-jump unit bar* which prograded upstream and downstream and formed a bidirectional cross set pattern.

5. With near-steady flow and only minor fluctuations in sediment flux, a series of *hydraulic-jump unit bars* developed, each above and upstream of the previous one and all above the massive basal unit. Each had a characteristic streamwise anatomy: passing downstream, a relatively fine-grained wedge of upstream-dipping laminae, a small volume of massive sand, a coarse-grained and a finer-grained foreset. A topset overlaid both types of foreset.

6. The fanning coset architecture of the *hydraulic-jump bar complex* has a character without counterpart in sedimentary geology, and as such is diagnostic of the presence of a hydraulic jump in the flow when the sand was deposited, but not of the nature of the hydraulic jump or the sand flux (which was specific to the experiment). The juxtaposition of the *hydraulic-jump bar complex* and the massive *basal wedge* is also a signature of the presence of a hydraulic jump.

7. Steep backsets (as classically attributed to hydraulic jumps when observed in the rock record) did not form over a non-erodible bed in a single experimental run involving sediment input to the hydraulic jump. Rather, upstream dipping laminae form the stoss sides of *hydraulic-jump unit bars* and gently upstream-dipping set boundaries occur between unit bars in *hydraulic-jump bar complexes*.

4.7 MODEL OF FORMATION OF A *HYDRAULIC-JUMP BAR COMPLEX*

A five stage model describes the inception and growth of a *hydraulic-jump unit bar* (Fig. 4.12). The model is based mainly on observations through the flume sidewalls. Initially there is no sediment in the system. Sand added to the system is all transported in the supercritical flow and into the hydraulic jump. Some of this sand drops to the bed underneath the detached jet at the standard *jet up* condition. This bedload is periodically pushed downstream into the slowing tailwater when the jet is deflected downward to sit closer to the flume floor in *jet*

down state. A single isolated feature (the proto bed feature) begins to build where bedload comes to rest. When the contact of the upper surface and lee slope, of this proto feature becomes sufficiently abrupt and its height sufficient for a lee slope separation eddy to form, this is the transition from proto bed feature to non-equilibrium *hydraulic-jump unit bar*.

Finer sand falls out of suspension downstream of the proto bed feature to form a wedge (Fig. 4.11B) with a preferential length scale at which slowing flow, decreasing in turbulence, and decreasing suspended sediment concentration combine most effectively (i.e. the length scale is dependent on settling velocity). The non-equilibrium *hydraulic-jump unit bar* grows upstream, and downstream over the wedge. The established deposit slows the flow so that finer grains are preferentially trapped at the leading edge due to a boundary layer blocking effect (Fig. 4.11 inset i – iii). Downstream progradation continues separately. The upstream face of the *hydraulic-jump unit bar* becomes less steep, reducing the blocking effect and permitting increasingly finer bedload to traverse the feature. Pulses of fine sand reach the lee avalanche face; a streaky character appears within the coarse foreset (Fig. 4.11D). Once the leading edge gradient becomes sufficiently gentle, all bedload traverses the feature and upstream growth of the unit bar stops. All further bedload traverses the equilibrium *hydraulic-jump unit bar* to the foreset. As the foreset grows it receives more sediment which falls out from suspension. Subsequently the grain size distribution deposited on the lee avalanche face approaches that of the bulk load. The topset aggrades as the lee side avalanche face progrades and the elevation of the brink point increases (the set climbs; Fig. 4.11D and E). Because the growing deposit causes the tailwater surface to rise, the hydraulic jump migrates upstream, to maintain the balance of pressure gradient versus momentum change across the hydraulic jump, and a new unit bar may be initiated further upstream. The association of a resultant climbing and upward-thinning coset with the underlying massive *basal wedge*, is here defined as one unit: a *hydraulic-jump bar complex*.

5. Flow patterns, sedimentation and deposit architecture under a hydraulic jump II

5.1 INTRODUCTION

5.1.1 Placing Chapter 5 in context

Chapter 4 described first of all the flow through a hydraulic jump without sediment (Run 1). It then described the flow and sediment transport patterns that resulted from one regime of sediment-input to it (Run 2). *Hydraulic-jump unit bars* and *hydraulic-jump bar complexes* were defined. The depositional architecture was documented. Chapter 5 describes two subsequent runs (Run 3 and Run 4), both with initial flow conditions (at $t = 0$) identical to Run 1, each involving a different regime of sand input (Table 4.1). The interaction of the flow and the sediment in Runs 3 and 4 are described and the deposit architectures are documented (§5.3 and §5.4). The sediment deposits of Runs 3 and 4 were similar in appearance to each other, and have similarities but some major differences with the *hydraulic-jump bar complex* of Run 2. The differences and similarities are discussed in Section 5.5.

5.1.2 Rationale for undertaking Runs 3 and 4

Chapter 1 showed that a wide range of hydraulic jumps form and affect sediment transport in a wide range of environments. A large matrix of flume runs would indicate the variety of sediment features that form. Within the constraints of a PhD, I chose to focus on variations in flow patterns and deposit patterns that result from my defined variations in the regime of sediment flux to the hydraulic jump (described below). Chapter 3 described sediment transport patterns involving different hydraulic jumps.

5.1.3 Procedure for Runs 3 and 4

Initially (at $t = 0$), the hydraulic jump in Runs 3 and 4 had inflow with a partially developed streamwise velocity profile, a near-stationary mean position and a detached submerged jet that oscillated in space through time (§4.2). Initially $Re_s = 282000$, $Re_d = 270000$, $Fr_s = 2.73$ and $Fr_d = 0.24$ (§4.1.1). These properties are true of many natural situations in which hydraulic jumps occur (§1.6); they are the same as the Run 1 hydraulic jump and the initial condition of

the Run 2 hydraulic jump. Initially the test channel floor was non-erodible (representative of flow over bedrock, frozen or otherwise hard ground). At $t = 0$ sediment input began by shovelling onto the conveyor (§2.3). In total 5000 kg of sand were shovelled into the flume, from six crates, in Both Run 3 and Run 4. Sand entered the test channel of the flume after having passed through more than 15 m of recirculation pipes and the flume pumps.

Following Run 2, the sediment was removed to the crates and allowed to dry. In Run 3 this sediment was put back into the flume over 45 minutes, compared to 75 minutes in Run 2 (Table 4.1). In this way the mean mass input rate of sand was varied. Sediment input was constant, whereas there had been haiatuses in the input in Run 2. Following Run 3 the sediment was removed from the flume and disposed of (procedure for sediment removal described in §2.2.2). To document the changing shape of the deposits the sand surface was traced onto the flume sidewall 19 times. The water surface was traced 16 times.

Run 4 had the same mean mass input rate as Run 2 (Table 4.1) but of finer and better sorted sand, of the type used in the hemisphere runs (Fig. 3.3). The sand input rate was near constant except for a gap of 1 minute between inputs from Crates 5 and 6. To document the changing shape of the deposits the sand surface was traced onto the flume sidewall 21 times in Run 4. The water surface was traced 22 times. During Run 4, fifteen 0.125 kg portions of black blast furnace abrasive were added directly to the supercritical flow at the approximate position $x \sim 0.5$ m. This black abrasive had grain size of coarse sand (Fig. 5.1) and density of 1442 kg m^{-3}. It moved down-flume in a hydraulically-different way to the finer and denser bulk load. It deposited to highlight lamination within the sand deposit. Highlighting was necessary because the bulk load was well sorted and the lack of variation in grain appearance made laminae poorly distinguishable by eye.

Procedure for recording velocity in Runs 3 and 4

The UDVP array was fixed at $x = 6.10$ m, with profilers facing upstream (profiler operation described in §2.4.2). The distance over which velocity was measured was set at $0.075 - 0.345$ m upstream of the probes, compared to $0.175 - 0.185$ m in Run 2. The sediment deposit that developed in Run 2, buried the lowermost profilers as it grew and in consequence the last useful datum recorded by each buried profiler was 0.175 m upstream of the deposit. In Runs 3 and 4, buried profilers recorded velocity 0.075 m upstream of the deposit and this allowed the

149

flow and upstream growth of the deposits to be better understood. Compared to Run 2 a finer time-resolution of measurements was also achieved without compromising the accuracy of UDVP readings.
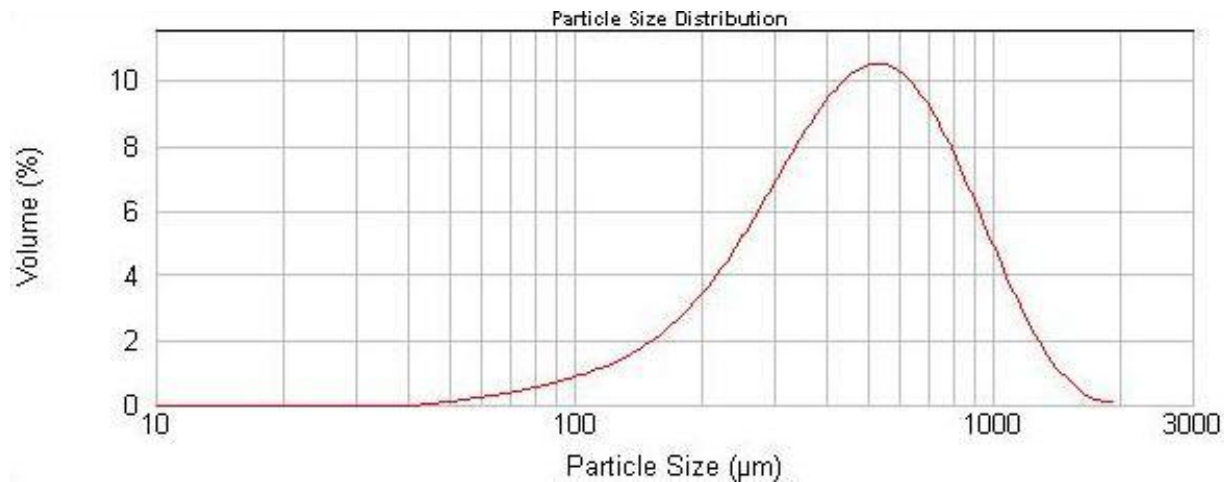
Figure 5.1 Grain size distribution of the black blast furnace abrasive used to highlight lamination.

Procedure for sectioning and sampling sediment deposits in Runs 3 and 4

As in Run 2, stream parallel and stream transverse sections were cut to see the architecture within the deposits. The deposits were also sampled.

First I documented and photographed the deposit adjacent to the right hand sidewall, and observed the deposit at the left hand sidewall. Second I drained the flume slowly. Third I dug out the deposit to the right hand side of the line $y = 0.7$ m to form a stream parallel section (Fig. 5.2A). I documented and photographed the pattern of lamination and compared it to the lamination seen through the sidewalls. Fourth I marked the locations of the stream-transverse cuts with stream transverse lines scratched into the deposit surface (Fig. 5.2B). Fifth I carefully removed the thin layer of clay which had settled onto the deposits post-run and sampled sediment from the deposit, several days after the respective run (Fig. 5.2C). Specific sampling regimes for Runs 3 and Run 4 depended on the nature of the resulting deposits and are described in Sections 5.3.6 and 5.4.6. The samples were analysed using the Mastersizer, to determine grain size distribution within the deposits (Mastersizer and operating procedure described in §2.6). Sixth I cut the stream-transverse sections (Fig. 5.2D), documented and photographed the pattern of lamination.
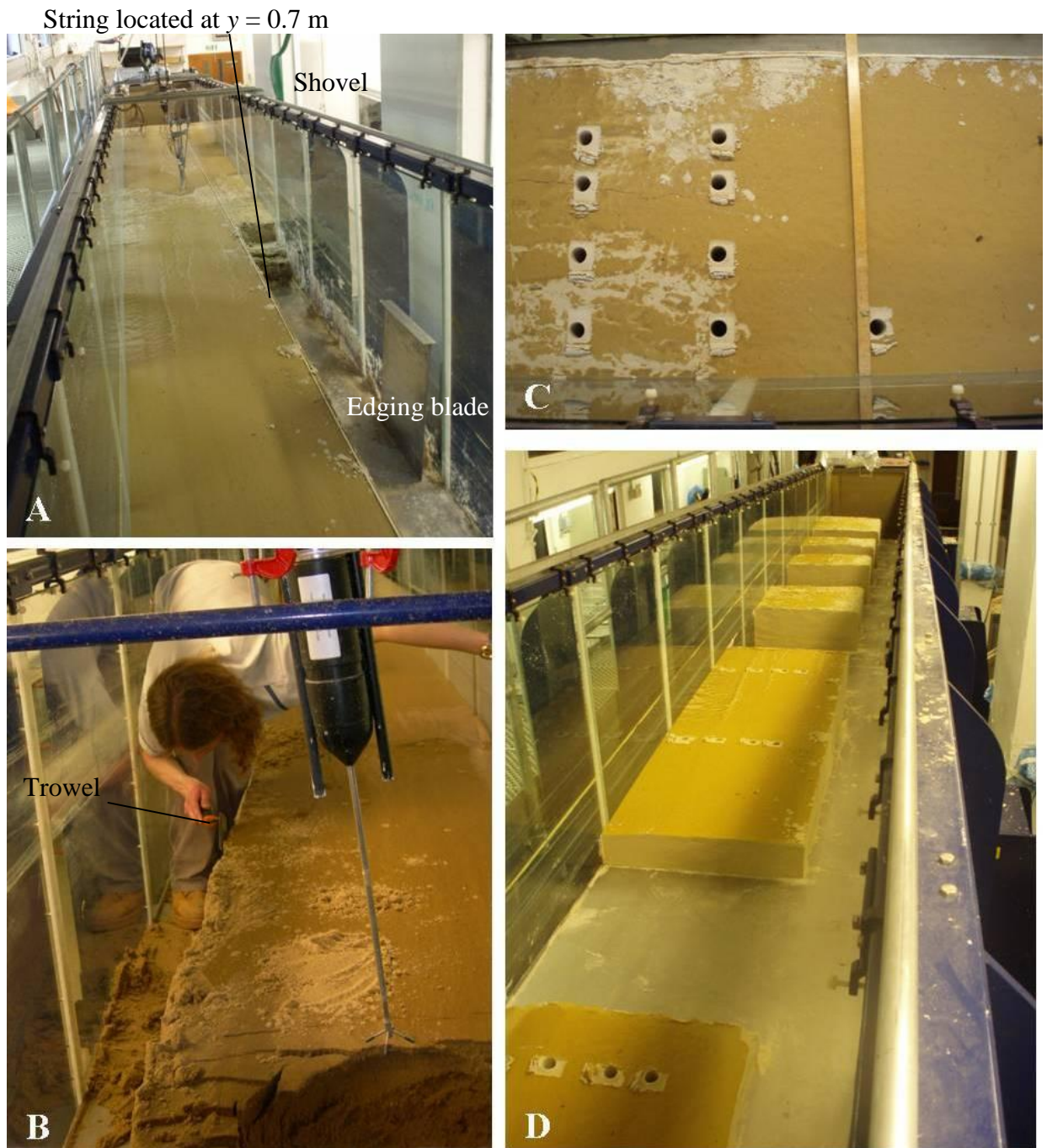
Figure 5.2 Sequence of sectioning and sampling the deposits that formed in Runs 3 and 4. (A) A stream-parallel section was cut in the deposit, 0.3 m from the right hand sidewall of the flume using a shovel. An edging blade and (B) a trowel, were used to clean the face of the section. (C) A thin layer of clay that had settled onto the deposit post-run was carefully removed at the location of sediment samples. Samples were taken vertically downwards using a metal tube of 0.029 m internal diameter. (D) Stream-transverse sections were cut and cleaned using an edging blade and trowel.

5.2 RUN 3: HYDRAULIC JUMP WITH SAND FLUX II

5.2.1 Changes to the supercritical flow and hydraulic jump through Run 3

At all times after $t = 0$, sediment was suspended throughout the flow within the test channel, and obscured the view of both the channel floor and bubbles in the flow. Consequently, paths of flow within the hydraulic jump and tailwater were difficult to detect, as they had been in Run 2. Water surface patterns could be seen, and at any time the water surface of the front of the hydraulic jump had at least several folds, oriented both stream-parallel and stream-transverse (Fig. 5.3). Neither the shape nor the oscillating nature of the front of the hydraulic jump was affected by the presence (versus absence) of suspended sediment within the flow.
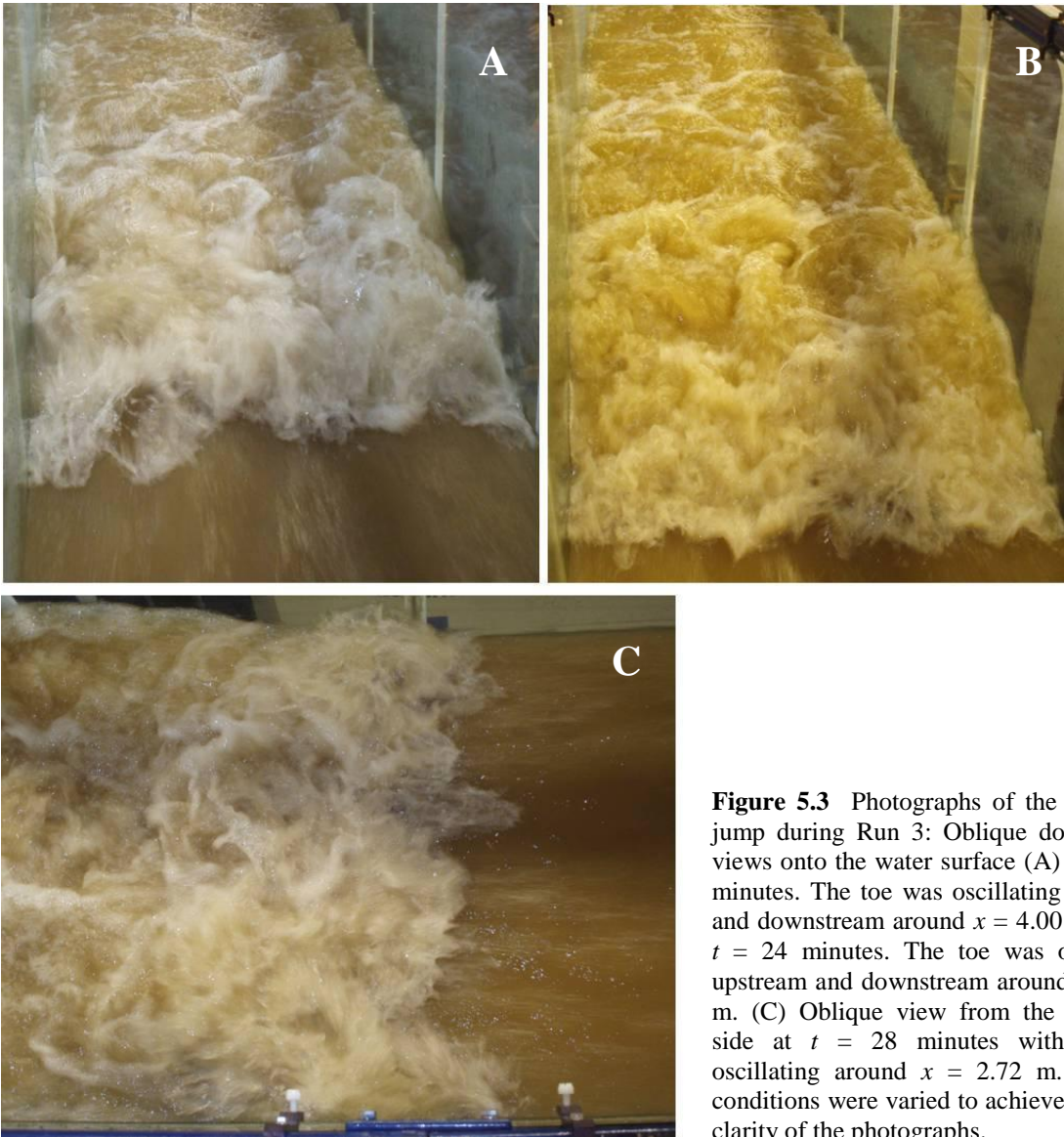
Figure 5.3 Photographs of the hydraulic jump during Run 3: Oblique downstream views onto the water surface (A) At $t = 10$ minutes. The toe was oscillating upstream and downstream around $x = 4.00$ m. (B) at $t = 24$ minutes. The toe was oscillating upstream and downstream around $x = 3.05$ m. (C) Oblique view from the left hand side at $t = 28$ minutes with the toe oscillating around $x = 2.72$ m. Lighting conditions were varied to achieve optimum clarity of the photographs.

Throughout Run 3 the hydraulic jump moved upstream in response to a deposit forming. As the hydraulic jump moved upstream, the thickness of the supercritical flow, h_1 increased from 0.09 m to 1.12 m. In association U of the supercritical flow decreased (Eqn. 1.1) but Re_s was unchanged (Eqn. 1.7). The value of Fr_s decreased from 2.73 to $Fr_s = 2.13$ so the hydraulic jump changed from an oscillating jump to a weak jump (cf. Massey, 's 1983 classification), with the transition at $t \sim$ 15 minutes. The timing of the transition cannot be defined exactly because the accuracy of Massey's divisions within the classification is unknown. As the hydraulic jump moved upstream, L increased by more than 10% (considering Eqn. 2.1); the velocity profile of the flow entering the hydraulic jump became increasingly less developed.

Because h_1 and Fr_s are known, we can write down that at the end of Run 3, $h_2 = 0.28$ m, $Fr|_{h=h_2} = 0.52$ and $U_2 = 0.86$ m s^{-1}, following Eqns 1.1 − 1.3. Compared to the initial conditions h_2 had decreased, $\overline{u_2}$ had increased and $Fr|_{h=h_2}$ had more than doubled by the end of Run 3.

5.2.2 Observations of the water flow and sediment transport

Sediment transport and accumulation patterns were generally the same as in Run 2 (§4.5). Sediment fell from suspension between the toe of the hydraulic jump and 2 m further downstream. It moved downstream as bedload and stalled 2.1 m downstream of the toe. The bedload accumulated in a non-migrating bed feature that was longer and thinner than the Run 2 mound. By $t = 2$ minutes this feature was a distinct proto-unit bar. Some sediment fell from suspension to the flume floor between the hydraulic jump and the discharge tank. It formed a downstream thickening massive bed; called the *basal wedge*, as in Run 2 (§4.5.2). The proto-unit bar and massive bed formed simultaneously.

Once the proto-unit bar formed, bedload accumulated in pulses every few tens of seconds at its upstream limit. This did not occur in Run 2. Each pulse temporarily added up to a few centimetres thickness of sediment over a streamwise distance of 0.1 − 0.2 m; sediment in the pulse was remobilised downstream within a few seconds. It moved over the bed feature and avalanched down its lee face, forming a prograding foreset with a brink (defined §4.5.2) by $t = 3$ minutes. Each pulse of sediment left no signature where it had temporarily stalled at

the upstream limit of the deposit, and because of this the sediment pulses are described as nascent bed features during the few seconds in which they were stationary.

A *hydraulic-jump unit bar*, with a brink at $x = 7.65$ m, was seen within a few minutes of $t = 0$. Its foreset prograded downstream and climbed the *basal wedge*. It thickened by 0.14 mm s^{-1} over the first 15 minutes and by 0.07 mm s^{-1} over the subsequent 12 minutes, reaching the downstream end of the test channel at $t = 27$ minutes. The associated topset continued to grow for 10 minutes after that. The *basal wedge* ceased to develop where it was overridden by the foreset. The *basal wedge* was 0.17 m thick at its downstream limit (compare 0.15 m in Run 2).

As in Run 2, the accumulation of sediment caused the height of the water surface above it to rise, which increased the hydraulic jump surface gradient. This made the hydraulic jump unstable and it responded by moving gradually upstream. The hydraulic jump and the upstream limit of the sand deposit moved upstream at the same constant rate but the pattern of deposition was not constant with time. Neither did *hydraulic-jump unit bars* repeatedly form (as in Run 2). Above the first *hydraulic-jump unit bar*, another feature formed, which may be a low amplitude *hydraulic-jump unit bar* (discussed in §5.5.5). Its inception was not directly observed, but occurred between $t = 33 - 34$ minutes. This foreset did not noticeably thicken downstream as it prograded, and it reached the end of the test channel by $t = 43$ minutes. Pumping was stopped at $t = 45$ minutes. A topset associated with the second foreset, thickened continuously until pumping was stopped.

Flow above the unit bar became thinner because the increase in water surface height did not keep pace with the increase in deposit surface height (they had kept pace in Run 2). Because flow above the deposit became thinner over time, $\bar{u}$ above the deposit increased. The possible transition to upper stage plane bed flow conditions is discussed in Section 5.5.5.

The magnitude of the change in hydrostatic pressure from upstream to downstream of the hydraulic jump did not vary. From the thickest flow at the downstream limit of the hydraulic jump, to the thinner flow in the tailwater, pressure decreased. As h decreased above the deposit, the downstream pressure gradient increased, and was increasing at the time Run 3 was ended.

Interaction between the sediment deposit growth and the hydraulic jump

The 5000 kg of poorly sorted sand formed a 3.84 m^3 deposit and in response the hydraulic jump moved upstream by 3.44 m (Fig. 5.4). The hydraulic jump and the upstream limit of the sediment deposit moved upstream at 4.8 m hr^{-1} in Run 3 (sediment input rate 6700 kg hr^{-1} for 45 minutes) compared to 3.5 m hr^{-1} in Run 2 (sediment input rate 4000 kg hr^{-1} for 75 minutes).
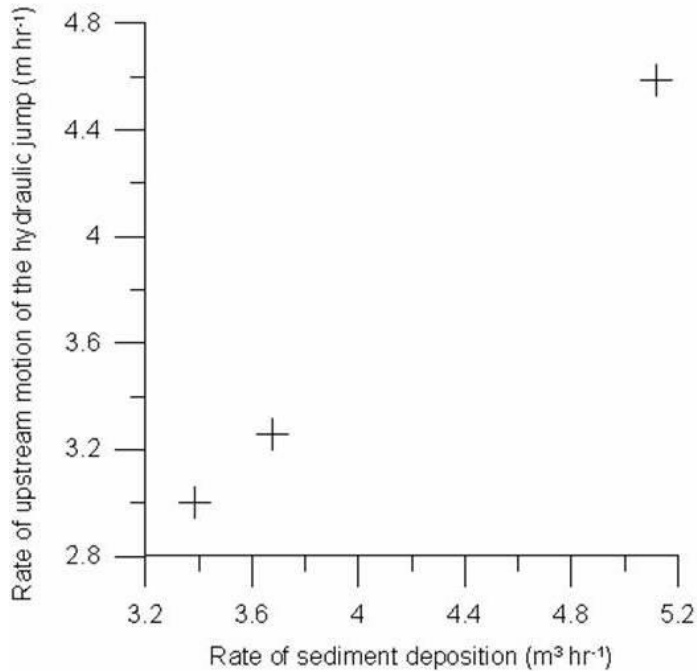
Figure 5.4 Plot of the volume rate of sediment deposition and the rate of motion (to upstream) of the mean streamwise position of the toe of the hydraulic jump for Runs 2 – 4 (one data point for each).

5.2.3 Profiles of time-averaged velocity

At $x = 6.10$ m, where the $\bar{u}$ profiles were recorded, flow thickness decreased from 0.42 to 0.37 m over the first 26 minutes whilst the deposit grew and the hydraulic jump moved upstream. Whilst flow at $x = 6.10$ m thinned, U increased from 0.62 – 0.70 m s^{-1}. Over the remainder of Run 3 ($t = 26 – 45$ minutes), the flow over the deposit at $x = 6.10$ m continued to thin but more slowly. Just before pumping was stopped it was 0.31 m thick and in association U was 0.84 m s^{-1}.

The $\bar{u}$ Profile A (Fig. 5.5) was recorded at a streamwise location equivalent to the region of jet detachment in the sediment-free hydraulic jump of Run 1 (Profiles F and G, Fig. 4.3). Peak time-averaged velocity in the profile, $\bar{u}_{max}$ was 1.15 m s^{-1}. Below the position of $\bar{u}_{max}$ the gradient of velocity was high ($\bar{u}$ increased from $0 – 1$ m s^{-1} between $z = 0 – 0.06$ m) and a lower jet edge could be detected (jet edges defined in §1.9.3). The value of $\bar{u}$ generally
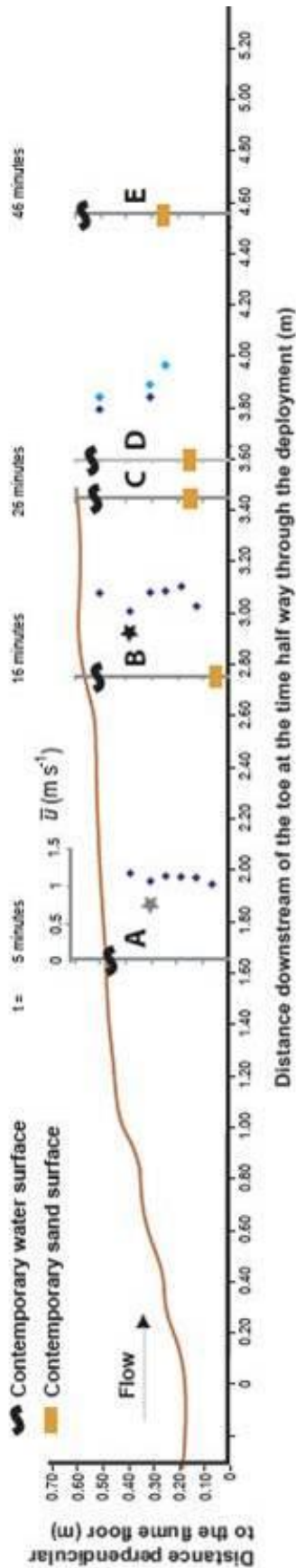
Figure 5.5 Profiles of the time-averaged streamwise velocity component $\bar{u}$ in Run 3 measured by ultrasonic Doppler velocity profilers (UDVP). Each mark data point is the average of measuring intervals of 600 s. The UDVP array was fixed at $x = 6.10$ m throughout Run 3 and the hydraulic jump moved upstream. The brown line indicates the lowest water surface position of the hydraulic jump: The profiles are drawn in positions relative to the contemporary hydraulic jump. The sand and water surfaces at $x = 6.10$ m, half way through each deployment are marked on the profiles using short black and yellow lines. Note the dip in magnitude of $\bar{u}$ in Profiles A and B: flow was faster above and below the positions marked with the stars. At $t = 26$ minutes, the dark blue symbols are associated with Profile C and the pale blue symbols are associated with Profile D.

156

decreased above the position of $\bar{u}_{max}$ and additionally there was a slight dip in $\bar{u}$ around $z =$ 0.31 m. Within the dip $\bar{u}$ was up to 9% less than that above and below it (grey asterisk, Fig. 5.5). Despite this dip in $\bar{u}$ no distinct upper jet edge could be detected.

The $\bar{u}$ Profile B (Fig. 5.5) was taken 1.1 m further downstream of the toe than Profile A, at a streamwise location equivalent to the region of the tailwater of Run 1 with pulses expanding downward into the water column (Profiles I and J, Fig. 4.4B). Between the flume floor and 0.25 of the flow height, $\bar{u}$ increased from $0 - 1.2$ m s^{-1}. A lower jet edge was detected close to the deposit surface. In Run 1 the detached jet had diffused by this streamwise position; the lower jet edge was at a similar height to the lower jet edge in the 'jet down' state of Run 1. Above this height $\bar{u}$ generally decreased upwards by a small amount and was 1.05 m s^{-1} at the water surface. As in Profile A, there was a dip in $\bar{u}$, but more pronounced, flow through the dip being up to 20% slower than flow above and below it (compare grey and black stars, Fig. 5.5). The shape of $\bar{u}$ Profile B gave the impression of a jet with a much more distinct upper edge than in Profile A; the jet spanned two thirds of the flow thickness and was detached by 0.05 m above the sand deposit.

Two profiles of $\bar{u}$ are displayed from the same deployment of the UDVP array around $t = 26$ minutes, at streamwise locations 0.15 m apart (Profiles C and D; Fig. 5.5). Both profiles were recorded slightly downstream of the position that would relate to the pulses within the Run 1 tailwater (§4.3.1). The $\bar{u}$ data in Profile C were processed in the same way as the $\bar{u}$ data in Runs 1 and 2. Profile D was analysed from bins 0.15 m closer to the profilers because at that distance the bins of all three non-buried profilers returned a complete dataset, whereas one malfunctioned part way through the deployment, at the streamwise position of the measurement bins which constitute Profile C. In both profiles the position of $\bar{u}_{max}$ was close to the sediment surface; $\dfrac{\partial \bar{u}}{\partial z}$ was higher in magnitude close to the flume floor than had been the case in the more upstream Profile B. At a position 0.05 m above $\bar{u}_{max}$, $\bar{u}$ was 20% slower (Profile D). Above this position velocity did not change with height. A jet appeared to be distinct, 0.45 times as thick as the Profile B jet, with its lower edge adjacent to the sand surface.

Whilst the UDVP array was deployed in Profile E it returned no data but the depth-averaged velocity through the section was 0.87 m s^{-1}, determined from the conservation of volume flux of flow through the flume.

5.2.4 Discussion: Effects of changing flow characteristics on the position of the jet

In Run 2 the default position of the jet within the hydraulic jump was separated from the flume floor ('jet up' position) whilst Fr was equal to 2.73 (oscillating jet) and the jet was recognised to oscillate both vertically and in length (§4.3.1). Compared to the Run 1 oscillating jump, the time-averaged jet was much lower in the flow whilst the Run 3 hydraulic jump was in the form of an oscillating jump ($t = 0 − $~15 minutes, 5.3.1; Profile B, Fig. 5.5), the , consistent with the value of Fr decreasing towards a weak jump ($Fr < 2.5$ from $t = 15$ minutes onwards). According to Massey (1983), on transition to a weak jump the jet would have ceased to detach from the flume floor and instead expanded in a simple way underneath the roller; this is apparent from Profile C. The lower position of the jet occurred despite the transition from higher to lower pressure above the sediment deposit, suggesting that the value of Fr is a greater control on jet position. The length of separated flow and the angle of detachment would also vary with the Reynolds number (Van Dyke, 1982), in general, but because Re was not varied between runs, its control on jet position was not determined. These are the direct influences of changing flow conditions on jet position. The influence of the developing deposit is discussed after the deposit architecture and Run 4 have been presented.

5.2.5 The depositional architecture: Another *hydraulic-jump bar complex*

In Run 3, with sediment mass input rate 67.5% higher than Run 2, three beds formed in an upward sequence (Fig. 5.6). Bed 1 was a *basal wedge*; a downstream-thickening volume of massive sand at the base of the sequence. The *basal wedge* pinched out upstream at $x \sim 6.8$ m. It made a sharp contact with the bed above. In its upstream-most 0.8 m the contact was not wavy but further downstream it was wavy, with amplitude on the order of millimetres per metre downstream but not rythmically.
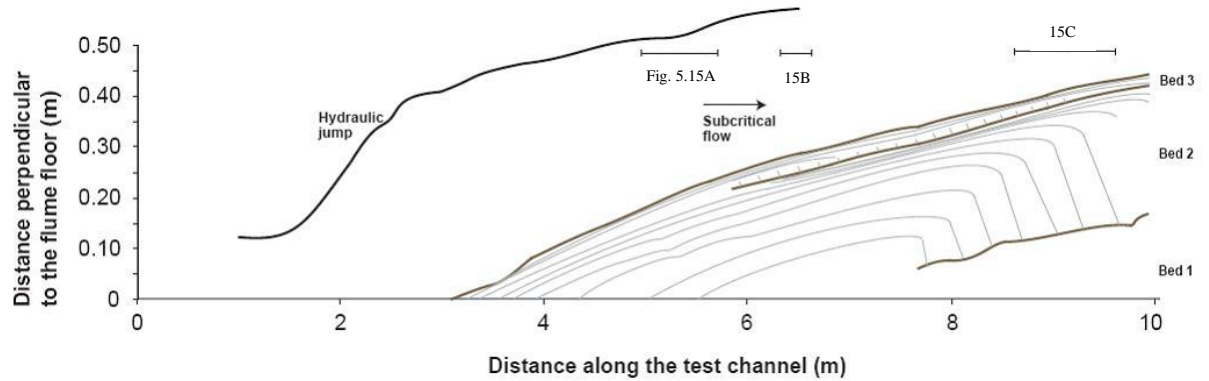
Figure 5.6 Pattern of lamination within the deposit that formed during Run 3 represented in stream-parallel section. The height scale is five times the streamwise length scale and the inclinations of the laminae are plotted with respect to this height exaggeration. The initial position of the toe of the hydraulic jump was at $x = 4.68$ m. The line representing the water surface corresponds to the position of the hydraulic jump at the end of each run. The solid brown lines indicate the upper limits of the beds. The change of dip with height exaggeration is derived in Appendix 4.

Beds 2 and 3, formed by *hydraulic-jump unit bars*, were both different in appearance to each of Beds 2 – 5 of Run 2. Beds 2 and 3 both consisted of a cross bed set and an associated topset, which were truncated by the downstream limit of the test channel. For convenience the foresets and topsets of Beds 2 and 3 are called Foreset 2, Foreset 3, Topset 2 and Topset 3.

Foreset 2 overlaid the *basal wedge*. It was 0.06 m thick at $x = 7.6$ m, which was its upstream limit (Fig. 5.6). It was 0.10 m thick 0.5 m further downstream, and 0.22 m thick at the downstream end of the test channel. Its laminae between $7.6 \leq x \leq 7.9$ m had a dip of 46° (dip is 79° in Fig. 5.6 because of the height exaggeration). Between $7.9 \leq x \leq 10.0$ m the dip of each lamina was within the range 24 - 32°. Each lamina within Topset 2 was convex-up in streamwise view and had low curvature. They could be traced on the order of metres in the streamwise direction. At its downstream end each lamina terminated at the top of the avalanche foreset, except for the uppermost 0.05 m of Bed 2, where it terminated at the downstream limit of the test channel. The length of the laminae increased and the curvature of the laminae decreased, upwards through Topset 2.

Foreset 3 was 0.06 m thick at $x = 7.6$ m, which was its upstream limit (Fig. 5.6). It was 0.14 m thick at $x = 8.1$ m and 0.22 m thick at $x = 10.0$ m. It made a sharp contact with the laminae of Topset 2, below it, and with the laminae of Topset 3, above it. Laminae within Topset 3 were convex up in streamwise view, had low curvature and could be traced on the

order of metres in the streamwise direction. When Run 3 was ended Topset 3 was still growing.

Stream-parallel sections

As in Run 2, the features observed through the right hand sidewall of the flume were also observed in a stream-parallel section cut at 0.3 m from the right hand sidewall, at comparable streamwise locations, with comparable thicknesses and geometries. The same features were also seen with similar shape, size and position, through the left-hand sidewall. The stream-parallel sections are "read" from upstream to downstream and photographs are presented in the same order (Fig. 5.7).

In the most upstream part of the deposit, Topset 2 was directly overlain by Topset 3. Upstream of $x = 5.20$ m the laminae of both topsets were several grains thick and convex up; no contact could be distinguished between the two topsets (Fig. 5.7A). Downstream of $x = 5.20$ m, stringers of the coarsest grains in the bulk load distribution were seen in the lower part of Topset 3; the stringers distinguished Topset 3 from Topset 2 (Fig. 5.7B). Grain size within Topset 2 did not change upwards through the lowermost 80% of the bed, but fined-upwards above this (Fig. 5.7B). Topset 2 also appeared to fine slightly from upstream to downstream.

Foreset 3 was seen further upstream than Foreset 2 (compare Foreset 3 between Fig. 5.7C and D, whereas Foreset 2 can be seen in Fig. 5.7D but not Fig. 5.7C). The upstream limit of Foreset 3 was at $x \sim 6.40$ m: At this streamwise location the upward sequence was Topset 2 overlain by Foreset 3 and then Topset 3. Foreset 3 was less than 0.02 m thick and had grain size characteristics similar to topsets above and below it, to the naked eye. The downstream dipping laminae of Foreset 3 could be seen by eye when observing the deposit but when observing photographs only the upper and lower bounds of Foreset 3 could be detected because of the drying pattern of the deposit (Fig. 5.7C). No grain size trends were seen from upstream to downstream within Foreset 3 or Topset 3.

Flow

Stringers

A

B

Bed 3 topset

Bed 2 topset

Beds 2 & 3 topsets

C

D

Bed 3

Bed 3

Bed 2 topset

Bed 2
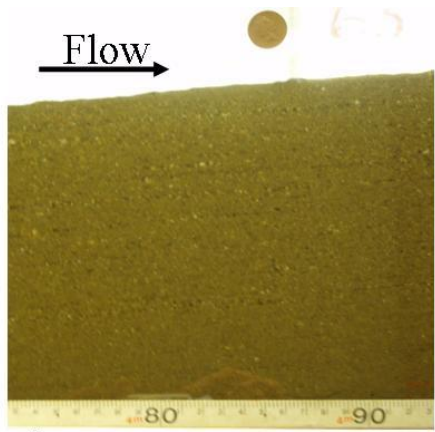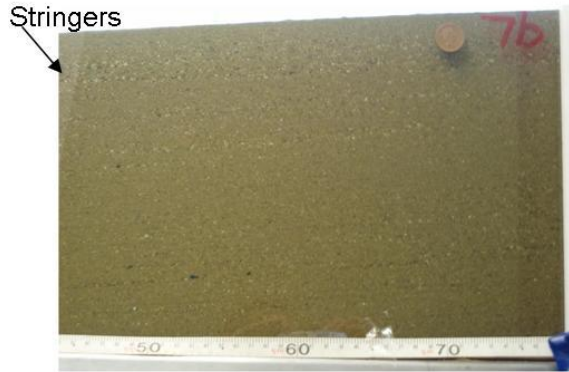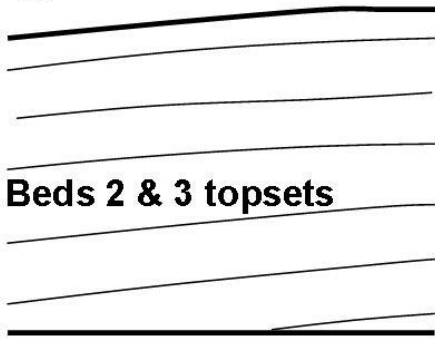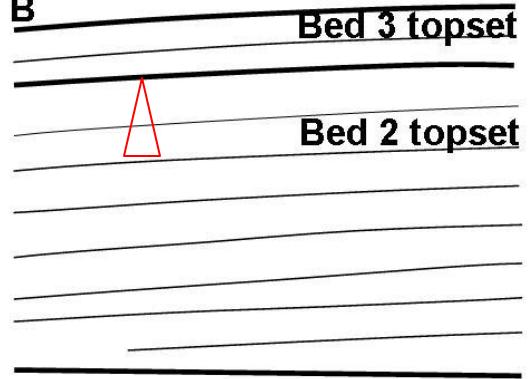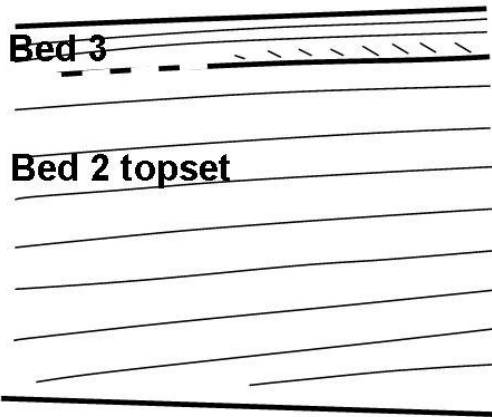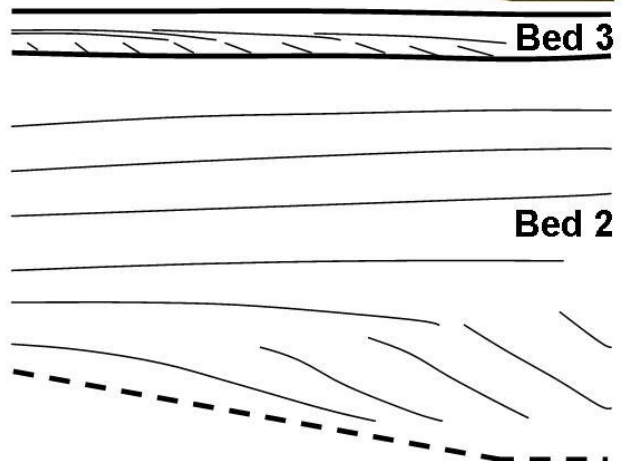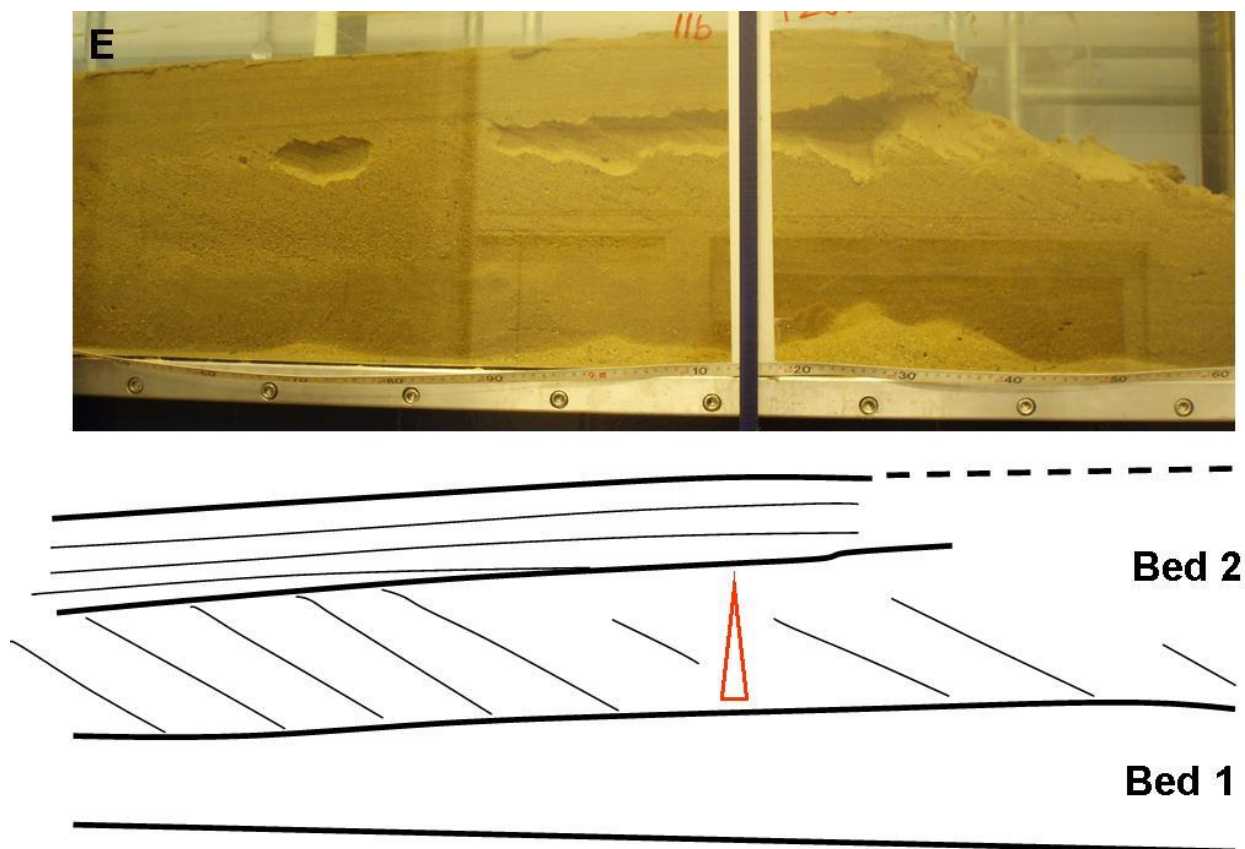
Figure 5.7 (above and previous page) Photographs taken of the Run 3 deposit through the sidewall of the flume (i.e. stream-parallel sections) and corresponding line drawings of the deposits. In A – D the deposit is adjacent to the sidewall and in E it is 0.3 m away from the sidewall (the stream-parallel cut). The location of each photograph is indicated in Figure 5.6. The lighting conditions were varied to highlight the lamination; this gives a false impression of variation in sand colour. The line drawings are labeled with bed numbers as in Fig. 5.6. The thick lines indicate bed contacts. The red triangle indicates grain size trends assessed by eye. The coin is 20 mm in diameter. The approximately horizontal lines of pale coloured sand in Photographs C and D are at the top and bottom of the Run 3 foreset; their pale colour is a result of the drying pattern over many hours. Some days after the stream-parallel section was cut and the sand samples taken, the top part of the foreset of Bed 2 had collapsed along its downstream-most metre, and in another patch 0.1 m long that was 0.16 m further upstream (Photograph E).

In the most downstream part of the deposit, the *basal wedge* (Bed 1) was directly overlain by Bed 2 and then Bed 3 (Fig. 5.7D and E). The *basal wedge* appeared massive. Within the deposit, the greatest prevalence of coarse grains was seen at the upstream limit of Foreset 2. The prevalence of coarse grains declined downstream within Foreset 2. This grain size pattern was more noticeable adjacent to the sidewall than in the cut section (compare Foreset 2 between Figs 5.7D and E). Beds 1 and 2, and 2 and 3 were more distinct from each other at the sidewall than at the cut face. Foreset 3 was difficult to detect downstream of $x = 8.50$ m from digital photographs (e.g. Fig. 5.7E) but was seen in the deposit downstream of $x = 8.50$ m.

5.2.6 Patterns of grain size distribution within the Run 3 deposit

Sediment sampling procedure

Initially, during excavation of the deposit, I did not distinguish Bed 3 as a distinct bed, but rather considered that Foreset 3 was some discontinuity in a larger Topset 2. With this misinterpretation, arrays of 2d sediment samples were taken using a metal tube of 0.029 m internal diameter. Sample Array 1 included fifty six samples taken in four channel-parallel rows between $y = 0.1$ (Row 1) and $y = 0.5$ m (Row 4), and 14 channel-transverse rows between $x = 2.30$ m (Row B) and $x = 9.80$ m (Row O) (Fig. 5.8). Sample Array 1 spanned Topset 2 and Bed 3, to the left hand side of the centreline. It was assumed that the grain characteristics would be symmetrical about the channel centreline.

Sample Array 2 consisted of twenty eight samples, taken at the same plan-view locations as Rows I – O of Sample Array 1 (blue dots, Fig. 5.8B). It spanned Foreset 2. Because all features of the architecture were at the same position both at the sidewall and cut face, the depth of Foreset 2 was taken to equal its depth at the sidewall at the same streamwise location as the associated sampling position.

The grain size distributions of all sediment samples were unimodal, and positively skewed by an amount similar to the bulk load. The median grain size, D_{50} was calculated as a representative grain size of the unimodal samples. The difference between sample D_{50} and bulk load D_{50} was contoured using the Kriging method of contouring (Fig. 5.9). The cross-channel mean of the four median values of grain size in the samples of Rows 1 – 4, was calculated for each of Rows B – O (Array 1) and Rows I – O (Array 2). These cross-channel mean values are assigned the nomenclature $\overline{D_{50}}\big|_x$ and their streamwise trend is presented in Figure 5.10. Values of $\overline{D_{50}}\big|_x$ for sample Rows A – H, K and N (at 0.9 m intervals) were further averaged to give a mean D_{50} for the beds. This averaged value is assigned the nomenclature $\overline{\overline{D_{50}}}$.
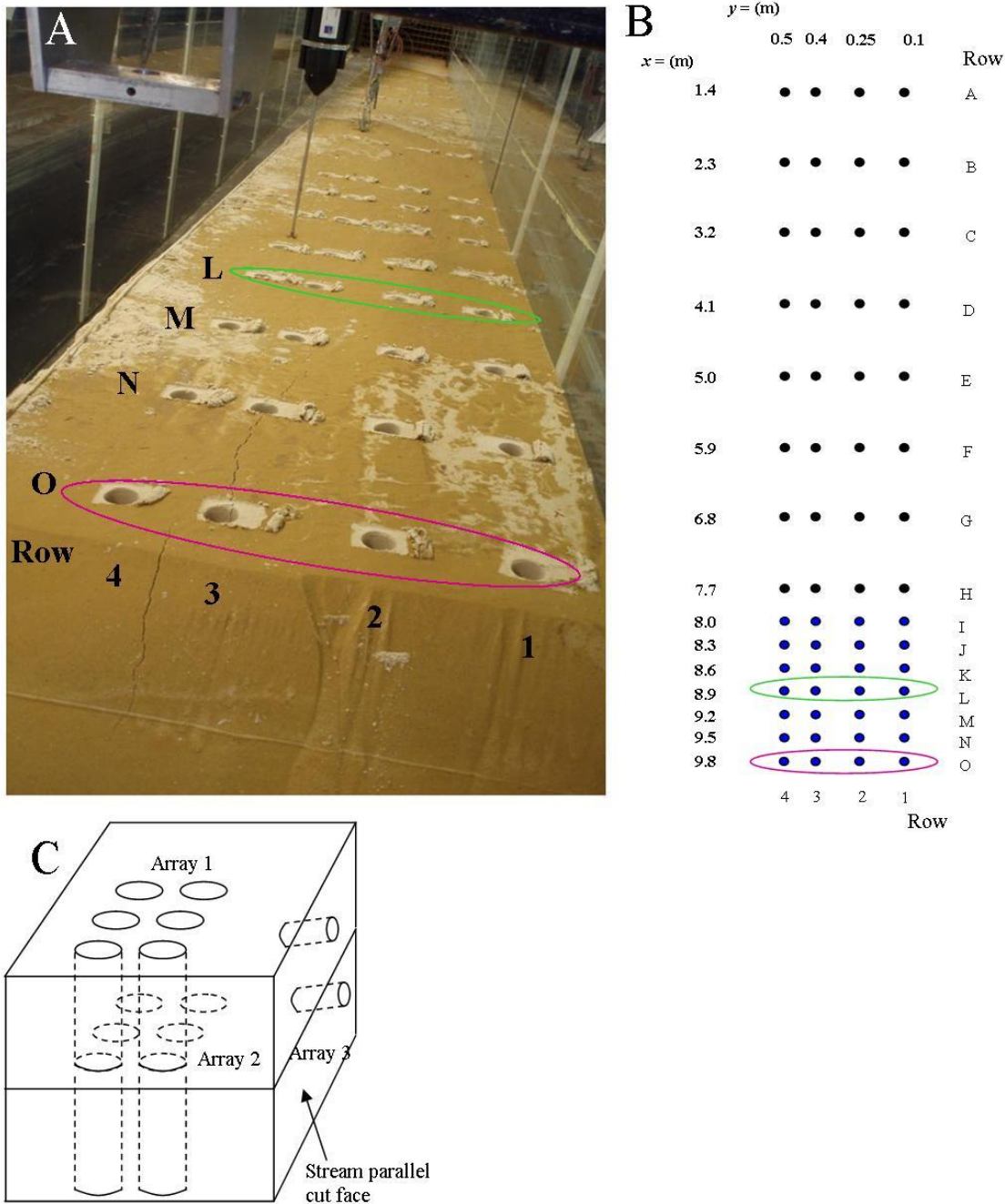
Figure 5.8 The sediment sampling arrays: (A) Photograph of the sediment surface pattern of the holes made in sampling Arrays 1 and 2 in Run 3. Flow had been obliquely out of the page. Each sample was taken vertically using a metal tube. The squares around the sample holes were made using a sharp-edged block to carefully remove the thin layer of clay that had settled onto the deposit after Run 3 had finished. The same practice was undertaken in Run 4. The head of one acoustic Doppler velocimeter and the lower part of the ultrasonic Doppler velocity profiler array were buried. (B) The plan view arrangement of samples taken using Array 1 (all dots) and Array 2 (blue dots only). Not to scale. Rows A – H, K and N are equidistant (0.9 m separation) and span the streamwise lengths of the deposits. Row codes A – O and 1 – 4 correspond between (A) and (B); both pink ellipses surround Row O and both green ellipses surround Row L. (C) Sketch of the orientation of samples taken using Arrays 1 – 3.

Grain size distributions in plan

All samples of Topset 2 and Bed 3 (combined, Array 1) had values of D_{50} lower than that of the bulk load (Fig. 5.9A). The value of D_{50} gradually decreased with distance downstream, by approximately 110 μm and varied by less than 30 μm across-stream at all streamwise locations. The value of $\overline{D_{50}}\big|_x$ was less than 10 μm finer than the bulk load at the upstream limit of Bed 3 and it generally decreased downstream, by 125 μm in Array 1 (Fig. 5.10). Variation in $\overline{D_{50}}\big|_x$ was approximately linear with *x*.
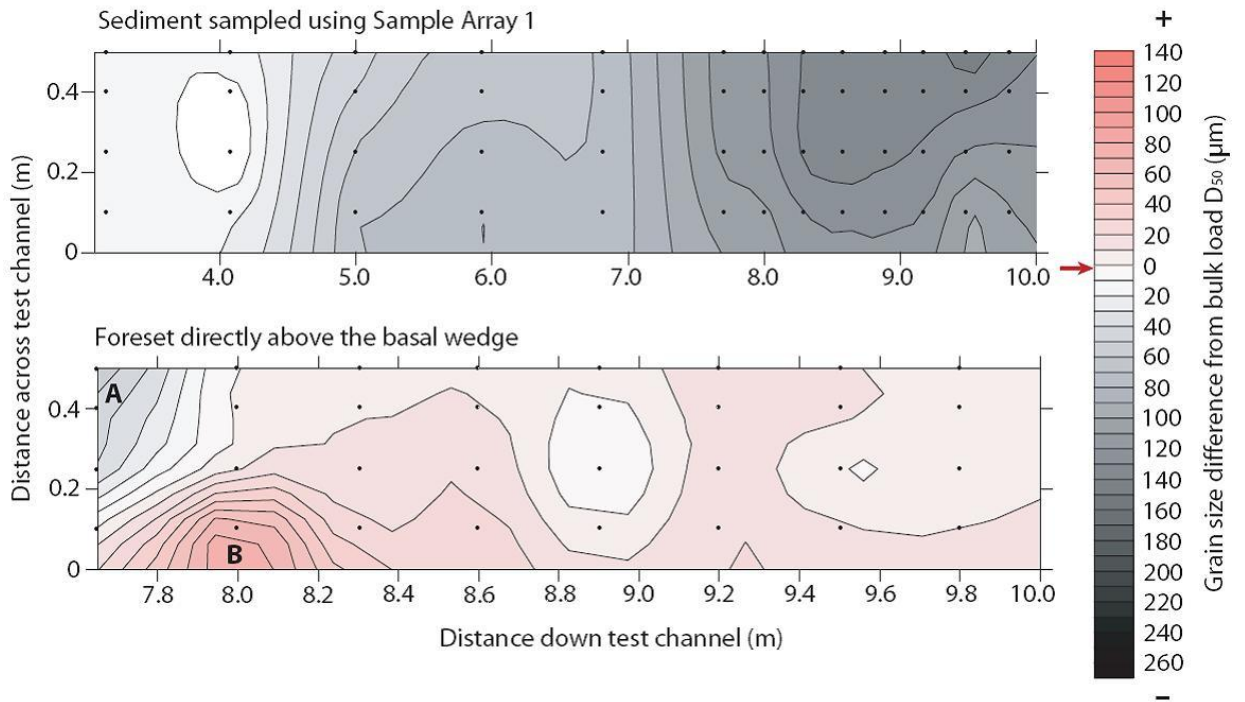
Figure 5.9 (above) Maps of the difference between D_{50} in the original sediment and in the deposit, made using Surfer 8 and the Kriging method of contouring. The first map is of Bed 3 and the topset of Bed 2 combined (Sample Array 1), the second map is of the foreset of Bed 2. Sample locations are depicted with dots (·). The colour scale depicts D_{50} greater than that of the bulk load (red), less than the bulk load (black) and equal to the bulk load (white) in 10 μm increments. The D_{50} value of the bulk load was 368 μm; this takes the value 0 on the scale and is marked with a red arrow. In the second map, one feature which was up to 45 μm finer than the bulk load is marked by the symbol **A** and one feature up to at least 85 μm coarser than the bulk load is marked by the symbol **B**.

Foreset 2 had a coarser $\overline{D_{50}}$ than the sediment sampled in Array 1 (Table 5.1). The D_{50} of individual samples ranged from 30 μm finer to 80 μm coarser than the bulk load, being finest near the upstream limit of Foreset 2, at *y* = 0.50 m (Position A, Fig. 5.9B) and coarsest towards the sidewall 0.3 m further downstream (Position B, Fig. 5.9B). Sediment at Position B

had the coarsest distribution within the deposit. The value of $\overline{D_{50}}\big|_x$ varied by less than 40 µm

along Foreset 2, with no obvious trend (Fig. 5.10). Near to the centreline, the value of D_{50} of the sediment samples taken from Foreset 2 increased downstream and the magnitude of the increase decreased downstream. Closer to the flume sidewall D_{50} decreased downstream in the most upstream metre of Foreset 2 and in the 1.5 m of Foreset 2 further downstream, D_{50} varied little across-stream. The stream-transverse variation in most upstream 0.3 m of Foreset 2 was associated with sediment initially mounding around the channel centerline and the mound growing towards the sidewall as well as downstream (§5.3.2).

Bed	D_{50} values [number of sample locations]			Trend in grain size	
	Mean (µm)	Standard deviation	Range (µm)	Upstream	Downstream
R3 Foreset 2	376 [28]	26	310 - 392	No trend	
R3 Topset 2 and Bed 3	286 [44]	39	219 - 373	◁ (fining downstream)	
R4 Bed 1	251 [22]	25	220 - 332	◁ (fining downstream)	
R4 Bed 2	288 [6]	7	278 - 297	No trend	
R4 Bed 3	279 [28]	13	255 - 311	▷ (coarsening downstream)	
R4 Bed 4	256 [60]	30	214 - 319	◁ (fining downstream)	

Table 5.1 Properties of the grain size segregation within the Runs 3 and 4 deposits. Bed numbers are equivalent to those in Figs 5.5 and 5.14. In Run 3 the bed of thin upstream inclined laminae (Bed 4) and the thin foreset within it (Bed 3) were taken within the same sample. No samples were taken from the Run 3 *basal wedge*.
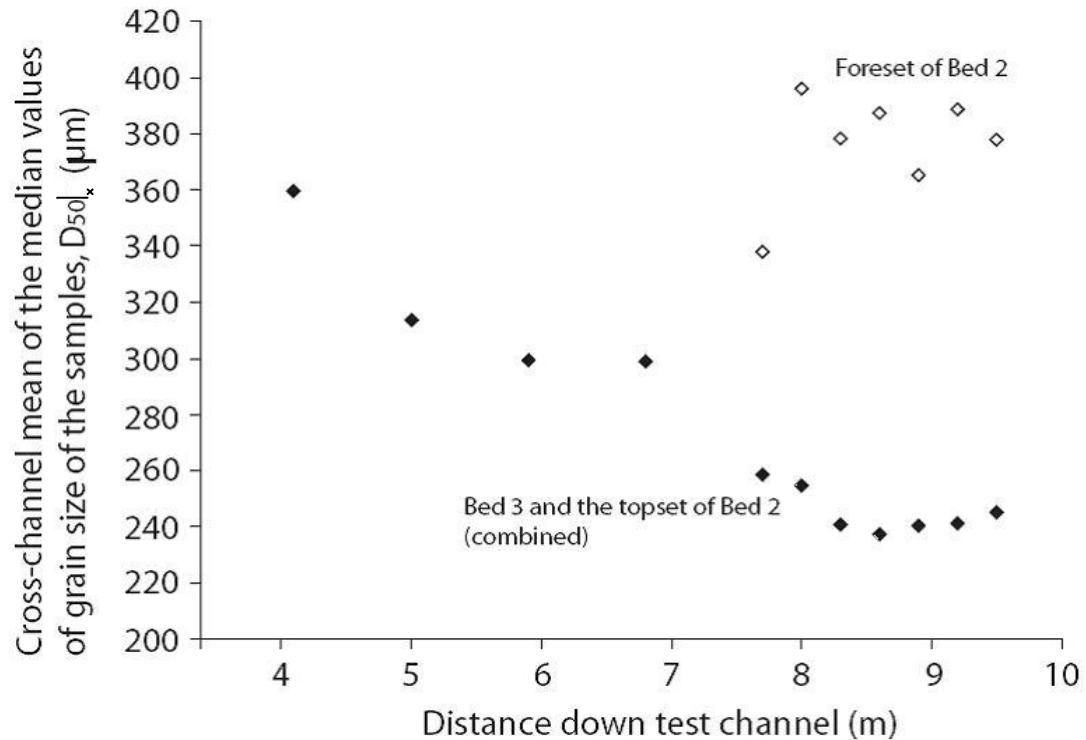
Figure 5.10 Plot of the streamwise variation in grain size along beds of the deposit which formed during Run 3. The D_{50} data of the four stream-parallel rows (Rows 1 – 4, Fig. 5.8) were collapsed to show the on-average variation in grain size along-stream, $\overline{D_{50}}\big|_{x=nm}$.

5.3 RUN 4: HYDRAULIC JUMP WITH SAND FLUX III

Run 4 had the initial conditions of Run 1 (§4.2). It was 75 minutes long and involved the near constant addition of a total of 5000 kg of sediment (Table 4.1). Compared to Run 2 the sediment was finer, and was input at the same mean rate, but with no hiaituses in sand loading.

5.3.1 The general flow character through Run 4

The water surface shape of the hydraulic jump was similar to that observed in Runs 1 – 3 (compare Figs 4.5, 4.8, 5.2 and 5.11). It generally did not change through Run 4 but the breaking pattern was complicated. As in Runs 2 and 3, suspended sediment was seen within all parts of flow within the test channel, and it obscured the view of the channel floor and bubbles within the flow. Consequently paths of flow within the hydraulic jump and tailwater were difficult to see.

167
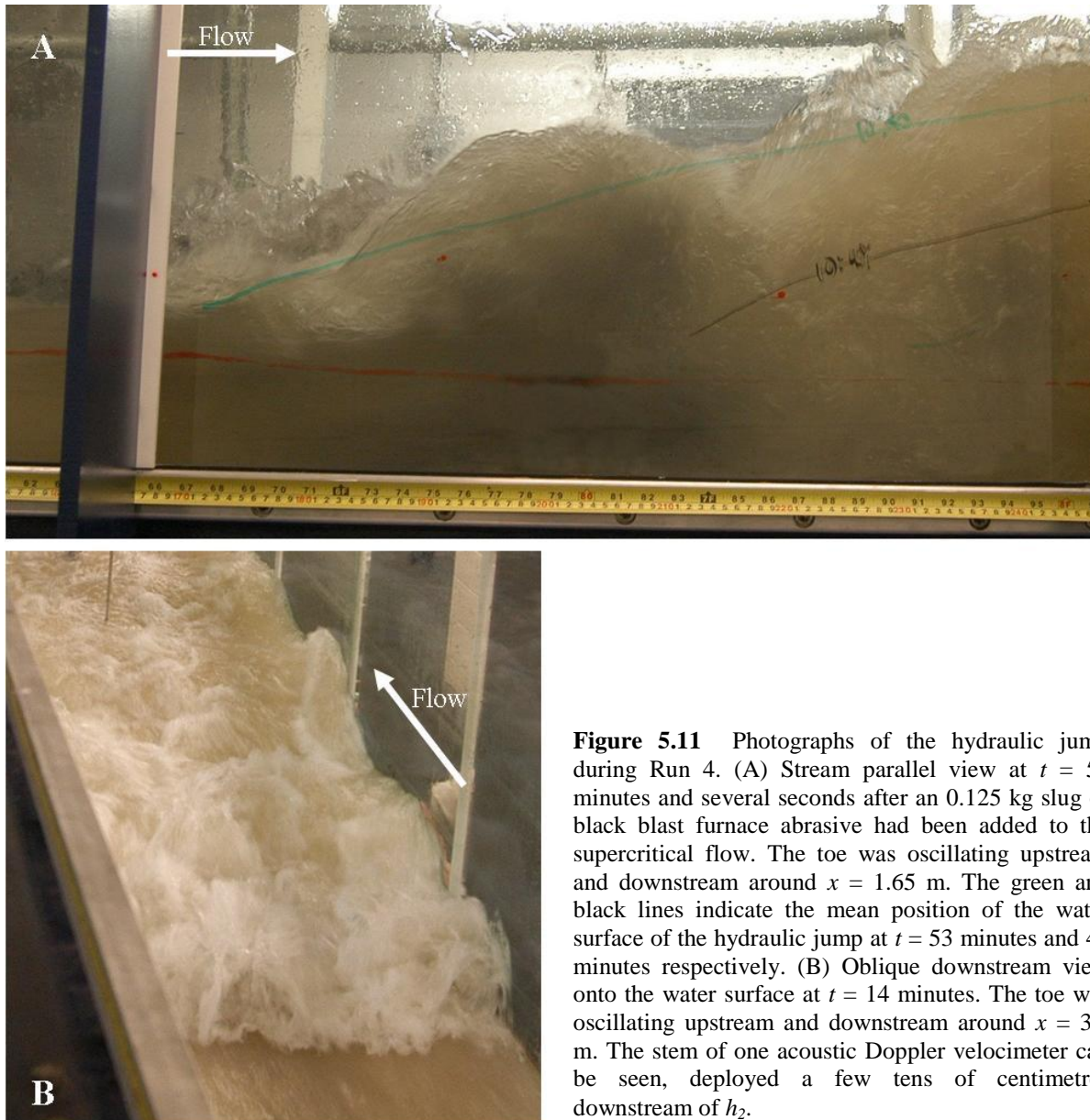
Figure 5.11 Photographs of the hydraulic jump during Run 4. (A) Stream parallel view at $t = 54$ minutes and several seconds after an 0.125 kg slug of black blast furnace abrasive had been added to the supercritical flow. The toe was oscillating upstream and downstream around $x = 1.65$ m. The green and black lines indicate the mean position of the water surface of the hydraulic jump at $t = 53$ minutes and 48 minutes respectively. (B) Oblique downstream view onto the water surface at $t = 14$ minutes. The toe was oscillating upstream and downstream around $x = 3.8$ m. The stem of one acoustic Doppler velocimeter can be seen, deployed a few tens of centimetres downstream of h_2.

Through Run 4 the general character of the flow changed in an almost identical manner to the changes observed in Run 3 (§5.3.1). A 4.6 m^3 deposit formed and the hydraulic jump moved upstream by 4.25 m. In association with this change, the supercritical flow increased in thickness by 0.03 m to 0.12 m and Fr_s decreased from 2.73 to 2.18. As Fr_s decreased the hydraulic jump changed in form, from an oscillating jump to a weak jump cf. Massey's classification (1983). The transition of form happened at $t \sim 29$ minutes (rather than $\sim$15 minutes in Run 3, §5.3.1). The accuracy of this timing is unsure because the accuracy of Massey's divisions within the classification is unknown. As the deposit grew, h above it

decreased and at the end of Run 4, $h|_{x=10m}$ was 0.14 m. In association, hydrostatic pressure decreased between the downstream limit of the hydraulic jump and the thinner flow above the sediment deposit. Because h_1 and Fr_s are known at the end of Run 4, it must be true that at the end of Run 4, $h_2 = 0.31$ m, $Fr|_{h=h_2} = 0.51$ and $\overline{u_2} = 0.90$ m s^{-1} (computations via Equations 1.2 – 1.4).

5.3.2 Observations of the pattern of sediment transport

The sediment response to changing flow conditions was different to the response in Run 3. Sediment travelled in suspension or saltated through the supercritical flow. Initially it fell from suspension to the flume floor between $x = 5.30$ m and the discharge tank (the toe of the hydraulic jump was at $x = 4.68$ m). Over Run 4 (total of 75 minutes) one *hydraulic-jump unit bar* formed, compared to six in 75 minutes, Run 2; possibly two in 45 minutes, Run 3. It developed in a similar way to the first hydraulic jump to form in both Run 2 and 3, but grew much bigger. The sediment that fell from suspension between $x = 5.30$ and 6.80 m, moved downstream as bedload and stalled in a mound (Fig. 5.12A). In contrast to Run 3, sediment mounded close to the sidewalls from the first few tens of seconds. The mound increased in volume up to $t = 7$ minutes (compare Fig. 5.12A and B), was twice as high and eight times as long as the Run 2 mound and did not migrate. By $t = 8$ minutes, the foreset of the hydraulic jump had formed (twice as long as for the Run 2 *hydraulic-jump unit bar* to develop). The foreset was initially 0.4 of the thickness of the mound, whereas in Runs 2 and 3 the brink was initially as thick as the mound. Over the first 11 minutes of its development the foreset thickened at a rate of 0.16 mm s^{-1} until it was 0.10 m thick and after this it thickened by 0.04 mm s^{-1}, as it prograded downstream. The foreset reached the downstream limit of the test channel at $t = 31$ minutes.

The sediment that fell from suspension downstream of the mound and foreset formed a *basal wedge* cf. Runs 2 and 3. A rippled surface formed on the downstream-most metre of the *basal wedge* within the first 2 minutes (before the foreset had developed) and extended to the downstream-most 1.5 metres by $t = 4$ minutes. Initially the ripples were asymmetrical (steeper lee side). Over time the ripples grew in height and wavelength and became more symmetrical (Fig. 5.12D). Specifically at $t = 12$ minutes, ripples were 0.01 m high and 0.07 m long. At $t =$

14 minutes, when the foreset had prograded to $x = 8.5$ m it became the upstream limit of the rippled bed. After this time the grains forming each new avalanche lamina fell onto the surface of a symmetrical ripple (Fig. 5.12E). No other deposit surface was rippled throughout Run 4. The ripples migrated downstream (Fig. 5.12D), by less than one wavelength during the time they developed. The variation in shape and size of the ripples is discussed in Section 5.5.5.

A topset formed with the foreset. Before $t = 11$ minutes a depression was seen in the upper surface of the topset, just upstream of the brink point and after this time no depression was seen. Between $t = 21 - 23$ minutes no topset was seen above the foreset a few tens of centimetres upstream of the brink, and the brink looked sharper than at all other times in Run 4. The topset continued to thicken. After $t = 23$ minutes it covered the foreset and it was still thickening at the end of the run.

The 5000 kg of well sorted quartz-dominant sand formed a deposit 4.60 m^3 in volume and in response the hydraulic jump moved upstream by 4.07 m. With a sediment input rate of 4000 kg hr^{-1}, the upstream-migration rate of the hydraulic jump was 3.5 m hr^{-1} and was constant (Fig. 5.4). The upstream limit of the deposit did not move upstream over the first 13 minutes, but did after $t = 13$ minutes at a rate of 5.5 m hr^{-1} as the topset grew. After $t = 13$ minutes the upstream limit of the deposit relatively converged with the toe of the hydraulic jump.

Motion of the black sand that highlighted lamination

When input, the black sand (§5.1.3) was suspended within the full thickness of the supercritical flow and hydraulic jump (Fig. 5.11A). Although not hydraulically equivalent with the bulk load, the black sand travelled throughout the whole flow. Most of it was deposited over the entire flume length downstream of the hydraulic jump within the first recirculation of it.

Figure 5.12 (below) Photographs of the sediment deposit underneath the tailwater during Run 4. (A) The proto-unit bar at $t = 3$ minutes. The blue vertical supports are 0.80 m apart. (B) Part of the upstream edge (in 2d) of the *hydraulic-jump unit bar* at $t = 7$ minutes. A vortex is developing 0.08 m above the deposit surface and slightly further downstream a puff of sediment was lifted into suspension. (C) The mound of sediment developing above the *basal wedge* at $t = 29$ minutes. The silver bolts underneath the measuring tape are 0.15 m apart. (D) The rippled surface of the *basal wedge* at $t = 20$ minutes. The red, orange and brown lines are tracings of the rippled surface at previous times during Run 4. The foreset is 0.3 m upstream of the photograph. (E) The foreset of Bed 2 at $t = 22$ m.

Sediment surface

Sediment surface
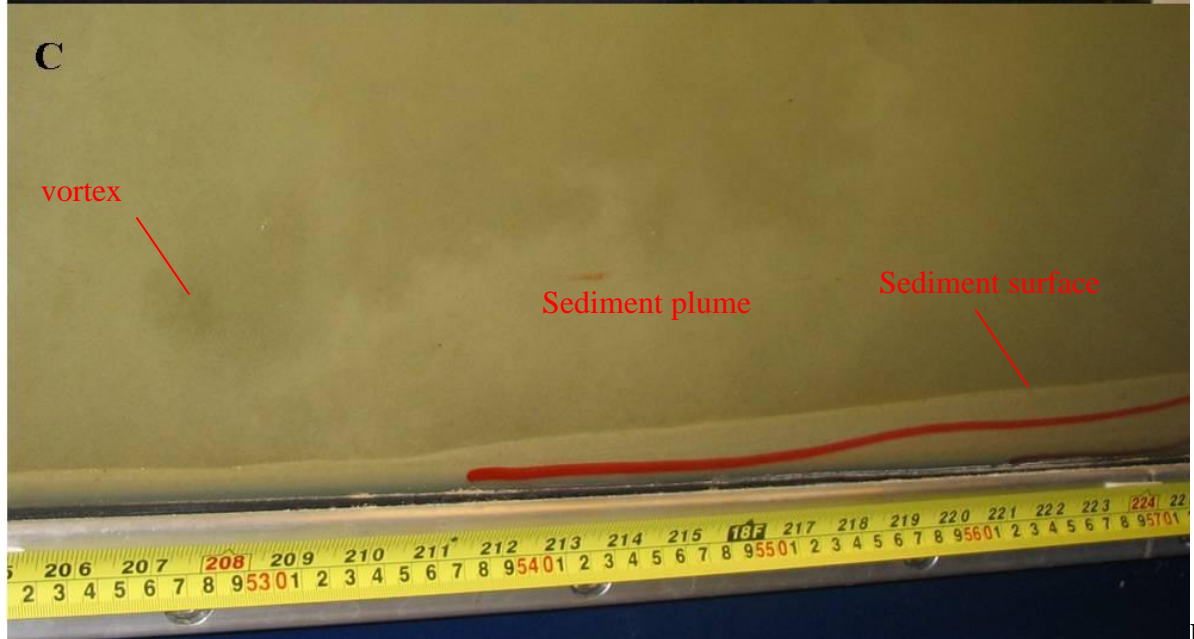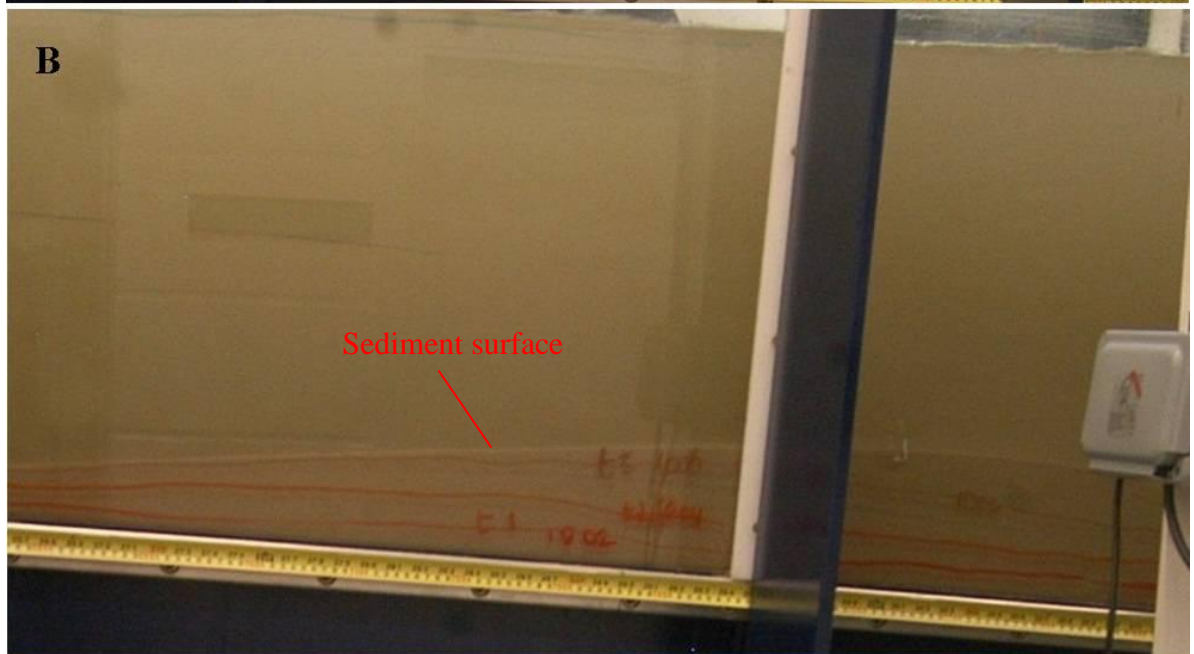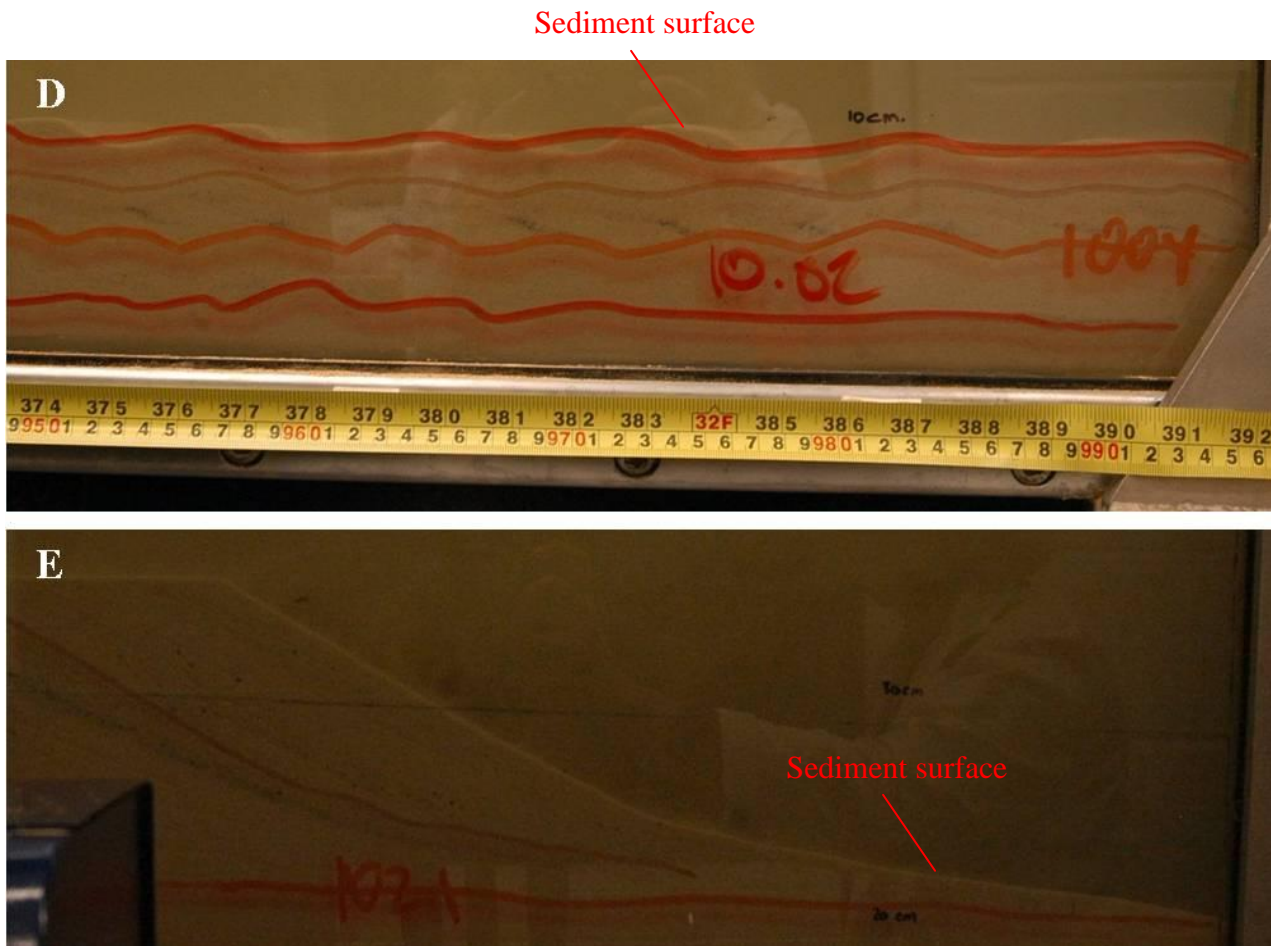
5.3.3 The motion of vortices in the flow

Vortices near the hydraulic-jump unit bar brink

Twenty five minutes into Run 4, vortices were seen to form immediately downstream of the prograding foreset brink. Generally these vortices were incepted at 15 second intervals, moved downstream approximately horizontally and were destroyed within the discharge tank. The diameter of the vortices was 0.08 – 0.10 m. They had a stream-transverse axis of rotation with the upper part of each vortex rotating downstream and the lower part rotating upstream (Fig. 5.13). Associated with each vortex was a dark region in the centre of the circulation, seen through the sidewall. It is unclear whether the dark region was due to an (unknown) change in flow or sediment transport that occurred around the axis of rotation or a pocket of air adjacent to the sidewall (cf. Fig. 5.13B). An air pocket in this position would have introduced a surface extending a short distance into the flow from the sidewall and would have introduced

172

shadows. Where two vortices were generated within a few seconds of each other they passed downstream together and interacted: They oppositely moved up and down curved tracks in a see-saw motion, with each track being a ~ 120° arc of a single circle (Fig. 5.13A). The circle centre was midway between the two vortices (grey asterisk, Fig. 5.13A) and moved downstream with the vortices (black arrow, Fig. 5.13A).

A vortex seen above the topset

One vortex was seen above the upstream limit of the proto-unit bar (Fig. 5.12C). It had a cross-stream axis of rotation with the upper part of each vortex rotating downstream and the lower part rotating upstream. It was 0.045 m in diameter with its centre 0.06 m above the sand surface and was detectable because it was darker in colour than the flow which surrounded it.
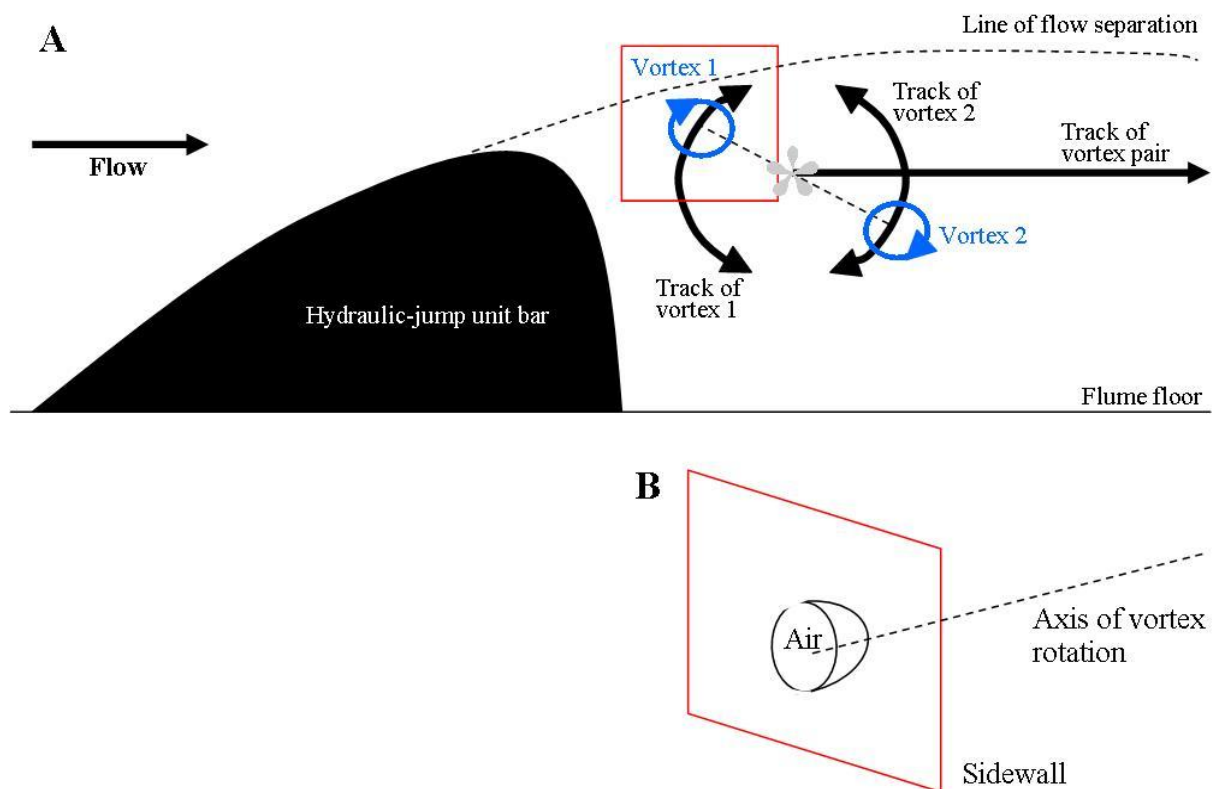
Figure 5.13 **(A)** Sketch of the interaction of two vortices incepted within a few seconds of each other, downstream of the prograding foreset brink. A *hydraulic-jump unit bar* is sketched to the left of the two vortices. Sketch is not to scale. Moving in the frame of reference of the centre of the vortex pair, the vortices rotate 120° clockwise and counter clockwise in an oscillatory see-saw motion. In the Eularian frame of reference the centre of the vortex pair (marked by the grey asterisk (*) moved downstream at approximately the height of the brink. (B) Sketch depicting the shape of a pocket of air adjacent to the flume sidewall which may have occurred at the centre of vortex 1, depicted in (A).

173

5.3.4 Profiles of time-averaged velocity

As in Runs 2 and 3 the UDVP was deployed at $x = 6.10$ m to measure streamwise velocity. The hydraulic jump moved upstream in response to the deposit forming (§5.4.3) and because the hydraulic jump moved 0.63 m further upstream than it did in Run 3, $\bar{u}$ was measured to 0.63 m further downstream of the toe than it was in Run 3. Seven velocity profiles are presented, between $0.5 - 5.3$ m downstream of the toe. At $x = 6.10$ m, flow thickness did not noticibly vary between $t = 0 - 25$ minutes. It decreased from 0.42 to 0.28 m between $t = 25 - 48.5$ minutes. In association with flow thinning, U increased from $0.62 - 0.93$ m s^{-1}. Over the remainder of the run (between $t = 48.5 - 75$ minutes), flow over the deposit at $x = 6.10$ m continued to thin but more slowly: At $t = 75$ minutes flow was 0.23 m thick at $x = 6.10$ m and in association $\bar{u} = 1.13$ m s^{-1}.

Streamwise velocity Profile F was the first recorded in Run 4, it was at a streamwise location equivalent to the region of jet detachment in the sediment-free hydraulic jump of Run 1 (Fig. 4.4). Maximum of time-averaged velocity, $\bar{u}_{max} = 0.85$ m s^{-1} occurred at 0.4 of the flow height; below this position $\bar{u}$ decreased to the flume floor, above this position $\bar{u}$ decreased to the water surface (Profile F, Fig. 5.14).

Further downstream from the toe, between Profiles F – L, $\bar{u}_{max}$ increased in magnitude from 0.85 to 1.5 m s^{-1} and the height at which $\bar{u}_{max}$ occurred rose (Fig. 5.14): $\bar{u}_{max}$ was half way up the water column in Profiles G and H and was immediately below the water surface in Profiles I – L. No distinct jet edge could be detected from any of the $\bar{u}$ profiles.

Effects of changing flow characteristics on the position of the jet

Unlike Runs 1 – 3, no jet was distinct within the hydraulic jump, neither in the oscillating jump state or weak jump state. The supercritical jet that entered the hydraulic jump instead expanded to occupy the full height of the water column within the tailwater: Even though Re was barely different to the sediment-free Run 1, and was even less different to Re in Runs 2 and 3, jet dynamics were very different. The co-developing jet shape and sediment deposit shape are discussed after the Run 4 depositional architecture is presented.
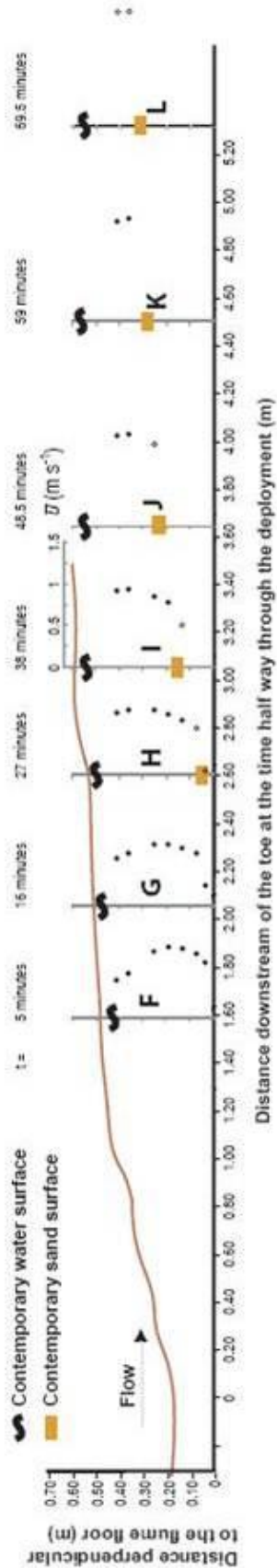
Figure 5.14 Profiles of the time-averaged streamwise velocity component, $\bar{u}$ in Run 4 measured by ultrasonic Doppler velocity profilers (UDVP). The solid symbols mark data points that were the average of measuring intervals of 600 s. Measuring intervals were shorter for the data points marked by the open circles because the associated profiler became buried part way through the deployment. The UDVP array was fixed at $x = 6.10$ m throughout Run 4 and the hydraulic jump moved upstream. The brown line indicates the lowest water surface position of the hydraulic jump. The profiles are drawn in positions relative to the contemporary hydraulic jump. The sand and water surfaces at $x = 6.10$ m, half way through each deployment are marked on the profiles using short black and yellow lines.

175

5.3.5 The depositional architecture: A *basal wedge* and a single *hydraulic-jump unit bar*

In Run 4 only two beds formed (Fig. 5.15). A *basal wedge* (Bed 1) was overlain by a single *hydraulic-jump unit bar* (Bed 2) that contained a mound of sediment (Element 2 of the streamwise anatomy of a fully developed *hydraulic-jump unit bar*, Fig. 5.16), a foreset (Element 4), a topset (Element 5) and a bottom set, which did not form in Runs 2 or 3.

The *basal wedge* was similar in appearance to the *basal wedges* that formed in Runs 2 and 3. It had an upstream limit at $x = 7.18$ m and thickened downstream, to 0.095 m thick at $x = 7.9$ m and 0.21 m thick at $x = 10.0$ m. It was massive in a lower region and in an upper region wavy laminae were seen (Fig. 5.12D, view using zoom on electronic version, Appendix 2). The lower limit of the upper region was downstream-dipping in a more upstream section and horizontal in a more downstream part (Fig. 5.15). The upper limit of the upper region was the contact with the bed above. The wavelength and amplitude of wavy laminae increased upward through Bed 1, and the laminae gradually changed in shape, from asymmetrical (steeper lee face) to symmetrical. The contact between the *basal wedge* and Bed 2 was sharp except for the most downstream 0.3 m where the contact was erosional. The contact had two distinct gradients: in the upstream-most part the gradient was relatively steep (upstream dipping) and in a more downstream part, including the erosional contact, the gradient was relatively shallow (Fig. 5.15). In the steeper part the contact fluctuated in height on the order of tens of millimetres in tens of centimetres. In the shallower part the contact fluctuated in height on the order of millimetres in tens of centimetres, associated with the ripples that had been on the surface of the wedge as the foreset had prograded over them.

The mound in Bed 2 was 0.15 m thick and 1.6 m long (Figure 5.15). It pinched out to upstream, 1 m upstream of the *basal wedge*. It pinched out to downstream above the *basal wedge*, and overlapped it by 0.60 m. It contained a very sparse pattern of downstream-dipping laminae amongst a generally massive texture and made a gradational contact with the upstream limit of the foreset.

The foreset was 0.02 m thick at the downstream limit of the mound and 0.1 m thick at the downstream limit of the test channel. The upper surface of the foreset had two distinct gradients: steeper in the upstream-most part, shallower in the more downstream part. The upstream limit of the steeper gradient was at the same streamwise position as the downstream

limit of the steeper gradient of the *basal wedge*. The foreset laminae dipped in the range 19 – 29° (increasing downstream).
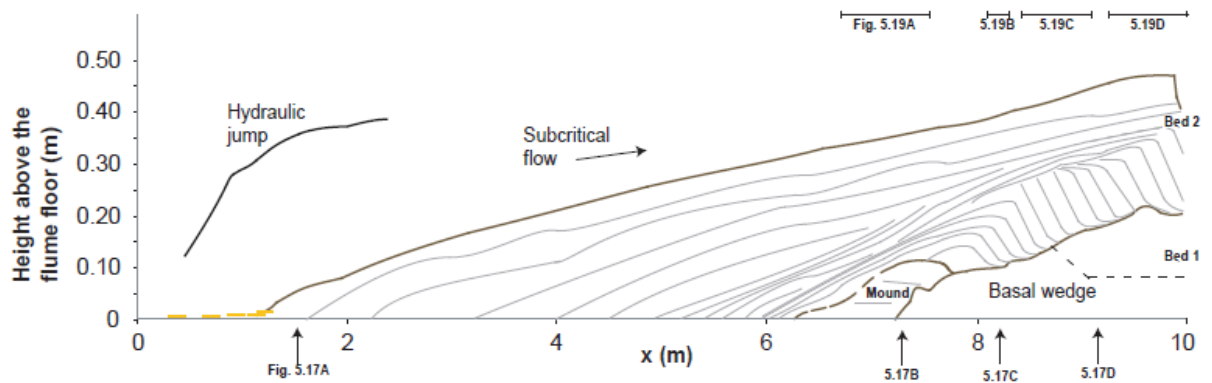
Figure 5.15 Pattern of lamination within the Run 4 deposit represented in stream-parallel section. The height scale is five times the streamwise length scale and the angles of the laminae are plotted with respect to this height exaggeration. The initial position of the toe of the hydraulic jump was at x = 4.68 m. The line representing the water surface corresponds with the position of the hydraulic jump at the end of Run 4. The solid brown lines indicate the upper limits of the beds. The dashed brown line indicates the upper surface of the mounded sediment. The ripple surfaces could not be clearly presented but indications of their shape are given in Fig. 5.12D. The change of dip with height exaggeration is derived in Appendix 4.

Associated with the foreset was an 0.01 m thick shallow-angled bottomset, as well as a thick topset. The bottomset is a new Element (6) of a fully developed *hydraulic-jump unit bar* (Fig. 5.16). The topset extended from 5 m upstream of the mound to the downstream limit of the test channel. It was thickest at the upstream limit of the *basal wedge*, where it was the thickest part of any bed. Grain size was not seen to vary between the upstream and downstream limits of the topset. Topset laminae could be traced for metres in the streamwise direction. The contact between the foreset and topset was sharp.
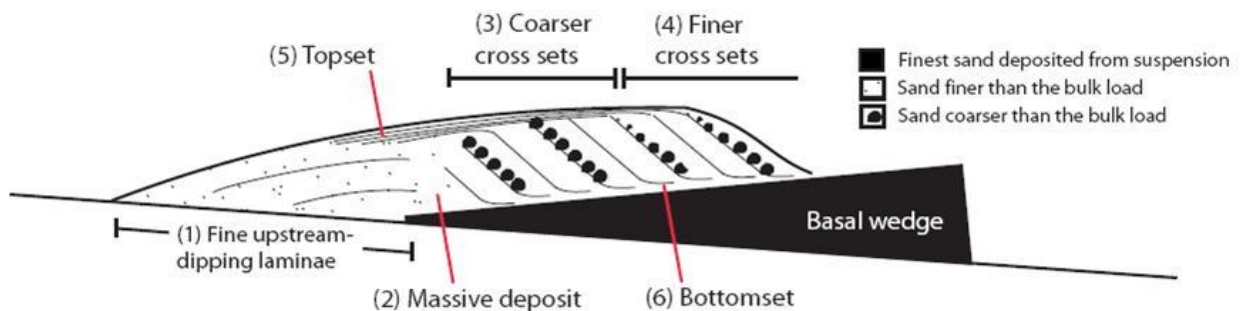
Figure 5.16 Diagrammatic representation of a "fully developed" *hydraulic-jump unit bar*, lying on top of a *basal wedge*: after three runs involving sediment six features had formed within eight or nine *hydraulic-jump unit bars*, none of which contained all six features, i.e. none were fully developed. The large (small) grains depict a location where grain-size distribution is negatively (positively) skewed with respect to the bulk load. The thin lines show the general orientation of laminae within the *hydraulic-jump unit bar*. The topset is drawn thinner than the foreset as if in an early stage of formation. Given sufficient time and sediment input and with no new feature forming on top of the *hydraulic-jump unit bar*, the topset could grow to be much thicker than the foreset.

Stream-parallel section

The slightly upstream dipping laminae in the topset upstream of the basal wedge were slightly convex up in stream parallel section. Further downstream, the absence of laminae within the *basal wedge* underneath the mound, distinguished it from the mound and the topset that overlay the mound when looking directly at the deposit. However, the distinction between the basal wedge and the mound did not reproduce in the photographs, despite attempts to vary brightness and contrast. The mound and topset could not be told apart by lamina thickness or grain size distribution, but the lowermost topset laminae appeared to diverge from the mound below (blue arrow, Fig. 5.17A; best viewed using zoom on the electronic version supplied in Appendix 2).

Further downstream than the mound, the topset overlay the foreset, which overlay the *basal wedge*. The basal wedge was massive. In a more upstream part the foreset was the darkest part of the section because it contained the most black sand. Foreset laminae had undulations along-lamina, with amplitude of 0.01 m (perpendicular to the dip of the laminae, Fig. 5.17B). Two to four wavelengths were present along any single lamina; the number of wavelengths tended to increase within the range 2 – 4 as the thickness of the foreset increased. The topset laminae were generally horizontal or dipped slightly upstream.

In a more downstream part the basal wedge contained wavy lamination, grading upwards from asymmetrical (steeper lee side) to symmetrical. Symmetrical wavy laminae directly underlaid the foreset (Figs 5.17C and D). The foreset was a similar colour to the *basal wedge* and topset. Foreset laminae dipped downstream with no undulations and each lamina passed smoothly downstream into a bottomset lamina. Passing downstream along the foreset, occasional patches at least several centimetres long were coarser than the rest of the foreset. Except for these patches no change in grain size was seen in the foreset (compare the foreset along Figs 5.17C and D).

Figure 5.17 (below) Photographs taken of the Run 4 deposit through the sidewall of the flume (i.e. stream-parallel sections) and corresponding line drawings of the deposits. The location of each photograph is indicated in Figure 5.15. The lighting conditions were varied to highlight the lamination; this gives a false impression of variation in sand colour. The line drawings are labeled with bed numbers as in Figure 5.15. Thicker lines indicate bed contacts and thinner lines indicate laminae. The coin is 20 mm in diameter. The location where the mound and topset laminae diverged downstream is highlighted by a blue arrow in the photograph and line drawing of (A). The silver circle in (B) is a reflection of the camera lens. Note the undulating nature of the foreset in (B) and the dark colour of some of the grains within it. Some of the black sand put into Run 4 highlighted the rippled basal layer (C and D). The dark blue object in (D) is part of the flume structure.

178

A

Flow

Topset of Bed 2

Mound of
Bed 2

B

Topset of Bed 2

Foreset of
Bed 2

C

Topset of Bed 2

Foreset
of Bed 2

Basal wedge, Bed 1

D

Topset of Bed 2

Foreset of
Bed 2

Basal wedge, Bed 1
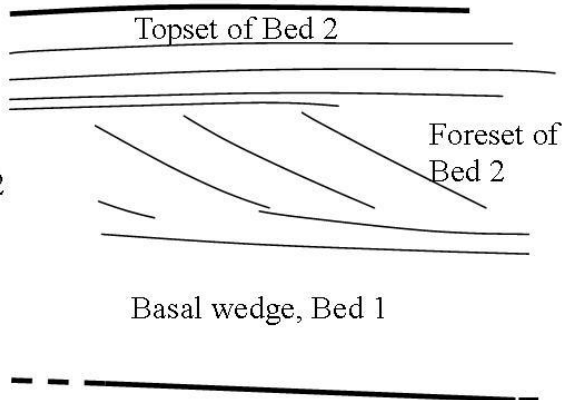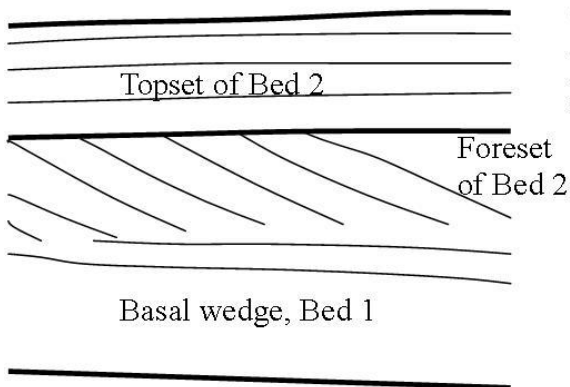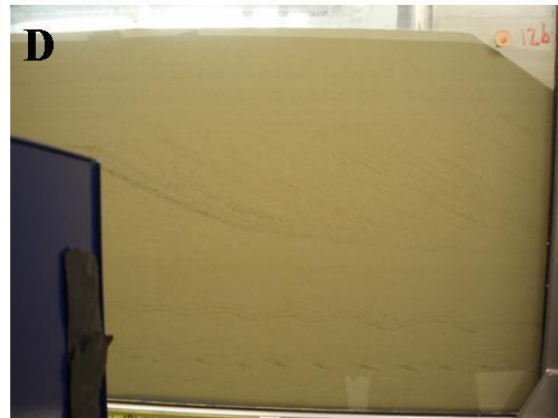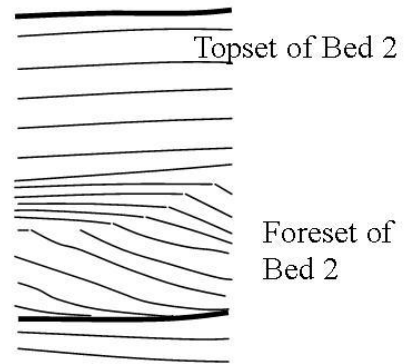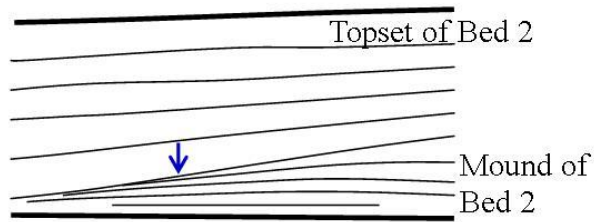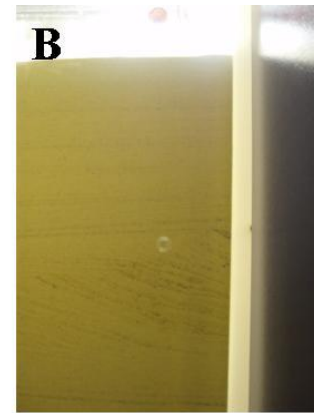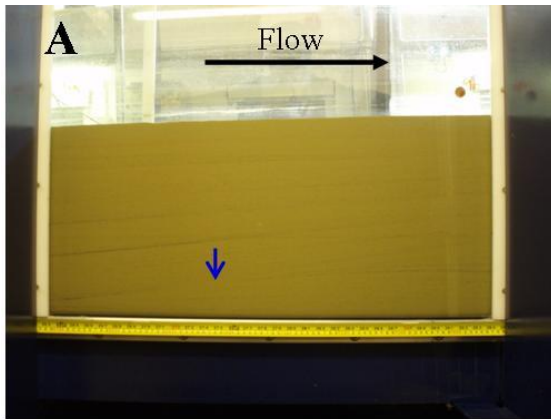
Stream-transverse sections

Eleven stream-transverse sections were cut (Fig. 5.18) and four photographs are used to illustrate the change in lamination pattern, from upstream to downstream (Fig. 5.19). At the upstream-most section, the topset was thinner near to the sidewalls than in the centre of the tank (Fig. 5.19A). Dips towards the position $y = 0.5$ m were seen in all laminae below 0.75 of the deposit height; the dip of several adjacent laminae can be seen from a photograph (Fig. 5.19A). The dip diminished in amplitude with height and with distance downstream. One metre further downstream than the section shown in Figure 5.19A, $x = 2.5$ m, the dip could not be seen.

At $x = 7.25$ m Bed 1, near its upstream limit, was discriminated from the mound above because of its massive texture, and its darker colour having retained more water. Within the mound a few stream-transverse laminae could be traced from one sidewall to the other. Topset laminae dipped at 4° from the channel centre to the flume sidewalls. At this streamwise location, in a region of the topset close to the flume sidewall, pores were seen, each several centimetres in diameter (Fig. 5.19B). Despite the differences in their appearance, the Bed 2 mound and topset were difficult to distinguish in stream-transverse section at $x = 7.25$ m (but had been easy to distinguish in stream-parallel section).
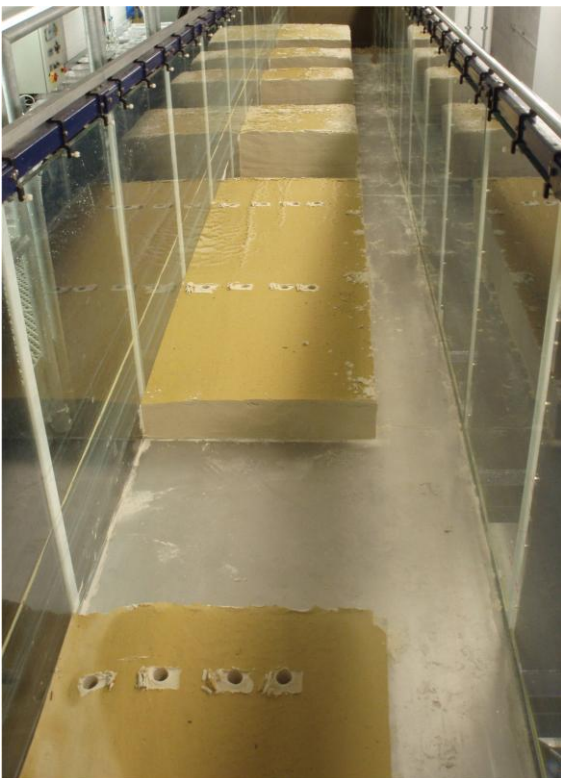
Figure 5.18 Photograph of the Run 4 deposit following cutting the stream parallel cut section, sediment sampling and cutting the eleven stream transverse sections. View was to downstream.

180

A

y = 0.5 m

Topset of Bed 2

B

Topset of Bed 2

Mound of Bed 2

Bed 1

C

Topset of Bed 2

Foreset of
Bed 2

Basal wedge, Bed 1

D

Topset of Bed 2

Foreset of
Bed 2

Basal wedge, Bed 1

181
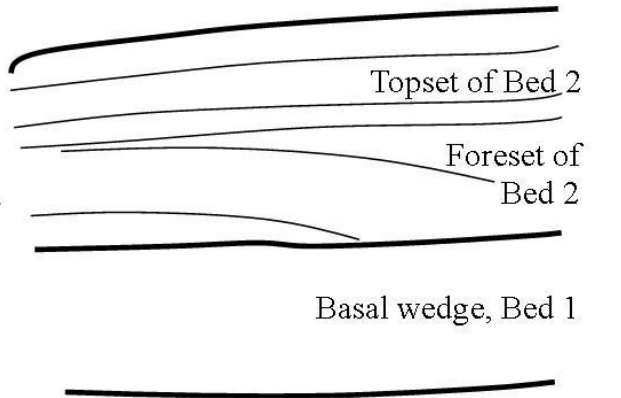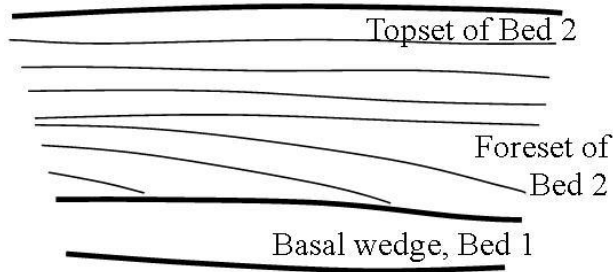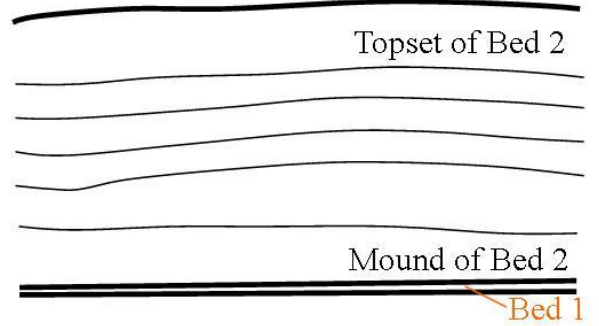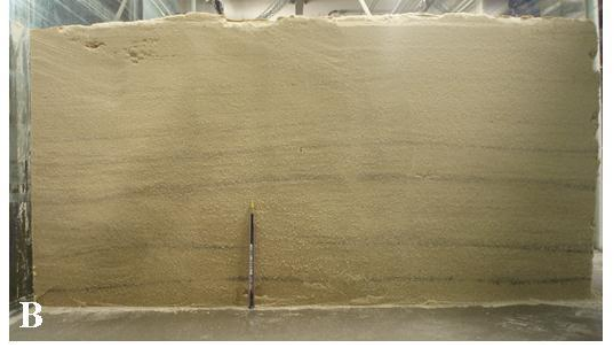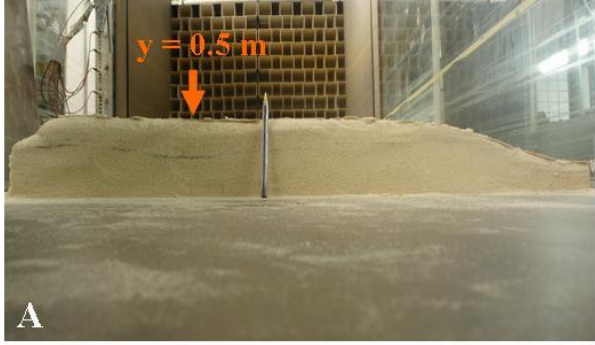
Figure 5.19 (above) Photographs and corresponding interpretative line drawings of stream-transverse sections cut through the deposit. Thicker lines indicate bed contacts and thinner lines indicate laminae. The lighting conditions were varied to highlight the lamination; this gives a false impression of variation in sand colour. The positions of these sections are indicated on Fig. 5.15. The pen is 0.145 m long. (A), (C) and (D) were photographed looking upstream and (B) was looking downstream. A small input of black sand highlighted lamination in (A). The pores that can be seen in the top-left corner of the deposit in (B) were exposed during cutting. The crack within the Bed 2 topset in (D) formed after that face was cut.

The *basal wedge* was massive in stream-transverse section between $x = 8.15 - 9.15$ m (Fig. 5.19C and D); there was no evidence of the ripples seen in stream-transverse section. The foreset was easily distinguishable from the *basal wedge* because it contained stream-transverse laminae and was lighter in colour having retained less water. Foreset laminae dipped from the channel centreline towards the sidewalls in a smooth curve (Fig. 5.19C). The curvature of the foreset laminae decreased downstream (compare Figs 5.19C and D). The topset laminae dipped towards the sidewalls at a much lower angle. They were easily distinguishable from the foreset laminae at $y = 0.5$ m but much less distinguishable towards the sidewalls.

5.3.6 Grain size distribution within the architecture

Sampling procedure

Sixty samples of the plan distribution of grain size within the topset were taken in four channel parallel rows between $y = 0.1$ m (Row 1, Fig. 5.8) and $y = 0.5$ m (Row 4), and 15 channel-transverse rows between $x = 1.40$ m (Row A) and $x = 9.80$ m (Row O) (Sample Array 1, Fig. 5.8). Samples were taken using a metal tube of 0.029 m internal diameter. Twenty eight samples of the plan distribution of grain size within the foreset were taken between $x = 8.0 - 9.8$ m (Rows I – O, Fig. 5.8) in four channel parallel rows between $y = 0.1$ m (Row 1) and $y = 0.5$ m (Row 4) (Array 2, Fig. 5.8).

Unlike procedure for Run 3, grain size distributions within the basal wedge were sampled in stream-transverse section. Twenty two samples were taken at five streamwise locations (0.5 m intervals), with an increasing number of samples at each location further downstream as the wedge thickened (black dots, Fig. 5.20C). Samples were taken 0.06 m into the face, each using a different plastic tube of 0.006 m internal diameter.

Grain size distributions in plan, Sample Array 1 (topset)

The grain size distribution of each sediment sample was unimodal and positively skewed. The mean D_{50}, $\overline{D_{50}}$ was 256 μm (Table 5.1), and the bulk load D_{50} was 250 μm. At its upstream limit the topset was coarser than the bulk load. It fined downstream, by 110 μm over 8.6 m (Figs 5.20A and 5.21) and varied little in grain size across-stream (Fig. 5.20A).
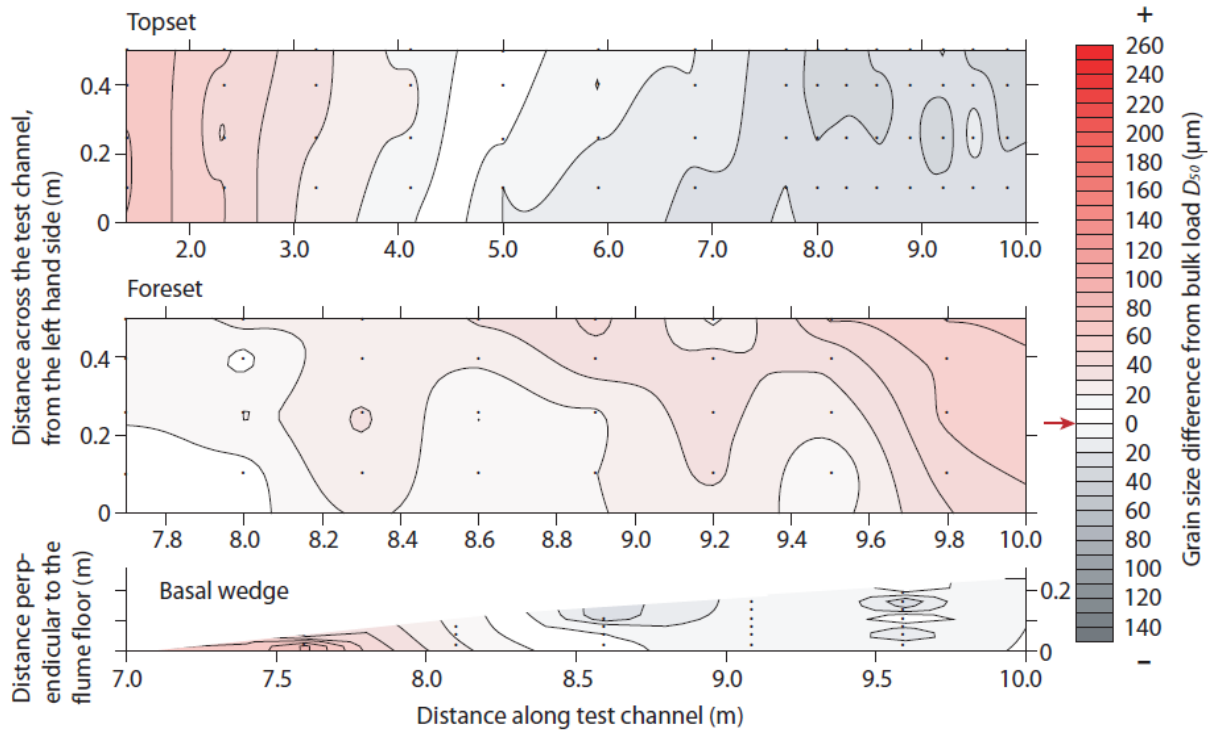
Figure 5.20 Maps of the difference between D_{50} in the original sediment and in the deposit, made using Surfer 8 and the Kriging method of contouring. The first map is of the topset of Bed 2 in plan view, the second map is of the foreset of Bed 2 in plan view and the third map is of the *basal wedge* in streamwise section with samples taken into the stream parallel cut face. Sample locations are depicted with dots (·). The colour scale depicts D_{50} greater than that of the bulk load (red), less than the bulk load (black) and equal to the bulk load (white) in 10 μm increments. The D_{50} value of the bulk load was 250 μm; this takes the value 0 on the scale and is marked with a red arrow.

Grain size distributions in plan, Sample Array 2 (foreset)

$\overline{D_{50}}$ was 279 μm (Table 5.1); 12% higher than the bulk load D_{50}. At the upstream limit of the foreset, values of D_{50} of the sampled sediment were similar to the D_{50} of the bulk load and the foreset became coarser downstream, with D_{50} increasing by 40 - 50 μm over 2.2 m (Figs 5.20B and 5.21). Downstream of x = 9.5 m, D_{50} increased towards the channel centre and further upstream D_{50} changed little across-stream at all streamwise locations.

183
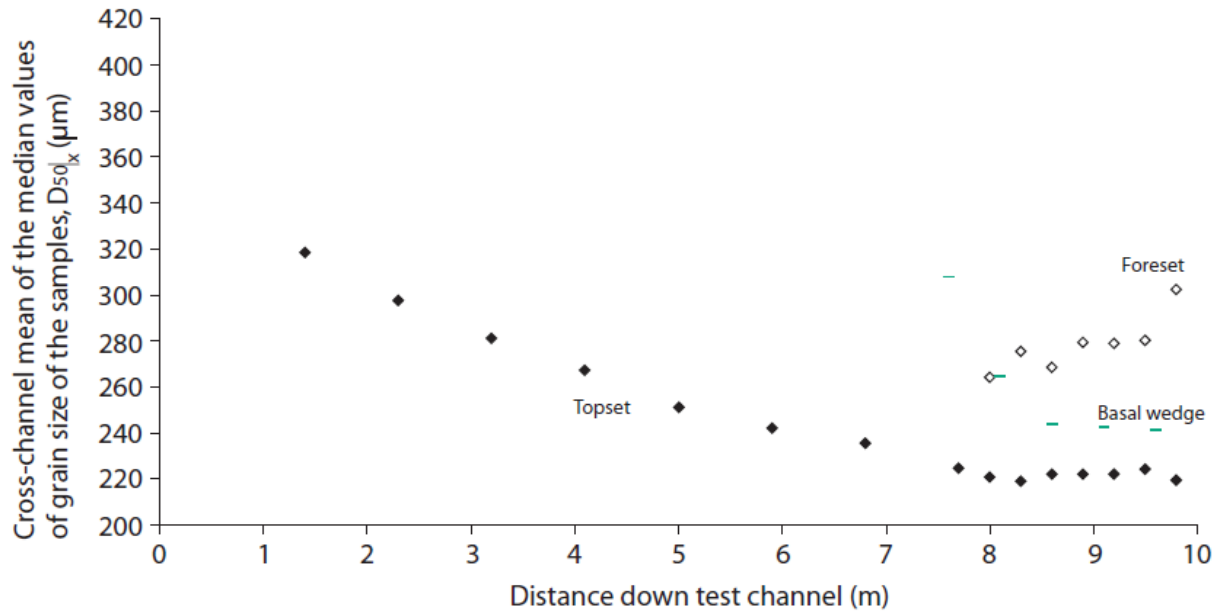
Figure 5.21 Plot of the streamwise variation in grain size along features of the deposit which formed during Run 4. The D_{50} data of the four stream-parallel rows (Rows 1 – 4, Fig. 5.7) were collapsed into one data point for each streamwise location: in the plot each datapoint represents one cross-stream average of D_{50} and variation can be seen along stream.

Grain size distributions within the basal wedge in stream-parallel section

$\overline{D_{50}}$ of the *basal wedge* was 251 µm (Table 5.1). At its upstream limit it was coarser than the bulk load. It became finer from its upstream limit to 1 m further downstream ($\overline{D_{50}}\big|_x$ decreased from 310 – 245 µm between $7.5 \leq x \leq 8.5$, Fig. 5.21) and changed little with distance further downstream of this position (green dashes, Fig. 5.21; Fig. 5.20C). No trend of grain size with height could be detected (Fig. 5.20C).

5.4 DISCUSSION

Different sediment inputs to the same hydraulic jump resulted in depositional architectures with marked differences. These differences in architecture resulted from differences in the feedback between the hydraulic jump and related flow patterns, and a deposit forming downstream of it.

5.4.1 Terminology: Full versus partial development of a *hydraulic-jump unit bar*

Macdonald *et al*. (2009) defined "full development" of a *hydraulic-jump unit bar* to be its development of a brink (hence its transition from a proto-unit bar). The five *hydraulic-jump unit bars* that formed in that published study, presented here in Run 2, Chapter 4, each had five anatomical parts. H*ydraulic-jump unit bars* also formed in Runs 3 and 4 and the ones in Run 4 had another anatomical part. In this way *hydraulic-jump unit bars* can be not fully developed with respect to anatomical parts: The use of the phrase *fully developed* by Macdonald *et al*. (2009) is not the most suitable. More suitably, a *fully developed hydraulic-jump unit bar* is redefined as having the six-component streamwise anatomy illustrated in Figure 5.16: by inference, *partially developed* is not containing the full six parts of the streamwise anatomy. The *hydraulic-jump unit bar* in its formative stages may be described as *incipient* or a *proto-unit bar*.

5.4.2 Requirements for the six elements of a hydraulic-jump unit bar to form

Whilst mounds and foresets were features of all eight *hydraulic-jump unit bars* that formed in Runs 2 – 4, none of the *hydraulic-jump unit bars* contained all the six-element anatomy depicted in Fig. 5.16. The most complete architectures developed in Run 2, which had (I) sufficiently wide bulk load grain size distribution and (II) suitable flow pattern, for grain segregation to occur. The steep upstream termination of each Run 2 mound was associated with a small region of flow in which grain segregation could occur (§4.5.2). The small region gradually diminished in size as the upstream termination of the *hydraulic-jump unit bar* became shallower. Elements (1) and (3), intimately linked in Run 2 and reliant on grains segregating by size, were both absent in Runs 3 and 4. The same small region would not have occurred in Run 3 because of the non-cylindrical shape of the mound. In Run 4 the microclimate may well have formed because the steepness of the upstream termination of the only mound to form was within the range that the microclimate formed within in Run 2. However, the finer grained and better sorted bulk load in Run 4 compared to Runs 2 and 3 resulted in the upstream face of the *hydraulic-jump unit bars* being smoother. Despite the greater availability of fine bedload to be blocked at the leading edge of the Run 4 mound, compared to the Run 2 mound, the smoother upstream face may have precluded the bedload from stalling.

5.4.3 Upstream migration of the hydraulic jump

Equivalent sediment mass-inputs in Runs 2 – 4 resulted in non-equivalent deposit volumes because of differences in grain shape and grain sorting by the flow. The Run 4 deposit was the biggest and contained the roundest grains. The Run 2 *hydraulic-jump unit bars*, with greater sediment sorting than the Run 3 *hydraulic-jump unit bars* formed a deposit slightly smaller in volume than formed in Run 3. The constancy of the rate of upstream motion of the hydraulic jump, in each run involving sediment, was related to the constancy of the volume rate of deposition downstream of the hydraulic jump (Fig. 5.4).

The magnitude of the rate of migration of the hydraulic jump was influenced by the deposit shapes. Although the shape of each deposit varied in a constant way as it formed (repeated bar formations in Run 2 and 3 and constant growth of the Run 4 bar), the shapes were different between runs: Deposit shape affected the particular constant rate of the motion of the hydraulic jump in Runs 2 – 4.

Considering the following thought experiment the differences in deposit shapes, volumes of flow over the deposits and other more minor factors influence the motion of the hydraulic jumps in different ways: Consider a hydraulic jump and a solid, impermeable cuboid block. In 2d view let the block have sides with relative length = 2 and width = 1 and let the hydraulic jump have h_2 = 2.5 (Fig. 5.22A). If the block is positioned downstream of the hydraulic jump, firstly with long side facing upstream, the hydraulic jump moves upstream (Fig. 5.22B). If it is secondly replaced with long side pointing upwards, one can imagine that the hydraulic jump will move to a more upstream position upon replacement: Although the volume of displaced water is conserved from the first state to the second, the actual change in orientation of the block causes (1) an abrupt decrease in h over the obstacle and the "backing up" of water upstream of it (Fig. 5.22C). (2) An increased volume of stagnant flow immediately upstream of the block when in the second orientation compared to the first. Being isolated from the free stream, the stagnant water effectively adds to the deposit volume.

In experimental Runs 3 and 4, flow thickness above the deposit decreased over time towards thickness of the supercritical flow, being 2.2 times h_1 at the end of the run; (1) was approached. In all runs involving sediment, (2) was satisfied in the isolated flow separation downstream of the avalanche foreset. In Run 2 there was a further small region of slow flow

immediately upstream of the deposit in which the upstream-dipping laminaset (architectural Element 1, Fig. 5.16) formed and this volume decreased over time (§4.5.2).
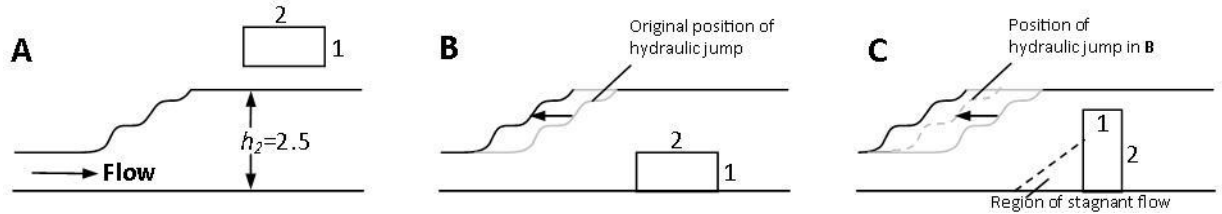
Figure 5.22 Three stages of a thought experiment depicted as line drawings. (A) Initially a hydraulic jump has a stationary mean position and height $h_2 = 2.5$. A block also exists and has sides with relative length of 2 and 1. (B) The block is placed downstream of the hydraulic jump, the hydraulic jump moves upstream and establishes a new mean streamwise position. (C) The block is replaced with long side pointing upwards and the hydraulic jump again moves upstream, establishing a new mean streamwise position. A volume of stagnant water concurrently forms upstream of the block and water backs up upstream of the block because of the abrupt decrease in flow thickness above the block.

5.4.4 Upstream migration of the pattern of sediment transport

Flow conditions associated with repeated hydraulic-jump unit bar formation

In Run 2 the toe of the hydraulic jump, the upstream limit of the deposit and the whole sediment transport pattern within the hydraulic jump moved upstream in tandem (Fig. 5.4). Sand fell from the flow to the flume floor under *jet up* conditions and was pushed to a mound further downstream in *jet down* conditions; mounds formed and *hydraulic-jump unit bars* developed from them. This sequence repeated until pumping was stopped. The same repeated formation of *hydraulic-jump unit bars* was not seen in Run 3 or 4. This can be explained by three factors.

Factor (I) the jet within the hydraulic jump ceasing to oscillate, both vertically and with respect to the length of the track of the jet. This change is associated with the change from oscillating jump to weak jump, cf. Massey's (1983) classification. Whilst $\dfrac{\partial \bar{u}}{\partial z}$ at the lower jet edge decreased during the transition to weak jump, the lower edge of the jet became very close to the sediment surface, promoting bedload transport. Because the jet within the weak jump diffused gradually downstream, sediment accumulated over a longer streamwise distance. In conditions of a weak jump, a second foreset formed in Run 3 but not Run 4.

187

Factor (II) shear stress and bedload transport rate increasing as h decreases above *hydraulic-jump unit bars*. As shear stress increased, flow conditions would approach being nett non-depositional or even erosional: the *hydraulic-jump unit bar* can be said to be "depth-limited" because in this state of flow it would not grow vertically. Depth limited bars are described by Carling (1990) and Davies (1987). Carling (1990) found that the uppermost bar crest of an upwards sequence of developing bars, flattened with decreasing h and this was also the case in the current runs, as the sand surface approached the water surface.

A hydraulic jump deposit grows, so long as bedload and suspended load flux to it is greater than bedload flux away from it. Even where sediment flux to a hydraulic jump is near-constant (cf. Runs $2-4$, Chapters $4-5$), bedload flux away from the deposit is controlled by the pattern of shear stress immediately above the deposit. The deposit will stop growing once a critical shear stress is reached; at which sediment flux away from the deposit equals sediment flux to it.

Factor (III) the non-cylindrical pattern of flow separation associated with the semi-elipsoidal Run 3 mound.

Changes in the pattern of suspended sediment over time

The pattern of suspended sediment would have varied with the flow and deposit and although no measurements of suspended sediment were made, the pattern of suspended sediment concentration is derived from simple physical reasoning. In the supercritical flow, C was nearly constant through time as it was controlled by the sediment supply and pumping conditions until the foreset(s) reached the downstream limit of the test channel. When the deposit reached the downstream limit of the test channel and bedload fell into the discharge tank, sediment recirculated with the water and C within the supercritical flow rose.

While the suspended sediment front passed downstream through the test channel in the first circulation of flow through the flume, just after $t = 0$, C had approximately the same value between the upstream limit of the test channel and the suspended sediment front. Further downstream than the suspended sediment front, $C = 0$. As soon as the suspended sediment front reached the hydraulic jump, sand fell from suspension due to the decreased competence in conveying the suspended material compared to the supercritical flow. The value of C decreased slightly through the hydraulic jump and tailwater (red line, Fig. 5.23A). Sediment

that fell to the flume floor directly underneath the hydraulic jump and was pushed downstream as bedload, added to the deposit whence it was permanently removed from suspension: In consequence of the deposit having formed, C within the hydraulic jump decreased (compare red lines between Fig. 5.23A – C). Because h decreased and u increased over time, above the sediment deposit, the competence of flow above the deposit increased (compare red lines, Fig. 5.23B – C); as h decreased towards the magnitudes of h_1, the competence of the flow over the deposit approached that within the supercritical flow. With no nett erosion, C remained constant over the deposit (red line, Fig. 5.23C). Later in time in the frame of reference moving upstream with the hydraulic jump, the pattern of C remained constant (compare red and blue lines, Fig. 5.23C).
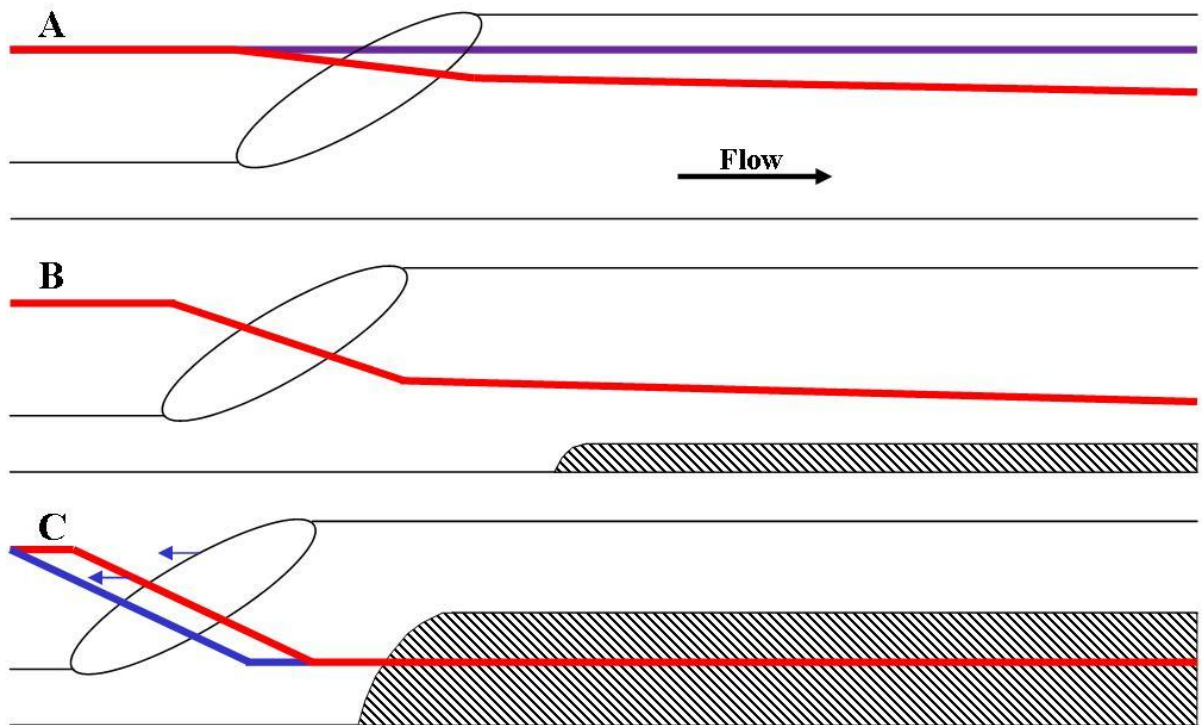
Figure 5.23 Sketches of the variation in suspended sand concentration, C (coloured lines), overlying sketches of the hydraulic jump and sand deposit. The variation is drawn relative to the positions and length scales of the hydraulic jump and the sand deposit. (A) The first circulation of sediment. The purple line denotes C of the downstream limit of the suspended sediment during the first recirculation of the sediment (first few seconds of a run). The red line denotes C after the first recirculation and before the deposit formed (first few tens of seconds of a run). (B) The early stages of formation of the sand deposit. The deposits received sediment fallen from suspension within the hydraulic jump that passed downstream as bedload. (C) Later stages of formation of the sand deposit. Note the decrease in h towards h_1 as the deposit grew between (B) and (C) and the gradient of C decreasing to 0. The blue line denotes the change in the pattern of C at an arbitrary later time compared to the red line; the line moved upstream in a simple way with the hydraulic jump (blue arrows).

5.4.5 General architectural differences with the *hydraulic-jump bar complex*

The pattern of laminae

As in Run 2, the Runs 3 and 4 deposit architectures were not similar in appearance to backset beds. Instead the deposits had two cosets of laminae; shallow upstream dipping laminae in a more upstream part and downstream dipping in a more downstream part. In contrast to Run 2, both of the Run 3 cosets involved only two sets and Run 4 only one set. The only ratios of anatomical dimensions that could be determined were within Run 4: [mound : foreset] being [1 : > 2.5] in the streamwise dimension and [1 : > 1.25] in the height dimension. These aspect ratios are lower than those of the *hydraulic-jump unit bars* that terminated within the test channel during Run 2 (§4.5.3); in reality the foreset could be very much bigger given more downstream space in which to prograde.

Trends in grain size in the deposits of Runs 3 and 4

Because no upstream dipping laminae formed (they had formed due to a hydraulic mechanism of grain size segregation in Run 2, §4.7), grain size patterns were different to the Run 2 deposit.The three foresets that formed in Runs 3 and 4 all coarsened downstream (Figs. 5.10 and 5.21). The downstream-coarsening would have been affected by *C* declining with distance downstream of the hydraulic jump. Because the foresets received continuously less sediment directly from suspension (the finer part of the bulk load distribution) as they prograded downstream, the grain size distribution of the exposed part of the foreset became less fine over time: the foresets coarsened downstream.

   The 3d shape of the mounds of sediment could not be seen through the flume sidewall as the mounds formed, but indications of their 3d shapes can be derived from the lamination patterns in cut sections and the pattern of D_{50} within the foresets (Figs 5.9 and 5.20). The Run 4 foreset changed little in D_{50} across-stream at all streamwise positions and so the *hydraulic-jump unit bar* was likely to be cylindrical since its inception. At the upstream limit of the Run 3 foreset, the juxtaposition of sediment finer than the bulk load around $y = 0.5$ m, sediment coarser than the bulk load close to the sidewall 0.3 m downstream (Features A and B, Fig. 5.9B; §5.3.5) and the curvature of the contours of sediment size in between indicates that the *hydraulic-jump unit bar* was not cylindrical when Features A and B formed. Instead bedload

initially mounded at the channel centre and the semi-ellipsoidal mound grew laterally as well as upstream and downstream; the mound appearing to have low amplitude at the flume sidewall was a consequence of this lateral growth.

5.4.6 Bed feature development in the region downstream of the hydraulic jumps

Was Run 3 Bed 3 a low amplitude hydraulic-jump unit bar?

According to the bedform stability field plot of Southard and Boguchwal (1990), flow downstream of the hydraulic jump did not enter the upper stage plane bed (USPB) field. According to others it did in both Run 3 and Run 4, but did not in Run 2. The possibility for Foreset 3 being a step discontinuity in Topset 2 instead of part of a partially developed *hydraulic-jump unit bar* would have required conditions below USPB during its continuous progradation. Whether the inception of Foreset 3 was from a mound or a discontinuity is discussed below.

Because the inception of Foreset 3 was not seen, it could have been preceded by a mound or a negative step. Now, Allen and Leeder (1980) showed that sufficient turbulent damping by a bedload layer prevents the progradation of a defect such as a shallow negative step. If formed from a negative step, for the thin avalanche foreset to have prograded several metres downstream, it is required that the layer of active bedload transport be thin compared with the step. Now, Hill (1966) suggested that a transition to upper stage plane bed conditions can occur when bedload transport becomes sufficient that the thickness of the bedload layer is not limited by the size of the grains being transported: The theoretical evidence of Hill (1966) indicates that USPB conditions were not reached if the foreset formed from a discontinuity not a mound.

USPB flow conditions would have been approached when Foreset 2 reached the downstream limit of the test channel and the volume of recirculated bedload increased. It would have also been approached as the thickness of the layer of bedload being actively transported thinned and in consequence $\frac{\partial \bar{u}}{\partial z}$ increasing close to the deposit surface. Both of these made the transition to USPB conditions (conceptually) increasingly possible, but no test is available.

Vortical motion, flow separation and the Run 4 ripples

The vortices seen within a lee separation zone were one visible component of the increasing unsteadiness as the lee face of the *hydraulic-jump unit bar* grew in height. The upper height limit of the motion of the Run 4 vortices as they passed to downstream (§5.4.4) suggests that they were trapped within the separated flow in the lee of the foreset and affected movement of the bedload. The inception of vortices downstream of a *hydraulic-jump unit bar* was associated with the sharpest brink, and in consequence of that fact, the highest levels of flow separation downstream of any of the brinks observed.

The change of shape from asymmetrical to symmetrical ripples was coincident with flow becoming increasingly complicated. Symmetry of ripples is known to require two or more flow tracks in opposing directions. The upstream part of the flow circulation within the separated flow downstream of the lee face was one permanent flow track directly involved with the sediment surface of the *basal wedge*. The track of the irregular stream of vortices incepted near the *hydraulic-jump unit bar* brink was in the opposite direction. In the early stages of *hydraulic-jump unit bar* formation, vortices were few and the ripples on the *basal wedge* were asymmetrical. The change to symmetrical ripples was associated with increasing rate of vortices forming and passing along the track. By the end of Run 4 the ripples migrated downstream because the stream of vortices mildly dominated the upstream flow. Given more time and a longer channel in which to form, ripple migration may have formed cross sets.

Two minutes of foreset development without topset development, Run 4.

The pattern of shear stress varied in time because of deposit formation, and at any time shear stress varied in space above the deposit. The topsets formed whilst depth-averaged shear stress increased (it must have done as flow thinned) and the brief non-deposition of topset(between $t = 21 - 23$ minutes in Run 3 (§5.4.2)) is inferred to be a local transition from shear decreasing to increasing. Rewriting Davies's (1982) equation for shear stress over the upper surface of a sediment bed feature in the form

$$\frac{\tau}{\rho} = g\bar{h}S + Q^2\frac{\theta}{h_b^2} \qquad (5.1)$$

temporal changes in shear stress imparted on the Runs 3 and 4 deposit surfaces can be considered.Throughout Runs 3 and 4 the constant g was 37 times bigger than the constant Q^2

when considering SI units. Hence changes in $\bar{h}S$ (term 1) had an order of magnitude bigger effect on the value of τ than changes in $\dfrac{\theta}{h_b^2}$ (term 2).

Early in Run 4, $\dfrac{\theta}{h_b^2} \sim 4\bar{h}S$. After the foreset formed and was prograding downstream, $\dfrac{\theta}{h_b^2}$ increased but $\bar{h}S$ decreased with the nett result of τ decreasing. As h decreased over the deposit and the water surface slope followed the upper surface of the deposit, $\bar{h}S$ became constant and $\dfrac{\theta}{h_b^2}$ continued to increase with the nett result of τ increasing: a transition from shear stress decreasing to increasing. Because Fr increased above the deposit as h decreased, given a longer run duration it is likely that the flow over the deposit would revert to supercritical and a new hydraulic jump develop downstream of the deposit, triggering a variation on chute and pool structure formation (§1.7; further discussion on the variation in §6.2.4).

5.5 CONCLUSIONS

1. Two regimes of sediment input to a hydraulic jump, each with one difference from the Run 2 sediment input, resulted in sediment deposition with patterns of lamination similar to each other but distinctly different from the *hydraulic-jump bar complex*. In Run 3 sediment was input at a greater rate. The resultant deposit was a complex of two *hydraulic-jump unit bars*, the upper one being low amplitude. In Run 4 finer sediment was input at the same rate and one *hydraulic-jump unit bar* formed.

2. Two important changes occurred in the character of the flow because the sediment deposit grew. (1) The Froude number of the supercritical flow decreased over time and the hydraulic jump changed from the classification of 'oscillating jump' to 'weak jump'. In association the oscillation of the submerged jet is inferred to have ceased and the pattern of deposition changed dramatically compared to that in Run 2. (2) A horizontal gradient of hydrostatic pressure is always present in a hydraulic jump (from low to high pressure from upstream to downstream). Because the flow became thinner

over the deposit over time, a gradient in pressure developed, from higher pressure at the downstream limit of the hydraulic jump to lower pressure above the deposit further downstream.

3. The earliest part of formation of each *hydraulic-jump unit bar* was sediment mounding on flume floor or sediment surface, within the tailwater. In Run 3, sediment initially mounded around $y = 0.5$ m, grew downstream and laterally. Once the mound grew to the same width as the flume sidewalls the feature only grew downstream. In Run 4 sediment mounded across the full width of the flume test channel as soon as mounding started. The Run 4 mound was cylindrical and much bigger than the Run 2 mound, associated with the jet becoming indistinct well upstream of the downstream limit of the roller.

4. When fully formed *hydraulic-jump unit bars* have at least a six component anatomy. (1) Set of upstream dipping laminae that is finer than the input sediment; (2) mound of sediment containing few or no bedding structures in streamwise view; (3) avalanche foreset coarser than the input sediment; (4) avalanche foreset similar in grain size to the input sediment; (5) topset overlying Elements (1) – (4); (6) bottomset underlying Element (4). Elements (2), (4) and (5) were present in all *hydraulic-jump unit bars* that formed in Runs 2 – 4.

5. Elements (1) and (3) are intimately linked, requiring segregation of fine grains upstream of the deposit from coarser grains of the bedload that pass over the deposit. Their formation is sensitive to sediment initially accumulating in steep mounds, a function of bedload transport rate and also requiring an abrupt transition from jet flow conditions to non-jet flow conditions within the tailwater. Their formation is also sensitive to the grain size pattern on the upstream limit of the mound; finer mounds being smoother and precluding bedload stalling.

6. The upstream growth of the sand deposit depends only on the water and sand fluxes that enter the hydraulic jump.

6. Discussion: Can hydraulic jump deposits be recognised in the rock record?

6.1 INTRODUCTION

Chapters 3 – 5 report sediment transport patterns and sediment accumulation patterns associated with hydraulic jumps in flume experiments. The architectures of the deposits involved patterns of lamination and grain size segregation that could be seen in field exposures. Here I discuss what makes these deposits distinctive. Aware of the lack of accommodation space for sediment deposition in the flume, I first discuss the potential characters of deposition in infinite time and streamwise space (§6.2). Second I reproduce the grain size and lamination patterns of *hydraulic-jump bar complexes* alongside grain size and lamination patterns of bedforms and barforms formed in other settings. Discussing their similarities and differences I propose diagnostic characteristics of *hydraulic-jump unit bars* and *bar complexes* on the basis of the laboratory examples (§6.3). Third I comment on interpreting the dimensions, original position and lifetime of the hydraulic jump that formed the hydraulic jump deposits and how this interpretation could be advanced by future work (§6.4). Fourth, I present outcrop photographs of an inferred proglacial delta and ground penetrating radar data from jökulhlaup deposits that are candidates for *hydraulic-jump unit bars* and *bar complexes* (§6.5 – 6.6). Fifth I use my experience of field data to comment on whether the depositional patterns found in the flume experiments can be identified in field exposures where the architectural element is partially exposed (§6.7). The discussion in Sections 6.2 – 6.8 leads to statements on how best to recognise *hydraulic-jump unit bars*, *hydraulic-jump bar complexes* and *basal wedges* in field exposures. Sixth I discuss environments in which *hydraulic-jump unit bars* are likely to be preserved (§6.8). Finally I draw conclusions about the recognisability of hydraulic jump deposits in field exposures at the current state of knowledge (§6.9 and §6.10).

6.2 THOUGHT EXPERIMENT: ARCHITECTURAL COMPLEXES IN INFINITE TIME AND SPACE

Some fully preserved hydraulic jump deposits in the rock record will look almost the same as the laboratory examples, indeed one rock record example presented in Section 6.5 has a striking resemblance to the Run 2 deposit (reported in Chapter 4). The appearance of other fully preserved hydraulic jump deposits in the rock record will differ from the laboratory examples because sediment transport to a hydraulic jump can persist for longer than 45 or 75 minutes (the durations of Runs 2 – 4) and the position of hydraulic jumps can vary with flow conditions (§1.4.3 and §1.6.1). Still other fully preserved hydraulic jump deposits will differ from the laboratory examples because (1) hydraulic jumps in rivers do not end in discharge tanks so the downstream end of deposits will be different, (2) hydraulic jumps can have more space to move upstream into so deposits can be longer and (3) some other open channels are deeper so deposits can be thicker. Some hydraulic jump deposits will not be fully preserved because they are truncated by erosion. The potential character and recognisability of truncated hydraulic jump deposits is considered in Section 6.7.

With few hydraulic jump deposits observed in modern environments (§1.6) I undertook two thought experiments to consider how the laboratory examples would have developed in infinite time and space. In Thought Experiment 1, below, the deposit grows because of suspended load fallout only. In Thought Experiment 2 there is suspended load-bedload segregation in the hydraulic jump and the deposit grows because of bedload transport and suspended load fallout, which happened in Runs 2 – 4 (Chapters 4 and 5).

6.2.1 Experimental setup

In both thought experiments the channel has unit width so that the results could be scaled by *Fr*. In both thought experiments the channel had rectangular cross section and non-erodible boundaries. The supercritical flow, hydraulic jump and tailwater were cylindrical and the channel floor was flat. The channel was infinitely long, and sufficiently deep to contain the flow and the deposits. The concentration of suspended sediment in the supercritical flow was constant so that the sediment pattern developed because of the hydraulic jump only. The volume of bedload transported in the supercritical flow was much less than the bedload segregated from the suspended load within the hydraulic jump.

6.2.2 Thought Experiment 1: suspended load fallout

Suspended sediment would enter the hydraulic jump by travelling downstream from the supercritical flow and some would fall from suspension in the tailwater (as in Runs 2 – 4). The fallen sediment would aggrade. The time rate of suspended sediment fallout would increase from the toe of the hydraulic jump downstream because sediment takes time (and therefore distance) to fall to the floor, because hydraulic jumps are abrupt transitions from thin fast flow to deep slow flow (§1.4.1) and because turbulence dramatically decreases downstream of the toe (§4.2.3). This contributes to the downstream-thickening shape of the *basal wedge* (Fig. 6.1A). Because the suspended sediment concentration decreases downstream of the toe of the hydraulic jump, theoretically there is necessarily a position at which the suspended sediment fallout rate would decrease downstream. (This position was downstream of the test channel in Runs 2 – 4.) In consequence the bed would thin from this position downstream; it would have a peak and would not be wedge shaped (Fig. 6.1A). However, the suspension fallout deposit was wedge shaped in Runs 2 – 4, in the length-limited flume. In this thesis I continue with the term *basal wedge* because no data are recorded to describe its full shape.

As the bed of sediment fallen from suspension thickens, initially its shape would remain approximately similar, with a peak at the same streamwise location (compare Fig. 6.1A and B). In association with the bed thickening, the hydraulic jump would move upstream in gradual adjustment to the tailwater surface elevation increasing. Because suspended sediment fallout in the tailwater is constant the upstream motion of the hydraulic jump would be constant too. Consequently the upstream motion of the pattern of sediment fallout would be constant and the upstream face of the bed would move upstream at a constant rate. The length and angle of dip of the upstream face would remain approximately constant over time (compare Fig. 6.1B and C). An upper surface of the deposit would develop upstream from the peak because the pattern of suspension fallout would spend a finite amount of time at any streamwise location; i.e. at any streamwise location the deposit would have a maximum, finite thickness (compare Fig. 6.1B and C). Infinite upstream motion of the hydraulic jump would result in a basal unit with upstream dipping upstream face, a near-infinitely long upper face with the same inclination as the channel floor, and a downstream dipping downstream face (Fig. 6.1D).
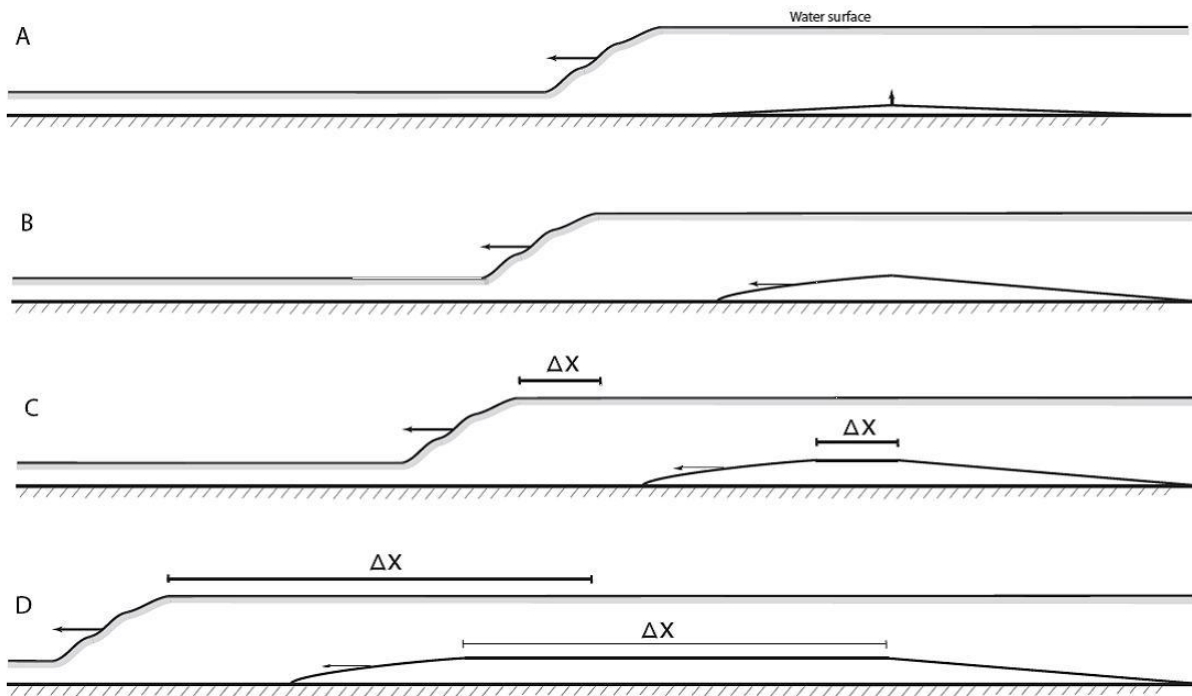
Figure 6.1 The development of the sediment accumulation pattern downstream of a hydraulic jump, where some of the suspended sediment falls to the channel floor in the tailwater and is not reworked when on the floor, depicted in stream parallel section. The channel has unit width, rectangular cross section and non-erodible boundaries and is deep enough to contain the flow and the sediment deposit. The hydraulic jump is cylindrical and a cylindrical deposit forms. (A) Initially the deposit develops in a wedge shape, with a peak, on the channel floor, downstream of the hydraulic jump. The wedge of sediment is asymmetrical about the peak (skewed to upstream). The downstream-thickening part of the wedge forms because sediment fallout rate increases from upstream to downstream above it. The downstream-thinning part occurs because the concentration of suspended sediment (available to fall out) decreases from the toe of the hydraulic jump downstream. (B) As the deposit grows the wedge grows. The hydraulic jump moves gradually upstream in response to the tailwater rising. (C) Because the sediment transport pattern moves upstream with the hydraulic jump the upstream limit of the wedge moves upstream too. With continued upstream motion of the hydraulic jump, the sediment fallout pattern spends a finite amount of time at any streamwise location. At any streamwise location the deposit would have a maximum, finite thickness and an upper surface develops on the wedge. (D) The upper surface of the wedge gets longer over time but the deposit gets no thicker.

6.2.3 Thought Experiment 2: bedload-suspended load segregation in the hydraulic jump

Suspended sediment would enter the hydraulic jump by travelling downstream. As in Runs 2 – 4, and potentially as in many river settings, some suspended sediment falls to the channel floor in the hydraulic jump and is mobilised as bedload. Some suspended sediment falls to the channel floor in the tailwater, and is not mobilised, cf. Runs 2 and 3. Two beds form simultaneously, a *basal wedge* of suspended sediment fallout and a *hydraulic-jump unit bar* that progressively overrides it (Fig. 6.2A).

198

At its most incipient the *hydraulic-jump unit bar* is too small to affect the suspended sediment fallout pattern and the *basal wedge* develops a peaked shape (Fig. 6.2A; cf. Thought Experiment 1). As the deposit grows, the hydraulic jump moves gradually upstream and the pattern of sediment transport moves upstream with it. Unlike Thought Experiment 1, the upper surface of the *basal wedge* would be short because the *hydraulic-jump unit bar* would override it (Fig. 6.2B). Because the *basal wedge* is overridden, suspended sediment falls onto the upstream end of it at a low rate for a short time and onto the downstream end of it at a higher rate for a longer time. In this way the upstream face of the wedge became steeper than it would have if a bedload feature had not progressively overridden it. The magnitude of downstream thickening of a *basal wedge* of a hydraulic jump deposit is a function of (1) the spatial pattern of suspension fallout and (2) the time taken for the *hydraulic-jump unit bar* to override the *basal wedge*. At least two possible architectures can develop. In the case that one *hydraulic-jump unit bar* forms above the *basal wedge* (cf. Run 4; Chapter 5), the *hydraulic-jump unit bar* will become very long over time (Fig. 6.2C). As it does the topset thickens and both the thickenss and length of the deposit have a maximum discussed below. In the case that new *hydraulic-jump unit bars* periodically form above and upstream of the previous one (cf. Runs 2 and 3; Chapters 4 and 5), the *hydraulic-jump bar complex* will consist of increasing numbers of *hydraulic-jump unit bars* over time (Fig. 6.2D).

Shear stress at the deposit surface increases as the deposit grows because tailwater thins, and the shear stress conditions at the deposit surface vary with position and track length of the jet within the hydraulic jump (§5.5.3). The hydraulic jump deposit reaches limiting thickness when shear stress conditions at the deposit surface cause sediment flux away from the deposit to equal the sediment flux to the deposit. The limiting deposit thickness is constrained by the initial tailwater depth. Less intuitively, the length of hydraulic jump deposits is also constrained by the initial tailwater depth. Flow would accelerate down the downstream-dipping downstream face of the deposit and flow would be erosional there because shear stress conditions would be higher. In this way the length of the deposit is limited. The flow down the downstream-dipping downstream face is likely to accelerate to supercritical (as did flow over the downstream half of the hemisphere described in Section 3.4). Downstream of the supercritical flow a second hydraulic jump would form in the flow and a second deposit would form (Fig. 6.2E). The two hydraulic jump deposits would be
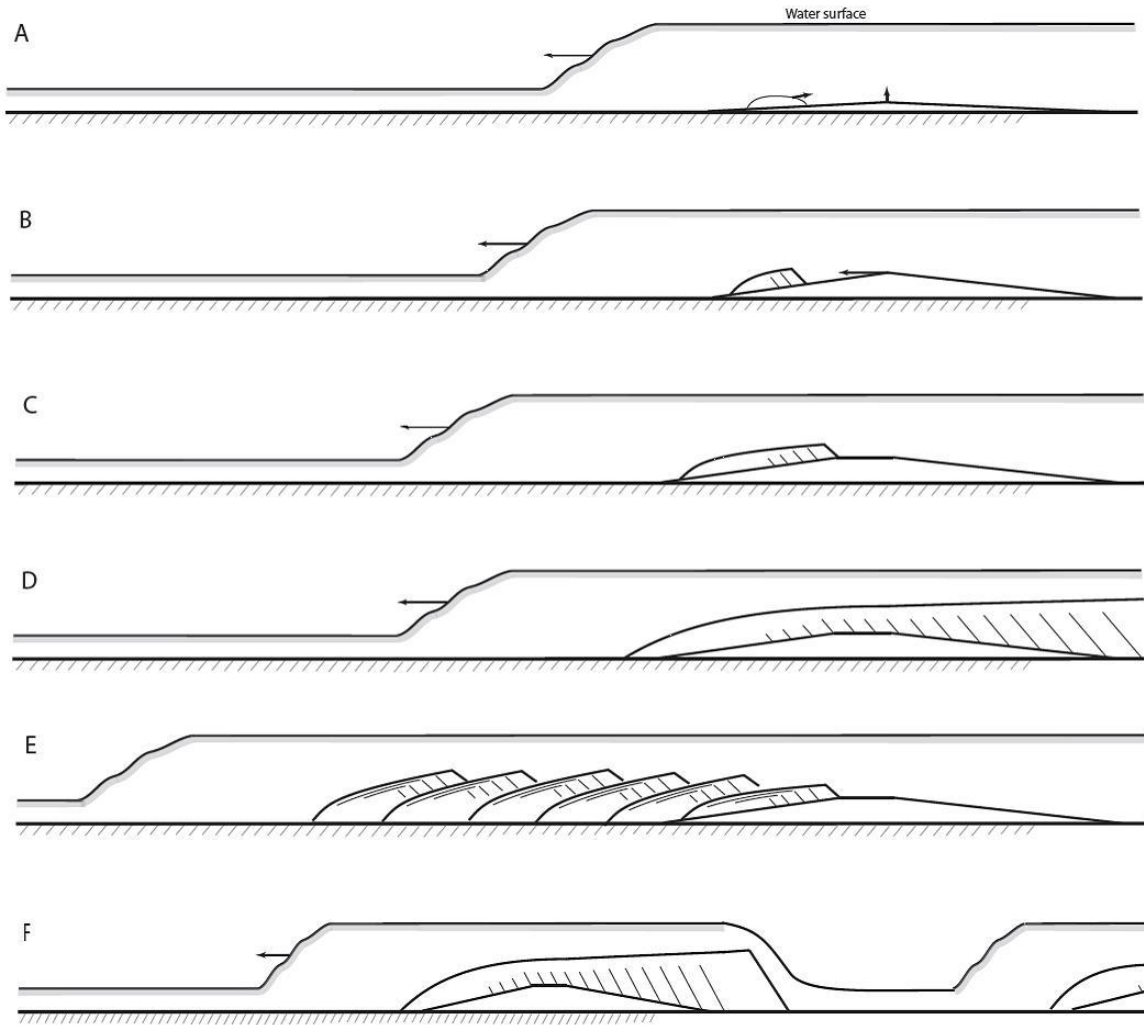
Figure 6.2 Sediment accumulation patterns downstream of a hydraulic jump, where some of the suspended sediment becomes bedload during passage through the hydraulic jump, depicted in stream parallel section. The channel has unit width, rectangular cross section, non-erodible boundaries and is deep enough to contain the flow and the deposit. The hydraulic jump is cylindrical and a cylindrical deposit forms. (A) Initially two beds form; a wedge shaped bed of sediment fallen from suspension and a bedload feature upstream of it (an incipient *hydraulic-jump unit bar*). (B) The wedge thickens over time. The incipient *hydraulic-jump unit bar* grows, also developing a brink and an avalanche face, whence it is no longer incipient. The *hydraulic-jump unit bar* illustrated does not have a set of upstream-dipping laminae at its upstream end (cf. the *hydraulic-jump unit bar* that formed in Run 4, Chapter 5). The hydraulic jump moves gradually upstream in response to deposit growth. (C) Because it moves upstream an upper surface forms on the wedge (cf. Fig. 6.1), and this gradually lengthens until the *hydraulic-jump unit bar* overrides it. (D) As time progresses, one possible development is for the *hydraulic-jump unit bar* to become very long, and the topset thick. (E) In the other possibility the upstream motion of the hydraulic jump results in repeated formation of *hydraulic-jump unit bars*, each upstream of the last. Six are shown but any number could develop until a limiting thickness is reached. (F) Whether stage (C) develops to stage (D) or stage (E), the deposit grows faster vertically than the tailwater rises. A limiting thickness is reached, where bedload transport from the upper surface of the deposit equals sediment arriving at the top of the deposit (by suspension fallout and bedload transport). Flow may become supercritical when passing over the deposit or as it accelerates down the downstream face. Flow would remain supercritical for a short distance downstream, a second hydraulic jump would form and with it a second hydraulic jump deposit. Although only two hydraulic jumps and hydraulic jump deposits are depicted, a train of them could form in this way.

separated by a streamwise distance equal to the length of supercritical flow over the non-eroding channel floor, plus the length of the second hydraulic jump. So long as the second hydraulic jump exists and forms a deposit, a third hydraulic jump and hydraulic jump deposit can form in this way. Eventually a streamwise sequence of *hydraulic-jump unit bars* or *bar complexes* could form. The formation of this train of bed features is a variation on chute and pool structure formation (Alexander *et al.*, 2001).

6.2.4 Discussion of the variation on chute and pool structure formation

As in cyclic steps the streamwise extent of individual regions of deposition is controlled by the position of the next downstream site of erosion. In cyclic steps this site may or may not involve flow becoming supercritical over a downstream-dipping downstream edge of a step. Deposit wavelength may increase with flow depth or grain size, in the non-cohesive range, up to the limiting thickness (§6.2.3). Deposit wavelength may also increase with the duration of sediment aggradation, until the limiting thickness is reached. Cyclic steps have a characteristic wave length 100-500 times the flow thickness (Taki & Parker, 2005), an aspect ratio that makes them particularly difficult to reproduce in flumes at scales that will generate significant deposits. The depositional units of hydraulic jump deposits were too long to determine their aspect ratio but much smaller hydraulic jumps could be devised in longer flumes and it might be possible to determine aspect ratios of hydraulic jump deposits in the future.

6.3 INTERPRETING *HYDRAULIC-JUMP UNIT BARS* AND *BAR COMPLEXES* FROM THEIR SEDIMENTARY STRUCTURES

The deposits that formed in Runs 2 – 4 (Chapters 4 – 5) were the direct result of the hydraulic jumps, which were on non-erodible floors in subaerial open channels. Taking the *basal wedge*, *hydraulic-jump unit bars* and *bar complexes* that formed (Chapters 4 and 5), and treating the flow that formed them as unknown (as if a geologist were looking at outcrop) it is possible to use the sedimentary structure of the deposits to infer that a hydraulic jump was present during their formation. If a fully developed *hydraulic-jump unit bar* is recognised, it should be interpreted that a hydraulic jump caused it, because it has an anatomy without counterpart in bedforms and other barforms (*fully developed* defined in §5.5.1). In particular it is unusual for

the complete topset, foreset and bottomset of any bedform or unit bar to be preserved (Alexander *pers*. *comm.*) It is also unusual for grain size to be segregated by finer grains accumulating at the upstream end of a bar and coarser grains accumulating at the downstream end of a bar. Together these characteristics of fully preserved, fully developed *hydraulic-jump unit bars* can be used as diagnostic criteria for beds associated with hydraulic jumps.

Test 1: Do *Beds X - Xn* have the anatomy of fully developed *hydraulic-jump unit bars*?

Outcomes: If they do, they were lain down in association with a hydraulic jump. If they do not, further tests are required.

Truncated fully developed *hydraulic-jump unit bars*, discussed in Section 6.7, are unlikely to satisfy Test 1. Other characteristics of sedimentary structure can be used to interpret a hydraulic jump deposit, where fully developed *hydraulic-jump unit bars* are not formed.

6.3.1 Interpreting *hydraulic-jump unit bars* from their juxtaposition with a *basal wedge*
The juxtaposition of mound overlying the most upstream part of the *basal wedge*, and foreset downstream of the mound is a criterion for interpreting a hydraulic jump deposit. The juxtaposition occurs in hydraulic jump deposits but is unlikely to form in other deposits. In some other settings suspended sediment may fall out at high rates downstream of prograding foresets but the juxtaposition is different. One example is a dune in shallow water. Saunderson and Lockett (1983) describe shallow flow at the dune to upper stage plane bed transition (their Fig. 3) and the wedge of suspended sediment fallout over which the dune migrates, thins downstream. Another example is a transverse bar (Fig. 6.3A), where flow can be thin over its upper surface and abruptly thicken downstream of it causing rapid suspended load fallout (Fig. 6.3B). Because the bedload feature forms first to create the abrupt flow thickening and rapid suspension fallout downstream of it, the upstream limit of the cross set is upstream of the upstream limit of the suspension fallout deposit (Fig. 6.3C). If a fine substrate, already present before the bedload feature forms, is not eroded by the flow that forms the bedload feature, it is
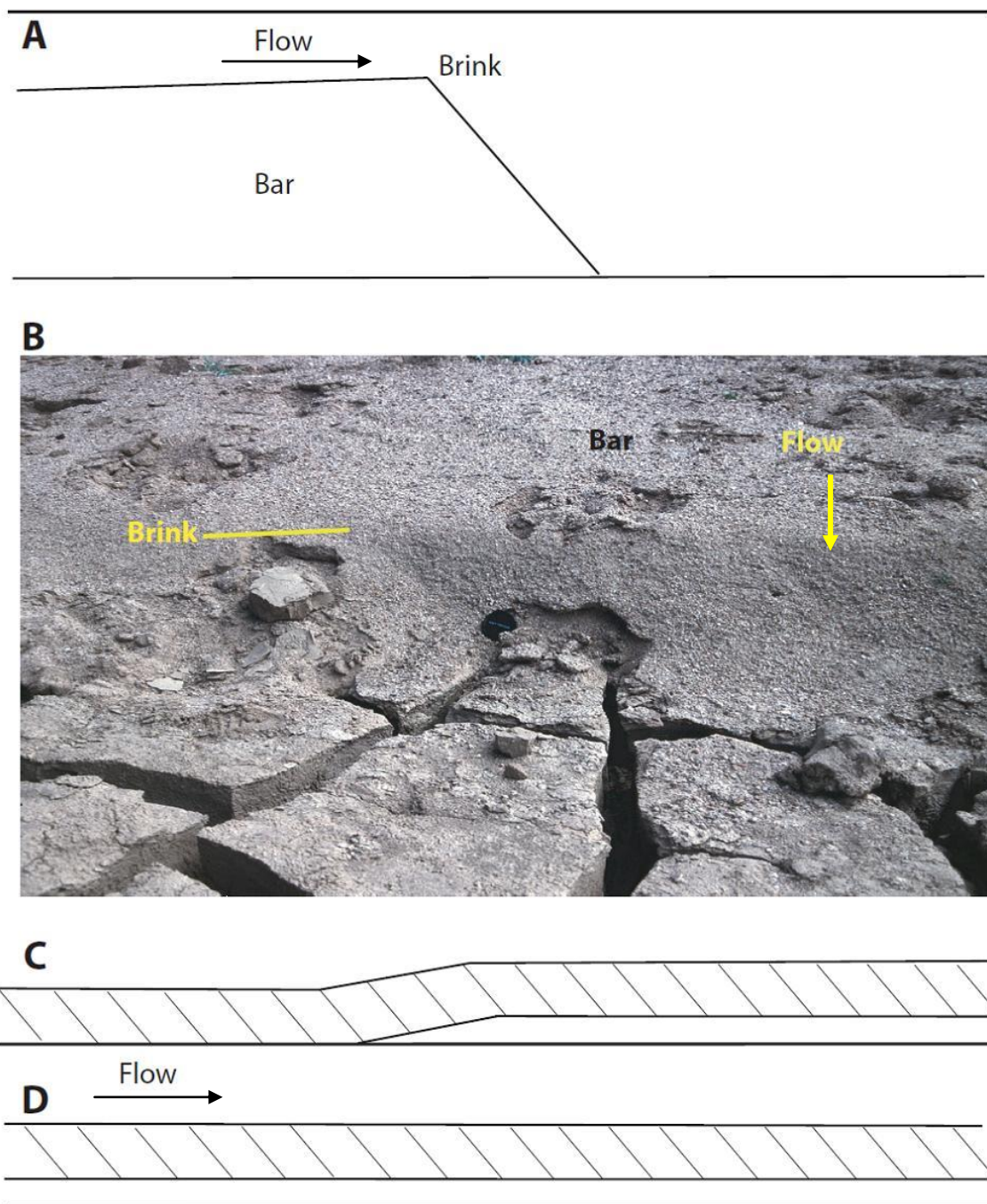
Figure 6.3 (A) The downstream end of a bedload feature with thick foreset compared to the thickness of flow above the feature. Suspended sediment preferentially falls out in the thicker flow downstream of the foreset compared to the thinner flow above the foreset, leading to two discrete beds. The suspended load bed formed second because the conditions for its formation were caused by the development of the bedload feature. (B) A transverse bar; an example of a bedload feature that had a thick foreset compared to flow thickness above the foreset. The process described in (A) occurred in this situation. (C) In the sedimentary structure that results from process (A) a basal unit of sediment fallen from suspension is overlain by a foreset of a bedload feature. The upstream limit of the foreset is upstream of the basal unit. (D) In the situation that a pre-existing fine substrate is overridden by a foreset that progrades over it, the base of the foreset is approximately parallel to the foreset.

unlikely to be wedge shaped. It may also have a recognisable contact with the suspension fallout deposit formed downstream of the bedload feature (Fig. 6.3D).

Test 2: Is the candidate *hydraulic-jump unit bar* directly above a downstream-thickening wedge, with the upstream limit of the unit bar a short distance downstream of the upstream limit of the wedge?

Outcomes: If it is, it was lain down in association with a hydraulic jump. If not it is not a hydraulic jump deposit.

The juxtaposition of *basal wedge* and *hydraulic-jump unit bar* suggests that both formed together. Had the *basal wedge* formed first, with no bedload transport, it would likely have been washed away by a subsequent flow event, unless it had been cemented or lithified. Whilst the magnitude of downstream thickening of the *basal wedge* did not vary with bedload transport pattern (being one unit thicker for every ten units further downstream in each of Runs 2 – 4), in the absence of bedload transport the magnitude would be lower (§6.2.2).

6.3.2 Interpreting *hydraulic-jump unit bars* without *basal wedges*

In the case where bedload is transported to a hydraulic jump, but there is no suspended load, no *basal wedge* would form. In other cases *basal wedges* may form but not be detected. For instance I detected two candidate *hydraulic-jump unit bars* in GPR data published by Cassidy *et al*. (2003, reported in Section 6.6) but the GPR did not penetrate down as far as where the *basal wedge* would be. In still other situations *hydraulic-jump unit bars* may be exposed but the *basal wedge* could be covered e.g. by scree or a retaining wall, so it cannot be seen. In these situations of partial exposure, partially developed *hydraulic-jump unit bars* have characteristics with counterparts in bedforms and other barforms. (1) *Hydraulic-jump unit bars* can be on the order of metres long but have no bedforms on their upper surface. (2) They have a downstream dipping cross set at their downstream end, which thickens all the way from the upstream limit to the downstream limit, unless they are partially eroded. (3) Given sufficient time and bedload transport, single *hydraulic-jump unit bars* (not in a complex) are very long compared to their height. (4) Topsets are preserved with the foresets. Whilst each

characteristic (1) – (4) has a counterpart in other bedforms or other barforms, the complete set of attributes has no obvious counterpart.

Test 3: Does *Bed X* have attributes (1) – (4) above?

Outcomes: If it does, it was lain down in association with a hydraulic jump. If it does not it is likely to be the signature of a bedform or another form of unit bar.

6.3.3 Interpreting *hydraulic-jump bar complexes*

If several beds in an upward sequence have the anatomy of a fully developed *hydraulic-jump unit bar*, Test 1 should be used to interpret that each bed was formed by a hydraulic jump and the architectural element is a *hydraulic-jump bar complex*. If several overlying beds have an anatomy that could be a partially developed *hydraulic-jump unit bar*, Test 3 should be called on first when interpreting whether or not it is a *hydraulic-jump bar complex*. However in a *hydraulic-jump bar complex* the foresets are unlikely to be very long compared to how thick they are (attribute 3, §6.3.2) because of the way new *hydraulic-jump unit bars* periodically appear and older *hydraulic-jump unit bars* become inactive during the formation of the complex.

From the limited data generated to date the attributes common to *hydraulic-jump bar complexes* are: (1) *hydraulic-jump unit bars* are the only barforms present in the bar complex and counter flow ripple cross lamination may be present. (2) Each *hydraulic-jump unit bar* has an upstream limit upstream of the *hydraulic-jump unit bar* below. (3) The upper surfaces of *hydraulic-jump unit bars* in the bar complex dip upstream and each one has a shallower gradient than the one below. These three attributes can also be true of climbing dune cross bedding or climbing ripple cross lamination within the upstream half of bars where dunes or ripples climb up the face of the bar (Villard & Church, 2005; Rice & Church, 2010). Unlike climbing cross bedding, *hydraulic-jump bar complexes* have the attributes that (4) topsets formed with each foreset and were at least as thick as the foreset they were associated with. (5) *hydraulic-jump unit bar* stacking patterns do not involve erosional contacts. It is common for dune cross bedding stacking patterns to involve complicated cross cutting relationships because of the scour in the dune lee (Leclair *et al.*, 1997; Leclair & Bridge, 2001). Because (4)

and (5) occur together in hydraulic jump deposits but not in other bar forms, all five attributes above can be used to interpret *hydraulic-jump bar complexes*.

Test 4: Do *Beds X - Xn* have attributes (1) – (5) above?

Outcomes: If they do, they are a *hydraulic-jump bar complex* and each bed was lain down in association with a hydraulic jump. If they do not they are not a *hydraulic-jump bar complex.*

6.4 INTERPRETING DETAILS OF THE FLOW FROM THE STRUCTURES OF *HYDRAULIC-JUMP UNIT BARS* AND *BAR COMPLEXES*

When an observer knows that they are looking at a hydraulic jump deposit, one at least of Tests 1 – 4 will be satisfied by the pattern of lamination. From some hydraulic jump deposits it should be possible to interpret details of the hydraulic jump and sediment transport pattern that formed it. The thickness of the tailwater can be assessed by the considerations of limiting thickness presented in Section 6.2. Other interpretations could be made; the ideas below derive from my work and could be assessed with further quantitative work, on a larger matrix of experimental runs.

6.4.1 Interpreting the transient character of the hydraulic jump

In a *hydraulic-jump bar complex*, the position of the mounds (anatomical part 2, Fig. 5.15) indicates the position of the incipient *hydraulic-jump unit bars*. The sequence of streamwise position of mounds in overlying beds indicates the streamwise movement of the hydraulic jump, caused by a combination of the deposit growth and changes in *Fr* of the hydraulic jump. An empirical relationship between (1) and (2) could be derived with a greater matrix of runs.

6.4.2 Interpreting the duration of deposition associated with a hydraulic jump

In the laboratory examples the foresets always formed within minutes of sand arriving at the hydraulic jump. Either one or two foresets prograded concurrently. Where a single *hydraulic-jump unit bar* forms, the length of the resulting cross bed indicates a combination of (1) the

length of time the hydraulic jump was active and (2) the sediment flux to the foreset. An empirical relationship between (1) and (2) could be derived with a greater matrix of runs. Such a relationship would be useful in interpreting modern or historical deposits where either (1) or (2) are recorded. Where a *hydraulic-jump bar complex* forms it is the total length of all downstream-dipping cross sets in the complex that indicates the combination of (1) and (2). In the ancient rock record neither can be assessed.

6.4.3 Interpreting flow and sediment transport conditions in the absence of a topset

The absence of a topset in a *hydraulic-jump unit bar* with no erosional upper surface (cf. the trial runs, §2.9) results from grains not stalling on the *hydraulic-jump unit bar* top as they travel downstream to the foreset. In the case of a small hydraulic jump this will be because flow was depth limited at the time the foreset formed. In other situations it may occur because all grains have sufficient momentum as they pass over the upper surface and the upper surface was sufficiently smooth (functions of grain size, shape and density).

If a sharp contact is recognisable between the upstream and downstream limits of a *hydraulic-jump unit bar* with no topset, it is likely that no topset formed. If the sharp contact extends upstream or downstream of the *hydraulic-jump unit bar*, it is likely that the topset was eroded. In this way it can be determined whether or not a topset formed. Where no topset formed, experiments presented in this thesis indicate that grain size distributions with significant quartz gravel fractions can have sufficient momentum to travel over the hydraulic jump deposit. Where the grain size distribution of the *hydraulic-jump unit bar* is finer than gravel, and no topset forms, flow was probably depth limited when the foreset formed.

6.5 STRONG CANDIDATES FOR A *HYDRAULIC-JUMP BAR COMPLEX* AND A *BASAL WEDGE*: PROGLACIAL DELTA DEPOSITS OF GLACIAL LAKE WESER, GERMANY

6.5.1 The geological setting

A candidate *hydraulic-jump bar complex* and *basal wedge* have been recognised in the bottomset deposits of the early Saalian age Emme coarse grained delta complex, which was

deposited in glacial Lake Weser (Winsemann *et al.*, 2010). In the early Saalian the Emme delta was at the southern margin of the Scandanavian ice shield (Winsemann *et al.*, 2004) at the mouth of an incised valley (Winsemann *et al.*, 2010). The delta complex is about 2 km long (north to south), 1.5 km wide and 70 m thick. The candidate *hydraulic-jump bar complex* and *basal wedge* were exposed in a quarry in the delta bottomset (Fig. 6.4A). The exposure was more than 60 m long and 5 m high and was oriented NNW to SSE. Palaeoflows in the delta complex were generally towards the southwest or south confirmed by foresets dipping towards SSE in the candidate beds. For greater detail and maps see the papers of Winsemann *et al*. (2004; 2010) and Hornung *et al*. (2007).

Modern physiographic setting

Until approximately one year ago the delta complex was exposed in Fell Pit, which is no longer quarried and has been filled in. I planned to study the exposure, to make field comparison with the flume results, but the exposure was buried before that was possible. The photographs in Fig. 6.4, taken by Prof. Winsemann before the pit was refilled, show lamina sets clearly. These photographs are provided in pdf form in Appendix 2 so it is possible to zoom in and view the deposits in greater detail.

Figure 6.4 (below) (A) Bottomset deposits of the Emme coarse grained delta complex, overlain by a steeply westward dipping foreset. Photograph taken by Jutta Winsemann in Fell Pit (now filled in). Photograph is reproduced in Appendix 2 in electronic form. The box indicates the position of photograph (B). Paleo flow was towards the southwest and south (right hand side of the photograph). There is a lateral facies transition from planar and trough cross-stratified sand and pebbly sand into trough-cross ripple-laminated sand and very thin- to thin-bedded sand, silt and clay alternations. (B) Close up of part of the delta bottomset deposits. Bed 1 is interpreted to be a *basal wedge* and Beds 2 – 6 a *hydraulic-jump bar complex* (complex of five overlying *hydraulic-jump unit bars*). Beds 2 – 6 formed downstream of the mouth of an incised valley during the Saalian period (Winsemann, *pers. comm.*) The associated line drawing is an interpretation of bed contacts and the general pattern of lamination, based on the photograph of the exposure.

Bed III

Bed II

Bed I

Bed VI Bed V

Bed IV

A

B

B

1 m
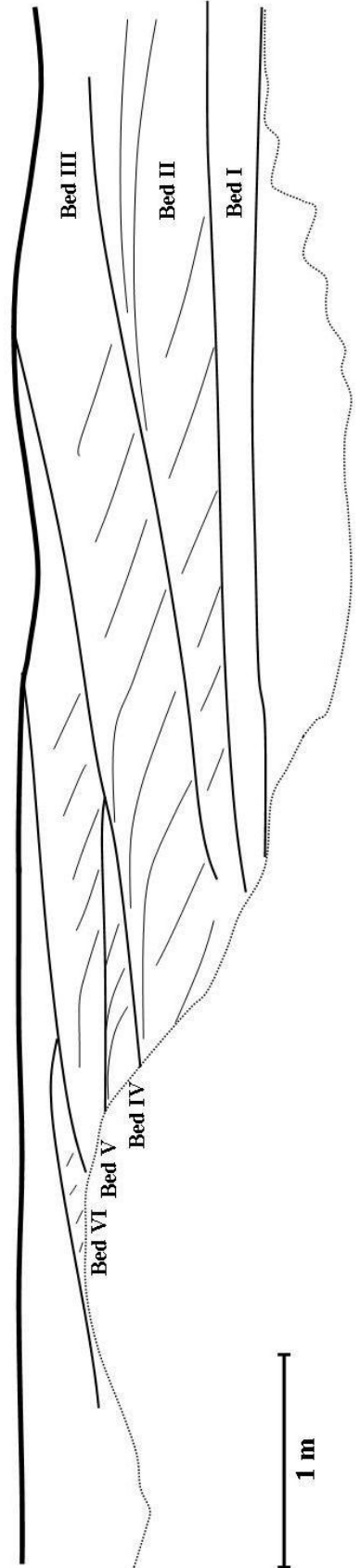
6.5.2 Attributes of the lamina sets

Attributes of the lamina sets in the candidate architectural elements

A sequence of six discrete beds within the exposure, is a candidate for a *basal wedge* (Bed I, Fig. 6.4B) and *hydraulic-jump bar complex* (Beds II – VI, Fig. 6.4A). Bed I, the lowermost in the sequence, was a downstream-thickening wedge of sand that was generally massive (Fig. 6.4B) but contained occasional slip faces (Winsemann, *pers*. *comm*.) Its upstream limit was obscured by a cover of talus (Fig. 6.4A). It was 0.3 m thick immediately downstream of the talus. It gradually thickened downstream, to 0.6 m thick 9 m downstream of the talus and pinched out 20 m downstream of the talus. Beds II – VI overlay Bed I (Fig. 6.4). Each dipped upstream and in an upward sequence the angle was shallower. Beds II – VI thinned upwards and had a downstream termination above the most upstream 0.9 m of Bed I. Generally in an upward sequence each successive downstream termination was further upstream than the last and the downstream termination was steep. The exception was Bed IV, which pinched out downstream further upstream than Bed V. Further downstream than Bed IV, Bed V directly overlay Bed III. The upstream terminations of Beds II – V were obscured by talus. Bed V was above the talus. It pinched out upstream, upstream of the talus.

The downstream part of Beds II - VI was a 3 m thick coset of five climbing foresets (Fig. 6.4). Each climbing foreset in the coset was 0.10 – 0.54 m thick and thinned upwards within that range. Each climbing foreset contained pebbly sand and medium- to coarse-grained sand and each foreset fined upwards within that range of grain size (Winsemann, *pers*. *comm*.) Each foreset had an associated topset and no associated bottomset. Each topset was approximately one third as thick as the foreset it was associated with. The laminae within the topsets were thin, slightly convex up to planar and could be traced on photographs for at least several decimetres in the streamwise direction (Fig. 6.4, Appendix 2; maybe a lot further if the exposure were still available to study directly). Laminae could be traced between the topset and some foresets on photographs; typically in the more upstream part of each set. The upstream limit of the foresets could be seen in Beds II and VI but was covered by the talus in Beds III, IV and V (Fig. 6.4). In Bed II the foresets passed upstream into a small region of massive sand that was obscured at its upstream end by the talus cover. Unfortunately Bed VI is too thin and out of focus in the photograph to detect what the foresets passed upstream into.

Attributes of the lamina sets surrounding the candidate architectural elements

The candidate *basal wedge* (Bed I) was underlain by 1 m thick thin- to medium- bedded sand (Fig. 6.4B). Because the thin- to medium-bedded sand was obscured both upstream and downstream by talus, the exposed part of it was shorter in the streamwise direction than Bed I.

In the paleo streamwise direction the coset of climbing foresets of the candidate *hydraulic-jump bar complex* passed into trough-cross ripple-laminated sand about 5 m long (Fig. 6.4). Further downstream this passed into very thin- to thin-bedded (2-10 cm) alternations of massive or planar parallel-laminated clay and planar-parallel or climbing-ripple cross-laminated silt and fine- to medium grained sand (Winsemann *pers. comm*). Soft sediment deformation structures were common. The topset of the Bed VI had a sharp contact with a 1.5 – 2 m thick cross set above it. Laminae in this cross set dipped in the opposite direction to the foresets in Bed VI. They contained a much wider grain size distribution than Bed VI and the rest of the candidate *hydraulic-jump bar complex* and the grains were generally darker. Unfortunately there was no opportunity to clean the talus and observe what the candidate *hydraulic-jump bar complex* passed upstream into and there is no photograph of what was upstream of the talus.

6.5.3 Testing the exposure for the presence of hydraulic jumps

The architecture of Beds I – VI look very similar to the architecture of a *basal wedge* and complex of five *hydraulic-jump unit bars* that formed in Run 2. To systematically interpret whether this is a *basal wedge* and *hydraulic-jump bar complex* I employ Tests 1 – 4 (§6.3).

Outcome of Test 1: Because the talus cover obscured the upstream parts of four candidate *hydraulic-jump unit bars* and the fifth candidate *hydraulic-jump unit bar* was small and out of focus in photographs, it was not possible to see if they were fully developed or not (fully developed defined in §5.5.1). Because the foresets of Bed 1 fined downstream and had an association with mounded sediment upstream of it, one may guess from the experience of Run 2 that Bed II at least was a fully developed *hydraulic-jump unit bar*. Beds II – VI could be a complex of partially developed *hydraulic-jump unit bars* but because no bed had the anatomy of a fully developed *hydraulic-jump unit bar* it is not possible to say from this test that a hydraulic jump was definitely involved in deposition.

Outcome of Test 2: The small mound of massive sand in Bed II does directly overly a downstream thickening wedge of almost structureless sand and does have a downstream-thickening downstream-dipping cross set immediately downstream of it. In consequence Bed II is almost certainly a *hydraulic-jump unit bar* and Bed I a *basal wedge*, both formed in association with hydraulic jumps.

Outcome of Test 3: Because all five candidate *hydraulic-jump unit bars* have the attributes listed in Test 3, those five beds were lain down in association with a hydraulic jump. Specifically each candidate is metres long, has no bedforms on its upper surface, has a downstream dipping cross set at their downstream end that thickens all the way from the upstream limit to the downstream limit, unless they are partially eroded and topsets are preserved with the foresets.

Outcome of Test 4: Because the candidate *hydraulic-jump bar complex* has the attributes listed in Test 4, they were lain down in association with a hydraulic jump. Specifically, the complex contains *hydraulic-jump unit bars* but no other bedforms or bar forms; each *hydraulic-jump unit bar* has an upstream limit upstream of the *hydraulic-jump unit bar* below; the upper surfaces of the *hydraulic-jump unit bars* dip upstream and each one has a shallower gradient than the one below; topsets formed with each foreset and were one third as thick as the foreset they were associated with; no erosional contacts can be detected in the *hydraulic-jump unit bar* stacking pattern.

Conclusions from Tests 1 – 4: Following Tests 1 – 4, and from experience of the flume deposits, I conclude that Bed I is a *basal wedge* formed by a hydraulic jump and Beds II – VI make up a *hydraulic-jump bar complex*. This is the first field example of a *hydraulic-jump bar complex* known. If this identification is correct it confirms that *hydraulic-jump bar complexes* can form in proglacial flows, can form up to several metres thick and can contain at least five *hydraulic-jump unit bars*. *Hydraulic-jump bar complexes* and *basal wedges* can be directly observed from a sufficiently good exposure without requiring grain size data or other analysis.

6.6 TWO STRONG CANDIDATES FOR *HYDRAULIC-JUMP UNIT BARS*: ICE-WALLED CANYON OF THE GIGJUKVISL CHANNEL, SKEIDARARSANDUR, ICELAND

6.6.1 History of the formation of the candidate *hydraulic-jump unit bars*

Skeiðarársandur is a modern and active proglacial outwash plain, more than 1000 km^2 in area. The deposits containing the candidate architectural elements are associated with the Gígjukvísl channel at the northern end of Skeiðarársandur, at the southern margin of the Vatnajökul ice cap (Cassidy *et al.*, 2003). The 1996 jökulhlaup scoured both an ice-walled canyon more than 500 m long and a double embayment at the head of the canyon (Cassidy *et al.*, 2003). Deposition occurred in the englacial channel, ice-walled canyon and proglacial outwash fan. Since the 1996 jökulhlaup, the ice margin has retreated and some of the sediment in the englacial channel can be seen as an esker (Burke *et al.*, 2008). Burke *et al.* (*loc. cit.*) reported the esker to be more than 700 m long and less than 30 m high with maximum width of 40 m. The esker was supported by underlying ice.

No exposures of the 1996 jökulhlaup deposit were available between 1996 – 2010 (A.J. Russell, *pers. comm.*) but I studied its architecture from ground penetrating radar (GPR) data reported by Cassidy *et al.* (2003) and Burke *et al.* (2008). The two architectural elements that are candidates for *hydraulic-jump unit bars* can be seen in strong reflection data from the ice-walled canyon (Fig. 6.5). The first candidate (Bed I) is upstream of the second (Bed II) and their combined streamwise length spans most of the ice-walled canyon. I detected no candidate architectural elements in Burke *et al*'s (2008) GPR data of the esker or Cassidy *et al's* (2003) GPR data of the outwash fan, but from these data I detected inflow conditions to, and outflow conditions from, the two candidates.

The 1996 jökulhlaup flowed out of an englacial fracture and shallow supercritical flows and hydraulic jumps were seen in the ice-walled canyon in its waning stages (Cassidy *et al.*, 2003). Hydraulic jumps may also have occurred in rising stages but most of the jökulhlaup was not seen due to inaccessibility or darkness (Cassidy *et al.*, *loc. cit.*). Flows through the ice-walled canyon had high sediment concentrations, which led to overcapacity of suspended sediment. Abrupt flow expansion between the ice-walled canyon and proximal fan was associated with rapid transfer of sediment from suspended load to bedload. In the distal fan

flow became supercritical when passing over or around stationary bed attached ice blocks, which were up to 45 m in diameter.

6.6.2 Attributes and interpretations of reflector data from the esker

Burke *et al*. (2008) undertook a GPR survey across almost all of the esker surface, in a grid with 5 m spacing (total line length of 3.8 km). The radar penetrated a maximum of 15 m and the depth at which reflections could be resolved was limited by underlying ice at most plan locations. My identification of lamina sets and interpretation of flow conditions in the jökulhlaup derive from the pattern of reflections in published analogue data (Burke *et al's* 2008 Figs 7 – 14). Patterns of GPR reflections in the esker are best seen in the online publication of Burke *et al*. (2008) because it allows profiles to be enlarged with no degradation of image quality.

Undular reflections at the base of the esker represent antidune deposits (Burke *et al*., *loc*. *cit*.; my own interpretation), which would have been lain down in flow of *Fr* > 0.84 according to Southard and Boguchwal (1990), and could have been lain down in supercritical conditions. To my eye most reflections above the antidunes were horizontal or parallel to the upper surface of the underlying ice and can be traced for many metres in the streamwise direction. These represent a pattern of laminae, lain down either under upper stage plane bed flow conditions or flow in antidune-forming conditions but with the antidunes suppressed by shear stress, sediment flux to the channel floor or limited vertical space. Flow could have become supercritical by becoming thinner, as the englacial channel filled with sediment.

Figure 6.5 (below) Ground penetrating radar data from jokulhlaup deposits within the ice walled canyon and proglacial outwash fan, Gigjukvisl channel, Skeiðarársandur, Iceland, reproduced from Cassidy *et al*. (2003, their Fig. 4). The four parts are a continuous survey line. The upflow limit of the transect ($s_t = 0$ m) was approximately 100 m downflow of the upflow limit of the ice walled canyon. My facies interpretations are depicted alongside. (A) One candidate *hydraulic-jump unit bar* was present between $80 \leq s_t \leq 410$ m. A second candidate *hydraulic-jump unit bar* has upstream limit at $s_t = 430$ m and extends into section B. (B) The downstream limit of the second candidate *hydraulic-jump unit bar* is at $s_t = 620$ m and the downstream limit of the ice walled canyon is at $s_t = 650$ m. Stoss side deposits of upstream migrating subcritical antidunes are interpreted immediately downstream of the second candidate *hydraulic-jump unit bar*. Cassidy *et al*. recognized occasional kettle scours up to 40 m long in the streamwise direction, which they interpreted to be associated with short stretches of supercritical flow around bed attached ice blocks. (C) The proglacial fan mainly contained sets of downstream dipping reflections and sets of horizontal reflections, which had abrupt contacts and complicated juxtaposition. In general there were more horizontal reflections below 7 m depth. (D) Similar to (C) and additionally one set of steeply upstream dipping reflections occurrs around $s_t = 1660$ m.

Depth estimate (m) based on uniform velocity of 0.07 m ns⁻¹
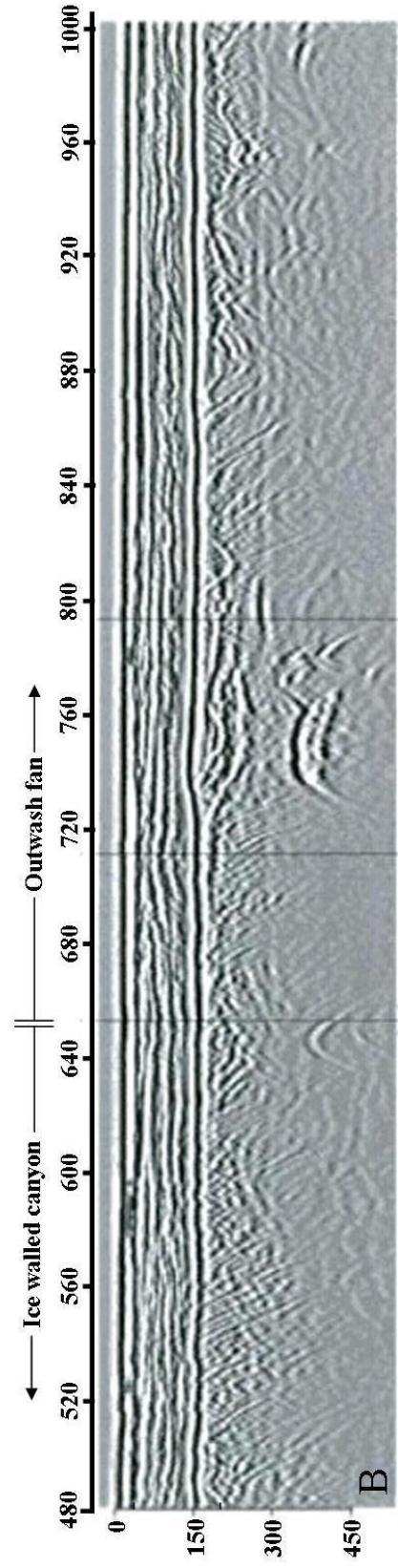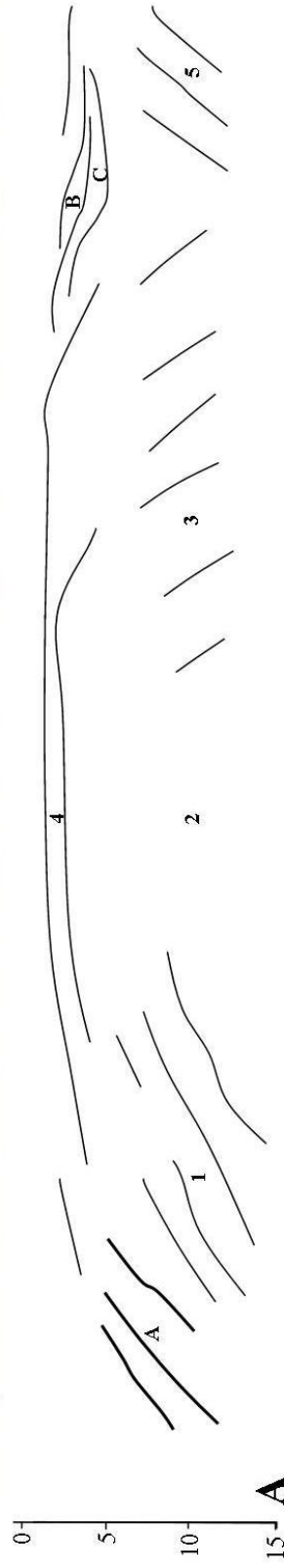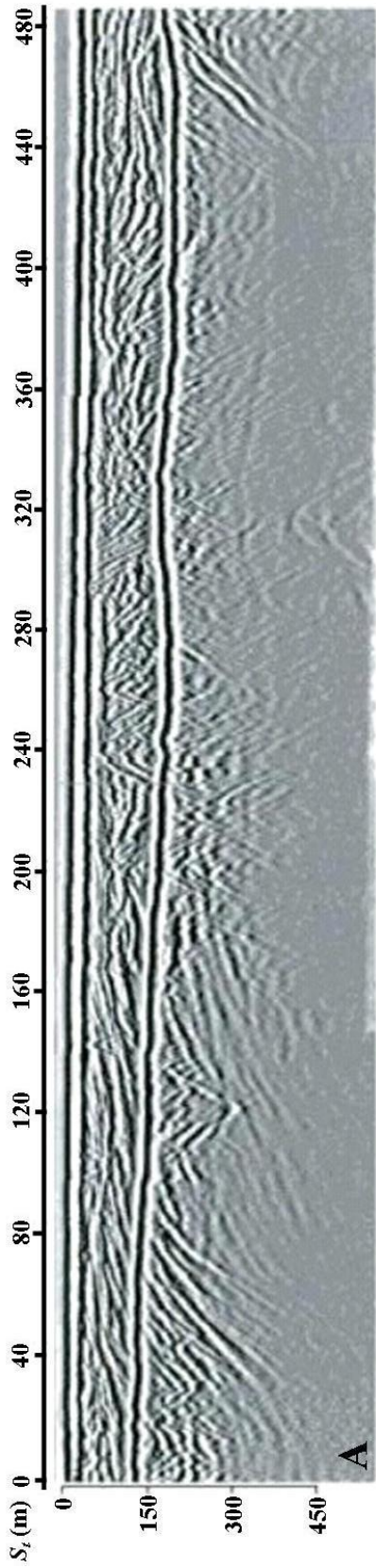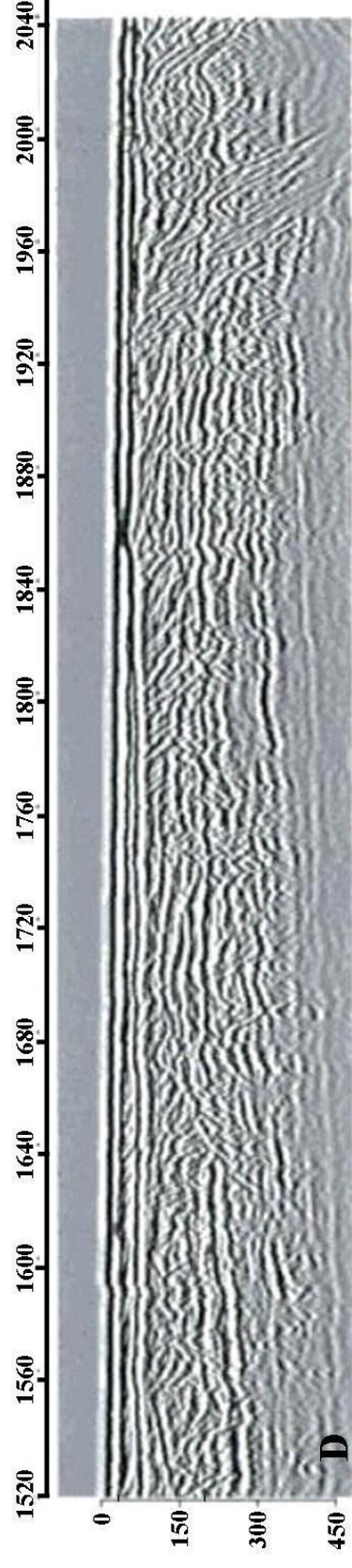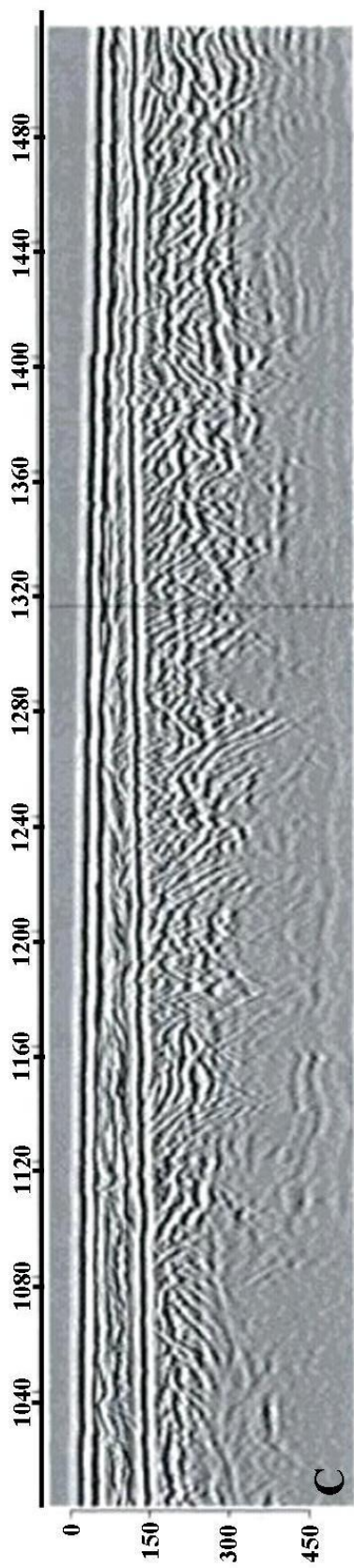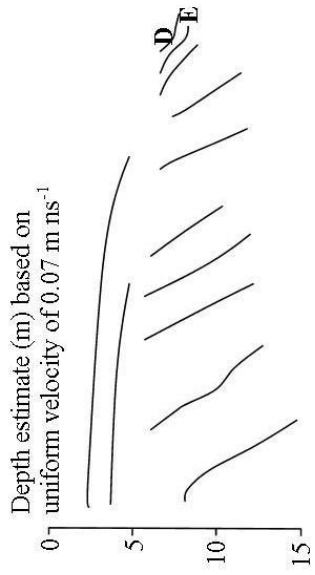
Two way travel time (ns)

6.6.3 Attributes and interpretations of reflector data from the ice-walled canyon

The lamina sets within two candidate hydraulic-jump unit bars

Two beds in the jökulhlaup deposit in the ice-walled canyon are, I think, *hydraulic-jump unit bars*; each associated with one hydraulic jump. These two beds are identified from Cassidy *et al's* (2003) GPR data along the jöhulhlaup flow path. The survey line started at a position about 100 m downstream of the upstream limit of the ice-walled canyon and finished at the downstream limit of the outwash fan, 2 km away (see Cassidy *et al.*, 2003, Fig. 2). I define the distance along-transect, s_t to have the value 0 at the upstream limit of the transect and s_t increasing along transect (up to $s_t = 2000$ km).

I interpret one *hydraulic-jump unit bar*, Bed I, from GPR data between $80 \leq s_t \leq 410$ m (Fig. 6.5A). It was close to the upstream end of the ice-walled canyon. It has an abrupt upstream termination, a 260 m long slightly convex up upper surface and an abrupt downstream termination. Passing from upstream to downstream it contained (1) a 100 m long set of reflections that dipped upstream in the range m, $8 - 13°$, (2) a 50 m long set of convex up reflections each ~ 15 m long and (3) a 180 m long set of steeply downstream dipping reflections (Fig. 6.5A). Above sets (1) – (3) is (4) a set of slightly upstream dipping slightly convex up reflections that could be traced for up to 80 m in the streamwise direction. At the downstream end of the candidate *hydraulic-jump unit bar*, (4) was obscured by convex up reflections that I interpret to represent boulders ($235 \leq s_t \leq 265$ m, Fig. 6.5 panel A). Set (4) varies between $0 - 4$ m thick (based on average velocity of 0.07 m ns^{-1} for the two way travel time of the radar signal, cf. Cassidy *et al.*, 2003) and sets (1) – (3) were at least 10 m thick but the bottom of all these sets of reflectors is not resolvable because signal strength decreased with depth. It is not possible to determine reflectors below sets (1) – (3); no candidate *basal wedge* is identified. Neither is it possible to determine whether the lower boundary is parallel to the ground surface.

A second candidate *hydraulic-jump unit bar*, Bed II is represented in the survey line between $430 \leq s_t \leq 620$ m (Fig. 6.5, candidate crosses panels A and B). It was close to the downstream end of the ice-walled canyon, which was at s_t ~ 650 m. The pattern of reflectors looks like the pattern of reflectors in Bed I. Specifically there is a set of gently upstream dipping reflections that is 40 m long (compare set 5 with set 1, Bed I). There is a coset of

convex up reflections that is 20 m long (set 6, Fig. 6.5). There is a set of steeply downstream dipping reflections that is 130 m long (set 7). There is a 5 m thick set of slightly undular reflections (set 8) that is directly above sets (5) – (7). Reflectors in set 8 could be traced for up to 65 m in the streamwise direction. The upper surface of sets (5) – (7) (the contact with set 8) was obscured by the strong reflection from the water table. Sets (5) – (7) are at least 7 m thick but the lower boundary is not resolvable because of the reflected signal decreasing with depth.

The lamina sets adjacent to the candidate hydraulic-jump unit bars

Neither candidate *hydraulic-jump unit bar* was overlain by any sediment. A set of steeply upstream dipping reflections is adjacent to the upstream limit of Bed I (set A, Fig. 6.5). It is distinct from the shallow upstream dipping reflections in set (1) of Bed I because of the greater angle of dip and the greater strength of reflections. The steeply upstream dipping reflections truncate the upstream limit of the shallow upstream dipping reflections. The contact between the two may have been erosional.

Between the reflections of Beds I and II, reflections are downstream-thickening downstream-dipping (set B) with a bottomset (set C), above the water table (Fig. 6.5). Below the water table the reflections between Beds I and II were weak. Each weak reflection was either horizontal or dipped downstream at a shallow angle. Each was approximately 5 m long. The contacts between the weak reflections and both sets 3 and 5 are sharp.

Immediately downstream of Bed II, there are downstream dipping reflections immediately below the water table reflection (set D) with a bottomset (set E). The reflections are stronger than the downstream dipping reflections at the downstream end of Candidate 4 and have a sharp contact with them. I interpret that this contact is erosional, as predicted at the downstream end of *hydraulic-jump unit bars* in thought experiment 2 (§6.2.3). Above the water table reflections were generally horizontal and could be multiples of the water table reflection.

6.6.4 Attributes and interpretations of reflector data from the outwash fan

The pattern of reflections in the proglacial fan indicates that flow over it during the jökulhlaup was generally subcritical. Data from the proglacial fan ($652 \leq s_t \leq 2044$) shows sets of downstream dipping reflections and sets of horizontal reflections, which had abrupt contacts

and complicated juxtaposition (Fig. 6.5). In general there were more horizontal reflections lower in the GPR panel (below 7 m depth, Fig. 6.5). I interpret these to be suspension fallout deposits. In general there were more downstream dipping reflections higher in the GPR panel (above 7 m depth, Fig. 6.5). I interpret these to be foresets of sand sheets or dunes, both of which form under subcritical conditions (e.g. Van den Berg & Van Gelder, 1993; Carling, 1999). Additionally there were horizontal reflections several hundreds of metres long, which were multiples of the water table reflection. Finally there were steeply upstream dipping reflections around $s_t = 1060$ m like the reflections immediately downstream of Bed II (compare sets D and G, Fig. 6.5). I interpret these reflections to be laminae formed in a scour hollow around an ice block. Finally, Cassidy *et al*. (2003) saw occasional sets of reflectors (and so do I) up to 40 m long in the streamwise direction, which they interpreted to be kettle scours, associated with short stretches of supercritical flow around bed attached ice blocks. No candidate *hydraulic-jump unit bars* or parts thereof could be detected.

6.6.5 Testing for the presence of hydraulic jumps

If flow into the ice-walled canyon was supercritical (§6.6.1) and flow out of it was subcritical (§6.6.1) there must have been a hydraulic jump in it, and a hydraulic jump deposit would have formed in the sediment-charged, decelerating flow. Tests 1 – 3 devised in §6.3 are used here to determine whether Beds I and II are *hydraulic-jump unit bars*. Test 4 is for a *hydraulic-jump bar complex* but I see no candidate *hydraulic-jump bar complex* in the GPR data.

Outcome of Test 1: Neither Bed I nor Bed II were fully developed *hydraulic-jump unit bars* (fully developed defined in §5.5.1). Both beds had patterns of lamination like the *hydraulic-jump unit bars* that formed in Run 2, except that the upstream-dipping laminae at the upstream end of Bed I and Bed II were steeper. However, Test 1 does not uniquely indicate that either bed was formed by a *hydraulic-jump unit bar*.

Outcome of Test 2: Because the reflectors were not strong enough to be resolved at the depth that a *basal wedge* would have occurred, Test 2 does not indicate that either Bed I or Bed II are *hydraulic-jump unit bars*.

Outcome of Test 3: Because Beds I and II have the four attributes in Test 3, they were lain down in association with a hydraulic jump. Specifically both beds are hundreds of metres long, have no bedforms interpreted on their upper surface, have a downstream dipping cross set at their downstream end and topsets are preserved with the foresets. It was not possible to determine whether the interpreted foresets thicken all the way from their upstream limit to their downstream limit because the strength of the reflectors decreased with depth. The attributes are more obviously like *hydraulic-jump unit bars* than sand sheets.

Discussion: Because no *basal wedge* or bottomset can be detected (GPR penetration too shallow) and because no grain size data are available, Beds I and II are only moderately good as candidates for *hydraulic-jump unit bars*. I think that they are the first examples of *hydraulic-jump unit bars* interpreted from GPR data. Hence I think that hydraulic jump unit bars exist on the order of hundreds of metres long and can form in jökulhlaups.

Although the upstream-dipping laminae at the upstream end of Beds I and II were steeper than the laboratory examples, they were shallower than classical backset beds (§1.8). Both jökulhlaup flows and supercritical flows have been associated with scouring, which could "dig out" the bed upstream of the hydraulic jump deposit. Should a hydraulic jump deposit form on an upstream-dipping face of a scour, laminae could dip steeply upstream. Because the floor of the ice walled canyon was frozen it would have been slowly erodible, that could account for the degree of dip of the upstream-dipping laminae in Beds I and II. Because the motion of the hydraulic jump over time is simply related to volume rate of sediment deposition (§5.5.3), I hypothesise that the general form of the hydraulic jump deposit would be unchanged by the erosional event.

6.7 IDENTIFYING PARTIALLY EXPOSED *HYDRAULIC-JUMP UNIT BARS* AND *BAR COMPLEXES*

The first candidates for *hydraulic-jump unit bars* and *bar complexes* were well captured in an exposure and a GPR profile (§6.5 – §6.6). Because most candidate *hydraulic-jump unit bars* and *bar complexes* will be partly exposed, truncated by erosion or changed by tectonic deformation or diagenesis they will be more difficult to recognise. Thresholds for recognising

truncated hydraulic jump deposits were sought by progressively cropping diagrams of a deposit architecture, known to be a *hydraulic-jump bar complex* overlying a *basal wedge*. The deposit architecture of Run 2 (Fig. 4.13) was used as the example because it contained the most *hydraulic-jump unit bars* (five as opposed to two in Run 3 and one in Run 4).

The architecture of the Run 2 deposit was truncated at its downstream end because of the end of the test channel (Fig. 6.6A), but even treating the flow that formed it as unknown, it could be identified as being a *hydraulic-jump bar complex* overlying a *basal wedge* (§6.3). The downstream end of the Run 2 architecture was a coset of avalanche foresets overlying the *basal wedge* and if it is truncated to several metres downstream of the upstream limit of the *basal wedge*, the architecture still has the attributes of a *hydraulic-jump bar complex* (compare Fig. 6.6A and B; attributes discussed in §6.3). If the coset of avalanche foresets is truncated further, so that the *basal wedge* is tens of centimeters long (e.g. Fig. 6.6C) or is removed entirely (e.g. Fig. 6.6D), Test 2 would not be successful. If the *hydraulic-jump bar complex* is made of many overlying fully developed hydraulic jump unit bars, Test 1 could still result in an interpretation that the uppermost unit bars in the complex are *hydraulic-jump unit bars*. If the *hydraulic-jump bar complex* is made of only a few *hydraulic-jump unit bars*, Test 1 is less likely to result in their identification.

If the coset of upstream dipping laminae at the upstream end of the Run 2 deposit architecture is truncated by a small amount at the upstream end, the architecture still has the attributes of a *hydraulic-jump bar complex* (compare Fig. 6.7A and B). If it is truncated to a position between the upstream terminations of the two lowermost *hydraulic-jump unit bars* in the complex, the attributes of a *hydraulic-jump bar complex* are still retained (compare Fig. 6.7A and C). The lowermost bed is still a downstream thickening wedge of massive sand. It is still overlain by a unit bar with mounded sediment near the upstream limit of the wedge and a long foreset further downstream. A recognisable *hydraulic-jump unit bar* still overlies it (recognisable by Test 1, §6.3). If the deposit architecture is truncated further downstream than the upstream limit of the *basal wedge*, the juxtaposition of *basal wedge* and foreset is lost (e.g. Fig. 6.7D) and in consequence Test 2 would be unsuccessful. The other tests would not definitively conclude that the deposit is a hydraulic jump deposit (§6.3).

Figure 6.6 The sedimentary structure of the *basal wedge* and complex of five overlying *hydraulic-jump unit bars* that formed in Run 2, successively cropped from the right hand side of the image, to simulate erosion in the downstream part of the deposit. (A) The full complex (with no erosion). (B) The sedimentary structure is eroded to within several metres of the upstream limit of the *basal wedge*. The *basal wedge* and all five *hydraulic-jump unit bars* can still be detected. (C) The sedimentary structure is eroded to within several tens of centimetres of the upstream limit of the *basal wedge*. Because there is little of the wedge left it would be speculative to define the lowermost bed as a *basal wedge*. The juxtaposition of *hydraulic-jump unit bar* and *basal wedge* cannot be detected. Because the uppermost *hydraulic-jump unit bar* in the sequence can still be detected as being fully developed it is still possible to define a *hydraulic-jump bar complex*. (D) The sedimentary structure is eroded to further upstream than the *basal wedge*. There is much less potential to distinguish the *hydraulic-jump bar complex*.

If both cosets were truncated from above, down to the highest point of the second *hydraulic-jump unit bar* in the upward sequence, the architecture still has the attributes of a *hydraulic-jump bar complex* (compare Fig. 6.8A and B). A complex of two *hydraulic-jump unit bars* directly overlying a *basal wedge* can still be seen in full (Fig. 6.8B). Because the upstream limit of each foreset was at a lower position than the highest position of the

222

hydraulic-jump unit bar below it, the coset of avalanche foresets would contain more than two foresets if more had formed (three more did in Run 2, Fig. 6.8B). The observer may reasonably infer a complex of as many *hydraulic-jump unit bars* as there are foresets in the coset. The more the *hydraulic-jump bar complex* is truncated downward, the fewer *hydraulic-jump unit bars* can be identified. For example when the Run 2 deposit is truncated to the top of
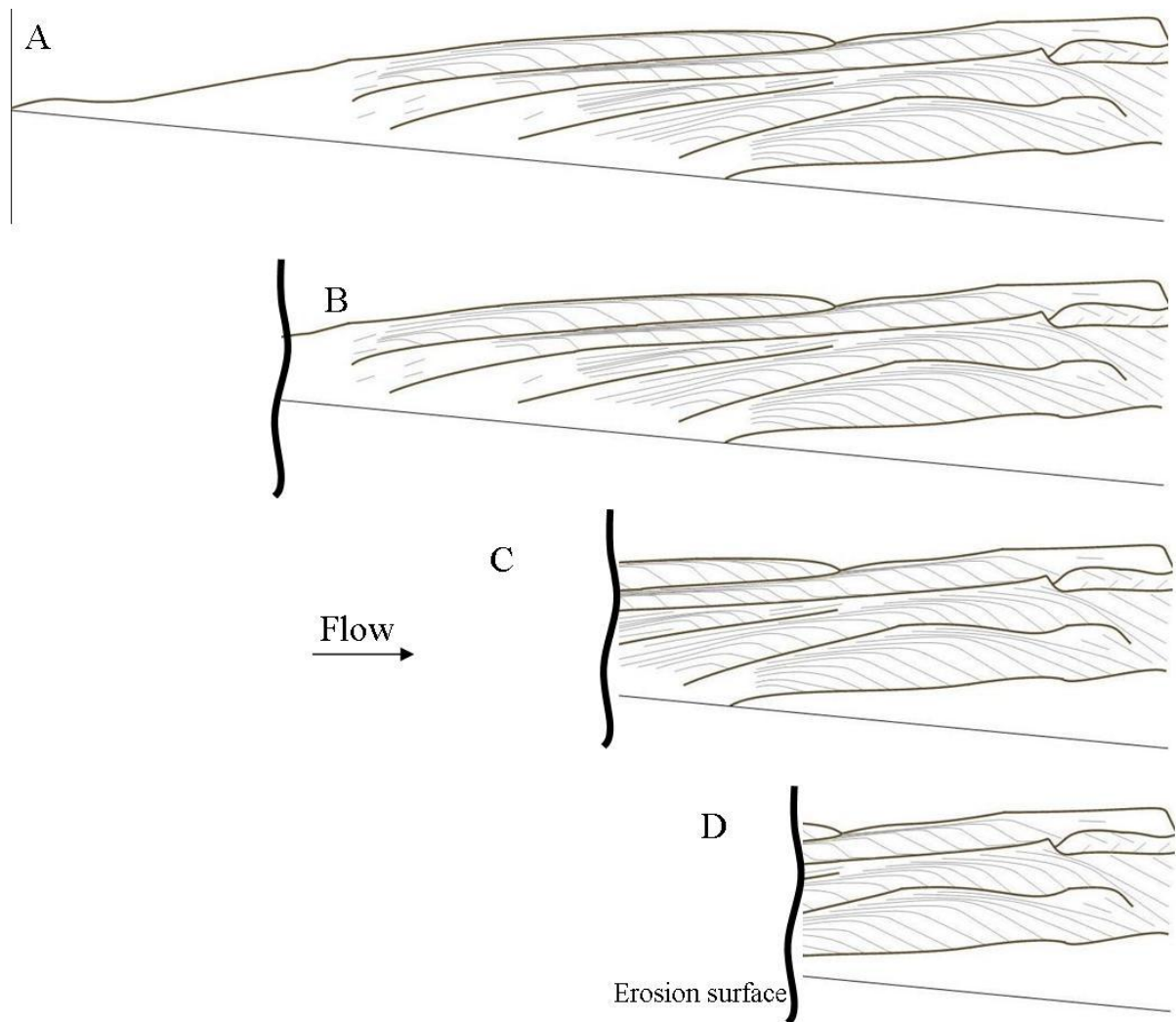
Figure 6.7 The sedimentary structure of the *basal wedge* and complex of five overlying *hydraulic-jump unit bars* that formed in Run 2, successively cropped from the left hand side of the image, to simulate erosion in the upstream part of the deposit. (A) The full complex (with no erosion). (B) The sedimentary structure is eroded by a few tens of centimetres from its upstream end. The incipient *hydraulic-jump unit bar* can no longer be seen but the *basal wedge* and all five *hydraulic-jump unit bars* in the *hydraulic-jump bar complex* can. (C) The sedimentary structure is eroded to a position between the upstream terminations of the two lowermost *hydraulic-jump unit bars* in the complex. Recognisable *hydraulic-jump unit bars* still overly it. (D) If the sedimentary structure is eroded to further downstream than the upstream limit of the *basal wedge*, the juxtaposition of *basal wedge* and foreset is lost and the *hydraulic-jump bar complex* cannot be detected.

the first *hydraulic-jump unit bar*, three foresets (hence three *hydraulic-jump unit bars*) can be detected (Fig. 6.8C). If the *hydraulic-jump bar complex* is truncated so far down that all foresets have been truncated, there is too little of the lamination pattern left to interpret a *hydraulic-jump unit bar* (Fig. 6.8D). Although it has a steep upstream termination, the shape of the *basal wedge* cannot be uniquely identified as a *basal wedge*.
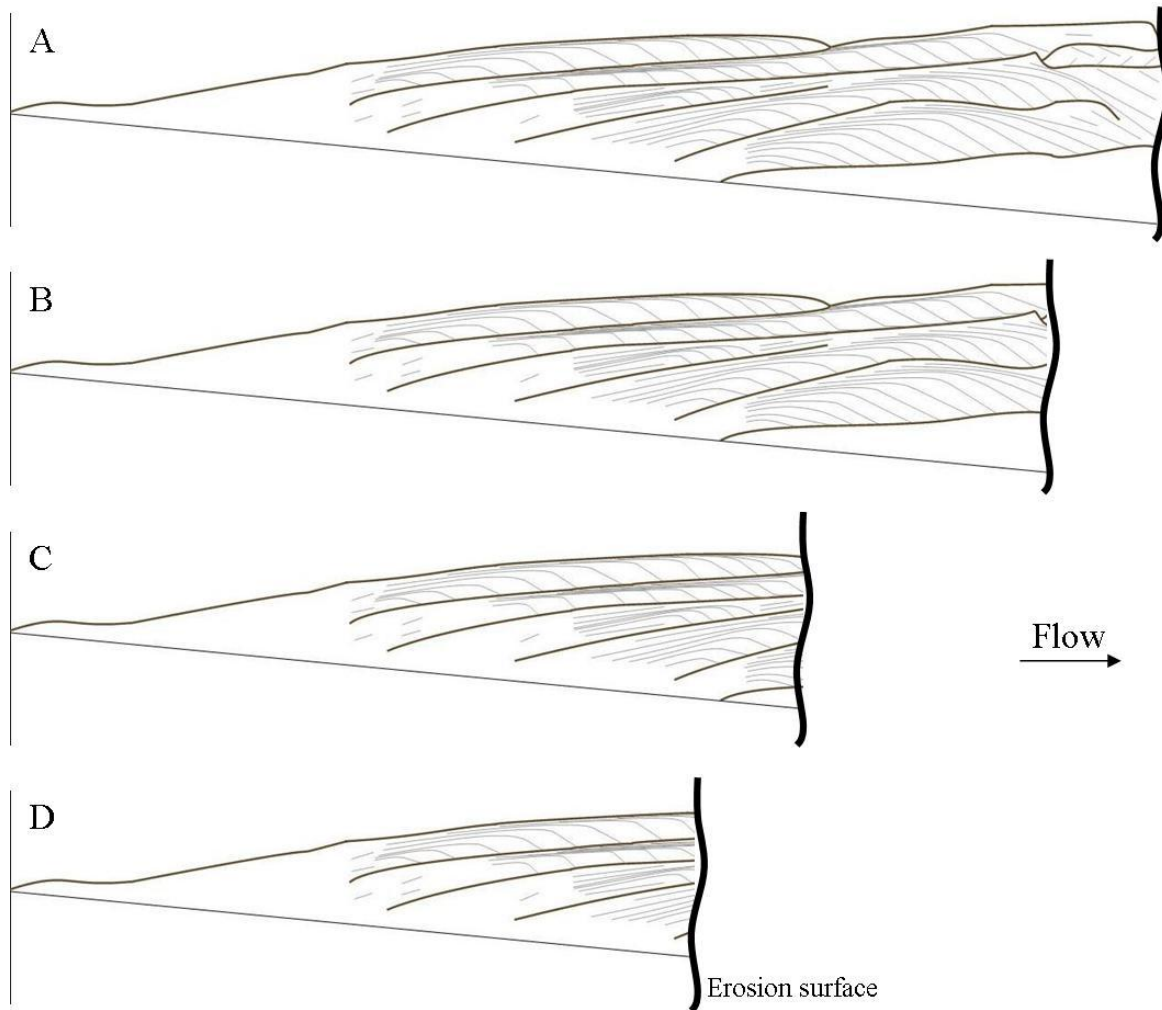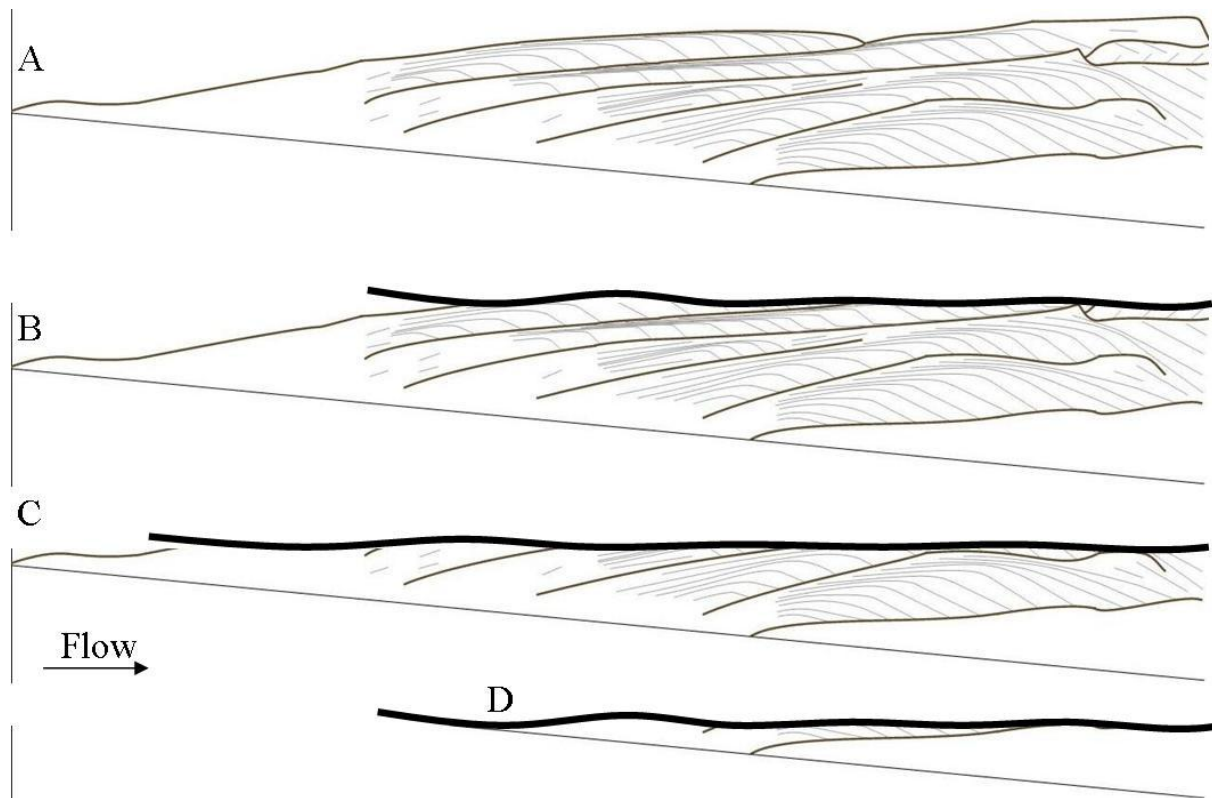

Figure 6.8 The sedimentary structure of the *basal wedge* and complex of five overlying *hydraulic-jump unit bars* that formed in Run 2, successively cropped from the top, to simulate erosion there. (A) The full complex (with no erosion). (B) The sedimentary structure is eroded to the highest point of second *hydraulic-jump unit bar* in the upward sequence. A complex of two *hydraulic-jump unit bars* directly overlying a *basal wedge* can still be seen in full. Five foresets of overlying *hydraulic-jump unit bars* can be detected and one may reasonably assume that they are looking at a complex of five overlying *hydraulic-jump unit bars*. (C) The sedimentary structure is eroded to the highest point of lowermost *hydraulic-jump unit bar*. The foreset of one further, overlying *hydraulic-jump unit bar* can still be detected and one may reasonably assume that they are looking at a complex of two overlying *hydraulic-jump unit bars*. (D) The sedimentary structure is eroded so far that no foreset is left. Part of the *basal wedge* has also been eroded. Too little of the sedimentary structure remains to interpret one *hydraulic-jump unit bar*. The *basal wedge* has an upper surface but the erosional contact that forms the upper surface is unlike the sharp contact of a *basal wedge* with upper surface in a longer channel.

Streamwise components of fully developed hydraulic-jump unit bars in vertical sequence

Because of the way *hydraulic-jump unit bars* can successively form upstream of each other, it is possible for the four streamwise components of the anatomy of a fully developed *hydraulic-*

224

jump unit bar to be seen in a vertical sequence, in some portions of *hydraulic-jump bar complexes*. Because there are four streamwise components, the complex must contain at least four *hydraulic-jump unit bars* for the sequence: upstream dipping laminae, overlain by mounded sediment, coarser foreset with topset and finer foreset with topset, to be preserved (Fig. 6.9). In the unusual case that one of these portions is left after major truncation it is strongly indicative of a *hydraulic-jump bar complex*.
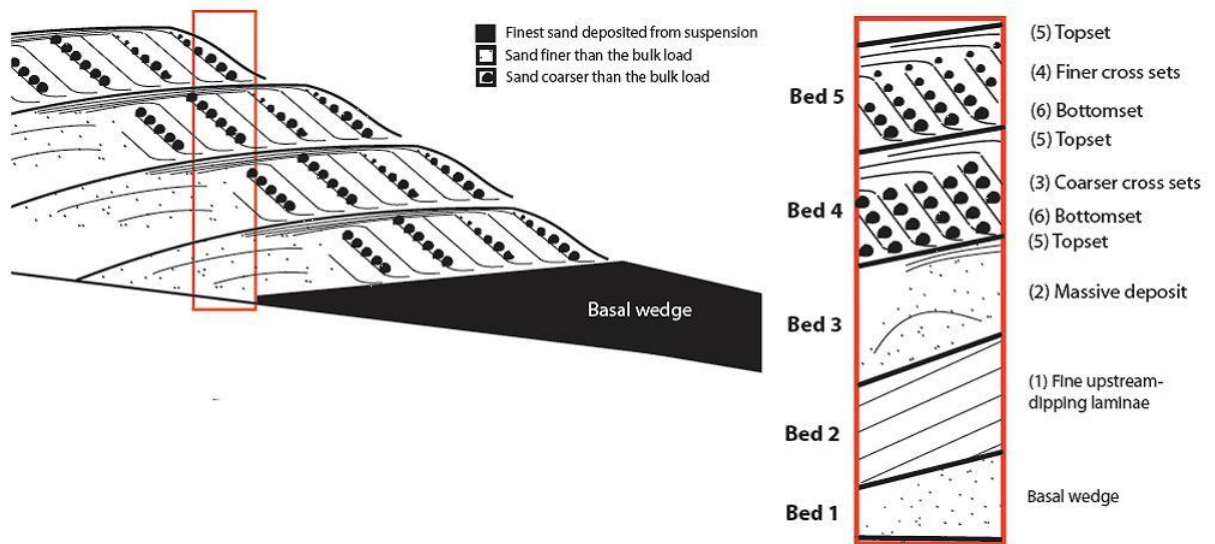
Figure 6.9 Line drawing representing a *basal wedge* and complex of four fully developed *hydraulic-jump unit bars*. The anatomical components (1) – (6) of a fully developed *hydraulic-jump unit bar* are illustrated in Figure 5.16. In the region highlighted by the red box the four beds above the *basal wedge* are composed in the main, of the four streamwise components of the fully developed *hydraulic-jump unit bar*, but in an upward sequence, namely anatomical component (1) is overlain by (2), (3) and then (4). The sedimentary structure of the part of the deposit in the red box is reproduced bigger on the right hand side and also includes topsets and bottomsets associated with (3) and (4).

6.8 ENVIRONMENTS IN WHICH *HYDRAULIC-JUMP UNIT BARS* AND *HYDRAULIC-JUMP BAR COMPLEXES* ARE LIKELY TO BE PRESERVED

Whilst hydraulic jumps occur and affect sediment transport in many rivers and other environments (§1.1.1), later erosion is likely to remove most hydraulic jump deposits in most settings. In order for a hydraulic jump deposit to be preserved, either a hydraulic jump has to be constantly present or repeatedly form at one location (e.g. because of a fixed topographic control), or following its formation it must be buried before significant erosion occurs. The latter might occur if, for example, a river avulses. If an avulsion occurs between the time of

deposition and a successive erosional event, and the avulsion point is upstream of the hydraulic-jump deposit then it is likely to consolidate and the chances for its preservation increase. Discussion of the preservation potential of *hydraulic-jump unit bars* or *bar complexes* in various river settings, presented below highlights settings where they may be expected in deposits.

6.8.1 Preservability of hydraulic jump deposits in proglacial channels

Because flow out of a glacier is generally much less pressurised than flow within or underneath a glacier, supercritical flows entering a proglacial channel are likely to go through a hydraulic jump within a short streamwise distance. Hydraulic jumps will form a short distance downstream of a subglacial or englacial channel as repeatedly as flow is supercritical – so in some channels very frequently. Hydraulic jump deposits may form frequently, especially where the channel is subglacial because the channel beds can be highly erodible and a lot of sediment can be transported.

Loosely packed sands and gravels tend to accumulate in the upstream reaches of proglacial channels. If the resulting sediment fan aggrades or the glacier front moves such that the site of hydraulic jumps changes through time, the hydraulic jump deposits in this setting will have a high preservation potential. However, each discharge event is energetic and subsequent flows are likely to truncate the tops of older deposits. Consequently proglacial channels are likely to have multiple examples of shallow upstream dipping laminae and shallow upstream dipping bed contacts, but recognisable *hydraulic-jump unit bars* or *bar complexes* may not be common.

The movement of an ice front may cause an avulsion because flow can travel through different sub or englacial channels and moraine can deflect channelised flow. Ice margins have been recorded to move several hundred metres in one jökulhlaup (§6.6). Jökulhlaups can deposit a lot of sediment, and that deposition can cause avulsion. Section 6.6 demonstrated that *hydraulic-jump unit bars* can be preserved in these settings.

Because proglacial channels generally flow over frozen ground, the channel floors are resistant to erosion. Hydraulic jump deposits in proglacial channels could well have similar architecture to the flume hydraulic jump deposits, which formed over an initially non erodible floor.

6.8.2 Preservability of hydraulic jump deposits in sub and englacial channels

Hydraulic jump deposits are unlikely to be preserved in sub and englacial channels because the pressurised conditions and limited space is frequently associated with flow being erosional or non depositional (Gorrell & Shaw, 1991; Russell & Arnott, 2003) and because the channels are confined they are not likely to avulse. Furthermore ice action can deform or destroy hydraulic jump deposits that form. Hydraulic jump deposits could be preserved in ephemeral subglacial or englacial channels because of infrequent flow or because the channel is short-lived. However, the ice may retreat before consolidation so the channel boundaries that support the deposit may be removed, causing post-depositional pre-compactional deformation, altering the hydraulic jump deposit out of recognition.

Because some features of subglacial and englacial channels fix the position of a hydraulic jump when flow is supercritical, hydraulic jumps and hydraulic jump deposits can form repeatedly at the same location. Because hydraulic jump deposits would also be repeatedly eroded it is likely that only the bottoms of hydraulic jump deposits will be preserved (cf. Fig. 6.10). Features fixing the position of hydraulic jumps include sub or englacial caverns, in which flow expands, and stationary obstacles such as boulders.
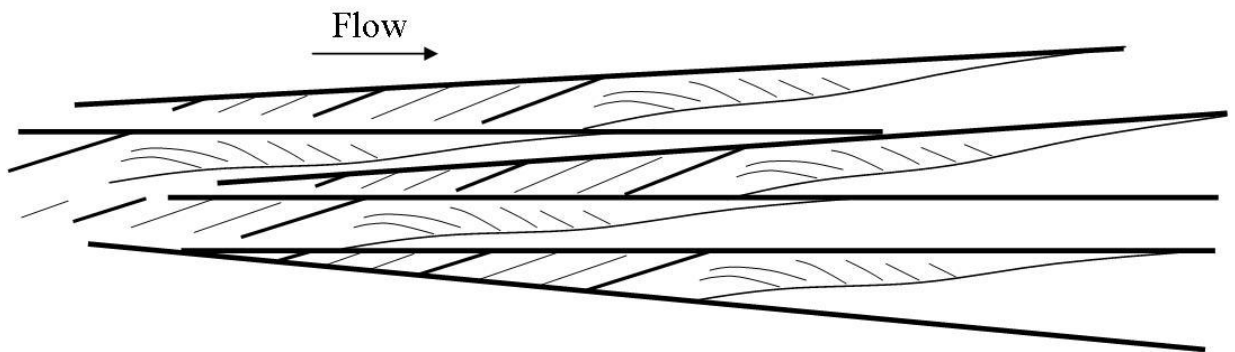
Figure 6.10 Hypothesised sedimentary structure in the situation that a hydraulic jump repeatedly forms at the same location and hydraulic jump deposits repeatedly form, but each one is subsequently eroded by a subsequent flow event. Five basal wedges and five *hydraulic-jump bar complexes*, eroded to the state in Fig. 6.8D are illustrated.

The likely orientation of a hydraulic jump deposit in sub and englacial channels

Because englacial channels are effectively non erodible compared to the timescale of a depositional event, hydraulic jump deposits in caverns of modern englacial channels would have a similar general orientation to the flume hydraulic jump deposits, and so would ancient

englacial hydraulic deposits if they could be preserved without subsequent deformation. The limited space in englacial channels could affect the orientation of hydraulic jump deposits in an unknown way: this would be an interesting area for future research. Large hydraulic jump deposits could only form and be preserved in large diameter branching channel systems and in caverns.

6.8.3 Preservability of hydraulic jump deposits in rivers with erodible channels

Although most hydraulic jump deposits will be eroded by subsequent flows, there may be greater possibility for their preservation than in the glacial rivers. The first reason is that there have been more non-glacial rivers over geological time than glacial rivers. Even though in major glacial periods this might be reversed, warm global conditions probably dominate earth history. In modern environments melt water may be more likely to be supercritical. However, in the geological past before flora developed, mean river channel dimensions were wider (Davies & Gibling, 2010a; Davies & Gibling, 2010b), hence flows are likely to have been thinner and supercritical flows may have been more prevalent.

The position of hydraulic jumps in historical and ancient channels will have been controlled by channel topography as it is in modern channels (§1.5.2). During mean annual and larger flows, jumps may shift size and type, and move downstream (Kieffer, 1985; Valle & Pasternack, 2002). Deposits associated with hydraulic jumps that do not form at repeated locations are most likely to be eroded away. Avulsion can allow hydraulic jump deposits to be preserved and hydraulic jumps can cause and be caused by hydraulic jumps. Hoyal and Sheets (2009) reported hydraulic jump deposits causing avulsion and bifurcation during an aggradational fan-delta experiment. Hydraulic jump deposits may also form and be preserved in flashy ephemeral rivers. Modern examples are rivers of north Queensland, Australia (Alexander *et al.*, 1999).

The likely orientation of a hydraulic jump deposit in erodible-bed rivers
Scour of the channel floor by supercritical flow could "dig out" the bed upstream of the hydraulic jump deposit. Because the motion of the hydraulic jump over time is simply related to volume rate of sediment deposition (§5.5.3), I hypothesise that the general form of the hydraulic jump deposit would be unchanged by the erosional event. I also hypothesise that the

228

deposit would be in a steeper orientation than hydraulic jump deposits in non-erodible or slowly erodible channels, should the deposit initially form on the upstream-dipping downstream face of the scour. This could be the reason why backset beds (often associated with hydraulic jumps, §1.8) dip steeply upstream.

My search in the field for hydraulic jump deposits in ancient erodible bed river environments
Following my experience of the laboratory examples I went hydraulic jump deposit spotting in outcrop of an Upper Carboniferous bank-attached fluvial lateral bar (reported by Haszeldine, 1983a; Haszeldine, 1983b), a Jurassic multistorey alluvial sandstone body (reported by Alexander & Gawthorpe, 1993) and partially consolidated Quaternary drift that has not been published on. The partially consolidated Quaternary drift was exposed in a 1 km set of generally north facing cliffs, west of Whitby West Cliff and directly north of Whitby Golf Club, North Yorkshire coast, England. I saw no depositional architectures like the laboratory examples but I expect that over the next ten years hydraulic jump deposits will become frequently recognised in deposits of erodible bed rivers.

6.9 CONCLUSIONS

1. I devised a series of tests to aid recognition of hydraulic jump deposits, presented in Section 6.3. If any one of the tests has a positive result, the observer is sure they are looking at a hydraulic jump deposit.

2. Some hydraulic jump deposits in open channels in nature have internal architecture like the laboratory examples of hydraulic jump deposits. Two architectural elements in the bottomset deposits of the Emme coarse grained delta complex (proglacial lake Weser, early Saalian, modern day Germany) are interpreted as a *basal wedge* and *hydraulic-jump bar complex*. These are the first candidates known from the rock record. The candidate *hydraulic-jump bar complex* has five overlying *hydraulic-jump unit bars*, each with an upstream-dipping upper surface. The dip decreases upwards in the upward sequence of the bars.

3. Two architectural elements in GPR profiles of the deposits of the 1996 jökulhlaup at Skeiðarársandur, Iceland, are interpreted as *hydraulic-jump unit bars*. One is a short distance upstream of the other. These may be candidates for a streamwise train of hydraulic jump deposits (described below) which is a variation on chute-and-pool.

4. The field hydraulic jump deposits confirm that such things can be preserved in glacial melt water flow. In particular they can form in jökulhlaups.

5. Hydraulic jump deposits can be on the order of hundreds of metres long and metres thick.

6. Hydraulic jump deposits can be recognised where they are partially exposed.

7. Hydraulic jump deposits should be preserved, and be recognisable, in erodible-bed rivers, submarine canyons and many other flows in natural open-channel unidirectional flows.

8. Sites where hydraulic jumps can repeatedly form, sites where hydraulic jump deposits can be rapidly buried, or sites downstream of previous avulsions are most likely to contain recognisable hydraulic jump deposits.

6.10 MODEL OF FORMATION OF HYDRAULIC JUMP DEPOSITS

In nature sediment deposition from suspension, downstream of a hydraulic jump in an open channel would accumulate in a shape not seen in the laboratory examples. Suspended sediment flux to the channel floor increases from the toe of the hydraulic jump downstream because flow velocity and turbulence dramatically decrease downstream of the toe. Suspended sediment concentration decreases downstream with deposition and so the rate of fallout peaks and decreases downstream. In the absence of bedload transport, sediment accumulation from suspension fallout causes the hydraulic jump to move almost constantly upstream in gradual adjustment to the tailwater level rising. The pattern of suspension fallout moves upstream at a near constant rate and the wedge of sediment can develop a long upper surface. The magnitude of downstream thickening of a *basal wedge* of a hydraulic jump deposit is a function of (1) the spatial pattern of suspension fallout and (2) the time taken for the *hydraulic-jump unit bar* to override the *basal wedge*.

In the presence of bedload transport the upper surface of the *basal wedge* would be short because bedload features rapidly override the wedge. Where only one *hydraulic-jump unit bar* forms it grows downstream over time. Otherwise, *hydraulic-jump unit bars* repeatedly form in a complex cf. the model presented in Section 4.7. Either way, deposit thickness is limited by the tailwater depth before deposition began. Flow over the deposit becomes thinner over time, and shear stress immediately above the deposit increases until it is sufficient that sediment flux away from the deposit equals sediment flux to it. Thin flow over the deposit accelerates down the downstream-dipping downstream end of the deposit and becomes supercritical. A second hydraulic jump and second deposit form. This second deposit reaches limiting dimensions with sufficient time and sediment flux and, eventually, a train of hydraulic jump deposits can form above a non-erodible floor in this way.

7. Conclusions

This thesis is on hydraulic jumps in rivers, although hydraulic jumps also occur in submarine and sublacustrine flows, air flows and granular flows. I determined flow and sedimentation patterns of hydraulic jumps. By undertaking the objectives set out in Chapter 1 and reporting my undertakings in this thesis I have increased knowledge and understanding of both the character of flow through hydraulic jumps and sediment transport processes that occur in association with hydraulic jumps. I used carefully devised experiments (Chapters 3 − 5) to systematically determine depositional patterns associated with hydraulic jumps. I recorded the depositional patterns so that hydraulic jump deposits can be recognised in the rock record. Architectural elements in the depositional record of one proglacial delta and one jökulhlaup have been identified as candidates for hydraulic jump deposits; because they have characteristics like my laboratory examples the study was successful. I expect that hydraulic jump deposits like my laboratory examples will also form and be preserved in environments with many other natural open channel flows.

7.1 FORMS OF HYDRAULIC JUMP

In modern open channel flows hydraulic jumps have toes with at least eight plan shapes: (1) Straight, oriented transverse to the stream. (2) Straight, oriented obliquely to stream transverse. (3) U shaped with the apex of the U pointing downstream. (4) V shaped with the apex of the V pointing downstream. (5) U shaped with the apex of the U pointing upstream. (6) W shaped with one apex pointing upstream and two apexes pointing downstream. (7) A shape sculpted by the underlying topography. (8) A new hydraulic jump with cross stream limits that were two arcs of overturning water. The arcs were several centimetres apart at their upstream limit and their cross tank separation increased with distance downstream. This shape has a counterpart with a flow feature called rooster tails described by Kennedy in 1963 but has not been defined as a hydraulic jump before. The report of the eight shapes of hydraulic jumps is useful because the breaking water surface of most hydraulic jumps is a source of vorticity to the flow the hydraulic jump is in; the toe bounds the upstream limit of this part of the vorticity

pattern. The eight shapes are not intended to be a classification of hydraulic jumps but are reported to show variation in hydraulic jumps.

Repeat visits to British river sites indicated that the range of lifetimes of supercritical flows and hydraulic jumps is between tens of seconds, and at least years. The time-persistence of supercritical flows is affected by discharge, stage and local channel conditions. All hydraulic jumps that I observed in British rivers formed at positions that were associated with one or more topographic controls, in regions of significant flow deceleration. The mean position of a lot of these hydraulic jumps did not change by more than the excursion of the oscillation of the toe because discharge did not vary significantly over individual observation periods.

7.2 HYDRAULIC JUMPS DOWNSTREAM OF BOULDERS

In one experiment a hemisphere was attached flat side down to the floor of a flume to act as a boulder on a stream bed. Water flowed around and over the hemisphere in conditions suitable for a hydraulic jump to form downstream of it. Flow became Froude-supercritical because it became thin as it overtopped the hemisphere, and accelerated down the downstream half of it within a dish shaped depression of the water surface. Although this mechanism of flow becoming Froude-supercritical is commonly seen in rivers, this is the first experiment that reproduced it in a flume. Now that the experimental method is proven it should make new science of hydraulic jumps downstream of boulders in stream channels straight forward to achieve and could lead to scientific advancement in wider sedimentological studies such as placer deposits and the formation of steps on river channel floors.

In each experimental series using the hemisphere, an undular jump with shape 5 (§7.2), a hydraulic jump with shape 5 (§7.2) and then a hydraulic jump with shape 8 (§7.2) were reproduced in a sequence of increasing discharge. The water surfaces of the flows involving each of these hydraulic jumps remained approximately stationary for at least tens of hours despite some parts of the water surfaces being steep. The pattern of vorticity known to form around a hemisphere under subcritical flow conditions was disrupted by the supercritical flow and the hydrostatic pressure gradient associated with the dish shaped depression. Vorticity was

not simply transported around the edge of the hemisphere but had a significant cross-stream component.

Distinct regions of bedload features developed. Most aspects of the sediment transport patterns around the hemisphere in supercritical conditions were controlled by the hemisphere and not the supercritical flow and hydraulic jump. Similarities to bedload transport patterns with subcritical flow included: (1) a region upstream of the hemisphere equivalent in streamwise length to 0.4 hemisphere diameters, in which sediment never entered; (2) immediately upstream of the gap, bedload features had a curved downstream face where elsewhere bedload features were not curved; and (3) a region directly downstream of the hemisphere where bedload transport rates were low, in which no bedload features formed. The supercritical flow, hydraulic jump and flume sidewalls caused regions either side of the hemisphere in which bedload features were washed out.

7.3 FLOW PATTERNS IN CYLINDRICAL HYDRAULIC JUMPS

Run 1, involving no sediment, was undertaken to determine flow patterns in a cylindrical hydraulic jump, as an initial condition for three runs involving sediment. The water, flume slope and pumping conditions were set so that a cylindrical hydraulic jump with toe with shape 1 (§7.2) formed in the test channel. Acoustic Doppler velocimeters and ultrasonic Doppler velocity profilers recorded detailed patterns of velocity upstream of, within and downstream of the hydraulic jump. Turbulent fluctuation in velocity time series generally decreased with distance downstream of the toe. A jet was recognised within the hydraulic jump. The core of highest velocity within the jet detached from the flume floor underneath the hydraulic jump and at any point in time it took one of two tracks, rising into the flow as water traveled downstream through it. In the *jet up* track the core of highest velocity reached three quarters of the way to the water surface and in the *jet down* track the jet was much closer to the flume floor. The jet continually switched between the two tracks.

7.4 SEDIMENT TRANSPORT AND ACCUMULATION PATTERNS IN CYLINDRICAL HYDRAULIC JUMPS

In Runs 2 – 4 sediment was added to the flume in a way that it was transported through the hydraulic jump both as suspended load and bedload. A deposit of almost 5000 kg of sand aggraded a short distance downstream of the hydraulic jump. This demonstrates that (1) large volumes of sediment can be deposited downstream of hydraulic jumps. Hence "hydraulic jump deposits" should be recognisable in fluvial deposits. (2) A method has been proven to achieve aggradational sedimentary experiments involving hydraulic jumps in a flume.

Most of the fine-grained sediment was deposited from suspension in the slowing tailwater to form a sheet, thickening downstream. Concurrently, coarser sediment dropped to the channel floor, from the flow within the hydraulic jump and was pushed downstream to a point just downstream of the upstream limit of the fine sheet, where it mounded. The mound developed into a *hydraulic-jump unit bar* which grew by prograding and progressively covered the fine sand sheet. In Run 2 the *hydraulic-jump unit bar* grew upstream and downstream and formed a bidirectional cross set pattern. With near-steady flow and only minor fluctuations in sediment flux, a series of *hydraulic-jump unit bars* developed, each above and upstream of the previous one and all above the massive basal unit. This series of overlying *hydraulic-jump unit bars* is defined as a *hydraulic-jump bar complex*. In Run 3 the same sediment was input at a faster rate. The resultant deposit was a complex of two *hydraulic-jump unit bars*, the upper one being low amplitude. In Run 4 finer sediment was input at the same rate as Run 2 and one *hydraulic-jump unit bar* formed. In both Runs 3 and 4 the Froude number of the supercritical flow decreased over time and the hydraulic jump changed from an 'oscillating jump' to a 'weak jump'. In association the oscillation of the submerged jet is inferred to have ceased and this may explain the different pattern of deposition compared to that in Run 2.

When fully formed, *hydraulic-jump unit bars* have an anatomy containing at least six components. (1) A set of upstream dipping laminae that is finer than the input sediment; (2) a mound of sediment containing few or no bedding structures in streamwise view; (3) an avalanche foreset coarser than the input sediment; (4) an avalanche foreset similar in grain size to the input sediment; (5) a topset overlying Elements (1) – (4); (6) a bottomset underlying the foreset. The mound, the finer foreset and the topset were present in all *hydraulic-jump unit*

bars that formed in Runs 2 – 4. The set of upstream dipping laminae and the coarser foreset were intimately linked, requiring segregation of fine grains upstream of the mound from coarser grains of the bedload that passed over the mound. Their formation was sensitive to the steepness of the upstream termination of the mound (a function of bedload transport rate), jet flow conditions and the grain size pattern on the upstream limit of the mound.

7.5 RECOGNISING HYDRAULIC JUMP DEPOSITS IN THE ROCK RECORD

The fanning coset architecture of the *hydraulic-jump bar complex* has a character without counterpart in sedimentary geology, and as such is diagnostic of the presence of a hydraulic jump in the flow when the sand was deposited. The juxtaposition of the *hydraulic-jump bar complex* and the massive *basal wedge* is also a signature of the presence of a hydraulic jump. Neither can be used to interpret the nature of the hydraulic jump or the sand flux, which was specific to the experiment. Because we know so little about hydraulic jumps or their deposit patterns in past sedimentary environments, they have been barely recognised in the rock record. Backset beds, classically attributed to hydraulic jumps, did not form in the flume experiments. Since this definition of *hydraulic-jump unit bars* and *hydraulic-jump bar complexes* was published, three strong candidates for them have emerged. Two candidates are from modern jökulhlaup deposits and one from an inferred proglacial delta. What is required now is for sedimentary geologists to be aware of these findings and to keep their eyes open. I expect that *hydraulic-jump unit bars* and bar complexes will be recognised in outcrop and GPR data over the coming decade or two.

7.6 SUMMARY OF MAJOR FINDINGS

1. Hydraulic jumps were formed above or downstream of a hemisphere in a flume by pumping water past it. The hydraulic jumps changed shape in series of increasing discharge.

2. A new shape of hydraulic jump was recognised; the same shape as Kennedy's "rooster tail" water surface feature but a different flow structure.

3. Submerged wall jets under hydraulic jumps can have tracks that detach from a channel floor and rise upwards in the flow. The length and position of the detached part of the track oscillate with time and can cause periodic releases of vortices from the roller.

4. *Hydraulic-jump unit bars* and *bar complexes* have been produced under cylindrical hydraulic jumps in a flume, described, recorded and related to flow conditions.

5. Three examples of deposits that involve *hydraulic-jump unit bars* have been described in literature. There are likely to be lots more hydraulic jump deposits in the geological record, and they can be recognised via diagnostic criteria presented in this thesis.

References

Agrawal, Y.C., McCave, I.N. and Riley, J.B. (1991) Laser diffraction size analysis. In: *Principles, Methods and Applications of Particle Size Analysis* (Ed J.P.M. Syvitski), 119-128. Cambridge University Press, Cambridge, UK.

Alexander, J., Bridge, J.S., Cheel, R.J. and Leclair, S.F. (2001) Bedforms and associated sedimentary structures formed under supercritical water flows over aggrading sand beds. *Sedimentology*, **48**, 133-152.

Alexander, J., Fielding, C.R. and Pocock, G.D. (1999) Flood behaviour of the Burdekin River, tropical north Queensland, Australia. *Geological Society Special Publication*, **163**, 27-40.

Alexander, J. and Gawthorpe, R.L. (Eds) 1993. *The complex nature of a Jurassic multistorey, alluvial sandstone body, Whitby, North Yorkshire*. (Eds C.P. North and D.J. Prosser), *Characterisation of Fluvial and Aeolian Reservoirs*, Geological Society Special Publication No 73, 123-142.

Alhamid, A.A. (2004) S-jump characteristics on sloping basins. *Journal of Hydraulic Research*, **42**, 657-662.

Allen, J.R.L. (1982) *Sedimentary Structures, Their Characteristics and Physical Basis.* Developments in Sedimentology, **30B**. Elsevier, Amsterdam, 663 pp.

Allen, J.R.L. and Leeder, M.R. (1980) Criteria for the instability of upper-stage plane beds. *Sedimentology*, **27**, 209-217.

Alonso, C.V., Bennett, S.J. and Stein, O.R. (2002) Predicting head cut erosion and migration in concentrated flows. *Water Resources Research*, **38**, 1303 - 1317.

Anderson, S. and Lohrmann, A. 1995. Open water test of the SonTek acoustic Doppler velocimeter. In: *Proc., IEEE 5th Working Conf. on Current Measurements*, pp. 188-192. IEEE Oceanic Engineering Society, St. Petersburg.

Annandale, G.W. (1995) Erodibility. *Journal of Hydraulic Research*, **33**, 471-494.

Armfield Limited. (2005) Product Manual AL12711. 30.

Baas, J.H. (1994) A flume study on the development and equilibrium morphology of small-scale bedforms in very fine sand. *Sedimentology*, **41**, 185-209.

Baas, J.H. and de Koning, H. (1995) Washed-out ripples: their equilibrium dimensions, migration rate, and relation to suspended-sediment concentration in very high sand. *Journal of Sedimentary Research*, **A65**, 431-435.

Bagnold, R.A. (1941) *The Physics of Blown Sand and Desert Dunes*. Meuthen, London, 265 pp.

Bakhmeteff, B.A. and Matzke, A.E. (1936) The hydraulic jump in terms of dynamic similarity. *Transactions of the ASCE*, **101**, 630-680.

Balachandar, R., Kells, J.A. and Thiessen, R.J. (2000) The effect of tailwater depth on the dynamics of local scour. *Canadian Journal of Civil Engineering*, **27**, 138-150.

Belanger, J.B.C.J. (1828) *Essai sur la Solution Numerique de quelques Problemes Relatifs au Mouvement Permanent des Eaux Courantes*. Carilian-Goeury, Paris, France.

Bellal, M., Spinewine, B., Savery, C. and Zech, Y. 2003. Morphological evolution of steep-sloped river beds in the presence of a hydraulic jump: Experimental study. In: *Proceedings of XXX IAHR Congress*, **C-II**, pp. 133-140, Thessaloniki, Greece.

Bennett, S.J. and Bridge, J.S. (1995) The geometry and dynamics of low-relief bed forms in heterogeneous sediment in a laboratory channel, and their relationship to water-flow and sediment transport. *Journal of Sedimentary Research*, **65**, 29-39.

Bennett, S.J. and Casali, J. (2001) Effect of initial step height on headcut development in upland concentrated flows. *Water Resources Research*, **35**, 1475-1484.

Best, J.L. and Brayshaw, A.C. (1985) Flow separation - a physical process for the concentration of heavy minerals within alluvial channels. *J. Geol. Soc. London*, **142**, 747-755.

Best, J.L., Kirkbride, A.D. and Peakall, J. (2001) Mean flow and turbulence structure of sediment-laden gravity currents: new insights using ultrasonic Doppler velocity profiling. *Spec. Publs int. Ass. Sediment.*, **31**, 159-172.

Bidone, G. (1819) Le romou et sur la propagation des ondes. *Report to Academie Royale des Sciences de Turin*, **XXV**, 21-112.

Binney, A.M. and Orkney, J.C. (1955) Experiments on the flow of water from a reservoir through an open horizontal channel. II. The formation of hydraulic jumps *Proceedings of the Royal Society A*, **230**, 237-246.

Blott, S.J., Croft, D.J., Pye, K., Saye, S.E. and Wilson, H.E. (2004) Particle size analysis by laser diffraction. In: *Forensic Geoscience - Principles, Techniques and Applications* (Eds K. Pye and D.J. Croft), Geological Society of London Special Publication, **232**. Geological Society Publishing House, Bath.

Blott, S.J. and Pye, K. (2006) Particle size distribution analysis of sand-sized particles by laser diffraction: an experimental investigation of sensitivity and the effects of particle shape. *Sedimentology*, **53**, 671-685.

Blott, S.J. and Pye, K. (2008) Particle shape: a review and new methods of characterization and classification. *Sedimentology*, **55**, 31-63.

Bradley, J.N. and Peterka, A.J. (1957) The hydraulic design of stilling basins. *Journal of the Hydraulics Division, ASCE*, **83**, 1401-1406.

Breda, A., Mellere, D. and Massari, F. (2007) Facies and processes in a Gilbert-delta-filled incised valley (Pliocene of Ventimiglia, NW Italy). *Sedimentary Geology*, **200**, 31-55.

Bridge, J.S. and Best, J.L. (1988) Flow, sediment transport and bedform dynamics over the transition from dunes to upper-stage plane beds: implications for the formation of planar laminae. *Sedimentology*, **35**, 753-763.

Bridge, J.S. and Best, J.L. (1997) Preservation of planar laminae arising from low-relief bed waves migrating over aggrading plane beds: comparison of experimental data with theory. *Sedimentology*, **44**, 253-262.

Brocchini, M. and Peregrine, D.H. (2001) The dynamics of strong turbulence at free surfaces. Part 1. Description. *Journal of Fluid Mechanics*, **449**, 225-254.

Brown, G. and Roshko, A. (1971) The effect of density differences on the turbulent mixing layer. AD0737731, Caltech graduate aeronautical labs, Pasadena, California.

Burke, M.J., Woodward, J., Russell, A.J., Fleisher, P.J. and Bailey, P.K. (2008) Controls on the sedimentary architecture of a single event englacial esker: Skeiðarárjökull, Iceland. *Quaternary Science Reviews*, **27**, 1829-1847.

Carling, P.A. (1990) Particle over-passing on depth-limited gravel bars. *Sedimentology*, **37**, 345-355.

Carling, P.A. (1995) Flow-separation berms downstream of a hydraulic jump in a bedrock channel. *Geomorphology*, **11**, 245-253.

Carling, P.A. (1999) Subaqueous gravel dunes. *Journal of Sedimentary Research*, **69**, 534-545.

Carling, P.A. and Reader, N.A. (1982) Structure, composition and bulk properties of upland stream gravels. *Earth Surface Processes and Landforms*, **7**, 349-365.

Cassidy, N.J., Russell, A.J., Marren, P.M., Fay, H., Knudsen, O., Rushmer, E.L. and van Dijk, T.A.G.P. (2003) GPR derived architecture of November 1996 jökulhlaup deposits, Skeiðarársandur, Iceland. In: *Ground Penetrating Radar in Sediments* (Eds C.S. Bristow and H.M. Jol). Geological Society of London, Special Publications, **211**, 153-166.

Chanson, H. (1995) Flow characteristics of undular hydraulic jumps. Comparison with near-critical flows. *Report CH45/95*, Civil Engineering, The University of Queensland.

Chanson, H. (1999) *The hydraulics of open channel flow. An introduction*, **56-67**. Butterworth-Heinemann, Oxford.

Chanson, H. 2007. Hydraulic jumps: bubbles and bores. In: *16th Australasian Fluid Mechanics Conference*, pp. 39-53, Crown Plaza, Gold Coast, Australia.

Chanson, H. (2008) Turbulence in positive surges and tidal bores. Effects of bed roughness and adverse slopes. CH CH68/08, Civil Engineering, The University of Queensland.

Chanson, H. and Brattberg, T. (2000) Experimental study of the air-water shear flow in a hydraulic jump. *International Journal of Multiphase Flow*, **26**, 583-607.

Darcy, H. and Bazin, H. (1865) Recherches hydrauliques. *Imprimerie Imperiale* Parties 1e et 2e, Paris, France.

Darghai, B. (1982) Local scouring around bridge piers - A review of practice and theory. *Bulletin No. 114*, Royal Institute of Technology Hydrological Laboratory, Stockholm, Sweden.

Darghai, B. (1990) Controlling mechanism of local scouring. *Journal of Hydraulic Engineering*, **116**, 1197-1214.

Davies, N.S. and Gibling, M.R. (2010a) Cambrian to Devonian evolution of alluvial systems: The sedimentological impact of the earliest land plants. *Earth-Science Reviews*, **98**, 171-200.

Davies, N.S. and Gibling, M.R. (2010b) Paleozoic vegetation and the Siluro-Devonian rise of fluvial lateral accretion sets. *Geology*, **38**, 51-54.

Davies, T.R.H. (1982) Lower flow regime bedforms - rational classification. *Journal of the Hydraulics Division, ASCE*, **108**, 343-360.

Davies, T.R.H. (1987) Channel boundary shape-evolution and equilibrium. In: *River Channels: Environment and Process* (Ed K.S. Richards), 228-248. Blackwell Scientific, Oxford.

Dey, S. and Sarkar, A. (2007) Effect of upward seepage on scour and flow downstream of an apron due to submerged jets. *Journal of Hydraulic Engineering*, **133**, 59-69.

Duller, R.A., Mountney, N.P., Russell, A.J. and Cassidy, N.C. (2008) Architectural analysis of a volcaniclastic jokulhlaup deposit, southern Iceland: sedimentary evidence for supercritical flow. *Sedimentology*, **55**, 939-964.

Euromag 2009. Sensor Wafer MUT 1000 EL.

Fielding, C.R. (2006) Upper flow regime sheets, lenses and scour fills: Extending the range of architectural elements for fluvial sediment bodies. *Sedimentary Geology*, **190**, 227-240.

Fielding, C.R. and Alexander, J. (2001) Fossil trees in ancient fluvial channel deposits: evidence of seasonal and longer-term climatic variability. *Palaeogeography, Palaeoclimatology, Palaeoecology*, **170**, 59-80.

Fildani, A., Normark, W.R., Kostic, S. and Parker, G. (2006) Channel formation by flow stripping: large-scale scour features along the Monterey East Channel and their relation to sediment waves. *Sedimentology*, **53**, 1265-1287.

Fiorotto, V. and Rinaldo, A. (1992) Turbulent pressure fluctuations under hydraulic jumps. *Journal of Hydraulic Research*, **30**, 499-520.

Fraenkel, L.E. (1961) On corner eddies in plane inviscid shear flow. *Journal of Fluid Mechanics*, **11**, 400-406.

Fralick, P. (1999) Paleohydraulics of chute-and-pool structures in a Paleoproterozoic fluvial sandstone. *Sedimentary Geology*, **125**, 129-134.

Froude, W. (1872) Experiments on the surface-friction experienced by a plane moving through water. *British Association for the Advancement of Science* 42nd meeting, U.K.

Gargett, A.E. (1976) Generation of internal waves in the Strait of Gibraltar, British Columbia. *Deep Sea Research*, **23**, 17-32.

Goring, D.G. and Nikora, V.I. (2002) Despiking acoustic Doppler velocimeter data. *Journal of Hydraulic Engineering*, **128**, 117-126.

Gorrell, G. and Shaw, J. (1991) Deposition in an esker, bead and fan complex, Lanark, Ontario, Canada. *Sedimentary Geology*, **72**, 285-314.

Goutiere, L., Soares Frazao, S., Savery, C., Laraichi, T. and Zech, Y. (2008) One-dimensional model for transient flows involving bedload sediment transport and changes in flow regimes. *Journal of Hydraulic Engineering*, **134**, 726-735.

Grant, G.E., Swanson, F.J. and Wolman, M.G. (1990) Pattern and origin of stepped-bed morphology in high-gradient streams, Western Cascades, Oregon. *Geological Society of America, Bulletin*, **102**, 340-352.

Gray, J.M.N.T., Tai, Y.C. and Noelle, S. (2003) Shock waves, dead-zones and particle-free regions in rapid granular free surface flows. *Journal of Fluid Mechanics*, **491**, 161-181.

Gray, T.E. (2004) *Sedimentation at subaqueous breaks in slope*, University of East Anglia, 298 pp.

Gregorian, T. and Thorp, J.H. (1992) Effects of microhabitat selection on feeding rates of net-spinning caddisfly larvae. *Ecology*, **73**, 229-240.

Gunatilaka, A. and Mwango, S.B. (1989) Flow separation and the internal structure of shadow dunes. *Sedimentary Geology*, **61**, 125-134.

Hager, H., Bremen, R. and Kawagoshi, N. (1990) Classical hydraulic jump: length of roller. *Journal of Hydraulic Research*, **28**, 591-608.

Hager, W.H. and Bremen, R. (1989) Classical hydraulic jump: sequent depths. *Journal of Hydraulic Research*, **27**, 565-585.

Haszeldine, R.S. (1983a) Descending tabular cross-bed sets and bounding surfaces from a fluvial channel in the Upper Carboniferous coalfield of north-east England. In: *Special Publication of the International Association of Sedimentologists*, **6**, 449-456.

Haszeldine, R.S. (1983b) Fluvial bars reconstructed from a deep, straight channel, Upper Carboniferous coalfield of northeast England. *Journal of Sedimentary Petrology*, **53**, 1233-1247.

Hertenstein, R.F. and Kuettner, J.P. (2005) Rotor types associated with steep lee topography: influence of the wind profile. *Tellus*, **57A**, 117-135.

Hill, H.M. (1966) Bed forms due to a fluid stream. *Journal of the Hydraulics Division, ASCE*, **95**, 1545-1558.

Hornung, H.G., Willert, C. and Turner, S. (1995) The flow field downstream of a hydraulic jump. *Journal of Fluid Mechanics*, **287**, 299-316.

Hornung, J.J., Asprion, U. and Winsemann, J. (2007) Jet-efflux deposits of a subaqueous ice-contact fan, glacial Lake Rinteln, northwestern Germany. *Sedimentary Geology*, **193**, 167-192.

Hoyal, D.C.J.D. and Sheets, B.A. (2009) Morphodynamic evolution of experimental deltas. *Journal of Geophysical Research*, **114**, F02009.

Huettel, M., Ziebis, W. and Forster, S. (1996) Flow-induced uptake of particulate matter in permeable sediments. *Limnology and Oceanography*, **41**, 309-322.

Imai, S. and Nakagawa, T. (1995) On longitudinal and transverse variations of the bed shear stress on the wetted perimeter of a sloped rectangular open channel in a hydraulic jump. *Acta Mechanica*, **111**, 141-150.

Johansson, C.E. (1963) Orientation of pebbles in running water: a laboratory study. *Geog. Annaler*, **45**, 85-112.

Jopling, A.V. and Richardson, E.V. (1966) Backset bedding developed in shooting flow in laboratory experiments. *Journal of Sedimentary Research*, **36**, 821-825.

Karcz, I. (1968) Fluviatile obstacle marks from the wadis of the Negev (southern Israel). *Journal of Sedimentary Petrology*, **38**, 1000-1012.

Karcz, I. (1972) Sedimentary structures formed by flash floods in southern Israel. *Sedimentary Geology*, **7**, 161-182.

Kemp, J.L., Harper, D.M. and Crosa, G.A. (2000) The habitat-scale ecohydraulics of rivers. *Ecological Engineering*, **16**, 17-29.

Kennedy, J.F. (1961) Stationary waves and antidunes in alluvial channels. *Rept. KH-R-2, W. M. Keck Lab. Hydraulics water resources* (Caltech, Pasadena).

Kieffer, S.W. (1985) The 1983 hydraulic jump in Crystal Rapids: implications for river-running and geomorphic evolution in the Grand Canyon. *Journal of Geology*, **93**, 385-406.

Kiger, K.T. and Pan, C. (2002) Suspension and turbulence modification effects of solid particulates on a horizontal turbulent channel flow. *Journal of Turbulence*, **3**, 019.

Kim, J.H. (2001) Hydraulic characteristics by weir type in a pool-weir fishway. *Ecological Engineering*, **16**, 425-433.

Kirkgöz, M.S. and Ardiçlioğlu, M. (1997) Velocity profiles of developing and developed open channel flow. *Journal of Hydraulic Engineering*, **123**, 1099-1105.

Koch, C. and Chanson, H. (2005) An experimental study of tidal bores and positive surges: Hydrodynamics and turbulence of the bore front. *Report No. CH56/05* Department of Civil Engineering, The University of Brisbane, Australia, 170 pp.

Koch, C. and Chanson, H. (2007) Turbulent mixing beneath an undular bore front. *Journal of Coastal Research*, **23**.

Kuettner, J. (1959) *The rotor flow in the lee of mountains*. Geophysics Research Directorate (GRD) Research Notes 6, Air Force Cambridge Research Center, USA, 20 pp.

Lane, S.N., Biron, P.M., Bradbrook, K.F., Butler, J.B., Chandler, J.H., Crowell, M.D., McLelland, S.J., Richards, K.S. and Roy, A.G. (1998) Three-dimensional measurement of river channel flow processes using acoustic Doppler velocimetry. *Earth Surface Processes and Landforms*, **23**, 1247-1263.

Laronne, J.B. and Carson, M.A. (1976) Interrelationships between bed morphology and bed-material transport for a small, gravel-bed channel. *Sedimentology*, **23**, 67-85.

Laronne, J.B., Garcia, C.M. and Reid, I. (2001) Mobility of patch sediment in gravel bed streams: patch character and its implications for bedload. In: *Gravel-bed Rivers V* (Ed M.P. Mosely), 249-280, Proceedings of the 5th International Gravel-Bed Rivers Workshop, Christchurch, New Zealand.

Leclair, S.F. and Bridge, J.S. (2001) Quantitative interpretation of sedimentary structures formed by river dunes. *Journal of Sedimentary Research*, **71**, 713-716.

Leclair, S.F., Bridge, J.S. and Wang, F. (1997) Preservation of cross-strata due to migration of subaqueous dunes over aggrading and non-aggrading beds: comparison of experimental data with theory. *Geoscience Canada*, **24**, 55-66.

Lennon, J.M. and Hill, D.F. (2006) Particle image velocity measurements of undular and hydraulic jumps. *Journal of Hydraulic Engineering*, **132**, 1283-1295.

Lewis, K.B. and Pantin, H.M. (2002) Channel-axis, overbank, and drift sediment waves in the southern Hikurangi Trough, New Zealand. *Marine Geology*, **192**, 123-151.

Lighthill, J. (1978) *Waves in fluids*. Cambridge University Press.

Liu, M., Rajaratnam, N. and Zhu, D.Z. (2004) Turbulence structure of hydraulic jumps of low Froude numbers. *Journal of Hydraulic Engineering-Asce*, **130**, 511-520.

Ljermitte, R. and Serafin, R. (1984) Pulse-to-pulse coherent Doppler sonar signal processing techniques. *Journal of Atmospheric and Oceanic Technology*, **1**, 293-308.

Long, D., Rajaratnam, N., Steffler, P.M. and Smy, P.R. (1991) Structure of flow in hydraulic jumps. *Journal of Hydraulic Research*, **29**, 207-218.

Long, R.R. (1954) Some aspects of the flow of stratified fluids-II. Experiments with a two-fluid system. *Tellus*, **6**, 97-115.

Macdonald, R.G., Alexander, J., Bacon, J.C. and Cooker, M.J. (2009) Flow patterns, sedimentation and deposit architecture under a hydraulic jump on a non-eroding bed; defining hydraulic-jump unit bars. *Sedimentology*, **56**, 1346-1367.

Macías, J.L., Espíndola, J.M., Bursik, M. and Sheridan, M.F. (1998) Development of lithic-breccias in the 1982 pyroclastic flow deposits of El Chichón Volcano, Mexico. *Journal of Volcanology and Geothermal Research*, **83**, 173-196.

Martini, I.P. (1977) Gravelly flood deposits of Irvine Creek, Ontario, Canada. *Sedimentology*, **24**, 603-622.

Massari, F. (1996) Upper-flow-regime stratification types on steep-face, coarse-grained, Gilbert-type progradational wedges (Pleistocene, Southern Italy). *Journal of Sedimentary Research*, **66**, 364-375.

Massari, F. and Parea, G.C. (1990) *Wave-dominated Gilbert-type gravel deltas in the hinterland of the Gulf of Taranto (Pleistocene, southern Italy). In: Colella, A. and Prior, D.B. (eds.)* Coarse-Grained Deltas, **10**. International Association of Sedimentologists Special Publication, 311-331 pp.

Massey, B.S. (1983) *Mechanics of Fluids*, **5th Edn**. Van Nostrand Reinhold, Wokingham, Berkshire, Art 11.10.

Materials, A.S.f.T.a. (2000) Standard Test Method for Determining Particle Size Distribution of Alumina or Quartz by Laser Light Scattering. In: *Annual Book of ASTM Standards, 15.02*, 375-376, Philadelphia.

McCorquodale, J.A. and Khalifa, M. (1980) Submerged radial hydraulic jump. *Journal of the Hydraulics Division, ASCE*, **106**, 355-367.

McLelland, S.J. and Nicholas, A.P. (2000) A new method for evaluating errors in high-frequency ADV measurements. *Hydrological Processes*, **14**, 351-366.

Menard, H.W. (1964) *Marine Geology of the Pacific*. McGraw-Hill, New York, 271 pp.

Met-flow (2002) UVP Monitor User's Guide. *Release 5*.

Montes, J.S. (1986) A study of the undular jump profile. In: *9th Australasian Fluid Mechanics Conference AFMC*, pp. 148-151, Aukland, New Zealand.

Mossa, M. and Tolve, U. (1998) Flow visualization in bubbly two-phase hydraulic jump. *Journal of Fluids Engineering*, **120**, 160-165.

Murzyn, F., Mouaze, D. and Chaplin, J.R. (2005) Optical fibre probe measurements of bubbly flow in hydraulic jumps. *International Journal of Multiphase Flow*, **31**, 141-154.

Needham, D.J. and Hey, R.D. (1991) On nonlinear simple waves in alluvial river flows: a theory for sediment bores. *Phil. Trans. Roy. Soc. Lond.* , **334**, 25-53.

Nelson, P.A., Venditti, J.G., Dietrich, W.E., Kirchner, J.W., Ikeda, H., Iseya, F. and Sklar, L.S. (2009) Response of bed surface patchiness to reductions in sediment supply. *Journal of Geophysical Research*, **114**, F02005.

Nemec, W. (1990) Aspects of sediment movement on steep delta slopes. In Colella, A. and Prior, D.B. (eds.): Coarse-Grained Deltas. *International Association of Sedimentologists Special Publication*, **10**, 29-73.

Nikora, V.I. and Goring, D.G. (1998) ADV measurements of turbulence: can we improve their interpretation? *Journal of Hydraulic Engineering*, **124**, 630-634.

Nortek AS. (2006) Vectrino - A new generation in 3D water velocity sensor!, http://www.nortekusa.com/lib/brochures/Vectrino%2006%20b.pdf.

Ozaki, Y., Kawaguchi, T., Takeda, Y., Hishida, K. and Maeda, M. (2002) High time resolution ultrasonic velocity profiler. *Experimental Thermal and Fluid Science*, **26**, 253-258.

Pagliara, S. and Chiavaccini, P. (2006) Flow resistance of rock chutes with protruding boulders. *Journal of Hydraulic Engineering*, **132**, 545-552.

Paola, C., Gust, G. and Southard, J.B. (1986) Skin friction behind isolated hemispheres and the formation of obstacle marks. *Sedimentology*, **33**, 279-294.

Parker, G., Fukushima, Y. and Pantin, H.M. (1986) Self-accelerating turbidity currents. *Journal of Fluid Mechanics*, **171**, 145-181.

Parker, G. and Izumi, N. (2000) Purely erosional cyclic and solitary steps created by flow over a cohesive bed. *Journal of Fluid Mechanics*, **419**, 203-238.

Pasternack, G.B., Ellis, C.R. and Marr, J.D. (2007) Jet and hydraulic jump near-bed stresses below a horseshoe waterfall. *Water Resources Research*, **43**, doi:10.1209/2006WR005774.

Paterson, A.R. (1983) *A first course in fluid dynamics*. Cambridge University Press, 528 pp.

Postma, G. and Roep, T.B. (1985) Resedimented conglomerates in the bottomsets of Gilbert-type gravel deltas. *Journal of Sedimentary Petrology*, **55**, 874-855.

Rajaratnam, N. (1965) The hydraulic jump as a wall jet. *Journal of the Hydraulics Division, ASCE*, **91**, 107-132.

Reynolds, O. (1883) An experimental investigation of the circumstances which determine whether the motion of water shall be direct or sinuous, and the law of resistance in parallel channels. *Philisophical Transactions of the Royal Society*, **174**, 935-982.

Rice, S.P. and Church, M. (2010) Grain-size sorting within river bars in relation to downstream fining along a wandering channel. *Sedimentology*, **57**, 232-251.

Richardson, P.D. (1968) The generation of scour marks near obstacles. *Journal of Sedimentary Petrology*, **38**, 965-970.

Robinson, K.M., Cook, K.R. and Hanson, G.J. (2000) Velocity field measurements at an overfall. *Transactions of the ASCE*, **43**, 665-670.

Russell, A.J. and Knudsen, O. (2002) The effects of glacier-outburst flood flow dynamics on ice-contact deposits: November 1996 jökulhlaup, Skeiðarársandur, Iceland. *Spec. Publs int. Ass. Sediment.*, **32**, 67-83.

Russell, H.A.J. and Arnott, R.W.C. (2003) Hydraulic-jump and hyperconcentrated-flow deposits of a glacigenic subaqueous fan: Oak Ridges Moraine, Southern Ontario, Canada. *Canadian Journal of Sedimentary Research*, **73**, 887-905.

Russell, H.A.J., Arnott, R.W.C. and Sharpe, D.R. (2003) Evidence for rapid sedimentation in a tunnel channel, Oak Ridges Moraine, southern Ontario, Canada. *Sedimentary Geology*, **160**, 33-55.

Sarma, K.V.N. and Newnham, D.A. (1973) Surface profiles of hydraulic jump for Froude numbers less than four. *Water Power*, **25**, 139-142.

Saunderson, H.C. and Lockett, F.P.J. (1983) Flume experiments on bedforms and structures at the dune-plane bed transition. *Spec. Publs int. Ass. Sediment.*, **6**, 49-58.

Savage, S.B. (1979) Gravity flow of cohesionless granular materials in chutes and channels. *Journal of Fluid Mechanics*, **92**, 53-96.

Savery, C. and Zech, Y. (2007) Boundary conditions in a two-layer geomorphical model. Application to a hydraulic jump over a mobile bed. *Journal of Hydraulic Research*, **45**, 316-332.

Schlichting, H. (1936) Experimentelle untersuchungen zum rauhigkeitsproblem. *Ing.-Arch.*, **7**, 1-34.

Schmincke, H.U., Fisher, R.V. and Waters, A.C. (1973) Antidune and chute and pool structures in the base surge deposits of the Laacher See area, Germany. *Sedimentology*, **20**, 553-574.

Seidl, M.A., Dietrich, W.E. and Kirchner, J.W. (1994) Longitudial profile development into bedrock - an analysis of Hawaiian channels. *Journal of Geology*, **102**, 457-474.

Shaw, J. (1994) Hairpin erosional marks, horseshoe vortices and subglacial erosion. *Sedimentary Geology*, **91**, 269-283.

Shillabeer, N., Hart, B. and Riddle, A.M. (1992) The use of a mathematical model to compare particle size data derived by dry sieving and laser analysis. *Estuarine, Coastal and Shelf Science*, **35**, 105-111.

Silberman, E. (1959) Discussion of turbulence characteristics of the hydraulic jump by Hunter Rouse, Tien To Siao and S. Nagaratnam. *Transactions of the ASCE*, **124**, 951-952.

Southard, J.B. and Boguchwal, L.A. (1990) Bed configurations in steady unidirectional water flows, Part 1. Synthesis of flume data. *Journal of Sedimentary Petrology*, **60**, 658-679.

Southard, J.B. and Harms, J.C. (1972) Sequence of bedforms and stratification in silt, based on flume experiments. *American Association of Petroleum Geologists Bulletin*, **56**, 654-655.

Stokes, G.G. (1851) On the effect of internal friction of fluids on the motion of pendulums. *Transactions of the Cambridge Philosophical Society*, **9**, 8-106.

Straub, K.M. and Mohrig, D. (2009) Constructional canyons built by sheet-like turbidity currents: observations from offshore Brunei Darussalam. *Journal of Sedimentary Research*, **79**, 24-39.

Sun, T. and Parker, G. (2005) Transportational cyclic steps created by flow over an erodible bed. Part 2. Theory and numerical simulation. *Journal of Hydraulic Research*, **43**, 502-514.

Sutton, S.L.F. and McKenna-Neuman, C. (2008a) Sediment entrainment in the lee of roughness elements: Effects of vortical structures. *Journal of Geophysical Research*, **113**, F02S09.

Sutton, S.L.F. and McKenna-Neuman, C. (2008b) Variation in bed level shear stress on surfaces sheltered by nonerodible roughness elements. *Journal of Geophysical Research*, **113**, F03016.

Svendsen, I., Veeramony, J., Bakunin, J. and Kirby, J. (2000) The flow in weak turbulent hydraulic jumps. *Journal of Fluid Mechanics*, **418**, 25-57.

Taggart, W.C., Pflaum, J.M. and Sorenson, J.H. (1984) Modifications of Dams for Recreational Boating. *Design Notes - Supplement to Flood Hazard News* 1-4.

Taki, K. and Parker, G. (2005) Transportational cyclic steps created by flow over an erodible bed. Part 1. Experiments. *Journal of Hydraulic Research*, **43**, 488-501.

Tamai, N., Asaeda, T. and Tanaka, N. (1987) Vortex structures around a hemispheric hump. *Boundary-Layer Meteorology*, **39**, 301-314.

Thompson, D.M. (2008) The influence of lee sediment behind large bed elements on bedload transport rates in supply-limited channels. *Geomorphology*, **99**, 420-432.

Toso, J.W. and Bowers, C.E. (1988) Extreme pressures in hydraulic-jump stilling basins. *Journal of Hydraulic Engineering*, **114**, 829-843.

Valle, B.L. and Pasternack, G.B. (2002) TDR measurements of hydraulic jump aeration in the South Fork of the American River, California. *Geomorphology*, **42**, 153-165.

Valle, B.L. and Pasternack, G.B. (2006) Submerged and unsubmerged natural hydraulic jumps in a bedrock step-pool mountain channel. *Geomorphology*, **82**, 146-159.

Van den Berg, J.H. and Van Gelder, A. (1993) A new bedform stability diagram, with emphasis on the transition of ripples to plane bed in flows over fine sand and silt. *Spec. Publs int. Ass. Sediment.*, **17**, 11-21.

van Dyke, M. (1982) *An Album of Fluid Motion*. The Parabolic Press, Stanford, 176 pp.

Vide, J.P.M., Dolz, J. and Del Estal, J. (1993) Kinematics of the moving hydraulic jump. *Journal of Hydraulic Research*, **31**, 171-186.

Villard, P.V. and Church, M. (2005) Bar and dune development during a freshet:Fraser River Estuary, British Columbia, Canada. *Sedimentology*, **52**, 737-756.

Waltham, D. (2004) Flow transformations in particulate gravity currents. *Journal of Sedimentary Research*, **79**, 129-134.

Werner, F. and Newton, R.S. (1975) The pattern of large-scale bed forms in the Langerland Belt (Baltic Sea). *Marine Geology*, **19**, 29-59.

Werner, F., Unsold, G., Koopmann, B. and Stefanon, A. (1980) Field observations and flume experiments on the nature of comet marks. *Sedimentary Geology*, **26**, 233-262.

Whipple, K.X., Hancock, G.S. and Anderson, R.S. (2000) River incision into bedrock: Mechanics and relative efficacy of plucking, abrasion, and cavitation. *Geological Society of America, Bulletin*, **112**, 490-503.

Whiting, P., Dietrich, W.E., Leopold, L.B., Drake, T.G. and Sherve, R.L. (1988) Bedload sheets in heterogenous sediments. *Geology*, **16**, 105-109.

Winant, C.D. and Browand, F.K. (1974) Vortex-pairing: the the mechanism of turbulent mixing and growth at moderate Reynolds number. *Journal of Fluid Mechanics*, **63**, 237-255.

Winsemann, J., Asprion, U. and Meyer, T. (2004) Sequence analysis of early Saalian glacial lake deposits (NW Germany): evidence of local ice margin retreat and associated calving processes. *Sedimentary Geology*, **165**, 223-251.

Winsemann, J., Brandes, C. and Polom, U. (2010) Response of a proglacial delta to rapid high-amplitude lake-level change: an integration of outcrop data and high-resolution shear wave seismics. *Basin Research* doi: 10.1111/j.1365-2117.2010.00465.x.

Wintwerp, J.C., Bakker, W.T., Mastbergen, D.R. and van Rossum, H. (1992) Hyperconcentrated sand-water mixture flows over erodible bed. *Journal of Hydraulic Engineering*, **119**, 1508-1525.

Wohl, E.E. (1992) Bedrock benches and boulder bars: Floods in the Burdekin Gorge of Australia. *Geological Society of America, Bulletin*, **104**, 770-778.

Wohl, E.E. and Cenderelli, D.A. (2000) Sediment deposition and transport following a reservoir sediment release. *Water Resources Research*, **36**, 319-333.

Wyrick, J.R. and Pasternack, G.B. (2008) Modeling energy dissipation and hydraulic jump regime responses to channel nonuniformity at river steps. *Journal of Geophysical Research*, **113**, F03003-.

Yüksel, Y., Günal, M., Bostan, T., Çevik, E. and Çelikoğlu, Y. (2004) The influence of impinging jets on hydraulic jumps. *Proceedings of the Institution of Civil Engineers-Water Management*, **157**, 63-76.

Appendix 1: Flow through a lateral constriction

Via Equations A1.1 − A1.5 Mark Cooker and I derived that flow through a constriction can be thicker than, the same thickness as or thinner than flow upstream of the constriction depending on the values of the Froude number upstream of the constriction and the ratio of channel widths upstream to downstream of the constriction. Symbols with subscript A are nomenclature for parameters of the flow upstream of the constriction and symbols with subscript B are nomenclature for parameters of the flow within the constriction.

For flow into a constriction it must hold that, following Bernoulli,

$$p + \frac{1}{2}\rho u_A^2 + \rho g h_A = p + \frac{1}{2}\rho u_B^2 + \rho g h_B \tag{A1.1}$$

and because mass is conserved through the constriction,

$$Q = b_A u_A h_A = b_B u_B h_B \tag{A1.2}$$

Rearranging Equation A1.2 in terms of u_B we find that

$$u_B = \frac{b_A u_A h_A}{b_B h_B} \tag{A1.3}$$

and substituting Equation A1.3 into Equation A1.1 we obtain

$$\frac{u_A^2}{2} + g h_A = \frac{u_A^2}{2}\left(\frac{b_A h_A}{b_B h_B}\right)^2 + g h_B \tag{A1.4}$$

Multiplying through by $\dfrac{h_B^2}{g h_A^3}$ and with some rearranging we get

$$\left(\frac{h_B}{h_A}\right)^3 - \frac{Fr_A^2}{2}\left(\frac{h_B}{h_A}\right)^2 - \left(\frac{h_B}{h_A}\right)^2 + \frac{Fr_A^2}{2}\left(\frac{b_A}{b_B}\right)^2 = 0 \tag{A1.5}$$

which is a cubic equation for $\dfrac{h_B}{h_A}$. Looking at Equation A1.5 we see that the value of h_B can be more than, less than or equal to the value of h_A, depending on the values of Fr_A and on $\dfrac{b_A}{b_B}$.

Appendix 2: Electronic copies of figures and video files

Videos and photographs are supplied on mini DVD at the back of this thesis. They are listed below and are listed on the mini DVD as well.

Fig. 4.14 The Run 2 deposit photographed in stream-parallel section.

Fig. 4.15 The Run 2 deposit photographed in stream-transverse section.

Fig. 5.7 The Run 3 deposit photographed in stream-parallel section.

Fig. 5.17 The Run 4 deposit photographed in stream-parallel section.

Fig. 5.19 The Run 4 deposit photographed in stream-transverse section.

Fig. 6.4 The exposure of the Emme coarse grained delta that contained a candidate basal wedge and candidate hydraulic-jump bar complex.

Video file 1 Non-breaking surface of a hydraulic jump during trial experiments reported in Section 2.9 of this thesis. A sediment deposit that formed during the trial experiment can be seen downstream of the hydraulic jump. The surface of the hydraulic jump was non-breaking before, during and after sediment transport.

Video file 2 Swash and backwash over a pebble on a beach. A hydraulic jump forms and changes shape twice, from arcuate fronted with the apex of the arc pointing upstream, to two arcs of overturning water, and back again.

Video file 3 Flow over the hemisphere in Run H3.05, involving an arcuate fronted hydraulic jump. Air is entrained into the flow in the form of bubbles. A particularly large bubble repeatedly forms in the supercritical flow adjacent to the downstream edge of the hemisphere, grows as smaller bubble coalesce and passes downstream.

Video file 4 Motion of bedload sheets around the hemisphere during Run MH2.2a.

Video file 5 Toe oscillation and splashing of the Run 1 hydraulic jump.

Appendix 3: Effect of vortices on velocity patterns

Consider a vertical profile of streamwise velocity in which velocity is constant with height (Fig. A3.1A). Consider then a vortex present at the location of the profile, with an upper half rotating downstream and a lower half rotating upstream (Fig. A3.1B). The presence of this vortex increases the streamwise velocity between the heights of the vortex centre and top (compare Fig. A3.1A and C). The presence of the vortex decreases streamwise velocity between the heights of the vortex centre and bottom. At the exact position of the vortex centre the magnitude of streamwise velocity is unchanged between the states of the vortex being absent or being present.
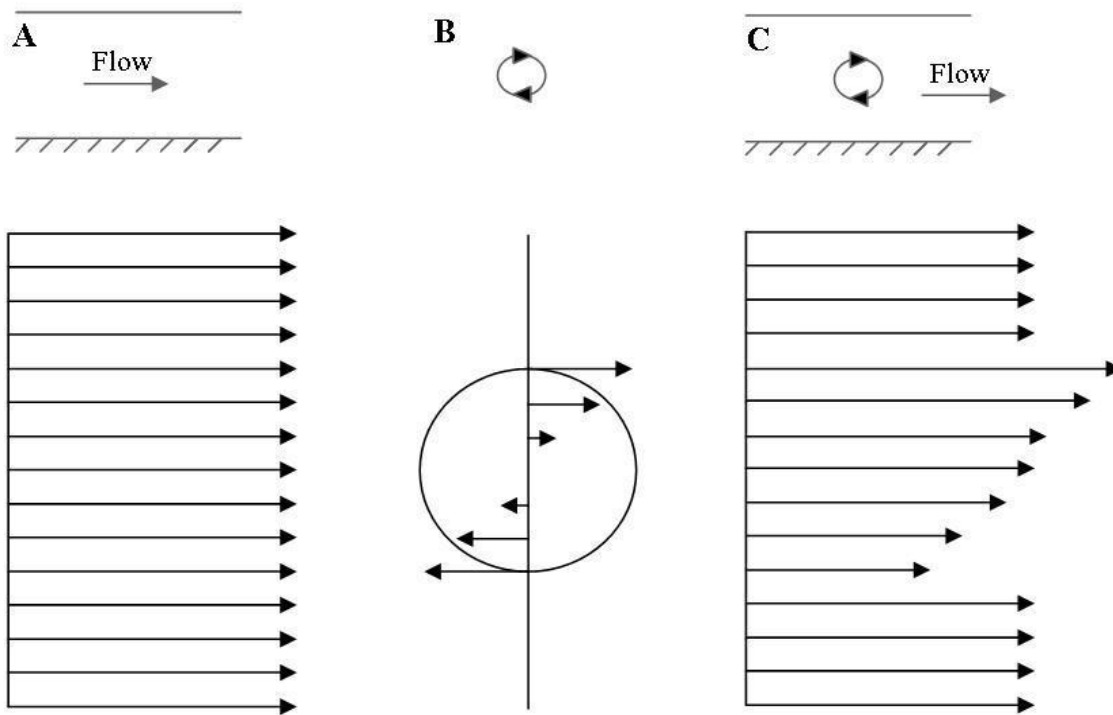

Figure A3.1 Line drawings of flows (grey lines and arrows) and their associated vertical profiles of streamwise velocity (black lines and arrows). The length of the black arrows indicates the magnitude of streamwise velocity. (A) Flow is left to right and streamwise velocity is uniform in magnitude with height. (B) A vortex in isolation. (C) A vortex present within Flow A. The vortex has a cross-stream axis of rotation. The upper half of the vortex has the same sense of rotation as the flow that surrounds the vortex and the lower half of the vortex has the opposite sense of rotation (grey arrows, Flows B and C).

Appendix 4: Change in angle (of laminae) due to height exaggerations imposed on diagrams: Derivation

The factor of change of lamina dip angle when an image is vertically exaggerated

Because of the long length : height ratio of the flume test channel, and of some sand deposits that formed within it, it has been necessary to depict the sand deposits diagrammattically using a vertical height exaggeration, notably in Figures 5.5 and 5.12. Dip angles do not change in a 1 : 1 relationship with height exaggeration in an image (imagine a 30° dip and a five-times exaggeration; the laminae would appear to dip in the wrong direction were the relationship 1 : 1). Instead the angles of dip of the laminae depicted in Figures 5.5 and 5.12 are exaggerated by a factor

$$\psi = \tan^{-1}\left(E\tan\varphi\right) \tag{A4.1}$$

where ψ is the exaggerated angle, E is the height exaggeration in the diagram and φ is the non-exaggerated angle of dip of the lamina. Equation A5.1 is derived from the following geometrical consideration.

Derivation of the factor ψ

Consider the original image of a right-angled triangle where the hypotenuse represents a dipping lamina (solid line, Fig. A5.1). Also consider it being exaggerated E-fold in the height dimension to form the exaggerated image (dashed line, Fig. A5.1). The height of the original image, y is simply

$$y = x\tan\varphi \tag{A4.2}$$

where x is the length of the base of the triangle and φ is the angle between the base and the dipping lamina. By simple transformation of Equation A5.2, the height of the exaggerated image, Ey is

$$Ey = Ex\tan\varphi. \tag{A4.3}$$

Now, by a simple trigonometric relationship the angle of the exaggerated dipping side, ψ is

$$\psi = \tan^{-1}\left(\frac{Ey}{x}\right) \tag{A4.4}$$

and combining A5.3 and A5.4 it is found that Equation 1 is the relationship of the original and exaggerated angles.
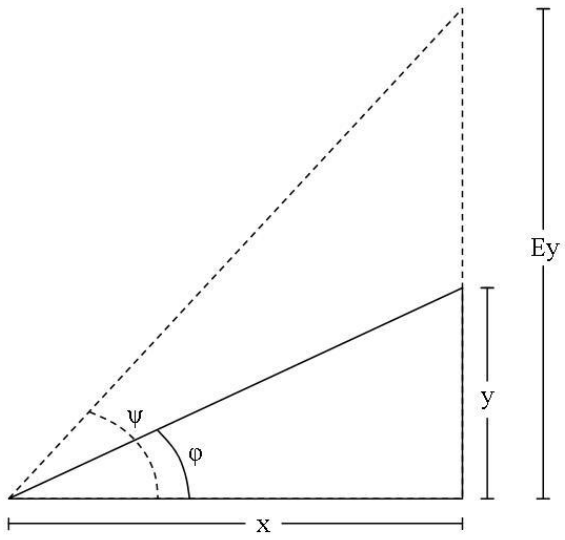
Figure A4.1 Two triangles with the same base length, *x* but different heights. The two hypoteneuses dip at different angles, φ and ψ. The reference triangle (solid line) has height *y* and the vertically-exaggerated triangle (dashed line) has height *Ey*.